Multi-Agent Systems - A new approach for assessing urban environmental conditions

This book was accepted in its original form as
post-doctoral habilitation thesis at the Faculty of Geoscience,
Ruhr-University Bochum, Germany

This edition contains updates to the original version

Michael Bruse

Multi-Agent Systems - A new approach for assessing urban environmental conditions

e-mail: michael.bruse@rub.de
www.botworld.info

Herstellung und Verlag: Books on Demand GmbH, Norderstedt

Multi-Agent systems as a new approach for assessing urban environmental conditions

Design and application of a Multi-Agent simulation system for analysing environmental conditions based on the simulation of individual-based assessment and the resulting behaviour shown by the example of thermal comfort in urban areas

Streets, open spaces or shopping malls – they all would be worthless without people filling them up with life. Regardless if ones looks at it from the sociologic, ecologic or economic perspective: The presence of pedestrians is a key indicator for the attractiveness of an urban environment. Moreover, it is an indicator that intensifies itself: If pedestrians stay out of an urban area, the available spending power decreases and streets and places begin to become desolate or being used as traffic axis only. As a consequence, the quality and quantity of the offered goods and services decreases and further pedestrians that might have become customers stay away. Hence, designing public places in a way that pedestrians feel comfortable is no luxury, but the indispensable basis for their functionality with unambiguous economic consequences if they fail to function.

For urban planners and architects it is therefore essential to have access to tools allowing them to analyse the dynamics of existing urban spaces and estimate the impact of future changes on the system. In practice it has turned out, that the application of static and local indicators for assessing the urban environment often does not reflect nor consider the dynamic character of the system. As people are usually in motion when they use the urban structure, the assessment of a specific location depends to a great extent on the experiences made before entering a certain location and the resulting expectations based on these experiences.

In this thesis, the simulation system *BOTworld* is presented as a new assessment approach based on the method of Multi-Agent simulations. This method focuses on the behaviour and environmental perception of the individual pedestrian and allows there through an assessment of environmental conditions seen from the user's perspective. By the example of urban microclimate and the resulting human thermal comfort it will be shown, how the *BOTworld* concept can be used for the analysis of complex environmental conditions.

Pedestrians and the urban microclimate

The way how pedestrians percept their urban surroundings and the question, whether they are satisfied with the situation or not depends on a multitude of influencing factors from which some are more and others are less quantifiable. From the quantifiable factors, the local climate conditions the pedestrians are exposed to during their passage through the urban area or while using open spaces contribute to a significant amount to the pedestrians' perception of the urban environment. Besides the actual state of the weather, it is often the right mix of sun and shade or the balance between wind protection and fresh air that tips the scales between success and failure of an open space.

Even though the local microclimate conditions explain the personal preferences for specific locations only partly, it is important for planners to know, how

the environmental design influences the local climate and how it interacts with the level of comfort and satisfaction of the pedestrians.

Very roughly, the urban climate conditions can be distinguished into two areas of influence: The *air quality complex*, dealing with the pedestrians' exposure to air pollutants and the *thermal complex*, describing the effects of microclimate on the human energy balance and the resulting heat- and cold sensation of the pedestrians.

In order to assess an urban area with respect to these two areas of influence and their impact on humans, a two-stage approach is typically used: In the first stage, the interactions between the physical urban structure and the investigated parameters are analysed using quantitative methods such as numerical models. In the second, often only qualitative and sometimes even subjective stage, the obtained data are then analysed with respect to their impact on the well-being of the pedestrians.

The methods and procedures used in the first stage are usually based on generally accepted fluid dynamical and thermodynamical principles and the discussion, whether model A is better suited than model B normally deals only with details. However, in the second stage of the process, the assessment of the data, the situation is fundamentally different: The quantitative data generated in the first stage correspond, depending on the method used, more or less with the reality, but in any case they are free from value judgements.

The spatial and temporal distribution of the urban microclimate as primary information is neutral first of all and does not provide any information whether the pedestrians are satisfied with these conditions or not. But after all, this information is crucial for the assessment of the environmental situation or for the choice between different alternative scenarios. Hence, it suggests itself to formalise the second stage of the assessment process through the fixation of threshold values and to relate the conclusion, whether the pedestrians are satisfied or not, to the question whether the defined limits are kept or not. However, this procedure induces some contradictions which should be discussed a bit further now.

Threshold values and indices

Starting the discussion by looking at the air quality component of the urban microclimate, most people think of the evaluation of air quality by comparing the actual pollutant concentration with the respective legislative threshold values. Most recently (2005), the new European legislative guideline for the maximum allowable concentration of fine dust particles came into the focus of public discussion. The application of this guideline means for many European cities that their pedestrians will not only feel unpleasant in several streets, but also have to expect health implications there.

This limit-motivated analysis of air quality can be confronted with a toxicological-motivated view at the problem: Seen from the health aspect, the optimal urban air situation is that situation in which the exposure of pedestrians and residents to air pollutants is minimised.

Though both approaches follow the same objective, the protection of the citizens against air pollutants, their practical application can result in quite different strategies: Seen from the aspect of keeping the threshold values, it might be reasonable to redistribute the car traffic over all available urban streets until all street segments fulfil the air quality limits. This approach is practically already realised through different traffic guidance measures. Evaluating such a procedure from the toxicological point of view, it might happen, if all streets are approximately equally frequented by pedestrians, that the situation has worsen as now more people are actually exposed to air pollutants compared to the situation with one single heavily polluted street. Though the local pollutant concentrations might now keep the legislative limits, the overall exposition of the citizens has increased. Hence, from the toxicological perspective, the situation is worse than before.

A local assessment in which the single locations are analysed independently from each other with respect to certain criteria is though problematic if the affected system, for which these criteria have been established, does not behave locally. This is the case for example when looking at pedestrians which move through different locations and are hence exposed to

the single local conditions only over a limited time.

This aspect becomes especially relevant if the concerned system reacts with a certain inertia on the external conditions and therefore the individual state at place x at time t depends also on the conditions the individual has been exposed before. Through this inertia, a temporal shift between the local environmental conditions and their actual perception establishes which generates space-time linkages in the analysed area. Without knowing and understanding these linkages, a realistic assessment of the environmental conditions and their impact on pedestrians is difficult.

Unfortunately, the second component of the urban climate, the thermal complex is such an inert system, in which the thermal sensation of a pedestrian at a specific location at a specific time depends to a huge amount on the microclimate conditions this pedestrian has been exposed to before. Hence, thermal comfort describes primary on the state of the user, not the conditions of a specific location. Consequently, it seems reasonable to focus the analysis on the affected system (the pedestrian) rather than on the triggering system (the microclimate).

In empirical studies this aspect is already considered implicitly: If pedestrians are interviewed about their actual assessment of the microclimate conditions, their response reflects in essence whether their actual thermal state and the local climate conditions correspond or not. An interviewer standing in the centre of a sunny open space will probably be confronted with different statements, depending whether the questioned person has already been exposed to the sun for a longer time or just came out of a shady street canyon.

Hence it is no surprise, that thermal assessment based on interview statements and thermal assessment based on local indices calculated using the meteorological conditions show significant differences (compare Module B of this thesis).

The individual in focus

Resolving the discussed contradictions requires not only a change of the method but particularly a change of the perspective: Instead of interpreting the microclimate system as a spatial patchwork of different meteorological conditions it would provide a solution to slip into the position of an user of the urban area and analyse the system from within.

That such a change of the perspective could lead to interesting and new discoveries was realised quite early for economic systems. In classical economy as represented by *Adam Smith* or *John M. Keynes*, the complex dynamics of an economic system are described similar to Newton' physics with a few parameters and general functions. Diametrically opposite to this concept is the interpretation of the economic system introduced by *John Nash*. In Nash's concept, the individual actor and his view of the system, especially his view of the other actors in the system stands in the focus of interest. Nash could prove that from this perspective, even complex macro economic processes could be simulated using relatively simple micro rules for the individual actor. These findings were not only honoured with the Nobel prize for economics in 1994 but also resulted in the Hollywood movie *A beautiful mind* in 2001.

It is the core idea of such an individual-based analysis to distribute the control of the system dynamic onto the individual actors deciding autonomously what to do rather than defining some explicit functions describing the different processes from a global perspective.

This concept corresponds to the idea of *Distributed Artificial Intelligence DAI* and its software realisation, the so-called *Multi-Agent-Systems*.

In general, an *agent* is a computer system or a piece of software code that *lives* in a specified environment and is able to percept this environment and, based on this perception, to make autonomous decisions and activities to reach a certain goal (compare Module A of this thesis).

Transferred to the topic of urban microclimate and thermal comfort of pedestrians this means that in such a Multi-Agent system each pedestrian is represented through a software agent moving autonomously through the urban environment while being exposed to different microclimate conditions. The reaction of the virtual body to these conditions is continuously monitored by internal models, in this case through a model of the human thermoregulatory sys-

tem. These models calculate all relevant indicators such as the skin temperature or the sweat rate. These indicators represent the internal state of the agent and serve as basis for the agent's assessment of the environmental conditions. In addition, it is possible to extend the behaviour rules of the agents so that they produce not only realistic movement patterns, but also take autonomously care of their well-being and take measures to improve their situation if their internal state exceeds the acceptable limits. To obtain a final assessment of the environmental situation, it is sufficient to observe the behaviour of the agents and to analyse the relevant internal conditions of the agents such as their thermal state. The space-time links mentioned above as well as their consequences for the assessment are considered automatically when using such a Multi-Agent system.

The practical application

In the practical application, such a Multi-Agent system allows a methodologically comprehensible and mathematically consistent assessment of environmental conditions seen from the users perspective. The danger of biasing the results through personal preferences is minimised.

In Multi-Agent systems, the focus of interest is set onto the single individual, hence it is possible to simulate dynamic and, seen from the urban structure, non-local processes. There through a much higher degree of realism can be achieved compared to local and static approaches. As it is possible to trigger the agents' routing behaviour in dependency to their internal state, the simulation does not only provide information about the pedestrians' assessment of a certain location but it can also be analysed which impact the environmental conditions have on the frequentation of the area. In daily practice the application of such a Multi-Agent model is more time expensive compared to the application of classic local approaches and assessment indices. But the more the complex the environmental conditions get in their spatial and/or temporal dimension, the more unsuitable the application of such simple local approaches becomes.

By the example of thermal comfort in urban open spaces it will be shown in this thesis in how far the assessment of environmental conditions based on the Multi-Agent simulation system BOTworld differs from the results obtained from static and local approaches.

Like each other model approach, BOTworld reduces the complexity of the complete problem by focussing onto some selected factors. The real behaviour of a real human depends of course on many other aspects impossible to be considered completely in a numerical or any other model. Hence it is not the aim of this simulation system to reproduce the complete human behaviour in urban areas, but to analyse to which extent urban microclimate has an impact on the behaviour of pedestrians and which conclusions can be drawn from this information.

Even though the emphasis of this thesis is on urban microclimate, the method of Multi-Agent systems can be applied to the assessment of many other environmental factors such as noise or the visual impression. To do so, the assessment rules of the system need to be extended with new rules for the environmental complex to be assessed.

Furthermore, the application of BOTworld is not restricted to urban situations. Those are only the worst-case conditions for simulating pedestrian behaviour. Another field of application could be for example the assessment of thermal comfort conditions on longer routes through terrain such as hiking paths.

Contents of this thesis

This thesis describes the different theoretical approaches used for the design of the Multi-Agent system BOTworld and shows through selected examples how BOTworld works and how it can be used to assess the urban microclimate and the thermal comfort of pedestrians.

The thesis is divided into the following modules:

Modul A *PedWalk* – A Multi-Agent Model for the simulation of pedestrian traffic in complex urban microscale environments

Modul B Simulating human thermal comfort in urban outdoor spaces using a simple dynamic model of the human thermoregulatory system linked to a Multi-Agent model system

Modul C The F-A-ST approach: A Fuzzy Logic based assessment model for the use in Multi-Agent model environments

Modul D Simulating human thermal comfort in urban open spaces using the Multi-Agent simulation system BOTworld

Modul E Simulating pedestrian exposure to traffic-induced air pollutants in urban areas using a Multi-Agent model system

Besides the theoretical modules, the developed software system BOTworld is the main outcome of this thesis. All of the results shown in this thesis have been generated using BOTworld and the software can be found, together with the simulation data, on the accompanying DVD. For the most recentversion of BOTworld, visit `www.botworld.info`.

Future perspectives

With the software system BOTworld developed in this thesis, a powerful tool for the assessment of urban environmental conditions based on the Multi-Agent simulation technique is available. Using the BOTworld concept it is not only possible to assess urban microclimate data, but also to assess other impact factors on pedestrian comfort such as noise or the visual environment if the system is extended with the respective assessment rules..

The next steps in the development of the BOTworld system will have to deal with the determination of suitable values for the different behaviour specific calibration factors used in the model. Through investigations carried out during the EU project RUROS an initial methodological framework has been established which needs to be refined and extended in further empirical and model theoretical studies.

Bochum/ Essen October 2005, February 2007


A

Module A

PedWalk – A Multi-Agent model for the simulation of pedestrian traffic in complex urban microscale environments

Pedestrian traffic is one of the main indicators for the vitality, attractiveness and economic power of urban areas. Especially in the larger cities of the northern hemisphere, the lack of affordable parking spaces, the closure of roads for individual traffic or legislative restrictions for car access have led to a significant increase in urban pedestrian traffic in the last decade. In view of more stringent threshold values for air quality becoming effective in the next years (e.g. guideline 1999/30/EG for Particulate Matters concentrations in the EU countries) and the resulting administrative measures to fulfil these criteria, it can be anticipated that this trend will continue.

When analysing pedestrian traffic on the microscale level focussing on a single street, an intersection or a public place, a huge spatial and temporal variability of usage of open space can be observed. Hence, when looking for the optimal environmental design, architects and urban planners are often faced with the problem how to assess the impacts of their design or planning decisions on the pedestrian traffic flows and frequentation of areas. Similar to car traffic, several analytical and numerical approaches exist to predict the influence of urban geometry on pedestrian traffic flows and the level of service which is achievable. On the microscale level, the application of Multi-Agent models is offering a promising approach to handle the complex system of pedestrian traffic by focussing on the behaviour of a single agent (pedestrian) rather than attempting to describe the whole system through macroscopic and explicit model equations. Through the iterative application of behaviour rules and the usage of a huge number of agents, even complex features of the observed system can emerge autonomously without being included explicitly through model equations, e.g through self-organisation.

In this paper, the Multi-Agent model *PedWalk* is presented (Part I) and selected model results are discussed (Part II). *PedWalk* is a numerical model designed to simulate pedestrian movement through urban structures on a very small spatial (typically 0.5 to 3 m) and temporal (around 1 sec) scale. As a specific feature, the model offers an interface to include additional quality information such as local environmental quality indicators in the simulation process. *PedWalk* is the basic component of the BOTworld simulation system designed for simulating and analysing the urban environment using the Multi-Agent technique.

Keywords: Pedestrian traffic, Multi-Agent Simulation, Microsimulation, Urban environment, Frequentation of outdoor spaces

Contents

List of Figures

List of Tables

Main Symbols (Alphabetical Index)

Main Symbols *PedWalk* Model		
Symbol	**Unit**	**Meaning**
ag	y	Age
a	ms^{-2}	Acceleration coefficient
b	ms^{-2}	Deceleration coefficient
d_{conflict}	m	Extention conflict zone
d^*	m	Desired clearance to next agent
im, jm	m	Distance from assigned navigation node
impatience	[0,1]	Impatience flag
t^*	sec	Save time interval
t_{lost}	sec	Lost time
timeout	sec	Timeout counter
talking	[0,1]	Talking flag
v_{pref}	ms^{-1}	Agent's preferred velocity
v_{act}	ms^{-1}	Agent's actual velocity
α	[deg]	Moving direction (angle)
ι		Hierarchy position in group
ϕ	[1..8]	Moving direction (index)
ξ	-0.3 to +0.3	Walking personality
ω_x	0 to 1	Impact factor profile
Δ	m	Real distance
Δ^v	m	Virtual distance
Ξ^v	m	Virtual Distance map
$\Pi(\text{act})$	$[i, j]$	Agent's assigned navigation node
Π_+	$[i, j]$	Next navigation node
Π^*	$[i, j]$	Next destination node
$\Upsilon = (x, y)$	m	Exact position from origin of model domain
Φ^q	-1 to +1	Quality of grids (individual)
$\Phi^{q,0}$	-1 to +1	Quality of grids (global)
Φ^0	-1 to +1	Routing assessment
Φ^*	-1 to +1	Reactive assessment
$\Phi^=$	-1 to +1	Dynamic assessment

Part I
Model Theory

1 Introduction

When thinking about traffic in urban areas, car traffic and the associated problems such as demand of space, pollutant emissions and traffic congestion are the first things that come into mind. But looking at an urban area more in detail, we soon discover another traffic component of at least equal importance: Pedestrians.

Especially in the core center of larger cities, the lack of affordable parking places or restrictions in car access (e.g. as practiced in London, Rome or Singapore) has shifted a significant part of the urban traffic load towards public transport and walking. Taking Central London as an example, the Transport Statistic Report from 2003 states that 54% of all trips in the Central London Area (34% in Greater London) are made by walking including those trips coming from or heading towards public transport connection nodes (GSS, 1997). In general, it was found for Great Britain, that 80% of all trips which are shorter than 1.6 km (1 mile, about 25% of all trips) are made by walking (ONS, 2001). For most other European countries and cities, similar figures can be found.

Through the next years, national and international guidelines will establish increasingly stringent new threshold values for air quality (e.g. the recently effective guideline 1999/30/EG for Particulate Matters concentrations in the EU countries). As a matter of fact, today most of the bigger cities in Europe are not able to satisfy the thresholds given by these guidelines and the only immediately effective measure that can be taken, is to ban cars out of the city cores at critical times. Hence it can be anticipated, that in the next years, the percentage of pedestrian traffic in urban areas will continue to grow, making its analysis even more important.

Although pedestrians are a significant component of the urban traffic network, the analysis of their demands and the design of public facilities with respect to these demands is a relatively new area of research. The main reason for this neglect is certainly based on the general attitude towards urban life and urban planning in the second half of the 20th century, which was well and prominently described through the *Charta of Athens*. This document, published by Le Corbusier (1943), summarized the results from the IV. Congress of CIAM (Congrès Internationaux

d'Architecture Moderne) in 1933 and propagated a spatial separation of the dimensions housing, labour, leisure and transportation in order to improve the living conditions in urban areas. Its remarkably strict application in urban planning especially between the 1950ies and 1970ies lead inevitably to a significant increase in travel distances and traffic volume between the different functional units of the city. Consequently, a modern and well-functioning city in this period was considered to be a car-optimized city and the calculation and optimisation of vehicular traffic flows was the prior interest to planners – Pedestrians were supposed to live with the remaining space after the car traffic facilities have been designed.

In the last twenty to thirty years there has been a general change in the common mind about cars and the role they are supposed to play in daily urban life. Car-free zones in the CBDs have been established and pedestrian walking was upgraded to - and promoted as - an individual form of traffic, bringing benefits to both the environment and the walker him or herself.

Nowadays, the presence of pedestrians is recognized as a major indicator for the vitality, attractiveness and economic power of an area. Planners have realized that achieving a high level of pedestrian satisfaction is not only pure luxury in urban planning, but also has a direct economical impact when considering the frequentation of shop locations and the mood of the passing pedestrians and their willingness to buy the offered goods. For example, the *Planning Policy Guidance 6: Town Centers and Retail Developments* (UK Department of Environment, 1996) explicitly names the

> "[...] numbers and movement of people on the street, in different parts of the center at different times of the day and the evening, who are available for business to attract in to shops, restaurants or other facilities [...]" *PPG6, 1996, p.11*

as an important indicator for assessing the vitality and viability of town centers.

Different to people commuting in cars, pedestrians are directly exposed to their immediate environmental conditions, which influence their moving decisions and their level of comfort. This level of comfort is composed out of many components from simple mobility aspects up to personal environmental preferences and has a direct impact on the individual perception of the environment and consequently on the behaviour in and the usage of public open spaces.

The increased importance of designing an urban environment in which pedestrians feel comfortable is also well notifiable in the "Bible" of traffic planners, the *Highway Capacity Manual*: Whereas in the 3rd edition from 1985 pedestrians (and bicycles) were presented in two short chapters and remained unedited until 2000, the 4th edition from 2000 does not only provide a much more sophisticated set of tools for designing pedestrian facilities, but goes even further in detail by also considering additional environmental factors (comfort, convenience) that contribute to the "*walking experience and therefore to perceived level of service*" (TRB, 2000). The Highway Capacity Manual 2000 concludes, that

> "[...] these supplemental (environmental) factors can effect pedestrian perception of the overall quality of service of the street environment" *HCM 2000, Chapter 11*

1.1 History of traffic modelling

With increasing consideration of pedestrian traffic, researchers and planners began to search for methods for the description and prediction of pedestrian traffic as an individual transport component. It soon turned out, that the movement of cars and the behaviour of pedestrians are too different from each other to allow a successful adoption of existing methods for vehicular traffic to pedestrian flows: Rules for car traffic are usually very strict and the possible movement options are restricted by lanes and consist basically of velocity adjustments and occasional lane changes. This limited set of microscopic behaviour options allows the successful application of simple and general macroscopic rules for traffic flow such as the *Fundamental Diagram* introduced by Greenshields (1934). These simple methods show a good agreement with the observed properties as long as the observed situation does not reach a critical stability (e.g. jam conditions). In contrast, the movement of pedestrians is significantly more complex: Pedestrians do not follow pre-defined lanes and the rules of pedestrian interactions are much less obvious and more subject to individual interpretation compared to traffic laws. Another difficulty in the prediction

of pedestrian flows is imposed through the microscopic character of pedestrian interaction processes in time and space: In order to understand and evaluate the quality of pedestrian facilities, the models applied demand a spatial and temporal resolution resolving the single pedestrian and his/her dynamic behaviour. This all together makes it significantly difficult to find simple rules describing the relationship between the design of facilities and the resulting flow of pedestrians.

Empirical rules and statistical relationships for the prediction of pedestrian traffic have been developed quite early using linear functions based on statistical analysis of observed data (Hanking and Wright, 1958; Oeding, 1963; Older, 1968; Navin and Wheeler, 1969; Stilitz, 1969; Fruin, 1971b; Sandahl and Percivall, 1972). The drawback of these macroscopic and analytical models, for car traffic as well as for pedestrian flows, is that they are limited either to very simple or to very specific situations and do not provide information about the internal characteristics of the traffic. In addition, it is not possible to analyse the consequences of modifications in the infrastructure on the pedestrian traffic flows.

Due to this limitations, researchers began to apply model theories from other areas of research, e.g. classical fluid dynamics, to the problem of pedestrian flows. Henderson (1971, 1974) was probably one of the first researchers who successfully compared the dynamics of a crowd to the dynamics of a fluid given by the Navier-Stokes equations. Other authors applied different methods such as queuing networks (Lovas, 1994), mass conservation partial differential equations (Al Gahdi and Mahmassani, 1991) or gas kinetic equations (Prigogine and Herman, 1971) to the problem. Helbing and Molár introduced the so-called *"Social Force Model"* for the simulation of small scale pedestrian traffic (Helbing and Molnár, 1995; Molnár, 1996). In their model, a new prognostic variable, the "social force field" is introduced which describes the different attracting and repelling parameters that influence the pedestrian movement. Another approach relating local movement in a street segment to the connectivity and accessibility of this segment in the context of the urban neighborhood can be found in the *"Space Syntax"* approach introduced by Hillier et al. (1993) in the Space Syntax Laboratory at the University College of London, a part of Sir Norman Forster's team.

Although these models are applicable to a much wider range of situations and can reproduce the qualitative distribution of pedestrian traffic more or less accurate, they still are not able to explain the mechanisms that caused the observed behaviour or to give information about individual dynamics and the interaction with the environmental design. As these problems are inherent to all macroscopic approaches in which complex mechanisms are described through only a few selected parameters and equations, a possible solution for a number of these problems was found in applying microscopic modelling approaches to the problem of traffic flows.

1.2 Microscopic Modelling of Pedestrian Traffic

Microscopic models describe the behaviour of the individual components (here pedestrians) of the observed system through a set of more or less simple and intuitive rules. There is a certain level of confusion concerning the question from which point on a model is called microscopic or not. There are models which are microscopic from the spatial resolution point of view, for example the social-force model (Helbing and Molnár, 1995; Molnár, 1996) mentioned before, but the simulated unit (particle) is driven by a larger scale potential field instead of being steered by autonomous decisions located at the level of the microscopic unit. In order to avoid confusion in formalism, we will use the existence of an individual based decision process in this paper as the required feature to call a model "microscopic". Doing so, two general approaches for modelling pedestrian traffic remain: Cellular Automata (CA) approaches and Multi-Agent (MA) models.

In **Cellular Automata** (models), the environment is represented by discrete cells in some regular arrangement and the state of each cell (e.g. the occupation by individuals) at time $t + \Delta t$ depends only on the state of a fixed and finite set of neighbour cells at time t. The same behaviour rules are applied to all cells of the automata at all times except those at the lateral boundaries of the model. CA models have been successfully applied to model car traffic flows (Nagel and Schreckenberg, 1992; Nagel and Rasmussen, 1994; Nagel, 1996) which encouraged scientists to apply this method also to model pedestrian traffic (Gipps and Marksjö, 1985; Blue

and Adler, 2001, 1998; Brustedde et al., 2001; Muramatsu and Nagatani, 2000a,b). The general architecture of these models is based on logical behaviour rules (Blue and Adler, 1998) like *"IF the neighbour cell is free THEN DO..."* or probabilistic calculations (Brustedde et al., 2001) like *"Move right with a 70% chance and left with a 30 % chance"* or, most common, based on a combination of both.

The second genre of individual based model types, the **Multi-Agent Models**, goes a step further and regards the microscopic entities as unique individuals (*"agents"*). These agents might not only move around and experience their environment, but also are able to establish plans, to learn and to interact with other agents. Whereas in a typical CA model the same behaviour rules apply to all actors and all actors are equal, the MA simulation allows the single agent to develop an own personality and select between different behavioural strategies depending on his recent internal state (goals, motivation, emotions,...) and external inputs.

The special strength of MA simulations lies in the ability to analyse systems for which the general Hamilton-Function is unknown and in which the dynamic of the complete system is driven by activities in between the actors as well as between the actors and the environment. Obviously, this is the case for most systems where human behaviour is involved in the spatial and/or temporal system dynamic. One of the earliest and most prominent approaches based on the concept of Multi-Agent Systems dates back to 1950 where John Nash showed for the simulation of economic strategies on markets, that the most successful behaviour and stable situations can be found if each individual actor (=agent) adjusts his strategies with respect to the other actors behaviour (*Nash Equilibrium*, Nash, 1950). This approach was honoured with the Nobel Prize in Economics 1994 and found its way into the Hollywood movie "*A beautiful mind*" in 2001.

The computer based application of MA systems did not play a significant role until the mid-1990ies when the machines became strong enough to handle the large amount of data and processes required for modelling up to a few hundred software agents. Since then, research on MA systems is an exploding field in science with uncountable theoretical concepts and practical applications. In this paper we will refrain from reviewing theoretical approaches of agent based systems such as different architectural concepts and restrict ourselves to the properties of Multi-Agent systems which are of relevance for the simulation of pedestrian movement. For a deeper study of this subject, Weiss (2000) and Jennings et al. (1998) are good starting points.

The promising capabilities of Multi-Agent systems soon attracted researches from the field of (pedestrian) traffic modelling. In fact, modelling the movement of pedestrians is a subject which seems to be made for the application of MA models, as the traffic is composed out of little, autonomous subjects interacting with each other and with the environment. One agent-based model, though not directly linked to pedestrian traffic but definitely notable when speaking about urban traffic flows and MA systems, is the *TRANSIMS* model developed at Los Alamos[1] which is based on the SWARM model environment[2]. *TRANSIMS* simulates individual car trips of agents over an urban street network based on the analysis of the network connectivity and the socio-economic structure of the city. A similar model called *STREETS* is presented by Schelhorn et al. (1999). Also based on the SWARM environment, *STREETS* focuses on pedestrian traffic in smaller sections of the urban area than *TRANSIMS*, but is still not going down to the microscopic level considered in this paper.

On the microscale level, Batty (2003), Jiang (1999) and Batty et al. (1998) present the agent based model *SimPed* (although they call it a CA-based model in their papers) which is driven by the random walker concept with agents following the gradient of a large scale attraction field. This model mixes a number of local and non-local, microscopic and non-microscopic elements, so that it is hard to classify. However, as the agents decide autonomously in this model, it falls into the microscopic category given the criteria established before. Although the model seems theoretically sound, its application shows significant difficulties in producing a realistic movement behaviour of the agents. Especially the usage of random routing instead of purposeful route selection and the absence of inter-agent interactions seems to be the main conceptual bottleneck of this model.

1. see website `www.lanl.gov`
2. see website `http://wiki.swarm.org`

Finally, the model *PEDFLOW* developed by Kulka et al. (2003, 2002) is worth mentioning. *PEDFLOW* is a microscale agent-based model of pedestrian traffic which allows not only the simulation of obstacle avoidance by pedestrians, but also the consideration of other dynamic aspects, for example the effects of walking with a partner. The approach used in *PEDFLOW*, especially in its revised version (Kulka et al., 2003) is very close to the objectives followed with the *PedWalk* model presented here. Unfortunately, *PEDFLOW* is still under development, the documentation is quite limited and it lacks information about important details, so that there was no possibility at this stage to include concepts or experiences from *PEDFLOW* into our model or to compare results.

1.3 The *PedWalk* model: Motivation and overview

As one might imagine from the long, but nevertheless incomplete list of models presented before, a magnitude of different approaches for pedestrian traffic models exists depending on the target of the research. The main motivation for adding with *PedWalk* another model to this list was the demand of a microscale agent-based model taking care of the route selection and pedestrian movement process inside urban structures as a sub-module of the Multi-Agent software system called *BOTworld*[3]. One of the main requirements in this context was that the model had to be able to simulate pedestrian traffic flows in *any* given urban geometry, not only for a set of pre-defined structures such as street canyons or intersections.

Secondly, the model had to provide the possibility to include additional local "quality" information (desirable walking areas, less pleasant locations,...) into the simulation process and consider them in the routing decisions of the agents. These quality information can also serve as an interface to other modules of *BOTworld* which provide additional factors potentially influencing pedestrian movement which are not explicitly treated in the context of the movement process, e.g. the effects of environmental conditions (climate, noise,...) found along possible routes.

These two requirements suggest the use of a relatively simple and transparent design of the evaluation rules. The more complex the rule system gets, the more complicated and often ambiguous will be the analysis of a given situation. In particular, it would become unclear where and how the impact of external factors should be incorporated into the decision process and how they would interact with other behaviour strategies.

The description of the *PedWalk* model is organized into the following parts: In the following section, and the principal design of the model will be presented (Section 2, p. 6 ff). This is followed by a description of the basic principles and rules of pedestrian behaviour and their mathematical implementation in the *PedWalk* model including the movement decision process (Section 3, p. 15 ff). Finally, results of some example simulations will be presented and the effect of different parameter settings on the traffic flow will be discussed in Section 4 p. 32 ff. The paper closes with some final conclusion about *PedWalk* (Section 5, p. 48ff).

On the gender of pedestrians and agents

Without doubt, pedestrians can be distinguished into male and female persons and the same applies to their virtual representation, the agents. In sake of a reader–friendly text flow, will will use the male gender when writing about the software agents and use the male and the female gender versions mixed in the text.

3. see website `www.botworld.info`

2 Model theory of *PedWalk*

2.1 General Model Design

In this paragraph, the basic properties and assumptions about the *PedWalk* model environment are presented and the key terms used are defined. It is shown how the virtual model environment is constructed and a brief overview is given how the agents are created and integrated into the system.

2.1.1 Layout of the model domain and definition of key terms

The **model domain** is organised as a two-dimensional data matrix of $I \times J$ elements (**grid cells**). Each cell covers a finite area of $\Delta x \times \Delta y$ m, summing up to a total model domain of $X \times Y = (I \cdot \Delta x) \times (J \cdot \Delta y)$ m. Inside the model domain, each grid cell is uniquely defined by its matrix coordinates (i, j) with $i \in [1 \cdots I]$ and $j \in [1 \cdots J]$. In order to keep the numerical methods as simple as possible, the model is restricted to square cells ($\Delta x = \Delta y = \Delta xy$) organized in an equidistant grid matrix (all cells have the same dimension). All information about the environment and other required model data are stored in **variables** on different layers on the model domain. Mathematically, the variables are defined in the geometric center of each grid cell and assumed to be constant over the grid cell area $\Delta xy \times \Delta xy$.[4] The state of the variable χ in grid cell i, j is referenced as $\chi(i, j)$ or $\chi_{\mathrm{i,j}}$.

To control the position and the movement of the agents in the model, an eight-point connected **navigation mesh** is used in the model. [5] The size and the layout of the mesh correspond to the grid cell layout mentioned before: Each **node** $\Pi(i, j)$ (or $\Pi_{\mathrm{i,j}}$) of the navigation mesh is uniquely assigned to the corresponding grid cell i, j and spatially located in the center of this cell. The **real distance** or **segment length** between two neighbouring navigation nodes Π_{a} and Π_{b} is referenced as $\Delta(\Pi_{\mathrm{a}}, \Pi_{\mathrm{b}})$ with $\Delta(\Pi_{\mathrm{a}}, \Pi_{\mathrm{b}}) = \Delta xy$ for non-diagonal connected nodes and $\Delta(\Pi_{\mathrm{a}}, \Pi_{\mathrm{b}}) = \sqrt{2}\Delta xy$ for diagonal connected navigation nodes. Non-passable navigation nodes e.g. those inside of buildings or over non-walkable terrain are excluded from the navigation mesh. As the spatial concept of the grid cell matrix and the layout of the navigation mesh are identical, no further formal distinction is made whether a variable $\chi(i, j)$ is used for the state of grid cell i, j or for the state of the associated navigation node $\Pi(i, j)$ or for both. Figure 1 (bottom) illustrates the concept of the grid cell matrix and the navigation mesh based on a 20×15 grid.

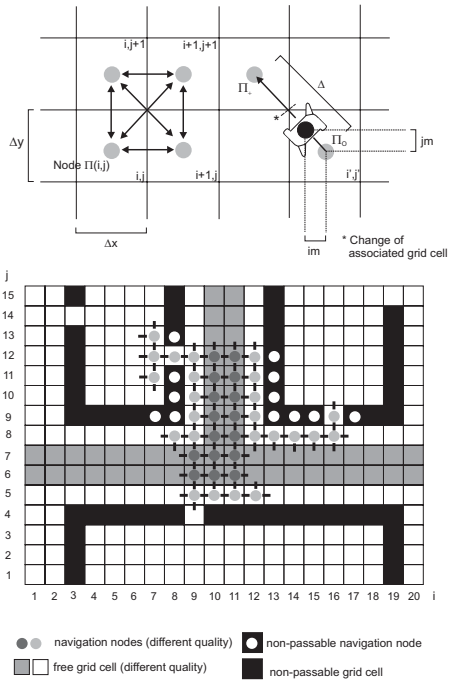

Figure 1: Organisation of grid cells and navigation nodes (top) representing the *PedWalk* model environment including the navigation mesh (bottom). The navigation mesh shown only partly and with 4 connections.

2.1.2 Representation of the model environment

To represent the environment in the *PedWalk* model, different information layer are assigned to the grid

4. If variables are imported from other sources, for example from models using a staggered grid system, they have to be recalculated so that they correspond to the grid center first

5. *Moore*-Neighborhood with diagonal connections between the nodes

cells of the model domain. The data provided by these layers are basically:

- Position of buildings
- Location of routing points with associated traffic data
- Additional data

Buildings are the basic components to describe the morphological structure of the environment (vegetation elements are displayed in the model but do not have an immediate effect on the *PedWalk* routines). The two basic functions of buildings in the framework of *PedWalk* are: (i) being an obstacle and (ii) being a target of pedestrian traffic. The effect of buildings as an obstacle to pedestrian traffic is realised by disabling those nodes of the navigation mesh, which are covered by building parts (compare lower part of Figure 1). To include the effects of buildings on pedestrian traffic, the concept of **routing points** is used in *PedWalk* . Routing points are special nodes of the navigation mesh, which can serve as entry points, intermediate destinations or exit points for pedestrians. These nodes are linked to a database, describing the traffic properties more in detail (frequentation, type of routing point, alternative points,...). Routing points are not only used to represent the entrances of buildings, but also to model other traffic relevant structures like tram stops, parking lots or other interfaces where pedestrians enter or leave the model area.

The third group of information stored in the model domain contains all other additional data needed and/or produced by the model. These data can be either generated inside the model framework (for example the assessment values mentioned before) or be obtained from external information (for example environmental data). Figure 1 (bottom) illustrates this by showing different "quality" of grid cells to indicate the area of the street.

2.1.3 Definition of the Multi-Agent Framework

The adequate design and implementation of the agents is the most crucial part for each Multi-Agent System. The general model layout as presented before only provides the basic data framework for the model system, the heart of the model lies in the design of the properties, characteristics and behaviour of the virtual pedestrians.

Table 2: Properties of the *PedWalk* environment and of the agent community. ([1]50-50 distribution, [2]Gaussian distribution)

Community Properties	
Gender distribution[1]	
Age distribution[2]	$\overline{ag}, \sigma(ag)$
	$ag \in [5, 80]$
Preferred velocity distribution[2]	$\overline{v}_{\text{pref}}, \sigma(v_{\text{pref}})$
	$v_{\text{pref}} \in [0.5, 2.0]$
Percentage groups	
Environmental Properties	
Routing points with traffic data	
Non-passable grids	
Quality of grids/nodes (global)	$\Phi^{q,0}$

As it can be seen from Table 2 and 3, the definition of the Multi-Agent framework is a two-level structure: On the community level, the basic characteristics of the whole agent population are defined (see Table 2). This level also interfaces with the relevant data of the model environment as presented before ("Environmental Properties"), for example the location of routing points or the quality of navigation nodes. These data are the same for all agents.

Based on the community properties, the exact data for the individual agent are generated. Depending on processed property, the generation method is based on statistical data (e.g. generation of age or the preferred walking velocity) or it involves a selection process (e.g. selection of destination nodes based on frequentation data).

The following sections give a very brief overview over the concepts used to implement the agents in the *PedWalk* model. Further details and explanations can be found in the corresponding sections of the detailed model description.

2.1.3.1 Basic properties of the agents

The basic properties define the general character of the agent and stay constant during the virtual life of the agent. The basic properties of an agent with respect to the *PedWalk* model are summarized in Table 3.

The gender of the agent is obtained using a random number based on a 50–50% distribution of male and female pedestrians. The age and the preferred velocity are obtained from Gaussian distributions f_{G} with

Table 3: Properties of the individual agent in the *PedWalk* model.

Basic Properties	
Gender (male, female)	*sex*
Age	*ag*
Preferred velocity	v_{pref}
Group member or single ped	
Walking personality	ξ
Impact factor profile	ω_x
Routing Properties	
Virtual Distance map	Ξ^v
Quality of grids (individual)	Φ^q
Assigned navigation node	$\Pi(\text{act}) = (i, j)$
Distance from assigned nav.-node	im, jm
Exact position in m from origin	$\Upsilon = (x, y)$
Next navigation node	Π_+
Routing point list	$\Pi\,(1..n)$
Next destination node	Π^*
Dynamical Properties	
Actual velocity	v_{act}
Moving direction (index, angle)	α, ϕ
Hierarchy position in group	ι
Lost time	t_{lost}
Timeout counter	*timeout*
Impatience flag	*impatience*
Talking flag	*talking*

$$ag \leftarrow f_{\text{G}}\left\{\overline{ag}, \sigma(ag)\right\}$$
$$v_{\text{pref}} \leftarrow f_{\text{G}}\left\{\overline{v}, \sigma(v_{\text{pref}})\right\}$$

using the mean values $\overline{ag}, \overline{v}_{\text{pref}}$ and standard deviations $\sigma(ag), \sigma(v_{\text{pref}})$ of the age and velocity distribution.

As age and preferred walking velocity are not independent (see §3 on page 15), the generated value of v_{pref} is reduced by 10% if the agent is between 50 and 65 years and by 20% if the age is above 65.

Depending on the community settings, a certain amount of agents are forming groups with other agents rather than walking alone. As this implies a special treatment, the membership as well as the strategic position inside the group needs to be stored for each agent. Finally, the *impact factor profile* and the *walking personality* variables are used to individualize the single agent (see next section).

2.1.3.2 Individualization of agents In reality, people differ in many aspects beyond the pure physiological properties like gender or age. These differences have a significant influence on the behaviour patterns and also can help in dissolving problematic situations. The classical example in pedestrian traffic is a deviation process, which fails as long as both involved pedestrians react at the same time in the same way. For Multi-Agent systems like *PedWalk* the same principle applies and due to the more limited behaviour options compared to the real world, the effect is even more dramatic. During the development of the model it was found out, that in an agent community in which the agents are too similar to each other, unrealistic smooth patterns as well as unsolvable deadlock situations frequently occurred. To overcome this problem, a set of "personality" parameters have been added to the definition of each agent providing him with some kind of artificial character. These values can be a function of the walking history of the agent (*impatience* flag) or, like the *impact factor profile*, represent a general preference of the agent by adjusting the impact of the model rules on the movement behaviour between "not important" and "very important".

2.1.3.3 Traffic generation using routing points In order to generate pedestrian movement through the model environment, a set of destination nodes (*Routing point list*) must be assigned to each agent. This set contains at least two points: the entry point, where the agent enters the model area, and the exit point, where he leaves. Depending on the model size and the simulation settings, a number of intermediate targets are added to this list.

The selection of the routing points are based on the frequentation data (agents per minute) explicitly assigned to each routing point through a database. The model tries to balance the distribution of agents entering and leaving the routing points in the model so that they approximately fit to the frequentation data for each point. If more than one routing point is assigned to the same object (e.g. different entrances to the same building), the model allows a dynamical switching between these alternative routing points, depending on the actual position of the agent or the actual traffic situation.

2.1.3.4 Positioning and steering concept Seen from the theoretical point of view, the Multi-

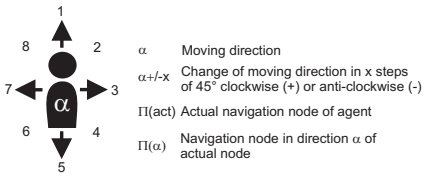

Figure 2: Reference scheme for the moving directions of the agent.

Agent concept of *PedWalk* belongs to the category of "*spatially explicit models with mobility*". The model is spatial explicit as the position of each agent inside the virtual map is clearly defined using the system of navigation nodes as explained in Section 2.1.1. Secondly, the term *mobility* implies, that the agents can move autonomously through the model environment using the connections offered by the navigation mesh.

Another classification criteria for MA models concerns the question, whether a model is *continuous* (the agents can hold any position inside the virtual map) or *discrete* (the agents are bounded to discrete points). The use of grid cells and navigation nodes in *PedWalk* suggests a classification as a discrete model, but in fact only the basic routing decisions of the agents are bounded to the nodes of the navigation mesh. While executing the movement decision, the model allows the agents to hold positions between the navigation nodes. This hybrid approach is the key feature for the realistic simulation of pedestrian traffic as it allows to simulate speed adjustments of the single agent due to conflict with other agents which would not be possible if the agent would "hop" from node to node like in a cellular automata environment.

While travelling from one node to the other, the agents can adjust their walking velocity, but cannot change the next navigation node. Technically, the position of the agent is always assigned to one distinct node of the navigation mesh: during the first half of the trip between two nodes, the agent is assigned to the node of origin ($\Pi^{\mathrm{A}}(\mathrm{act}) = \Pi_{\mathrm{O}}$ in Figure 1, top), after he has completed 50% of the way, he is assigned to the destination node ($\Pi^{\mathrm{A}}(\mathrm{act}) = \Pi_{+}$ in the same figure). The exact (continuous) position $\Upsilon^{\mathrm{A}} = (x^{\mathrm{A}}, y^{\mathrm{A}})$ of an agent A counted in meters from the model origin can be calculated as

$$\Upsilon^{\mathrm{A}} = i^{\mathrm{A}} \cdot \Delta xy + im^{\mathrm{A}}, j^{\mathrm{A}} \cdot \Delta xy + jm^{\mathrm{A}}$$

where $i^{\mathrm{A}}, j^{\mathrm{A}}$ are the coordinates of the recently assigned navigation node $\Pi^{\mathrm{A}}(\mathrm{act})$ and $(im^{\mathrm{A}}, jm^{\mathrm{A}})$ is the exact distance of the agent A from node $\Pi(i^{\mathrm{A}}, j^{\mathrm{A}})$. After travelling 50% of the distance to the destination node, $(im^{\mathrm{A}}, jm^{\mathrm{A}})$ holds negative values until the node Π_{+} has been reached.

The moving direction α^{A} of the agent is defined in relation to the map orientation as $\alpha \in [0, 1, 2, 3, 4, 5, 6, 7, 8]$ where 1 is *up*, 5 is *down* and so on. If α=0 the agents has no defined moving direction at the moment (=stands still). Moving directions relative to the actual direction are written as $\alpha + X$ where X is the number of 45 degree steps, counted clockwise for positive X and anti-clockwise for negative ones (for example $\alpha + 1$ denotes a right hand move seen from the agents perspective). Figure 2 illustrates the scheme of moving directions at a glance.

To avoid ambiguous spatial constellations, each node of the navigation mesh can only be used by one agent at a time. As each node also represents the surface area of the associated grid cell, one agent per grid cell area is also the maximum possible density in the model (non-compressibility). To achieve the optimal model results, the best size of a grid cell is close to the area occupied by a single pedestrian. According to TRB (2000), Fruin (1971b) and Pushkarev and Zupan (1975) an area of 0.6 m×0.5 m is considered as the minimum area covered by a standing pedestrian and 0.9 m×0.9 m of space should be expected for moving pedestrians (compare illustration in Figure 3).

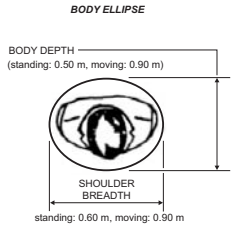

Figure 3: Typical area covered by person "Body ellipse" (modified after Fruin, 1971b)

Based on these figures, the optimal resolution of the environment Δxy for the simulation of pedestrian

traffic is about 1 m. However, the possible model resolution is also limited by available computer resources so a compromise between total model area covered and model resolution needs to be found. If only a single street canyon is simulated, the resolution can be selected close or at the optimum, but bigger systems like town centers will require a more coarse grid resolution. In practice, the optimal resolution depends both on the morphology of the structure analysed and on the properties of the traffic flows. If the selected resolution produces unrealistic bottlenecks, a refinement is inevitable. A detailed discussion on that issue can be found in Section 4.1, p. 32 ff.

2.2 Pedestrian movement control: The concept of assessment values and the Virtual Distance metric

2.2.1 The general concept

There is a wide range of different aspects influencing pedestrian movement decisions and the resulting traffic patterns. Each of these controlling components is linked to a certain context of pedestrian perception and behaviour, and, in most cases, these contexts are dealing with distinctly different topics. Hence, the general situation for designing a decision based model is remarkably different to the design of a numerical model related to some natural processes, for example a fluid dynamics model, in which physical constants and definite processes can be used to establish (numerical) links between the different components of the system.

If different entities and processes without a natural link between each other need to be linked numerically, it is common practice to define a simple numerical space as an interface which allows to relate the different modules and values to each other. A prominent example for this technique is *Fuzzy Logic*, where all components of the decision process, even if they are based on totally different backgrounds, are projected into a numerical space of $[-1, +1]$ and only in the last step ("de-fuzzification") a re-transformation into a crisp numerical value takes place (compare for example Zadeh, 1978).

In the *PedWalk* model, we use the concept of "*Assessment Values*" to allow the numerical handling of information generated by and required from the different decision modules. These assessment values are qualitative operators expressing relations between different types of information such as "higher than", "lower than" or "more important than" and "less important than". The *PedWalk* model uses a core assessment range between -1 and +1 to formulate suggestions or to define the quality of locations. All behaviour rules and associated processes are designed accordingly to produce results inside this interval.[6]

Figure 4 illustrates the concept of assessment values and their linguistic interpretation inside their core numerical definition space $[-1, +1]$. The *sign* of the assessment value defines, whether it represents a positive (attractive) or a negative (repulsive) factor and the *absolute value* represents the level of attraction/repulsion. At the same time, this value also represents the level of importance the assessed parameter plays in decision processes when being compared to other assessment values.

In Figure 4 the assessment values "Node quality (Φ^{q})", "Routing assessment (Φ^{0})" and, as an example for behaviour rules expressed through assessment values, the static value for "Keep Moving Direction ($\Phi^{=}_{\text{movedir}}$)" and the context dependent value "Avoid private territory ($\Phi^{*}_{\text{conflict}}$)" are shown.

In order to simulate different agent "characters" without modifying the code of the model, all assessment values are weighted with a personal *impact factor* (ω_{x}) which is used to trigger the level of impact the associated behaviour context plays in the decision process.

The impact factors are defined in the range of $[0, +1]$ in which "1" means that the associated rule or behaviour context is considered *very important* for the agent and "0" means that the context is considered as *not important* in the decision process. All other intermediate values scale the impact between these two extremes.

In overview, assessment values are used in the *PedWalk* model in the following contexts:

- to define the quality of navigation nodes with

6. After summing up all individual results, the final assessment (e.g Φ^{q}, compare eq. 2.2.2, p.12) might, of course, show values outside this "active" range [+1,-1]. This is no problem as this is still a valid qualitative statement

respect to the probability that they are used by pedestrians (Quality assessment Φ^{q})

- to identify the *best* available path from the recent position to a given destination while *best* includes both distance and quality information mentioned above (Routing assessment Φ^{0})
- to modify the moving decision by changing the quality of near-by navigation nodes on a short-term basis (Reactive assessment Φ^{*})
- to modify the moving decision by directly favouring or disfavouring certain directions relative to the actual moving direction of the agent (Dynamic assessment $\Phi^{=}$)

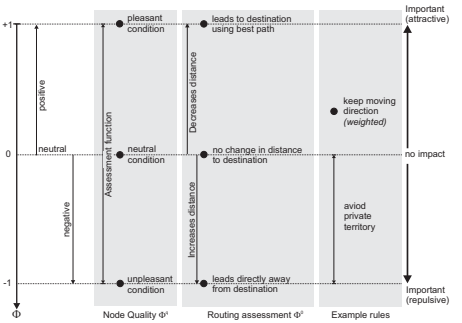

Figure 4: Graphical representation and interpretation of the numerical space of assessment values. The value of "keep moving direction" is displayed weighted with the default impact factor $\omega_{\mathrm{movedir}}$.

The virtual distance metric

The assessment values provide a good tool for the analysis of local conditions, but it has not yet been shown, how they can be used to determine the optimal route to the destination node. Apart from all quality aspects, the main route selection criteria for pedestrians is the aim to reach the destination point using the shortest possible route. Though, a metric is required which allows to combine the real spatial distance aspect with the available local quality information.

For the *PedWalk* model, we have designed the *virtual distance* (Δ^{v}, Ξ^{v}) as the reference metric to compare possible routing decisions and quality-weighted paths lengths among each other.

The basic idea behind this metric is that the virtual distance represents some kind of "felt distance" which increases above the real spatial distance if the route includes unpleasant conditions or, on the other hand, decreases below the spatial distance to simulate the effects of pleasant locations.

We define the virtual distance Δ^{v} of two nodes linked to each other through a path segment with

$$\Delta^{\mathrm{v}} = \Delta + (-\Phi \cdot \Delta) \text{ or } \Delta^{\mathrm{v}} = \Delta\,(1 - \Phi) \quad (2.1)$$

where Δ is the measurable spatial distance of the associated path segment and Φ is a local assessment value defining the "quality" of this segment. Using this definition, a coherence between the lingual association of the term "assessment" and the mathematical effect is established: the virtual distance increases for negative (=unpleasant) assessment values and decreases for positive (=pleasant) ones.

Analogously, a path segment of virtual length Δ^{v} can be transferred into the corresponding assessment value with:

$$\Phi = 1 - \frac{\Delta^{\mathrm{v}}}{\Delta} \quad (2.2)$$

2.2.2 Quality assessment Φ^{q}, Virtual distance map Ξ^{v} and Routing assessment Φ^{0}

As mentioned in the preceding section, the virtual distance metric is used as a reference metric to combine spatial distance and quality information in one parameter. Following the definition in (2.1), the virtual distance Δ^{v} between two nodes can then be calculated as

$$\Delta^{\mathrm{v}} = \Delta\,(1 - \omega_{\mathrm{q}} \cdot \Phi^{\mathrm{q}}) \quad (2.3)$$

where Φ^{q} is the quality meter modifying the distance between the nodes and ω_{q} is the impact factor for quality information on the routing decision.

The quality of navigation nodes can be defined on two hierarchical levels: On the global level and the level of the individual agent. Assessment values defined on the global level ($\Phi^{\mathrm{q},0}$) are recognised by all agents in the same way, each agent "sees" the same

numerical value of a navigation node. For example the "walkability" of a specific area is typically defined on the global level.

On the level of the individual agent, a quality assessment value Φ^{q} can be used to express the agent's individual opinion about the quality offered by a certain navigation node. This opinion can be the function of some general preferences of the agent or it can depend on the actual state of the agent. Though, for the same navigation node, different agents can come to different conclusions about the quality of this node and assign different quality assessment values to the same node.

If more than one quality assessment value exists for one node, the different relevant global and/or individual assessment values need to be summed up:

$$\Phi^{q} = \omega_{q}(1) \cdot \Phi^{q,0}(1) + \ldots + \omega_{q}(n) \cdot \Phi^{q}(n) \quad (2.4)$$

and ω_{q} is dropped from (2.3).

In other applications, these kind of functions are often called "cost functions" because they estimate the "costs" of travelling from one node to another.

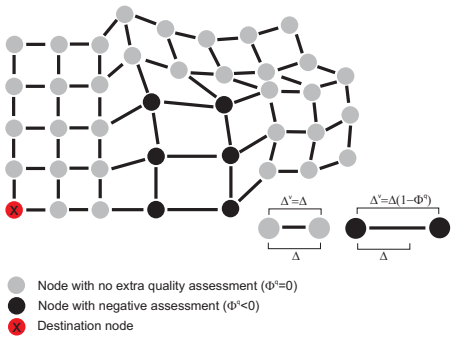

Figure 5: Effect on negative quality assessment values on path lengths. Navigation nodes with negative quality assessment are drawn in black. Diagonal connections between nodes are not shown for simplicity.

Figure 5 illustrates the impact of local negative assessment values on the virtual length of connecting segments and the resulting navigation mesh. The grey navigation nodes are without extra assessment values ($\Phi^{q} = 0$), whereas some negative assessment is assigned to the black nodes making path segments connected with this node virtually "longer".

The total virtual distance for the complete path between a start node $\Pi_{i,j}$ and a destination node Π^{*} is calculated by summing up the length of the connecting path segments:

$$\Xi(i,j) = \sum \Delta^{v} \left(\Pi_{i,j} \longrightarrow \Pi^{*}\right) = \sum_{n=1}^{N-1} \left\{ \Delta\left(\Pi_{n}, \Pi_{n+1}\right) \left(1 - \omega^{q} \cdot 0.5 \left(\Phi_{n}^{q} + \Phi_{n+1}^{q}\right)\right) \right\} \quad (2.5)$$

where N is the number of navigation nodes forming the path (including the nodes $\Pi_{1} = \Pi_{i,j}$ and $\Pi_{N} = \Pi^{*}$ themselves) and Φ_{n}^{q} is the quality assessment of the n-th navigation node Π_{n} (as Φ^{q} is defined in the center of the associated grid cell, the quality assessment of the path segment between two cells is averaged between the two adjacent nodes).

The Virtual Distance Map Ξ^{v}

Once the destination node Π^{*} of the agent has been selected, the virtual distance between this node and all other nodes of the navigation mesh can be calculated based on (2.5). The resulting $i \times j$ matrix of virtual distance values is called the **Virtual Distance Map** (Ξ^{v}).

For each node, the Virtual Distance Map holds the least accumulated quality-weighted distance for getting to the destination cell. Figure 6 illustrates the concept by picking up the situation used in the preceding paragraph: The real distance between the nodes was set to Δ=1 m and the quality assessment of the black nodes was assumed to be Φ^{q}=-1.

Using the virtual distance values, the optimal path from any node to the destination point can be found by connecting, or, in terms of a moving agent, by moving to the neighbour node with the lowest available Ξ^{v} value (see Figure 7). [7]

A detailed description of the numerical methods used to calculate the Virtual Distance nap can be found in Appendix A, p. 52 ff.

7. Please note, that the figures used in this section are only for general illustration purposes and do neither take into account nor show the diagonal connections between the nodes. In the final *PedWalk* model, all values are calculated using an 8-point connected node mesh

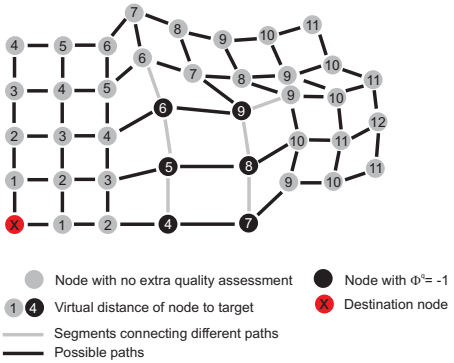

Figure 6: Example of calculated Virtual Distance Map Ξ^v. Black nodes have negative quality assessment of Φ^q=-1. Diagonal connections between nodes not shown for simplicity.

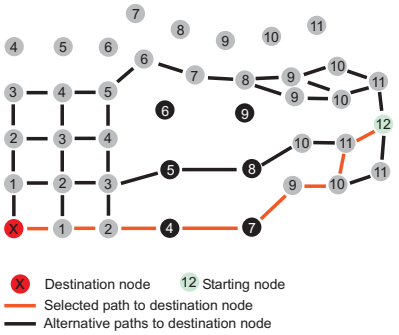

Figure 7: Example of calculated Virtual Distance Map Ξ^v with nodes connected to possible paths. Diagonal connections between nodes not shown for simplicity.

Routing assessment Φ^0

The *routing assessment* Φ^0 finally re-transforms the combined distance and quality information from the virtual distance map back into a local assessment value. This value then expresses the suitability of navigation nodes to bring the agent closer to the desired destination node with respect to the best available path.

For each position Π(act) of the agent, eight possible values $\Phi^0(\alpha)$ can be calculated to assess the routing quality of the neighbouring nodes:

$$\Phi^0(\alpha) = \frac{\Xi^v(\Pi(\text{act})) - \Xi^v(\Pi(\alpha))}{\Delta(\Pi(\text{act}), \Pi(\alpha))} \quad (2.6)$$

where $\alpha \in [1, 2, 3, 4, 5, 6, 7, 8]$ is the relative moving direction as illustrated in Figure 2 and Δ is the real distance between Π(act) and $\Pi(\alpha)$. Navigation nodes with positive assessment values indicate moving directions that will lead the agent towards the next destination whereas negative values show directions that lead into the opposite direction.

However, the final moving decision of the agent also needs to take into account further reactive and dynamic assessment values that might influence the local routing decision to a huge extent.

2.2.3 Reactive Assessment Φ^*

The desirability of navigation nodes is not only influenced by general and long–termed quality aspects as described through the quality assessment, but also by short–termed effects arising from the dynamic character of the model such as the interactions with other agents. To describe the impact of such local variations of the navigation node quality, the type of *reactive assessment* Φ^* is used in the model.

Different to the quality assessment, the reactive assessment has no influence on the general path selection, but triggers the local moving decision of the agent. An agent can only "see" and consider reactive assessment values from his direct neighbour nodes, data from nodes further away remain unknown, that is why they are called "reactive". Hence, the reactive assessment values represent all navigation node information not known by the agent when planning the route.

Like all other assessment values, reactive assessments can have a repulsive character (e.g. collision avoidance) but might also serve as an attractive force (e.g. short–termed attraction to shopping windows).

2.2.4 Dynamic Assessment $\Phi^=$

The last type of assessment values, the *dynamic assessment* $\Phi^=$, is used to favour or disfavour certain moving directions relative to the actual (last) mov-

ing direction of the agent. The dynamic assessment is therefore not linked with fixed navigation nodes but moves with the individual agent and is only of importance during the selection of the next navigation node.

3 Simulating pedestrian behaviour: Model Design

The degree of realism and therefore the quality of a Multi-Agent model depends in essence on the behaviour- and interaction rules implemented in the model system. However, the key point when compiling the rule system is not to implement as many rules as possible, but to find a common level of detail on which the decision process takes place. It is not very convenient to implement rules which operate on a very general, almost macroscopic level side-by-side with rules based on very microscopic analyses. It is foreseeable that such a rule system will produce contradicting suggestions in complex situations. In the following sections, the basic rules of pedestrian behaviour are summarized and it will be shown, how they are linked mathematically with the theoretical model framework.

It should be noted again, that the majority of parameters and equations presented here must be interpreted as mathematical representations of different (behaviour) "*rules*" and decision processes. Their outcomes are projections of the possible range of results onto a defined numerical scale (the assessment values) so that they can be compared to each other. The most important issue are the relations between the different assessment values, not their individual crisp numerical value.

3.1 Basic rules of Pedestrian behaviour in urban environments

Although pedestrian behaviour seems to follow an almost infinite number of rules and strategies, some dominant behaviour rules can be identified. The following list summarizes those features of pedestrian movement which appear most important in the context of the *PedWalk* . The rules are extracted from literature (e.g. Helbing, 1997; Wolff, 1973) or based on knowledge from everyday observations.

§1. Pedestrians normally choose the fastest available route. If alternative routes have the same length, the one where the pedestrian can walk straight ahead as long as possible is chosen.

§2. Pedestrians try to minimize detours. Walking opposite to the desired walking direction is avoided whenever possible.

§3. Each pedestrian tries to walk with his or her individual preferred velocity. In an average pedestrian crowd, the preferred velocities are Gaussian distributed with a mean of $\bar{v}$ =1.34 ms^{-1} and a standard deviation of σ_v=0.26 ms^{-1} (Weidmann, 1993; Henderson, 1971; Navin and Wheeler, 1969). For the design of pedestrian facilities, the Highway Capacity Manual (TRB, 2000) suggests an average design speed between 1.2 ms^{-1} (most cases) and 1.5 ms^{-1} (free sidewalk flow). For the individual pedestrian, the maximum average speed is around the age of 22 and is significantly decreasing above the age of 50 (compare Helbing, 1997, p.7). If the amount of elderly people (older than 65 years) if above 20%, TRB (2000) suggests the use of 1.0 ms^{-1} as design speed.

§4. Pedestrians try to keep certain distances to other pedestrians and obstacles. This distance gets smaller with growing density (TRB, 2000; Brilon et al., 1993). The preferred distance is a function of the social and cultural background of the pedestrians (Navin and Wheeler, 1969). In average, pedestrians without luggage prefer to keep a lateral distance of around 0.7 m to each other. In the walking direction, this distance increases up to 1.0–1.5 m, depending on the walking velocity (Weidmann, 1993; Helbing, 1997).

§5. Pedestrians estimate other pedestrians routing trajectories and change their own routing to allow other people to pass ("yielding"). The distance for starting a deviation manoeuver is ranging from 2 m at low density to almost none in high density traffic (Wolff, 1973).

§6. If two pedestrians are confronted with each other and need to deviate, one direction is preferred (the right hand side in most countries; Helbing, 1997).

§7. If the density is high, pedestrians form lanes of uniform walking direction (Oeding, 1963). Similar to pheromone markers used by insects (see e.g. Schweitzer et al., 1997) pedestrians tend to follow each other with the same walking direction in groups ("streaming").

§8. Individuals that know each other form groups that behave like an individual. Group sizes are poisson distributed (Coleman, 1964). Around

40% of the pedestrians in urban areas are moving in groups of two or more .

Some of these behaviour rules are only applying to "purposeful" pedestrians moving towards a specific destination (e.g. §1, §2). For "aimless pedestrians" such as tourists or shoppers, these rules might be less strict or other personal goals may be used to select the optimal route. These effects can be modeled by changing the associated impact profile accordingly (compare Section 2.2.1, p. 10).

As it can be seen from the list above, the majority of behaviour rules become relevant, when pedestrian begin to interact with each other. If only one agent would exist in the environment, the virtual distance map would be sufficient to navigate the agent successfully to the destination node. Hence, the main objective of the behaviour model presented in the next sections is the detection, solution and avoidance of conflicts between the virtual pedestrians.

3.2 Mathematical implementation of the *PedWalk* rules

The model rules presented in the following sections are designed for evaluating certain aspects and situations of pedestrian traffic and their impact on the movement process. The section is basically divided into the parts "Basic movement strategies" handling the fundamental aspects of motion like acceleration, deceleration or collision avoidance and "Complex behaviour and interaction strategies" describing more sophisticated behaviour rules like group formation or the impact of moods on the pedestrian movement.

3.2.1 Implementation of basic movement strategies

The main objective driving pedestrian behaviour is to avoid collisions with other pedestrians while maintaining the personal preferred velocity.

From the general behaviour rules presented in Section 3.1, p.15 we can extract three basic strategies that are relevant for the simulation of pedestrian behaviour:

1. Spatial avoidance (deviating)
2. Adjustment of walking velocity, and
3. Considering alternative navigation nodes to maintain the preferred velocity (e.g. overtaking)

In addition, two general behaviour strategies, "keep the walking direction" and "prefer right hand side" are added to the model rules which help to reproduce a realistic behaviour of the agents.

3.2.1.1 The Conflict Zone Model

The conflict zone model is based on the idea, that a certain territory around a person can be interpreted as "private space" possessing a repulsive potential ρ_{conflict} against other persons ("territorial effect", compare Scheflen and Ashcroft, 1976). Besides the more psychologically motivated aspects of the territorial effect, standing inside the private territory of a moving person also signals a potential danger of collision.

Lewin (1951) suggests to interpret the spatial structure of this private space as an ellipse which is directed along the moving direction and has a maximum repulsive force close to the pedestrian. In the *PedWalk* model this ellipse is represented through the "Forward zone" (compare Figure 8). In addition to this zone, a much smaller conflict zone behind the moving person ("Backward zone" in Figure 8) is used in the model. Although no immediate danger of collision exists in this area, people normally avoid to move too close towards the back of another person except they are in a hurry and aim to push the preceding person.

The main task of the forward conflict zone is to indicate areas in which a potential danger of collision with the associated agent exists. Therefore, its spatial extension depends on two parameters: a) the walking velocity of the agent v_{act} and b) the save time interval t^*. The latter is defined as the time period between the first realization of the conflict and the moment when the collision would actually happen if all parameters remain unchanged.

As the sense of the conflict zone model is limited to agents in motion, a lower velocity threshold for creating a conflict zone is used in the model. This threshold is set to 0.3 ms^{-1}. Slower moving or standing agents create no dynamical conflict zone.

To define the spatial extension d_{conflict} of the forward conflict zone, a simple formulation based on the required safety distance is used:

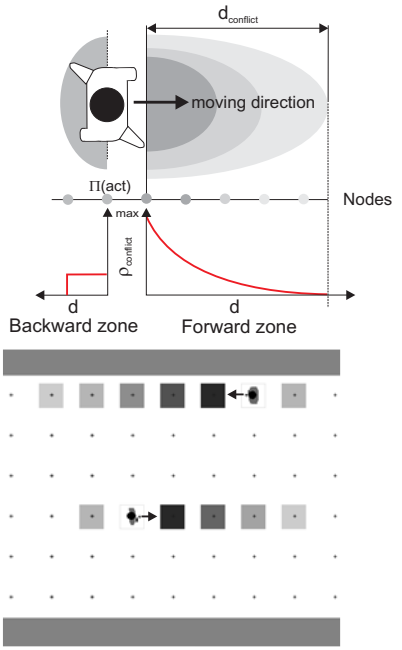

Figure 8: Schematic illustration of the conflict zone model (top) and example of two moving agents with conflict zones in the model environment (bottom). Darker colours indicate stronger repulsive potentials.

$$d_{\text{conflict}} = d_0 + 2 \cdot v_{\text{act}} \cdot t^* \tag{3.1}$$

where d_0 is the physically required minimum distance between two standing pedestrians (around 0.5 m, compare body ellipse in Figure 3, p. 9) and t^* is the save time interval.

For the save time interval t^*, values around 1 s seem to be realistic for pedestrians moving with average velocity and attitude. With t^*= 1 s, we obtain a safety distance of 1.34 m in case of the average velocity of 1.34 ms^{-1} which fits with empirical observations suggesting a safety distance between 0 and 2 m depending on the actual pedestrian density (compare §5, p. 15).

In order to consider the worst-case scenario of two agents approaching frontally, the reference velocity of the agent is multiplied by 2. This is of course a huge simplification as it both can under- and overestimate the velocity relation between two agents. But for the purposes of the *PedWalk* model this formulation is sufficient, as the velocity adjustment of the agent (see next section) will also take care of the upcoming collision.

The repulsive force ρ_{conflict} at a navigation node $\Pi(i,j)$ inside the forward conflict zone is calculated using a simple cubic function:

$$\rho_{\text{conflict}}(i,j) = \rho_{\text{conflict,max}} \cdot \left(1 - \frac{d(i,j)}{d_{\text{conflict}}}\right)^2 \tag{3.2}$$

where $d(i,j) = \Delta\left(\Pi(\text{act}), \Pi(i,j)\right)$ is the distance between the analysed node i,j and the position of the agent $\Pi(\text{act})$ counted from the first node in front of the agent with ρ_{conflict}=$\rho_{\text{conflict,max}}$ at $d = 0$ and ρ_{conflict}=0 at $d = d_{\text{conflict}}$ (compare Figure 8).

If the forward conflict zone reaches a non-passable navigation node (e.g. building), the zone is truncated at this node as the agent cannot walk over this node and consequently cannot generate conflicts behind this node.

The backward conflict zone is limited to the navigation node directly behind the agent. As it does not indicate a real danger of collision, its repulsive force is assumed to be much lower than for the forward zone.

For ρ_{conflict} behind the agent we define:

$$\rho_{\text{conflict}}(i,j) = 0.25 \cdot \rho_{\text{conflict,max}} \tag{3.3}$$

To fit into the concept of the *PedWalk* model, the repulsive force finally needs to be transformed into a reactive assessment value with:

$$\Phi^*_{\text{conflict}}(i,j) = -\rho_{\text{conflict}}(i,j) \tag{3.4}$$

The maximum repulsive level $\rho_{\text{conflict,max}}$ is set to 1, so that the outcomes of this behaviour module automatically fit into the active range of assessment values with the maximum repulsive force of |-1| directly in front of an approaching agent.

For each moving agent, a forward and backward conflict zone is generated and maintained with respect to the actual velocity and moving direction. If conflict zones of different agents overlap, the zone with the strongest repulsive force is selected. If agents are part

of a group, they do not react on the conflict zones of other group members.

Finally it has to be mentioned, that conflict zones are not only applying to frontally approaching agents, but also to agents coming from all directions, even from the back. This represents some kind of monitoring process that enables the agents also to react on situations in their back. If for example, a running person is approaching from the back, the pedestrians in front are also deviating to avoid a collision.

3.2.1.2 The Intelligent Walker Model IWM

Adjusting the walking velocity is the second basic strategy for the avoidance of collisions in pedestrian traffic. In the *PedWalk* model the velocity adjustment is restricted to the reduction of speed although in practice short-termed accelerations might also help to solve potential conflicts between pedestrians.

To simulate the velocity adjustment, the idea of the so-called "*Intelligent Driver Model (IDM)*" presented by Treiber et al. (2000) have been adapted to pedestrian traffic. The IDM was originally developed to describe the optimal accelerating and breaking behaviour of a car driver trying to avoid collisions with other vehicles while driving as close to the preferred velocity as possible at the same time.

In the adopted version (called "*Intelligent Walker Model (IWM)*" now) the change of the velocity v_{act} is given by

$$\left[\frac{\partial v_{\text{act}}}{\partial t}\right]_{\text{IWM}} = a\left[1 - \left(\frac{v_{\text{act}}}{v_{\text{pref}}}\right)\right] - b\left(\frac{d^*}{d\,(A,B)}\right)^2 \tag{3.5}$$

The first term on the right hand side describes the acceleration of the agent depending on the ratio between actual v_{act} and preferred velocity v_{pref} and the maximum comfortable acceleration coefficient a. The second term describes the deceleration process if another agent B is within a critical distance of the considered agent A. The amount of deceleration depends on the actual distance $d(A,B)$ between the two agents related to a reference distance ("desired clearance", d^*) describing the general distance preference of the agent.

As the agents are able to change their velocity at any time during the simulation, even between two navigation nodes, the distance $d(A,B)$ between agent A and B is not calculated from navigation node to navigation node but instead the exact position Υ^{A} and Υ^{B} of the agent is used:

$$\begin{aligned} d(A,B) &= \Upsilon^{\text{A}} - \Upsilon^{\text{B}} = \sqrt{dX(A,B)^2 + dY(A,B)^2} \\ dX(A,B) &= \left(i^{\text{A}} - i^{\text{B}}\right)\Delta xy + im^{\text{A}} - im^{\text{B}} \\ dY(A,B) &= (j^{\text{A}} - j^{\text{B}})\Delta xy + jm^{\text{A}} - jm^{\text{B}} \end{aligned}$$

where $(i^{\text{A}}, j^{\text{A}})$ and $(i^{\text{B}}, j^{\text{B}})$ are indices of the assigned navigation nodes of agent A and B and im, jm is the exact position relative to the center of i, j respectively. If non-passable navigation nodes are found between the agents, the distance calculation is obsolete and stopped as those two agent collide with each other.

The desired clearance d^* is a function of the actual approaching rate of the two agents and a desired safety distance:

$$d^* = d_0 + \max\left(t^* \cdot v_{\text{act}} + \frac{v_{\text{act}} \cdot \Delta v(A,B)}{2\sqrt{a \cdot b}}, 0\right) \tag{3.6}$$

Here, d_0 and t^* are the physical minimum distance and the save time interval as used in (3.1). The last term of the right hand side in (3.6) represents an "intelligent braking strategy", where the pedestrian decelerates the harder the closer a possible collision comes.

Two special cases are considered in the IWM model when calculating the desired clearance: If the two agents in a possible conflict are members of the same group, the required distance is much smaller than between two unknown agents. In this case the desired clearance is set to

$$d^* = 2 \cdot d_0 \tag{3.7}$$

Secondly, if the agent is in the "impatience" mode (see Section 3.2.2.2, p. 24), the distance kept to other agents also reduces significantly to

$$d^* \equiv 0.1 \cdot d^* \tag{3.8}$$

If no other agents are within the clearance zone d^*, the deceleration term $-b\,(d^*/d(A,B))^2$ in (3.5) becomes zero.

The velocity difference $\Delta v_{\mathrm{A,B}}$ between two pedestrians A and B is calculated with respect to their relative angle of movement:

$$\begin{aligned}\Delta v(A,B) &= \left|\vec{v}^{\mathrm{A}}_{\mathrm{act}} - \vec{v}^{\mathrm{B}}_{\mathrm{act}}\right| \\ &= \left|\begin{pmatrix}\sin\phi^{\mathrm{A}}\cdot v^{\mathrm{A}}_{\mathrm{act}}\\ \cos\phi^{\mathrm{A}}\cdot v^{\mathrm{A}}_{\mathrm{act}}\end{pmatrix} - \begin{pmatrix}\sin\phi^{\mathrm{B}}\cdot v^{\mathrm{B}}_{\mathrm{act}}\\ \cos\phi^{\mathrm{B}}\cdot v^{\mathrm{B}}_{\mathrm{act}}\end{pmatrix}\right| \\ &= \Big[\left(\sin\phi^{\mathrm{A}}\cdot v^{\mathrm{A}}_{\mathrm{act}} - \sin\phi^{\mathrm{B}}\cdot v^{\mathrm{B}}_{\mathrm{act}}\right)^2 \\ &\quad + \left(\cos\phi^{\mathrm{A}}\cdot v^{\mathrm{A}}_{\mathrm{act}} - \cos\phi^{\mathrm{B}}\cdot v^{\mathrm{B}}_{\mathrm{act}}\right)^2\Big]^{0.5}\end{aligned}$$

with $v^{\mathrm{A}}_{\mathrm{act}}$ and $v^{\mathrm{B}}_{\mathrm{act}}$ being the actual velocity of agent A and B and $\phi^{\mathrm{A}}, \phi^{\mathrm{B}}$ the absolute angle of the actual walking direction α with

$$\phi \in [0, 45, 90, 135, 180, 225, 270, 325] \qquad \forall\alpha \in [1, 2, 3, 4, 5, 6, 7, 8]$$

(compare Figure 2, p.9). If the other agent is not moving $\Delta v(A,B)$ equals $v^{\mathrm{A}}_{\mathrm{act}}$.

Finally, the acceleration and deceleration coefficients a and b need to be defined. Different to the acceleration and deceleration time required in car traffic, a pedestrian can reach any realistic walking velocity almost immediately. Following Helbing (2001), the average time until a pedestrian reaches his preferred velocity is 0.5 s. Based on an average preferred velocity of v_{pref}=1.34 ms^{-1} (compare §3 p. 15) this equals an acceleration coefficient of a=2.68 ms^{-2}.

For the deceleration coefficient b a similar, slightly higher value seems reasonable, so we use b=3.0 ms^{-2} in the *PedWalk* model. Anyway, as mentioned above, the acceleration and deceleration phase is less critical in pedestrian traffic compared to car traffic, so the model is not sensible to the selection of a and b.

3.2.1.3 Maintaining the preferred velocity

If the actual possible walking velocity of a pedestrian falls below an acceptable percentage of the preferred velocity, she begins to consider alternative routes on which she thinks she can walk with the preferred speed. On a longer term basis, this might result in the selection of an alternative route towards the destination node omitting potential bottlenecks, but on a short term basis it will only influence the local routing decision between alternative navigation nodes with equal or similar suitability (virtual distance values). The most obvious example for this behaviour strategy is to overtake a slower pedestrian walking ahead and use a parallel lane. As the *PedWalk* model does not explicitly define and use *lanes*, the impact of velocity reductions on the routing decision is realized by imposing a negative dynamic assessment value onto the recent walking direction.

To avoid unrealistic quick responses of the agent, the actual velocity must fall below a defined threshold value v_{crit} with

$$v_{\mathrm{crit}} = 0.01(100 - f_{\mathrm{crit}}) \cdot v_{\mathrm{pref}} \tag{3.9}$$

before it has an effect on the routing decision. The tolerable slow down f_{crit} from the preferred velocity v_{pref} is given in percent with a default value of 30 %.

To calculate the required assessment value, we express the effect of walking with $v_{\mathrm{act}} < v_{\mathrm{pref}}$ as an increase in distance compared to the situation where the agent can walk the distance Δ with the preferred velocity:

$$\Delta^{\mathrm{v}} = \frac{v_{\mathrm{pref}}}{v_{\mathrm{act}}} \cdot \Delta \tag{3.10}$$

where Δ^{v} is the virtual distance of a segment with length Δ taking into account the reduced walking velocity v_{act}.

The associated assessment value can then be obtained by inserting (3.10) into the definition of the assessment values given in (2.2):

$$\Phi = 1 - \frac{\Delta^{\mathrm{v}}}{\Delta} = 1 - \frac{v_{\mathrm{pref}}}{v_{\mathrm{act}}} \tag{3.11}$$

As the speed reduction is not a local property of a specific navigation node, but belongs to the recent walking direction α of the agent, the assessment value is directly assigned to the recent walking direction α using a dynamic assessment value (compare section 2.2.4, p. 13):

$$\Phi^{=}_{\mathrm{v\_ass}}(\alpha) = \max\left(-1, 1 - \frac{v_{\mathrm{pref}}}{v_{\mathrm{act}}}\right) \tag{3.12}$$

The max-function cuts the assessment values to a lower limit of -1 in order to fit the outcomes to the interval $[-1, 0]$ as discussed in Section 2.2,p.10 f.

3.2.1.4 Additional dynamic and avoidance behaviour preferences There are two additional behaviour characteristics that can be observed in pedestrian traffic but have not been considered explicitly in behaviour rules so far, nor develop automatically: (i) the preference to walk straight ahead as long as possible, and (ii) the tendency to prefer one certain moving direction if equal alternatives exist

Both strategies cause a certain asymmetry in the selection of the next navigation node, which becomes especially relevant if alternative choices of more or less the same quality exists. This asymmetry plays an important rule concerning the behaviour of the agents in the *PedWalk* model: The tendency to keep the old walking direction *smoothes* the trajectories of the agents whereas the preference for one direction *supports the self-organisation* process inside the model, such as the formation of lanes of uniform walking direction.

Strategy (i), "keep the walking direction" (compare §1, p.15) plays an important role through filtering the impact of small variations in the routing assessment field on the resulting agent behaviour. As the routing decision is based on crisp numerical values, the agent would follow *exactly* the optimal route to the destination node, regardless how curvy or complex this path might be. As this behaviour is not realistic, some attractive component is added to the recent walking direction using the additional dynamic assessment value $\Phi^{=}_{\text{keepdir}}$.

The second strategy, "prefer right hand side" hereafter, considers the aspect, that a certain asymmetry in the selection of the moving direction supports the success of a deviation manoeuver. In most countries, people prefer to pass each other on the right hand side (compare §6, p.15) which leads to a traffic flow organized in right hand side orientated lanes of uniform walking direction analogously to car traffic. If people prefer to deviate to the left hand side, the self-organisation effect is the same, but the lane structure is mirrored with respect to the dominating walking direction. If no preference for either side is given, the organisation of the traffic flow becomes significantly more chaotic as frequent conflicts with other pedestrians are occurring. To impose a certain asymmetry onto the node selection process, the dynamic assessment value $\Phi^{=}_{\text{rhs}}$ is added to the *PedWalk* model. This additional assessment value supports the successful deviation of two agents approaching frontally as well as the formation of lanes with uniform walking direction. A detailed analysis of this effect is given in Section 4.1.6, p. 39 ff.

Different to the other assessment values used in the model, $\Phi^{=}_{\text{keepdir}}$ and $\Phi^{=}_{\text{rhs}}$ do not depend on a specific traffic situation or another agent based context. The selection of their absolute values depend on the subjective decision, how important "keep the walking direction" and "prefer right hand side" should be in the simulated situation. To allow such an adjustment, both assessment values are initially set to their maximum attractive value "+1" and then modified through the associated impact factors ω_{keepdir} and ω_{rhs}. From numerical experiments (compare Sections 4.1.6 and 4.1.7), the values of ω_{keepdir}=0.5 and ω_{rhs}=0.8 have been found to be good choices for average pedestrian traffic situation.

3.2.2 Implementation of complex behaviour and interaction strategies

In addition to the presented basic behaviour strategies from which most of the observable pedestrian movement patterns emerge, there are some more sophisticated rules for agent interactions which are not absolutely necessary to run the model, but whose consideration increases the degree of realism of the simulation. The first strategy presented here deals with the formation and coordination of pedestrian groups, the second one adds the effect of "moods" on the walking behaviour to the *PedWalk* model.

3.2.2.1 Group coordination strategies As around 40% of the pedestrians in urban areas move in groups of two or more (compare §8 p. 16), the consideration of the special behaviour of agents as parts of a group is an important step towards the realistic simulation of pedestrian traffic.

Although it is said that a pedestrian group behaves principally like a single person (compare Coleman, 1964) this statement is of limited help for the implementation in a microscopic model as it does not provide information about the *internal* microdynamics that arise between group members and drive the macroscopic behaviour of the group in total.

No doubt pedestrian groups are very complex social systems and their internal and external dynamics

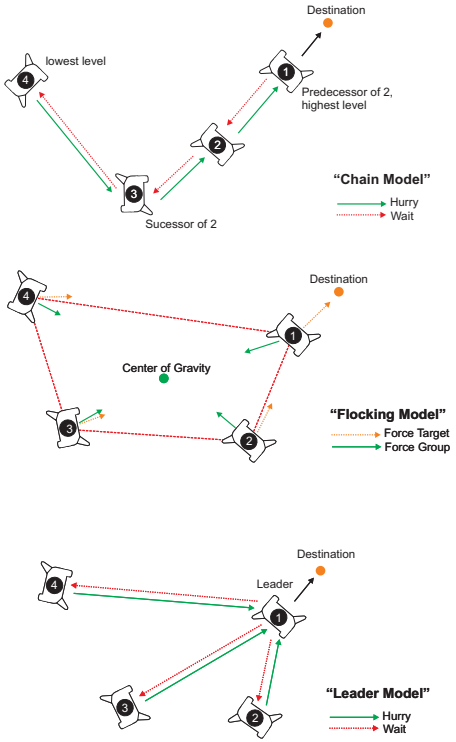

Figure 9: Different organisation concepts of pedestrian groups. From top to bottom: Chain model, Flocking model and Leader model.

are influenced by various factors like the social relationship between group members, attracting forces along the way or the knowledge of the actual destination. But beneath all these different goals, there is one main objective which is of prior importance to all group members: the maintenance of the spatial group organisation, or, in other words, not to loose group members or to get lost oneself.

In the context of the *PedWalk* model, group coordination strategies are understood as additional behaviour rules that become active as soon as a member of the associated group separates too far from the group and risks to get lost. However, even if only the spatial group formation is considered as a coordination strategy, it is not always obvious how this goal is established in a group of people. The question, who will look after and wait for whom depends again to a high degree on the social and personal relations inside the group. To handle these aspects in a numerical model, it is assumed, that the only aspect driving the internal group coordination is the spatial and hierarchical organisation of the group. With this simplification, three general types of group organisation can be distinguished:

1. Groups with implicit dynamic hierarchy organised as a chain including pairs ("Chain model")
2. Groups with no hierarchy organised as a flock or herd ("Flocking model")
3. Groups with explicit static hierarchy ("Leader model")

Figure 9 illustrates these three basic concepts of group coordination. [8]

The concept represented by the **Chain model** is probably the most frequently observable group organisation mode. Here, the group coordination task is distributed among all group members in a way that each group member links to one person walking ahead ("predecessor" in Fig. 9) and to one person walking behind ("successor"). If the distance to the predecessor increases above a critical value, the agent increases his walking velocity to catch up with the predecessor. Analogously, an agent will decrease his speed, if the distance to the successor begins to increase too much. As the relations between the agents are assumed to be symmetric, a critical distance between two linked agents will result in an increase of speed of the agent falling behind as well as in a (smaller) decrease of speed of the predecessor.

The hierarchy of the group is not given explicitly in the Chain model but derived from the spatial distribution of the agents: the agent closest to the (common) destination is set to the highest organisational level in the group ($\iota = 1$) and the other agents are classified accordingly. From time to time, the organisational structure is verified and, if necessary, reclassified according to the position of the agents.

The **Flocking model** is based on the concept of the popular *Boids* model introduced by Reynolds (1999, 1987). In this model, the complex behaviour of groups (flocks of birds, herds,...) is decomposed into three basic rules for the steering behaviour on

8. In this figure, as well as in the whole model, it is assumed that all members of the group have a common destination

the individual level: *separation*, *cohesion* and *alignment*. The formation and preservation of the spatial group structure is implemented by applying an attractive steering force to each individual directed into the geometric center of gravity of the group (compare Figure 9, middle). Although the flocking model reproduces a quite realistic behaviour for big swarms of individual actors, there are only very few cases in pedestrian movement where this kind of behaviour can be observed. In order to keep the *PedWalk* model as simple as possible, it was assumed that the Chain Model and the Leader model presented next are sufficient to simulate the behaviour of pedestrian groups.

Finally, the **Leader model** is a form of group organisation typical for groups where one person is responsible for all group members and defines the moving direction (e.g. school classes, group of tourists). The responsible agent ("Leader" in Figure 9 bottom) is defined explicitly and does not change during the simulation time. Like in the Chain model, the leader will wait if one or more of the linked group members separates too far and the concerned group members will increase the speed to catch up with the leader.

Mathematical implementation

The group coordination strategy in *PedWalk* is composed out of two components: a dynamical component (velocity increase or decrease) and a spatial component (orientation towards the linked agent). Both components become active as soon as the distance between two linked agents exceed a critical value. In addition, the formation of dense groups is also supported implicitly by modifying the desired safety distance d^* in the IWM model (see section 3.2.1.2, eq. 3.7, p.18).

The distance $d(A, B)$ between two linked agents A and B is transferred into a normalised value d^0 with

$$d^0 = \begin{cases} 0 & ; d(A,B) < d_{\text{lower}} \\ \frac{d(A,B) - d_{\text{lower}}}{d_{\text{upper}} - d_{\text{lower}}} & ; d_{\text{upper}} \leq d(A,B) \leq d_{\text{lower}} \\ 1 & ; d_{\text{upper}} < d(A,B) \end{cases} \tag{3.13}$$

where $d(A, B)$ is calculated like in the IWM model and d_{lower} and d_{upper} are predefined threshold values defining the active range in which the group's dynamic decisions take place. The lower threshold d_{lower} represents the minimal distance before an agents gets aware that a group member (including himself) is going to be lost and d_{upper} is the associated maximum value of tolerable distance. Distances lower than d_{lower} will have no effect on the behaviour and distances bigger then d_{upper} will be cropped to the maximum active distance.

The smaller the absolute values of the interval boundaries $[d_{\text{lower}}, d_{\text{upper}}]$ are, the closer the group members will stick to each other. If a group only consists of two people (=pair), d_{lower} and d_{upper} will be decreased by 50% to consider the effect that people walking in pairs normally stick much closer together compared to two people as apart of a bigger group.

The individual reaction to an upcoming separation is normally not linear but begins with a moderate velocity adjustment as long as the distance to the separating group member is low and then increases significantly when the distance approaches the critical upper threshold value d_{upper}. To model this effect, the linear distance d^0 is transformed into the non-linear distance function f_{d}: [9]

$$f(d^0) = 0.5 \log_{10}\left(\frac{1 + 0.98 \cdot d^0}{1 - 0.98 \cdot d^0}\right) \tag{3.14}$$

giving a sub-linear increase of f for d^0 between 0 and 0.5 and an exponential rise afterwards (compare Figure 10).

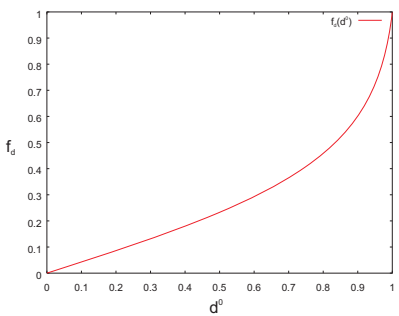

Figure 10: Plot of the $f_d(d^0)$ function to simulate the effects of a separation of group members on the velocity adjustment.

The velocity adjustment is then defined as:

9. Other authors, e.g. Molnár (1996) prefer the usage of a linear function

$$\left[\frac{\partial v_{\text{act}}}{\partial t}\right]_{\text{group}} = a \cdot f_{\text{d}}(d^0\,(\text{pre})) - 0.5 \cdot b \cdot f_{\text{d}}(d^0\,(\text{succ})) \tag{3.15}$$

In the Chain model, $d^0(\text{pre})$ and $d^0(\text{succ})$ are the distances between the agent and his predecessor and his successor respectively. If the group is organised following the Leader Model, $d^0(\text{pre})$ equals the distance of an agent to the group leader and $d^0(\text{succ})$ is the maximum distance found between the leader and rest of the group (the wait relation only applies for the leader agent).

The coefficients a and b are the maximum comfortable acceleration and deceleration as used in the Intelligent Walker Model (see 3.2.1.2, p. 18). The impact of the waiting component (second term in (3.15)) on the velocity adjustment is weighted with 0.5 to simulate that the agent falling behind normally makes the bigger efforts to reestablish the group formation. In order to obtain a final velocity control of the agent, the suggestions formulated in this module will be evaluated together with the results from the IWM model (see eq. 3.19, p. 30).

In addition to the dynamic component of the group coordination model, a spatial trigger is used to ensure that separating agents will move towards the associated predecessors rather than running directly towards the next destination node or being attracted by other forces along the way. This spatial strategy is implemented using a dynamical assessment value $\Phi^{=}_{\text{group}}$ which increases linearly with the distance to the predecessor and has a maximum attractive value of +1 in the direction of the predecessor:

$$\Phi^{=}_{\text{group}} = 1 \cdot d^0(\text{pre}) \tag{3.16}$$

Dynamic group formation and talking

The concept of group organisation as it is presented so far assumes that the group connections have been established by the time the assigned agents are released into the model environment so that the actual amount of groups depends only on the *percentage groups* value as it is defined in the simulation settings. In reality, groups might also form spontaneously, if two or more pedestrians knowing each other meet at any location. In most of these cases, those meeting agents will stand together for some time and talk, but they might also decide to form a temporary group and walk some distance together.

In order to consider this dynamical interaction in the *PedWalk* model, a random list of "known agents" is created each time a new agent is generated and released into the model world. If two agents knowing each other meet on neighbouring navigation nodes, the simulation system decides between three behaviour options: "ignore"," talk to" and "form temporary group".

If the two meeting agents have the same destination node or a common target is found on their routing point list, both of them choose this target as their next destination node and form a temporary group until they have reached the destination node. This rule represents the situation when two people knowing each other find out that they intend to visit the same locations and, if necessary, change their itinerary to walk some distance together.

In case no common routing points exists, the agents begin to talk to each other (=stand still) for some random time period and will continue their original plans afterwards. [10]

Finally, if one of the agents is in the *impatience* mode, no interaction takes place as the agent is assumed to be in a hurry (compare Section 3.2.2.2, p. 24). A detailed description on how this behaviour is incorporated in the main decision process can be found in Section 3.3.5, p. 28.

10. Once talked to each other, the conversation is stored in order to avoid an unrealistic continuation of talking if they meet again. Talking agents can be joined by other agents knowing one of the agents involved in the existing "conversation"

3.2.2.2 Effects of past walking conditions on pedestrian behaviour (*"Moods"*)

Pedestrian walking behaviour is not only determined by the actual traffic situation, but also by the walking conditions a person has experienced before and that influences its recent behaviour. This applies especially to conditions in which the pedestrian had been forced to walk slower than originally planned, which might result in a certain level of impatience and hurry influencing the recent walking behaviour. Up to a certain degree, these effects can be interpreted as "*Moods*" or "*Emotions*" triggering the behaviour of the individual agent.

Although emotions play a significant role in daily decision processes, many people feel uncomfortable when it comes to computer-based analysis of these processes. In fact, many people think that there is a dichotomy between emotional (=irrational) and logical (=rational) decision processes. However, recent research in psychology denies the destructive character of emotions on decision processes and considers them as factors that modulate a given process without violating its rational or logical character (compare e.g. PSI–Theory by Dörner, 1993). Without starting a debate of principals, we will adopt this point of view in the *PedWalk* model and treat emotions as a set of exceptions modifying the behaviour rules defined so far.

To include emotional effects into the behaviour model, two counter variables t_{lost} and t_{stand} plus an associated flag *impatient* is introduced in the *PedWalk* model. Each time the walking velocity of an agents falls below the critical threshold value v_{crit} (compare eq. 3.9, p.19), the value of t_{lost} is increased by the amount of time the agent looses per time step Δt due to walking slower than intended:

$$t_{\text{lost}}(t + \Delta t) = t_{\text{lost}}(t) + \frac{v_{\text{pref}} - v_{\text{act}}}{v_{\text{pref}}} \Delta t$$

Analogously, the counter t_{stand} sums up the time during which the agent does not move at all (v_{act}=0):

$$t_{\text{stand}}(t + \Delta t) = t_{\text{stand}}(t) + \Delta t$$

If t_{lost} increases above a critical value (20 s have been considered as a realistic value in the model, but can be adjusted by the user), the flag *impatient* is set to `TRUE`. In this state, some of the behaviour rules and decisions processes are modified to reflect the impatient "mood" of the agent:

- The preferred velocity is increased by 30% to simulate the efforts of the pedestrian to catch up lost time if possible: $v_{\text{pref}} = 1.3 \cdot v_{\text{pref}}$.
- The desired clearance d^* used in the IWM model is set to 10% of the original value. This results in a relative careless behaviour of the agent with respect to the velocity adjustment when approaching other agents: $d^* \equiv 0.1 \cdot d^*$ (compare eq. 3.8, p. 18 of the IWM model).
- The reaction on the conflict zone generated by other agents is reduced by 50% through reduction of ω_{conflict} (compare eq. 3.17 in Section 3.3.2, p. 27).
- The behaviour of an impatient agent when confronted with occupied navigation nodes is modified. Impatient agents will always try to keep moving and do not interact with other agents (see Section 3.3.5, p.28).

In conclusion, an active *impatient* flag initiates a behaviour that can be characterised by a faster and more aggressive movement through the model environment.

Once the agent has reached the impatient state, the counter t_{lost} is not increased any more.

As soon as the agent is able to move again with a velocity above the threshold v_{crit}, the budgets of t_{lost} and t_{stand} are decreased using the following rules:

$$t_{\text{lost}}(t+\Delta t) = t_{\text{lost}}(t) - \begin{cases} 0.1 \cdot \Delta t & ;\text{not impatient} \\ 2 \cdot \Delta t & ;\text{impatient} \end{cases}$$

and

$$t_{\text{stand}}(t + \Delta t) = t_{\text{stand}}(t) - \Delta t$$

The decrease of the lost time budget is split into two quite different phases: In the first stage, when the agent has not reached the impatience mode (yet), the time decrease equals 10% of a time step. This formulation can be interpreted as a kind of "forgetting" function which simulates the fading impact of past traffic conflicts on the actual behaviour. Contrary, once the agent has reached the impatience mode, he tries to recover the lost time by increasing the preferred walking velocity (see above).

Numerically, from the given increase of v_{pref} by 30% in the impatience mode, this would result in decrease of lost time by $0.3\Delta t$ if the agent is able to walk with the higher preferred velocity. Psychologically, the increased speed and the more aggressive behaviour gives the pedestrian the impression, that much more lost time is recovered than actually is.

3.2.3 Some final remarks on the behaviour model

There is an almost unlimited number of further behaviour strategies that can be observed in reality and could be included in the numerical model. Up to this stage, the key behaviour rules that should solve the majority of possible traffic situations are implemented and each new feature increases the complexity of the whole model though adding only few new functionality to the model.

However, the concept of assessment values provides an open interface to add other modules into the *PedWalk* model without modifying the existing ones. If demand exists for further behaviour rules, they can be easily added.

3.3 The movement process: Selection of navigation nodes

3.3.1 Overview

The movement process of an agent from his recent position $\Pi(\text{act})$ towards the actual destination node Π^* is composed out of several sequential decision processes selecting the optimal next navigation node Π_+ out of the eight competing neighbour nodes. The basic criteria for these selection processes are the assessment values calculated for the potential moving targets, which represent the suggestions formulated by the different behaviour strategies as well as the optimal path information obtained from the virtual distance map. In addition, the presence of other agents on the desired navigation nodes might cause a modification of the initial movement plan on a short-term basis.

The process of selecting the next navigation node can be divided roughly into 4 different phases (see also Figure 11, p.26): In the first step ("A" in Fig. 11), the overall assessments for all eight neighbouring navigation nodes from the recent position of the agent are calculated. Then, in the sequential step ("B"), the minimum required assessment value for a potential movement target is fixed. Navigation nodes with a lower assessment value are not concerned as potential choices. From the remaining nodes, the one with the best (highest) assessment value is suggested as next navigation node ("C"). Finally, it has to be checked, if this node is free or occupied by another agent. In the latter case, several options arise for the agent including to deviate, to stand still or to interact with the other agent. In the following sections, some details are given on the steps of the navigation node selection.

3.3.2 Phase A: Calculation of overall assessment Φ^{Σ} for each moving direction

For each of the eight neighbour nodes of the recent agent position the overall assessment Φ^{Σ} needs to be calculated. The only exception are those nodes of the navigation mesh which are explicitly marked as non-passable (e.g. obstructed by buildings) or missing nodes at the lateral boundaries of the model domain.

The overall assessment of a node in direction α of the agent is obtained by summing up all available assessment values:

$$\Phi^{\Sigma}(\alpha) = \underbrace{\Phi^{0}(\alpha)}_{\text{Routing}} + \sum \underbrace{\Phi^{=}(\alpha)}_{\text{Dynamic}} + \sum \underbrace{\Phi^{*}\Pi\left((\alpha)\right)}_{\text{Reactive}}$$

In the first step (**A1**) in Figure 11, the Routing assessment Φ^{0} (which implicitly includes the local quality assessments Φ^{q} and $\Phi^{q,0}$) is calculated for each of the eight moving directions (see Section 2.2.2, p.13 ff.).

In the next steps (A2 to A5), the dynamic assessment values are collected and summed up over the associated moving direction:

- **A2** and **A3**: Static assessment values for "keep walking direction" ($\Phi^{=}_{\text{keepdir}}$) and "prefer right hand side" ($\Phi^{=}_{\text{rhs}}$), both with a static base value of +1 (see Section 3.2.1.4, p.20) weighted with

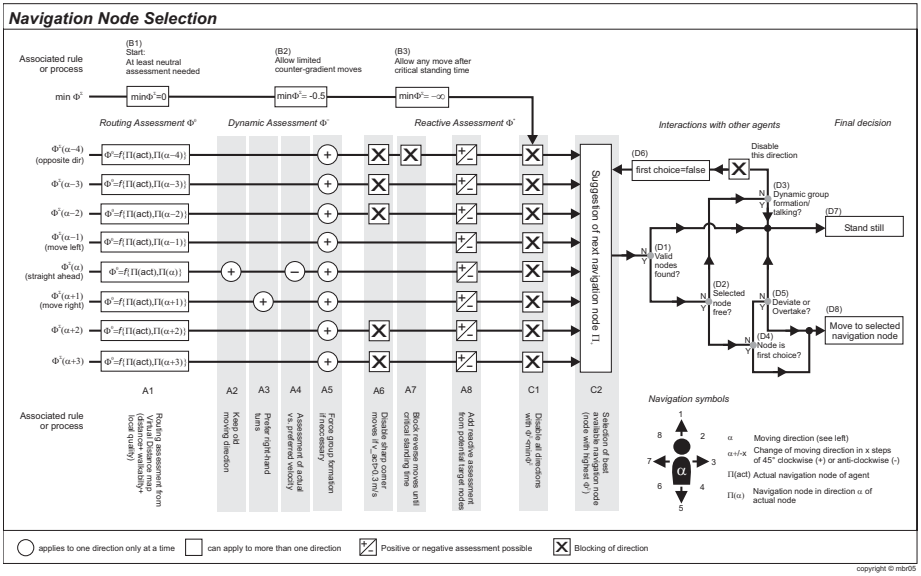

Figure 11: Flow chart of the navigation node selection process. The process splits in 4 phases: (A) calculation of overall assessment for all 8 moving directions, (B) estimation of minimum required assessment value, (C) selection of best suitable node, and (D) verification of suggested node with respect to conflicts and possible interactions with other agents.

the personal impact factors ω_{keepdir} and ω_{rhs} respectively

- **A4**: Velocity assessment $\Phi^{=}_{\text{v\_ass}}$ (see Section 3.2.1.3, p.19), weighted with $\omega_{\text{v\_ass}}$
- **A5**: Assessment value to force group formation $\Phi^{=}_{\text{group}}$ (see Section 3.2.2.1, p.20 ff.), weighted with ω_{group}

Two additional criteria A6 and A7 are added to the decision process in order to produce a more realistic dynamic behaviour of the agents. These rules are not based on empirical behaviour observation but are required for the software implementation of the model:

- **A6**: If the actual velocity of the agent is above 0.3 ms^{-1}, all directions resulting in an moving angle bigger than 45 degree are disabled as such a movement is dynamically not realistic
- **A7**: The moving direction directly opposite to the last moving direction is blocked until the agent stood still for a defined time (user-definable). This rules prevents unrealistic back-and-forward moves between the same navigation nodes if all other options are occupied by other agents

The last step of the assessment value collection (**A8**) sums up the reactive values found on the possible destination nodes. In the version of the model used here, these values only origin from the conflict zones of other agents ($\Phi^{*}_{\text{conflict}}$, see Section 3.2.1.1, p.16). If the reactive assessment values are used to include further external or internal information into the model, more data might be collected and summed up at this point.

After these steps, the exact formulation of the overall assessment value for the moving direction α is:

$$\begin{aligned}\Phi^{\Sigma}(\alpha) &= \Phi^{0}(\alpha) \\ &+\omega_{\text{keepdir}} \cdot \Phi^{=}_{\text{keepdir}}(\alpha) + \omega_{\text{rhs}} \cdot \Phi^{=}_{\text{rhs}}(\alpha) \\ &+\omega_{\text{v\_ass}} \cdot \Phi^{=}_{\text{v\_ass}}(\alpha) + \omega_{\text{group}} \cdot \Phi^{=}_{\text{group}}(\alpha) \\ &+\omega_{\text{conflict}} \cdot \Phi^{*}_{\text{conflict}}(\Pi(\alpha))\end{aligned} \tag{3.17}$$

with ω_{x} being the impact factor of the associated behaviour context.

As mentioned in Section 3.2.1.4, p.20, the impact factors ω_{keepdir} and ω_{rhs} are important parameters to adjust the behaviour of the agents with respect to the smoothness of the walking behaviour and the degree of spatial self-organisation. A more detailed analysis of the values of ω_{keepdir} and ω_{rhs} can be found in Section 4.1.6, p. 39 and Section 4.1.7, p. 42 respectively.

3.3.3 Phase B: Calculation of required minimum assessment value

In phase B of the node selection process, the minimum required assessment value $\min \Phi^{\Sigma}$ is fixed. Nodes with an overall assessment below this threshold value are not considered as potential next navigation nodes. If no nodes with at least the minimum assessment value are available, the agent will stand still.

Initially, at least a neutral assessment is required for a potential target node (**B1**, $\min \Phi^{\Sigma}$=0). With respect to the routing assessment, this condition means that the agent is allowed to move to all nodes which have at least the same virtual distance to the destination node than the node the agent is standing on (white grid cells in Figure 12). Even if further dynamic or reactive assessment values will cause some distortion on the assessment field, it is very unlikely that the agent will move into the opposite direction of the destination node.

However, under certain conditions it is necessary to relax this criteria in order to obtain a realist movement behaviour and to avoid obdurate stays in front of temporary obstacles like pedestrian jams.

The first relaxation (**B2**) allows limited counter gradient moves by setting $\min \Phi^{\Sigma}$=-0.5. This condition is sufficient to allow a smooth overtaking of standing pedestrians by accepting movement directions slightly directed away from the destination (light grey grid cells in Figure 12). Relaxation B2 is applied in all situations where the Euclidian distance of the agent to the destination node is above 30 m. If the distance is below 30 m, the agent is very close to the destination and, in view of the target point, normally detests all kind of deviations.

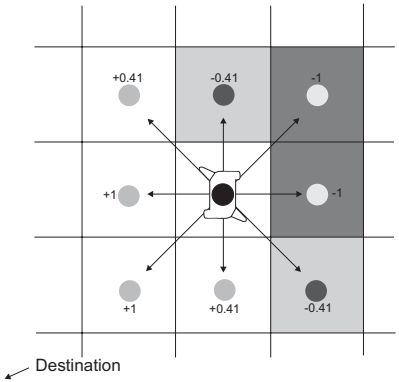

Figure 12: Example situation for local routing assessment Φ^{0} with no further assessment values regarded. White grids are accessible with $\min \Phi^{\Sigma} = 0$ (B1), light grey grids with $\min \Phi^{\Sigma} = -0.5$ (B2) and dark grey grids with $\min \Phi^{\Sigma} = -\infty$ (B3). The destination node is somewhere in the lower left, outside the figure.

If the traffic situation becomes even more dense and complicated, the agent might get stuck in a deadlock situation with no obvious escape. In this case, he has to search for alternative possibilities to reach the destination and this process involves walking around, including trying those directions that lead further away from the destination. To allow this behaviour, the final and maximum possible relaxation criteria of $\min \Phi^{\Sigma}$=$-\infty$ (**B3**) is set, if the standing time t_{stand} (see Section 3.2.2.2, p.24) reaches a critical threshold value (default 20 sec, adjustable in the software).

In severe traffic situations, a real pedestrian who is familiar with his environment will consider to use a totally different route to the destination omitting the critical traffic bottlenecks. This behaviour can easily be included in the model by marking those navigation nodes as either non-passable or assign a very bad quality assessment value to them and then re-run the calculation of the virtual distance map to find an alternative route if one exists.

3.3.4 Phase C: Suggestion of next navigation node Π_+

After all relevant assessment values are summed up and the minimum required overall assessment for the given traffic situation is fixed, the best available navigation node can be determined.

First, all directions leading to neighbour nodes with an overall assessment Φ^{Σ} lower than $\min \Phi^{\Sigma}$ are disabled (**C1**). These nodes join the other nodes which are non-passable in general or being disabled before (e.g through steps A6, A7). From the remaining nodes, the node with the highest assessment value "wins" and is suggested as next navigation node Π_+ (**C2**).

Up to this point, it has not been checked whether this node is available as target or if it is blocked by another agent. This is done in phase D of the decision process.

3.3.5 Phase D: Interaction with other agents and final movement decision

The final phase of the navigation node selection process deals with the interactions with other agents in general and with the solving of conflict between them in particular.

The navigation node suggested by phase C as the optimal next target may be temporary not available because it is blocked by another agent. In this case it has to be decided what the agent should do. In general, there are two options: i) to stand still and wait if the projected node becomes available in the next time steps or, ii) to consider an alternative navigation node as next target and try to move on. If the agent decides to stand still in front of an occupied node, two further options arise: a) to talk to the other agent or b) to form a dynamic group with the other agent and walk together some distance.

The decision process handled in phase D consists of 5 single decision modules (D1 to D5) explained next and their logical linkage as shown in in Figure 11, p. 26.

Module **D1** initially checks if the prior module C2 has provided some navigation node suggestion at all. If no further valid and free nodes exist, the agent has no other option than to stand still and wait (D7).

If C2 did suggest a navigation node, it has to be checked if this node is recently available as a target node or if it is occupied by some other agent (**D2**). At this point, the decision logic split up into two main branches, one handling the case of being faced with an occupied navigation node and the other dealing with a free navigation node.

On the first branch, associated with an occupied node, the next module (**D3**) checks, if the agent occupying the navigation is "known" to the agent. If this is the case, the agent can decide to either talk to the other agent or to form a temporary dynamic group (see Section 3.2.2.1, p. 20 for details). In both cases, the agent will decide to stand still as the outcome of the node selection process. If the occupying agent is unknown to the agent, the suggested node and the associated moving direction respectively will be disabled and the module C2 will be called again to suggest a different navigation node. In addition, it is stored that the following node suggestions are not the first choice any more (**D6**).

The second branch of the decision tree comes into play if the suggested navigation node is available as a next target. In this case it is important for the further process, whether this node is the first (optimal) suggestion or a second-best choice (**D4**). If the node is the first choice, the situation is clear: the node is accepted as next navigation node, it is reserved for the agent and the agent moves towards the node (**D8**).

For a free navigation node that is only second-best (or third or forth best, depending on the number of loops already executed in phase D), the situation is more complex, as it is not obvious if the agent should accept this suboptimal move or decline it and stand still (**D5**). This decision depends mainly on the quality of the alternative node compared to the optimal direction and, to a fewer extend, on the general personality of the agent.

In order to formalize this decision process, we assume, that there is a link between the probability of accepting an alternative node and the quality difference towards the optimal node: The more equal the quality of the alternative node is to the first choice node, the more likely it is that the agent accepts this deviation possibility and vice versa.

The formal decision is based on a Gaussian distributed random number $\chi(\mu, \sigma = 0.25)$ which is generated for each decision case. The mean μ of the

distribution is a function of the quality difference between the overall assessment of the optimal (first choice) node $\Phi^{\Sigma}(\text{opt})$ and the overall assessment of the suggested alternative node $\Phi^{\Sigma}(\Pi_{+})$with

$$\mu = 1 - \left(\frac{\Phi^{\Sigma}(\text{opt}) - \Phi^{\Sigma}(\Pi_{+})}{\Phi^{\Sigma}(\text{opt})} \right) + \xi \qquad (3.18)$$

With this formulation, the mean of the Gaussian distribution moves towards +1 for nodes of similar quality and approaches 0 and negative numbers for alternative nodes with much lower assessment values.

The concrete movement decision is then made based on the value of $\chi(\mu, \sigma)$ using the rule

$$\chi(\mu,\sigma) \begin{cases} < 0.5 & \rightarrow \text{decline, stand} \\ \geq 0.5 & \rightarrow \text{accept, move} \end{cases}$$

The factor ξ used in (3.18) is an additional agent-dependent factor ("*walking personality*") introducing some artificial character into the model. Ranging from -0.3 (stubborn, rejecting most of the alternatives) to +0.3 (flexible, deviating often), it defines the general tendency how the agent behaves in view of conflicts.

If the module decides to accept the suggested node, it is selected and reserved as next target and the agent moves towards it (D8). In case of rejection, the agents remains on the navigation node and stands still until the new selection process in the next time step (D7).

Finally, it has to be mentioned that special conditions apply in the decision modules (D3) and (D5) if the agent is in the *impatience* mode (see Section 3.2.2.2, p. 24): In this case, the agent will neither talk to other agents nor form a dynamical group (D3), and, in case of occupied navigation nodes, he will always try to keep moving ($\chi = 1.0$ in D5).

3.4 The complete simulation loop

In this final section of the theoretical part of the model documentation, the complete simulation loop as seen from the perspective of a single agent is presented. Figure 13 shows the general structure of the simulation as flow chart divided into 5 logical units with several sub-processes referring to the modules presented so far.

Phase 1

Phase 1 ("Initialisation of agent") includes all modules associated with the setup of the individual agent. First, the individual properties of the agent are derived from the properties of the agent community (Module 1.1 in Fig. 13, compare also Section 2.1.3.1, p. 7) and the list of destination points is generated from the available routing points in the model area with respect to their assigned traffic data (Module 1.2, compare 2.1.3.3, p. 8). Next, a random list of known agents is created and it is decided whether the agent is a part of a group or a individual walker. Finally the agent is released into the model world by being placed on the assigned entry node.

Phase 2

In Phase 2, the next destination node Π^{*} is selected from the agents routing point list (Module 2.1). In order to identify the most suitable target, the Euclidian distance between the actual position of the agent and the remaining unvisited points on the list is calculated and the closest point is selected. The *PedWalk* model allows defining groups of routing points, for example points defining different entrances to the same building. The agent is able to dynamically exchange routing points if, for example due to modifications of the actual route, another point of the same group is finally closer than the originally projected destination point. After selecting the next destination node, the virtual distance map is generated (Module 2.2, compare Appendix A, p. 52).

Phase 3

The main moving process towards the next destination node is handled in Phase 3. First, the next navigation node out of the 8 neighbour nodes from the recent position of the agent is selected as described in Section 3.3, p. 25 (Module 3.1).

The inner loop of phase 3 (Modules 3.2–3.3–3.4–3.5) then moves the agent towards this node until it is reached. Inside this loop, the agent cannot change the node he moves to, but the velocity can be adjusted at any time. As there are two modules in *PedWalk* that can produce velocity suggestions, namely the *Intelligent Walker Model* (Section 3.2.1.2, p. 18) and the group coordination model (Section 3.2.2.1, p. 20) a mediator function must be used to solve potentially contradicting suggestions.

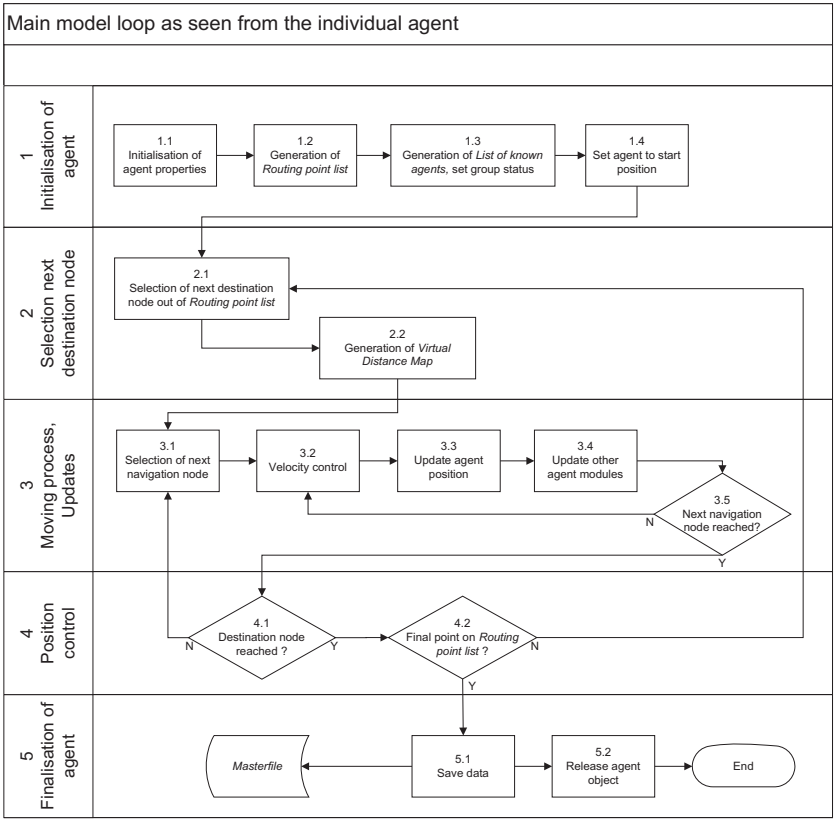

Figure 13: Flow chart of the main simulation loop as seen from the perspective of the individual agent.

The following rules are used to determine the required velocity change:

- if both IWM and group coordination module suggest acceleration or one of them provides no suggestion, the maximum acceleration rate is used
- if one of the modules suggests deceleration, the agent will decelerate with the suggested value regardless of the other suggestion
- if both modules suggest deceleration, the minimum value (if deceleration is counted negative) will be relevant

Mathematically, the mediator rules can be written as

$$\frac{\partial v_{\text{act}}}{\partial t} = \begin{cases} \max\left(\partial_{\text{gr}}, \partial_{\text{IWM}}\right) & ; \partial_{\text{gr}} \geq 0 \wedge \partial_{\text{IWM}} \geq 0 \\ \min\left(\partial_{\text{gr}}, \partial_{\text{IWM}}\right) & ; \partial_{\text{gr}} < 0 \wedge \partial_{\text{IWM}} < 0 \\ \partial_{\text{gr}} & ; \partial_{\text{gr}} < 0 \wedge \partial_{\text{IWM}} \geq 0 \\ \partial_{\text{IWM}} & ; \partial_{\text{gr}} \geq 0 \wedge \partial_{\text{IWM}} < 0 \end{cases} \tag{3.19}$$

with $\partial_{\text{IWM}} = (\partial v_{\text{act}}/\partial t)_{\text{IWM}}$ from eq. 3.5, p. 18 and $\partial_{\text{gr}} = (\partial v_{\text{act}}/\partial t)_{\text{group}}$ from eq. 3.15, p. 23.

Next, the recent position inside the navigation mesh is updated. If the agent has executed more than half

of the way to next navigation node, he will be logically assigned to this node $\Pi(\text{act}) = \Pi_+$ and the node of origin Π_O is released for the use of other agents.

Phase 4

After reaching the next navigation node, it is checked in Phase 4 if this node is the assigned next destination node (Module 4.1). If not, the next navigation node is selected in Module 3.1 and the moving process continues. In case the agent has reached the destination node, it is checked if this point was the last point on the routing point list and the agents exits the model or if other unvisited destination nodes remain (Module 4.2). In the latter case, the outer loop is repeated by selecting the next destination node from the list (Module 2.1).

Phase 5

If the agent has reached his last unvisited point from the routing point list, the data stored inside the agent object (e.g. data logged during the trip through the environment) are written into the so-called "*Masterfile*" for further analysis and the agent object is finally released (Phase 5).

3.5 Numerical aspects

The time step used to move the agents through the virtual environment depends on the size of the grid cells on the one hand and on the walking velocity of the agents on the other. Although no real numerical instabilities will happen in the case of too large time steps, it must be assured that no navigation nodes are "overjumped" between two calculated positions. This condition can be satisfied if the selected time step Δt is smaller or equal to the maximum possible time step according to the well-known Courant-Lewis stability criteria:

$$\Delta t_{\max} = 0.5 \frac{\Delta xy}{\max v_{\text{act}}(1..n)}$$

where Δxy is the horizontal resolution of the grid mesh and $\max v_{\text{act}}$ is the maximum actual velocity over all active n agents in the model system.

In order to avoid unnecessary calculations, the selected time step is set equal to $\Delta t_{\max}$.

Part II
Model Results

4 Model results and analysis

There are many ways how the data generated by the *PedWalk* model can be analysed and interpreted. For example, the analyst can take different perspectives like observing the traffic dynamics focussing on a single agent, or he might be interested in the flow patterns emerging in different parts of a specific structure. On the temporal scale, the fundamental parameters of the traffic can be described using averaged conditions or the analyst might be interested in the dynamics of short-termed peak situations.

The comparison of simulated traffic data with observational data is as complex as the phenomena of pedestrian traffic is complex per-se. Many typical phenomena (e.g. deviation processes) exists or take place only over a very short time and will not be represented adequately by averaged data. Also, there is a very high spatial variance in the pedestrian traffic data, making the data very sensible to the spatial resolution of the observation and to the exact placement of the area observed. For example, high density traffic situations will only be captured accurately if the area of analysis is located directly and exclusively where the jam situation occurs. If the observation area is too large, high density values will be diluted by averaging with data from model areas where few or no agents are present (which is typically the case when people agglomerate at one specific location).

In the following sections, some typical traffic situations will be simulated and, where possible, the results will be compared to other pedestrian traffic models or to relations based on empirical data.

4.1 The street canyon test case

4.1.1 Model layout

To gain insight into the model dynamics, a very simple test case of a street canyon as shown in Figure 14 is used in the following sections. The canyon possesses two entry/exit areas at each end implemented through a set of routing points used to generate the traffic inside the model area.

To analyse the traffic data in more detail, the BOT-world simulation system in which the *PedWalk* model has been integrated, allows the definition of so-called ”*Survey Areas*” inside the model area. For

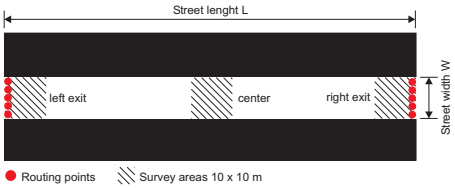

Figure 14: Layout of the model area for the street canyon test case showing the routing points and the survey areas.

Table 4: Agent release rate assigned to the routing points at the left and right end of the street (left end/right end.)

Agents per minute unidirectional	Agents per minute bidirectional	Scenario
20/0	10/10	
50/0	25/25	
100/0	50/50	
150/0	75/75	Light traffic
200/0	100/100	
300/0	150/150	(Dense traffic)
600/0	300/300	Heavy traffic

this test case, three survey areas, 10 m$\times$10 m each, have been defined: "left exit" and "right exit" at the two ends of the canyon and "center" in center of the canyon (see Figure 14). The street dimensions are set to a width of W=10 m and a length of L=100 m for most of the simulations except for the numerical tests on lane formation shown in Section 4.1.6.

The street canyon simulations have been carried out with two spatial resolutions: a) a coarse grid with Δxy=1 m $\times$1 m resolution and b) with a fine grid with a cell size of Δxy=0.5 m $\times$0.5 m. The total amount of grid cells and navigation nodes respectively vary with model resolution and street width and length. All simulations have been run over a time period of 15 minutes.

4.1.2 Traffic generation

In order to generate pedestrian traffic inside the test area, different frequentation data ranging from 20 agents/minute up to 600 agents/minute have been assigned to the routing points at both ends of the street. For the unidirectional flow simulations, all agents enter the area on the left end and walk over to the right hand side. For the bidirectional flow scenarios, agents can enter the street canyon at both sides. Table 4 summarises the different simulation scenarios and their associated agent release rate.[11] The simulations labeled *"Light traffic"* and *"Heavy traffic"* are used to study certain aspects of pedestrian traffic more in detail. For the bi-directional simulation with coarse grid, the *"Dense traffic"* scenario replaces the the "Heavy traffic" scenario in order to avoid immediate traffic jams in the entry/exit areas.

In the default configuration, the routing points on one side are equal and can be used alternatively, so that it is sufficient that an agent reaches any of these points to leave the model.

4.1.3 Other model settings

In addition to the spatial layout and the definition of the traffic properties, the values of some constants used in the *PedWalk* model need to be defined.

For the age distribution an average community mix with $\overline{ag}$=40 y and σ_{ag}=0.15 y was selected. Likewise, a standard distribution was selected for the preferred velocity v_{pref} with $\overline{v}$=1.34 m/s and σ_{v}=0.26 m/s (compare §3, p. 15).

Also, the suggested default values are used for the save time interval t^* (=1 s, compare Section 3.2.1.1, p. 17) and the tolerable slow down f_{crit} (=30 %, compare 3.2.1.3, p. 19).

Finally, the values for the different impact factors ω_{x} are selected as shown in Figure 15 (except of course those values that are adjusted for the different numerical tests).[12]

4.1.4 Fundamental flow characteristics: The Level-Of-Service (LOS) indicator

The Level-Of-Service (LOS) indicator is one of the most established parameters to describe traffic flows and to characterise the resulting quality of service. Originally developed for vehicular traffic (compare

11. Note that for the unidirectional scenarios, the traffic at the right end of the street is generated only by arriving agents, therefore the release rate is set to zero. The emission rate on the left end of the street is then increased accordingly to generate the equal amount of traffic like in the bidirectional scenarios

12. For simplicity, we will use the same impact factor profile for all agents in this study

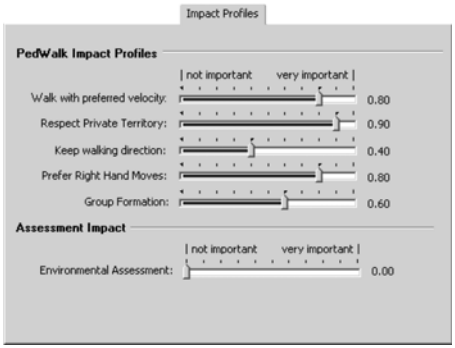

Figure 15: Values for the different impact factors used in the simulation (snapshot from the BOTworld software interface). The impact values are, from top to bottom, referring to the following assessment contexts: *Velocity assessment* (ω_{v_ass}=0.80), *Consideration of conflict zones* ($\omega_{conflict}$=0.90), *Preference of keep walking direction* ($\omega_{keepdir}$=0.40), *Preference of right hand moves* (ω_{rhs}=0.80) and *Importance of group formation* (ω_{group}=0.60). The *Environmental assessment* component is not used in this study.

Table 5: Different categories of Level-Of-Service (LOS) for pedestrian traffic and their characteristics compiled after Weidmann (1993); Fruin (1971a); TRB (2000).

LOS	*Density* $[P/m]^2$	*Name*	*Character of traffic / Average velocity* $[ms^{-1}]$
A	0.00–0.10	Open	No restriction, $\leq$1.32
B	0.10–0.30	Impeded	Free movement, 1.27–1.32
C	0.30–0.45	Constrained	Occasional obstruction 1.22–1.27
D	0.45–0.60	Crowded	Partially restricted, 1.14–1.22
E	0.60–0.75	Crowded	Significant obstruction, 0.76–1.14
F	0.75–1.00	Congested	Dense traffic, $\leq$ 0.76
G–I	above 1.00	Jammed	Moving queue, $\leq$ 0.76

TRB, 2000), it has been adopted to pedestrian traffic conditions by Fruin (1971a). The LOS indicator relates traffic quality to pedestrian density (available space) using a nine class scheme (A to I) as shown in Table 5. It has to be noted, that the values associated with the different LOS of pedestrian traffic vary significantly between the different authors and with the observed contexts. The data used here are a synthesis of the values used most frequently in literature and studies.

With respect to the application target of the *PedWalk* model, the analysis presented in this paper will focus mainly on the simulation of average urban pedestrian traffic conditions (typically LOS A to F) rather than analysing high-density crowd scenarios (LOS G to I). Figure 16 shows an illustrative interpretation of LOS A to F taken from the Highway Capacity Manual (TRB, 2000).

The traffic scenarios as shown in Table 4 have been designed to generate traffic flows associated with the LOS B ("Light traffic"-Scenario) and around LOS D ("Heavy traffic"-Scenario) in the uni-directional simulation mode. Figure 17 shows the simulated agent density in the center survey area for both traffic sce-

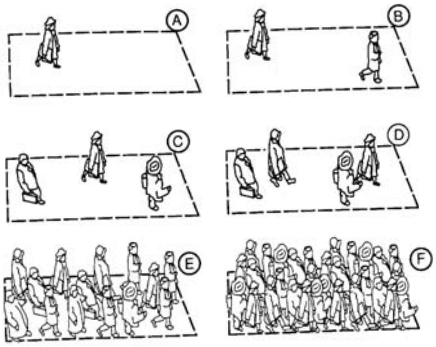

Figure 16: Illustration of the Level-Of-Service A to F (TRB, 2000).

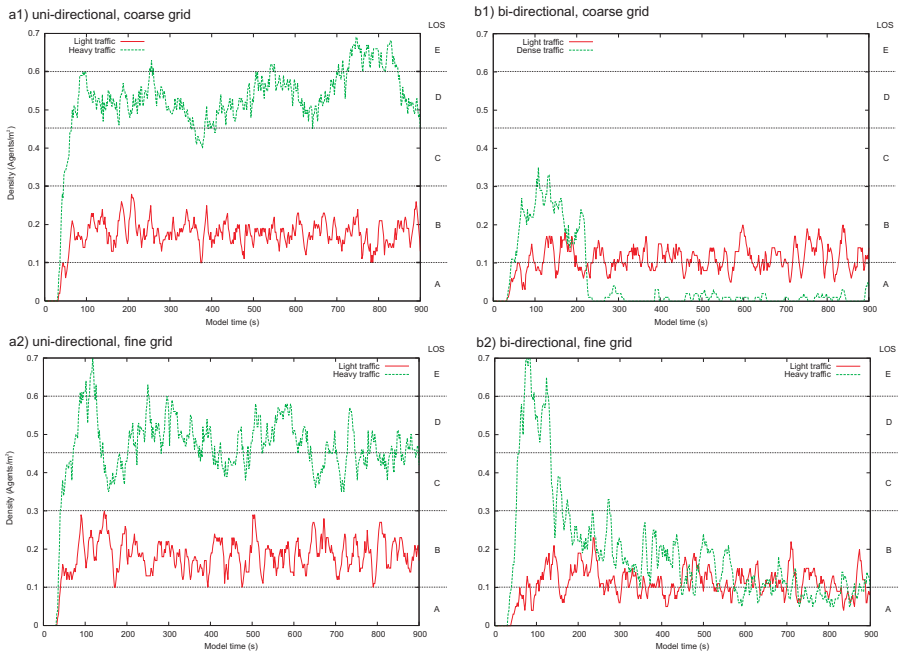

Figure 17: Traffic density during the 900 sec of simulation time shown for the center survey area. In the top row the results for the coarse model grid are shown for the uni-directional (a1) and bi-directional (b1) simulations. The bottom row shows the corresponding results for the simulations using the fine grid (a2 and b2).

narios. In the upper row, the results for the simulation using the coarse grid in the uni-directional (a1) and bi-directional (b1) mode are shown and in the row below, the same is plotted for the fine grid simulations (a2 and b2).

In the uni-directional modes, the simulations produce, apart from the stochastic variations, similar and stable traffic data for both traffic scenarios. For the bi-directional simulations, the situation is remarkably different: Here, the agent flow in the ”Dense traffic / Heavy traffic” scenario collapses shortly after the start of the simulation and the resulting agent density in the center survey area is only marginally above the ”Light traffic” scenario (b2), or, in case of the coarse grid simulation (b1), fluctuates around zero.

The reason for this behaviour is based in the significant number of conflicts between agents entering the model area and those aiming to leave it using the same routing points at the same time. In the uni-directional mode, these conflicts do not exists as the routing points are used exclusively for entering the model (left side) or leaving it (right side). To illustrate this process further more, Figure 18 shows the development of agent density in the survey area at the right exit and in the center of the street for the ”Dense / Heavy Traffic” bi-directional scenario (for the left exit, the situation is analogous).

In the coarse grid simulations, the maximum achievable capacity (all navigation nodes are occupied) equals 1 agent/m^2 (=LOS G after Tab. 4), whereas in the fine grid runs a maximum density of 4 agents/m^2 is possible (=LOS I). As it can be seen from Figure 18, the density in the right exit survey area increases quickly after the start of the simulation. For the coarse grid (Fig. 18 a), it approaches its saturation value about 200 sec after the simulation start

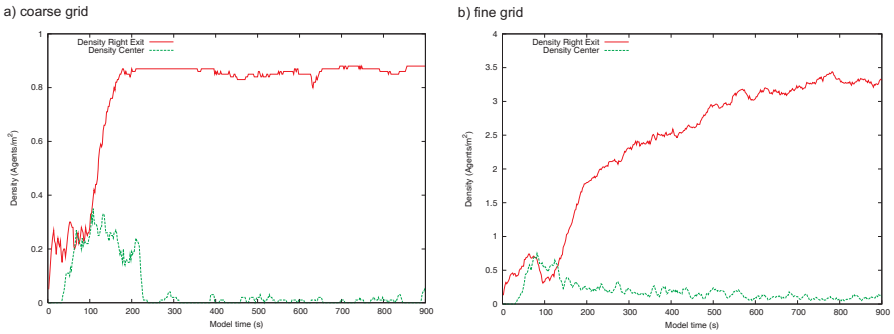

Figure 18: Traffic density in the survey areas at the right exit and in the center of the street in the bi-directional mode: Coarse grid results for the "Dense traffic" scenario (a) and fine grid results for the "Heavy traffic" scenario (b).

with a corresponding drop of density to almost zero in the center survey area. In the fine grid simulation (Fig. 18 b), the agent density at the right exit also increases significantly, but due to the larger amount of available navigation nodes the agent circulation through the center area remains on a higher level compared to the coarse grid simulation.

Speed distribution

Not only the density of pedestrians, but also the distribution of actual walking velocity compared to the desired velocity is one of the main quality criteria for the Level-Of-Service index. According to the LOS criteria shown in Table 5, the "Light traffic" scenarios with LOS B should allow the virtual pedestrians to walk more or less unrestricted with their personal preferred velocity whereas in the "Heavy Traffic" scenarios (LOS D to E), a plain difference between the desired and the actual velocity distribution should be observable.

Figure 19 (a) shows the velocity distribution in the center survey area for the uni-directional simulation scenario "Heavy traffic" simulated with the coarse grid. The data were collected over the complete simulation time of 15 min using the "Virtual interview" method of the BOTworld environment, in which the data of each agent are analysed once the agent enters the survey area. For better visualisation, a smoothing Bezier curve is drawn over the histogram steps in the diagram. The broken lines show the distribution of the preferred walking velocity v_{pref} as generated from the community properties (compare Section 2.1.3.1, p. 7) whereas the solid lines represent the distribution of the actual velocity v_{act}.

As it can be seen, the original single-peak distribution of preferred velocity has changed to a two-peaked distribution with a significant amount of agents moving slower than with their preferred velocity. In addition, there is a significant number of agents which do not move at all (velocity class 0 ms^{-1}).

The two-peaked shape of the distribution curve clearly indicates that in this scenario there is no general slow down of all agents, but a clear split into two groups of agents: One group of agents moving unrestricted with their preferred velocity and a second group, moving with a velocity restricted by dense traffic. This matches well with the definition of LOS D, defining the choice of velocity of "partially restricted". If the agent density increases more, it is likely that the velocity distribution would become single-peaked again, with all agents being restricted in their choice of velocity.

Figure 19 (b) shows the same phenomenon, but this time in the light of the difference in v_{act} and v_{pref} distribution comparing the data against the results from the "Light traffic" scenario simulation. As expected, the velocity distribution for the low density simulation (LOS B) shows only small deviations between the preferred and the actual velocity, most of them probably due to short-timed local conflicts.

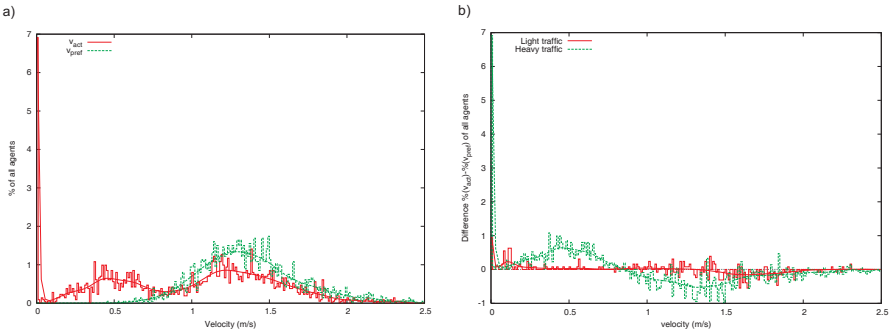

Figure 19: Velocity distribution in the center survey area for the uni-directional simulation (coarse grid): Distribution of actual velocity v_{act} versus preferred velocity v_{pref} for the "Heavy traffic" scenario (a), Difference between the preferred velocity distribution and the actual velocity distribution for the "Light traffic" and the "Heavy traffic" scenario ($\%(v_{\text{act}}) - \%(v_{\text{pref}})$, b).

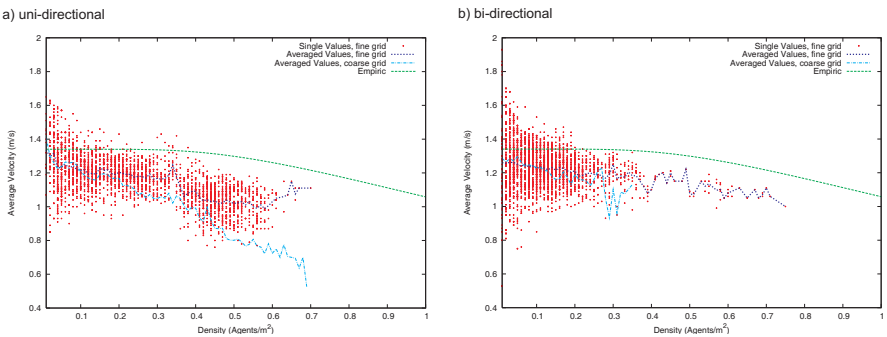

Figure 20: Velocity–Density curve for the center survey area. Single values are shown for the fine grid simulations only: Uni-directional traffic (a) and bi-directional traffic (b).

4.1.5 Relationship between agent density and speed

In the previous section the traffic flow has been analysed from the qualitative point of view. To analyse the relation between agent density and average walking velocity more in detail, we will now analyse simulated density/velocity constellations and make a comparison with an empirically obtained relationship.

To approximate the relation between pedestrian density and average walking velocity on plain terrain, Weidmann (1993) suggests the following simple equation:

$$\overline{v}(\rho) = 1.34 \left[1 - \exp\left(-1.913 \left(\frac{1}{\rho} - \frac{1}{\rho_{\max}} \right) \right) \right] \tag{4.1}$$

where $\rho_{\max}$ is the maximum pedestrian density which is assumed to be 5.4 Peds/m^2 in this relation. This equation is derived from the so-called "*Fundamentaldiagramm*" which describes the relation between traffic flow Q (agents/sec) and traffic density ρ (agents/m^2) in the equilibrium state.

Figure 20 shows the simulated constellations of agent density (ρ) and average agent velocity ($\overline{v}_{\text{act}}$) obtained for the center survey area. The small crosses are the individual simulated $\rho/\overline{v}_{\text{act}}$ data pairs collected over all traffic scenarios and over the complete 15 min of simulation. These data pairs are then again averaged to one single value per agent density and connected with the dotted line. The individual data are plotted for the fine grid simulations, the results from the coarse grid simulation runs are shown as averaged line only. Finally, the results from the empirical function (4.1) are plotted to be compared with the simulation data.

In the uni-directional simulation (Fig. 20 a), the maximum simulated agent density is about 0.7 Agents/m^2 for both the simulation with the coarse grid and with the fine grid. In the bi-directional runs (Fig. 20 b), the fine grid runs reach a maximum density of about 0.8 Agents/m^2 (but with very few data in the higher density regions above 0.4 Agents/m^2 which should not be over-interpreted) whereas in the coarse grid simulations the density gets not higher than around 0.35 Agents/m^2 due to the conflicts at the entry and exit points already mentioned.

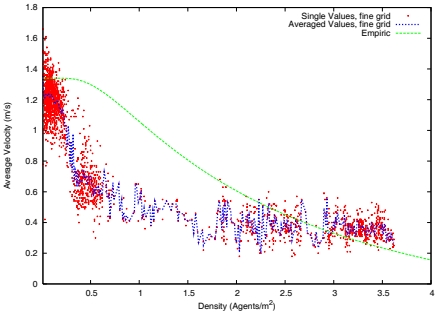

Figure 21: Velocity–Density curve using additional data from the left and right exit survey area obtained from the fine grid simulations with bi-directional traffic.

When comparing the data from the coarse grid simulation with the fine grid counterparts, it is obvious that the impact of the model resolution increases as the density values increase. Before this effect will be discussed, we will throw a short glance at the Velocity–Density constellation for high-density situations.

Although the *PedWalk* model focuses on low to average density traffic situations, it is interesting to see how the density-velocity relation behaves for higher density values when the traffic flow approaches Level-Of-Service conditions above F. Figure 21 shows the speed–density curve for the fine grid simulation, with bi-directional traffic using additional data from the survey areas at the right and left end of the street.

There are three agglomeration areas of $\rho/\overline{v}_{\text{act}}$ data pairs which can be identified in Figure 21: One accumulation of data points can be found in the low density areas up to 0.3 Agents/m^2 which originates probably mostly from the traffic in the center survey area. Clearly separated from this group there is a patch of data around the 0.5 Agents/m^2 density value indicating a synchronisation of agent velocity in this density range. Finally, a number of data points can be found in the high density regimes between 2 and 3.5 Agents/m^2. These data originate mainly from the traffic close to the routing points at the right and the left end of the street. For these data, the variance between velocity values assigned to the same density is larger than their dependency on the density value.

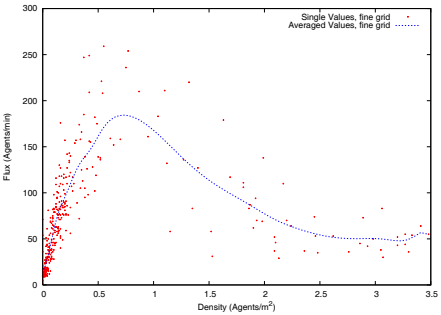

Figure 22: Flux–Density curve (*Fundamentaldiagramm*) for all survey areas obtained from the fine grid simulations with bi-directional traffic.

When comparing the simulated data with the empirical Weidmann-relationship, it is obvious, that the average velocities simulated by the model are constantly lower than those obtained from equation (4.1). On the other hand, the indicator variables given by TRB (2000) as shown in Table 5 do not match these data either, but fit better with the model data. It seems, that pedestrian traffic is much too chaotic to be described by simple statistical parameter. For that reason, this section closes with some general remarks on the characteristics of the *PedWalk* model as far as the speed–density dynamics is concerned.

There are basically three main factors that have to be kept in mind when comparing the model output with other data in general and with the data presented before in specific: 1) the model lacks compressibility, 2) the definition of density values is ambiguous and 3) the *Fundamentaldiagramm* is not valid for higher traffic densities:

1. The model is non-compressible, therefore it is not able to compensate short-termed fluctuations in density but transports shock waves from navigation node to navigation node.
2. The usage of the density parameter is ambiguous for two reasons: a) as mentioned in the introduction of this section, the density values depends on the size and the location of the analysed area, over which the density value is averaged, and, b) the *PedWalk* model mechanism reserves not only the actual navigation node for the agent, but also the projected next target node (compare step D8 in Section 3.3.5, p. 28). Due to this procedure, the amount of usable navigation nodes is much lower than the amount of grid points actually occupied by agents.
3. Finally, it is known for vehicular traffic and it is even more true for the more chaotic pedestrian traffic, that the equilibrium assumption of the *Fundamentaldiagramm* is only valid for low-density traffic. If the traffic flow approaches higher densities and begins to develop a non-homogeneous structure, different phases of traffic with different properties exist parallel to each other and the simple velocity-density relation implied by the *Fundamentaldiagramm* no longer usable (compare Helbing, 1997, p. 67 ff). Figure 22 shows the *Fundamentaldiagramm* extracted over all survey areas from the bi-directional simulations with the fine grid. Similar to the data shown in Helbing (1997), it can be seen that for densities above 0.3 to 0.4 Agents/m^2, the scattering of the data becomes too large to use the average value as a representative indicator.

4.1.6 Influence of impact factor $\omega_{\mathbf{rhs}}$ on pedestrian lane formation

Contrary to the repulsive effects that normally arise when unknown persons compete for space, we can also observe attractive forces that lead to the formation trails of pedestrians walking into the same direction, especially when the pedestrian density is high (compare §7, p.15 and see Figure 23 showing a high-density situation at the South Bank of the River Thames, London as an example).[13]

The development of this phenomenon is steered by two parameters: a self-organising component and a purposeful component. The self-organising part of the trail effect is based on the fact that following other pedestrians walking in the same direction reduces the amount of other persons approaching frontally. Thus the number of conflicts and successive direction changes is reduced and pedestrians following the trail are more likely to walk unobstructed

13. As it can be seen on the picture from Great Britain, the pedestrian traffic does not necessarily prefer the same walking side as the road traffic (right-hand pedestrian traffic versus left-hand road traffic)

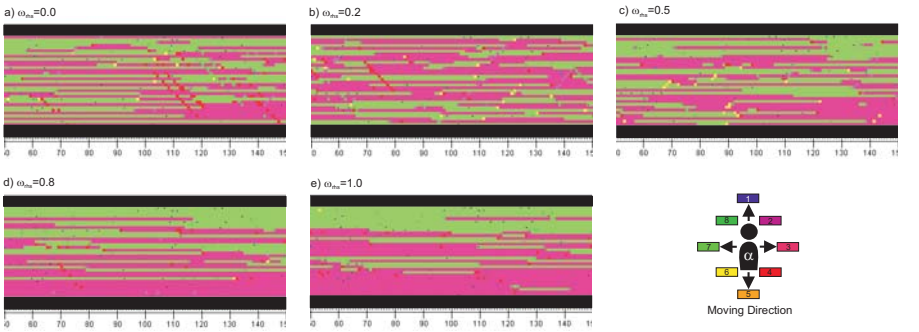

Figure 24: Lane formation for different impact factors ω_{rhs} observed after 15 min of simulation time for the 32 m wide street (middle segment between 50–150 m only shown). Colors indicate the direction of movement of the last agent visiting the grid cell.

Figure 23: Pedestrian lane formation at the South Bank of the River Thames, London, UK.

and keep their walking direction than those walking outside the trail. On a longer term basis, following the trail is the more successful strategy.

The second aspect concerns the active search of pedestrians for other people moving into the same direction within a certain range in order to benefit from the phenomenon described before. This behaviour is often compared to the chemotaxis used by insects, where a path is marked using chemical or hormonal substances which other individuals of the same species receipt and use for their routing decision.

When designing a numerical simulation model for pedestrian traffic, it has to be decided, how this lane formation effect should be handled in the model. Some authors, e.g. Brustedde et al. (2001) handle the trail formation process explicitly by simulating some virtual pheromone field whereas others, e.g. Nagel (1996) rely totally on the self-organisation aspect of the phenomenon. In the *PedWalk* model the lane formation process is not included explicitly as a behaviour rule and will only emerge through self-organisation processes. However, as already mentioned in Section 3.2.1.4, p. 20, imposing a certain behaviour preference onto the moving decision process supports this self-organisation process to a huge extend. This behaviour preference is numerically realised in the *PedWalk* model through the impact factor ω_{rhs}.

In the following section, the impact of different ω_{rhs} values on the lane formation process will be analysed.

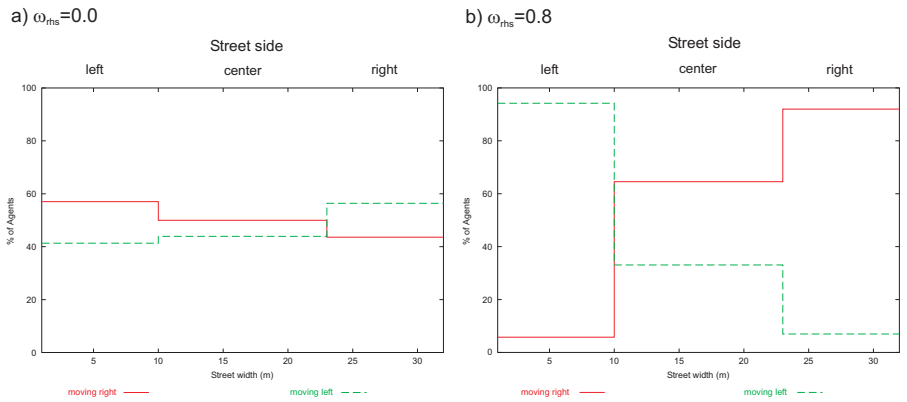

Figure 25: Distribution of agents walking left and right accumulated over 15 min of simulation time for ω_{rhs}=0.0 (a) and ω_{rhs}=0.8 (b). The street side labels refer to the perspective of an agent walking from the left to the right.

Modifications of the model layout

For the simulation of the lane formation process, the model layout as presented in Section 4.1.1, has been altered in two points: 1) the street length has been extended to 200 m in order to allow a longer distance for the self-organization, and 2) additional studies have been made with a street width of 20 m and 32 m. The model has been run over a time period of 15 minutes in the coarse grid resolution (1 m $\times$ 1 m) using the "Light traffic" scenario in the bi-directional mode.

Simulation results

To analyse the formation of pedestrian lanes, a snapshot of the model state after 15 min of simulation time has been taken. [14] The amount of lanes have then been extracted by counting and averaging the number of lanes found at the street length positions 70 m, 100 m and 130 m. Figure 24 shows the spatial distribution of pedestrian lanes for five different impact factors ω_{rhs} varying between 0.0 and 1.0 for the 32 m wide street focussing on the street segment between 50 and 150 m. In support, Figure 25 shows the amount of agents moving left and right in the center survey area accumulated over the complete 15 min of simulation time. The remaining model results for the street widths of W=10 m and 20 m are plotted in Figure 26.

As it can be seen from Figure 24 and from the corresponding values in Figure 26, the number of lanes decreases significantly with increasing values of ω_{rhs}, for example from 22 lanes (ω_{rhs}=0.0) to 11 lanes (ω_{rhs}=1.0) in the 32 m wide street. Also, the distribution of the moving direction (Fig. 25), clearly indicates a preference of right-hand traffic imposed if the impact factor is set to 0.8.

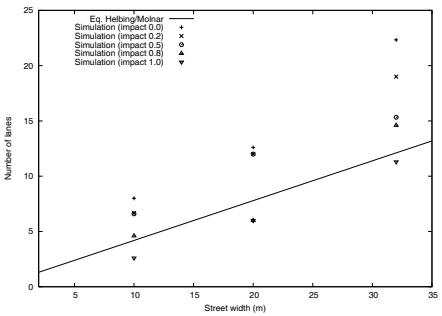

Figure 26: Number of emerging lanes for different street widths and impact factors ω_{rhs}. Points indicate simulated data from *PedWalk* after 15 min of simulation time for street widths W=10, 20 and 32 m. The solid line represents simulation data obtained by Helbing and Molnár (1995).

14. The model is stable at this time and no significant differences in the model state happen after these 15 min

In order to select a suitable value for ω_{rhs}, a comparison of the *PedWalk* results with other models and observational data would be desirable. Unfortunately, there is only very few material available and the only comparable data found were simulation results obtained using the *Social Force Model* (Helbing and Molnár, 1995; Helbing, 1997).

In their paper, Helbing and Molnár (1995) derived the relationship

$$N = 0.26W + 0.59$$

between the street width W and the number of emerging lanes N. The plot of this function is shown as a solid line in Figure 26. Comparing the number of lanes simulated using the *Social Force Model* with the different *PedWalk* results, a value of ω_{rhs} around 0.8 appears to match well with the data obtained by Helbing and Molnár (1995). There is of course a large variance in the amount of lanes generated from simulation to simulation as for example only one agent separating from the main lane will increase the number of lanes by 2. However, in order to obtain a general estimation of the order of magnitude for ω_{rhs} this comparison is sufficient. As the default value, ω_{rhs}=0.8 is suggested for the *PedWalk* simulations.

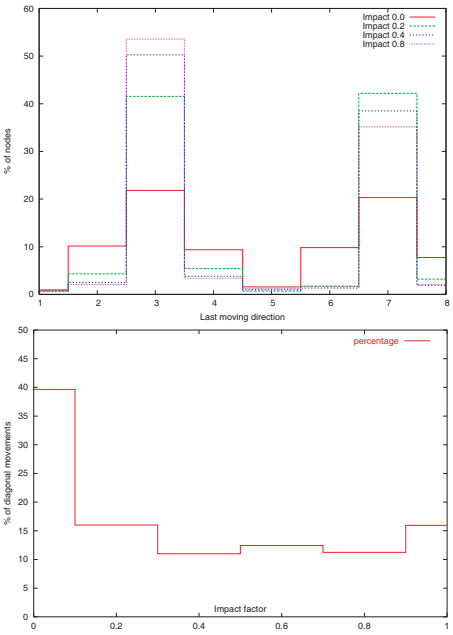

Figure 27: Distribution of the last agent moving direction for different values of ω_{keepdir}. Data were obtained taking the last registered moving direction from all navigation nodes in the 10 m wide street. Top: Distribution by moving direction, Bottom: Amount of diagonal moves by impact factor ω_{keepdir}.

4.1.7 Influence of impact factor ω_{keepdir} on movement patterns

The objective of imposing an additional attractive assessment value onto the recent walking direction is to avoid unrealistic frequent changes of the moving direction and a too sensitive reaction on small variations in the Φ^0 field (compare Section 3.2.1.4, p. 20). In other words, ω_{keepdir} acts as a filter smoothing the direction selection process. The selection of an appropriate value for ω_{keepdir} is relatively uncritical as long as no extreme values are selected. In case ω_{keepdir}=0.0 is chosen (which effectively disables this behaviour rule), the movement of the virtual pedestrians will appear unrealistically hectic, but the model itself will still be able to work. On the other hand, a value of ω_{keepdir}=1.0 will promote the objective of keeping the direction equal important to the objective of reaching the destination, which is unrealistic as well, but the modell will still work either. Hence, suitable values for ω_{keepdir} can be expected to lie somewhere between the two extremes.

Figure 27 shows the effect of different values for ω_{keepdir} ranging between 0.0 and 1.0 on the distribution of the agent's moving direction. The data presented are obtained from the simulation using the 10 m wide street case with bi-directional traffic, fine grid resolution and the "Heavy traffic" scenario. To obtain the distribution data, the last registered moving activity was taken from all navigation nodes of the model area (4000 in total). From these data, the amount of agents moving diagonally (directions 2, 4, 6 and 8; compare Fig. 2, p. 9) are the most interesting values. These diagonal movements indicate changes in the agents moving direction (e.g. due to deviation manoeuvers) as normally in this scenario only the movement directions 3 (left to right) and 7

(right to left) occur.

The lower panel in Figure 27 sums up the relative amount of diagonal moves versus different ω_{keepdir} values between 0.0 and 1.0. As it can be seen, the amount of direction changes drops significantly from about 40% for ω_{keepdir}=0.0 to values between 10 and 15% for ω_{keepdir} values above 0.0. There is only little difference for values between 0.2 and 0.8. Remarkably, for the value of ω_{keepdir}=1.0, the amount of diagonal moves increases again as the objective to keep the moving direction starts to interfere with other conflict avoidance strategies and the agent's moving behaviour gets a stubborn component. In summary, the selection of an adequate value for ω_{keepdir} is uncritical and a default of ω_{keepdir}=0.4 is used in the model.

4.1.8 Conclusions for the street canyon test case

Using the example of a simple street canyon, the basic behaviour of then *PedWalk* model and the influence of the adjustable parameters ω_{rhs} and ω_{keepdir} have been shown. The model has been run using different spatial resolutions with results underlining the importance of selecting an adequate fine grid resolution especially if high-density scenarios are analysed. Despite its significant random component, the obtained results are coherent and follow the results obtained by other models or observation.

Based on numerical test, values of ω_{rhs}=0.8 and ω_{keepdir}=0.4 are suggested as default settings in the model. However, the numerical tests have also shown these parameters only have a minor impact on the main functionality of the model so that they should be regarded as rather cosmetic tuning parameters.

4.2 The crossroads test case

4.2.1 Model layout

The second test case aims to demonstrate the usage of quality assessment values Φ^{q} to influence the moving behaviour of the virtual pedestrians in a slightly more complex environment. The model scenario consists of a symmetric crossroad with two intersecting streets as shown in Figure 28. Each street

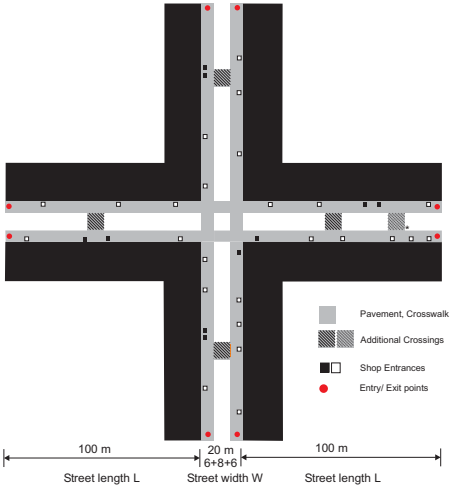

Figure 28: Layout of the model area for the crossroads test case showing the entry/exit points, shop entrances and the location of pavements and the position of the additional crossings.

segment is 100 m long and 20 m wide with entry/exit points at the end. The associated agent release rate is 15 agents per minute for all entry points. In order to generate and distribute traffic inside the model area, 30 routing points representing shop entrances are distributed more or less randomly over the area (little squares in Fig. 28). Analogous to the entry and exit points, these routing points posses assigned frequentation data from which the traffic in the model area is distributed and the trips of the individual agents are generated with a maximum of 5 intermediate targets per agent. The routing points indicated by white squares are representing single shop entrances with frequentation values between 0.2 and 1.0 agents per minute. The filled black squares indicate more popular shops with frequentation values of 2 visitors per minute. To avoid traffic jams, two routing points (=entrances) which can be used alternatively by the agents are assigned to these shops ("*dynamic target swapping*", compare Section 2.1.3.3, p. 8).

The main conceptual difference to the simple street canyon test case in the preceding section is that in this scenario a distinction is made between the pave-

ment area and the road area. The pavement area can be used freely by the virtual pedestrians, whereas the road area will only be entered under certain conditions, namely (like in real life) if crossing the road reduces the walking distance to the next target significantly. To simulate this aspect in the model, a negative (=repulsive) quality assessment value Φ^{q} is assigned to the grid cells and navigation nodes respectively lying inside the road area. The absolute value of this quality assessment can be obtained in many ways. One straight forward solution could be to relate it to the traffic volume Q of the assigned street segment:

$$\Phi^{q}(i,j) = -f\left(Q(i,j)\right)$$

where f is some scaling function transforming the traffic volume into an assessment value. To find an appropriate transformation function, the definition of the assessment values must be kept in mind: Travelling over a grid cell with an assessment value of Φ^{q}= -1 doubles the distance for this section of the path compared to the "real" distance (compare eq. 2.3 p. 11). In other words, crossing a 10 m wide road with Φ^{q}=-1 will only be accepted if the resulting path is at least 10 m shorter than competing paths (this will be illustrated more in detail later on).

For the presented case, we have selected two different quality assessment values for the horizontal and the vertical street representing different traffic volumes and pedestrian crossing possibilities ("*walkability*"): For the horizontal street, a negative quality assessment of $\Phi^{q,0}$=-10.0 (dense road traffic) and for the vertical street $\Phi^{q,0}$=-3.0 (less road traffic) was selected. The selection of these values is relatively arbitrarily, but – as mentioned in Section 2.2, p. 10 ff.– they aim to represent some qualitative behaviour concept rather than some mathematical constant. The quality assessment values are implemented on a global level, hence they are static and apply to all agents in the same way. The impact factor for the walkability quality parameter is set to $\omega_{q,0}$=1.0, which means that this aspect is very important for all agents.

The additional crossings shown in Figure 28 are only inserted into the model area for the numerical test presented in Section 4.2.3, p. 45 f.

4.2.2 Analyses of the influence of $\Phi^{q,0}$ on the routing choice

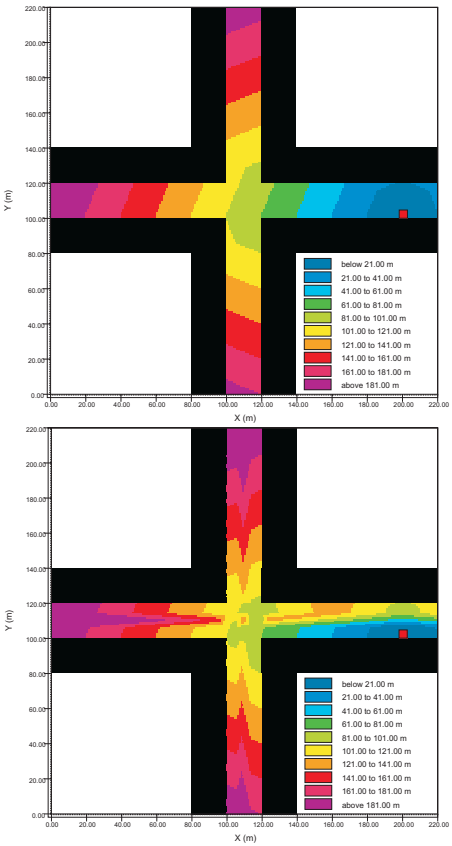

Figure 29: Distance maps for the crossroad test case. The routing target is indicated with the red square. The upper figure shows the real walkable distance Ξ, the lower figure displays the associated Virtual Distance Map Ξ^{v} taking into account the local quality assessment values.

Figure 29 shows as an example the real walkable distance (upper figure) and the associated Virtual Distance Map Ξ^{V} (lower figure) for the routing target indicated by the red square. The real walkable distance takes into account non-passable objects (buildings in this case) but no further quality information which results in a rather simple spatial distance distribution. In contrast, the structure of the Virtual Dis-

tance Map is remarkably more complex. Here, the local quality assessment values are also taken into account when calculating the least possible distance from each point of the model area towards the selected target.

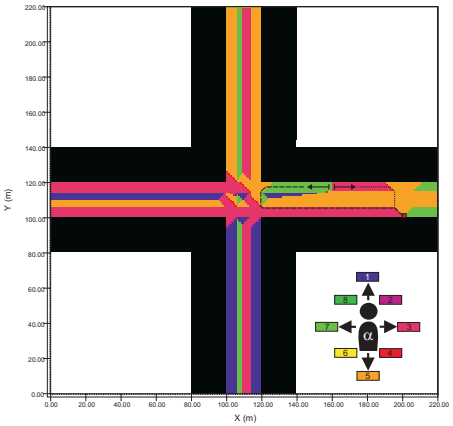

Figure 30: Map of the optimal moving direction from each navigation node to reach the routing target while minimizing the virtual distance walked. Two example paths are shown to illustrate the effect of local quality assessment values on the routing decision.

To understand the effect of the local assessment values Φ^{q} more in detail, Figure 30 maps the optimal moving direction from each navigation node to reach the routing target while minimizing the virtual distance. The optimal moving direction for a navigation node is derived directly from the Virtual Distance Map by calculating the routing assessment $\Phi^{0}(\alpha)$ for all 8 possible moving directions and then select the best available direction. This process is analogous to the selection of navigation nodes as shown in Section 3.3, p. 25 except that no further behaviour rules and interactions are considered. If no further interactions with other agents exist, the optimal path (=the path minimizing the virtual distance walked) towards the routing target could be obtained directly from Figure 30 by following the suggested moving directions from grid cell to grid cell.

Figure 30 can also be used to discuss the effects of the selected quality assessment values on the routing decision. For that, two different paths leading towards the example target are marked. Path one (broken line) leads towards the target without entering any road area whereas path number two (dotted line) crosses the horizontal road. Both paths represent optimal routes towards the target. Which of both would be selected by an agent depends on the actual position of the agent when selecting the target. The threshold position for selecting the one or the other is clearly visible and marked at x=160 m.

In this example we have chosen a quality assessment value of $\Phi^{q,0}$=-10.0 for the horizontal road with a width of 8 m. This lengthens all paths crossing the road perpendicularly from 8 m (real distance Δ) to 10·8+8=88 m (virtual distance Δ^{v}), hence the road will only be crossed if all other alternative paths are at least 80 m longer.

Comparing this calculation to the path constellation illustrated in Figure 30, the route avoiding the road area is about 130 m long at the threshold point. As it does not use navigation nodes with extra quality assessment values, these 130 m are identical to the real walkable length of this path. Contrary, from the same starting point, the length of the alternative path crossing the road is only about 50 m in real distance, but as it includes the road segment, another 80 m have to be added to obtain the relevant virtual distance. So, in total the length of this path is about 130 m in virtual distance as well, which explains the position of the break even point between the two alternative walking possibilities.

4.2.3 Analysis of pedestrian movement patterns and re-design suggestions

Figure 31 (top) shows traffic distribution inside the test area after one hour of simulation time. The maximum traffic is about 180 agents in the core region of the area and falls down to 20 agents and lower in the far ends of the crossing streets. The different quality assessments of the horizontal and the vertical street are also reflected by the amount of agents crossing the road uncontrolled outside the ”legal” (=paved) areas in the center of the crossroad: Along the vertical street, especially in the upper street arm, agents are crossing the street at several positions whereas in the horizontal street, uncontrolled street crossing is limited to a few sections of the street.

One question that might be of interest for urban planers concerned about the health of pedestrians

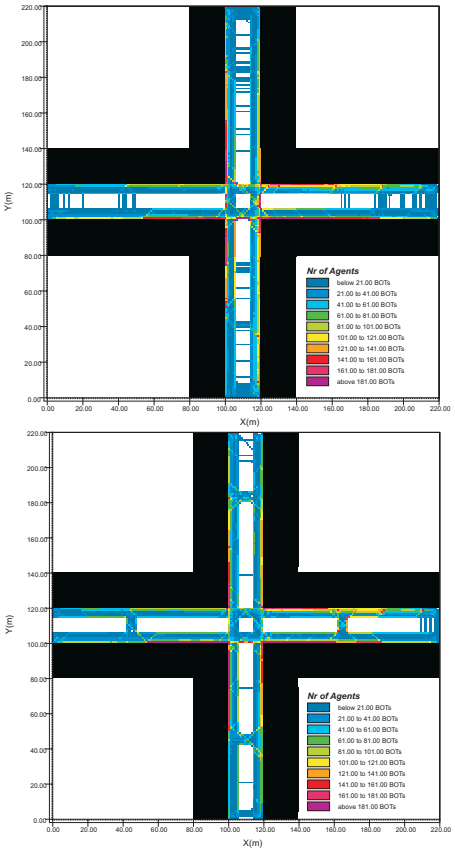

Figure 31: Traffic distribution in the crossroad scenario without (top) and with (bottom) additional crosswalks. Traffic is counted in number of visiting agents per navigation node in one hour of simulation time.

(or interested in undisturbed traffic flows) might be, how the placement of additional crossings influences the crossing behaviour of the pedestrians. Figure 31 (bottom) shows the simulation results in case of additional crosswalks in the model area (compare Fig. 28). In this first design scenario, a symmetric distribution of the crossings (excluding the crossing marked with "*").

For the left arm of the horizontal road, the new crosswalk reduces the amount of pedestrians crossing the

Figure 32: Traffic distribution in the crossroad scenario with a shifted crossing. Traffic is counted in number of visiting agents per navigation node in one hour of simulation time (same color scale as in the preceding figure).

road just as they like to zero. On the right arm of the same street there is still some considerable crossing activity at the end of the street, that should be regarded further. On the vertical street, the effect of extra crosswalks is more limited. The additional crossings attract pedestrians to some extend, but the area of influence is more limited compared to the horizontal street, uncontrolled crossing still exists at several positions of the street. This effect is logical and agrees with daily observations: The desire to use the official crossings decreases rapidly as the chances to cross the street unharmed or without long waiting periods increase.

With respect to the remaining crossing activity on the end of the right arm of the horizontal street, the question arises, if a different position of the crosswalk would improve the result. To test the assumption, the crossing right was shifted to the position indicated with "*" in Figure 28.

Figure 32 shows the resulting traffic in the horizontal street with the modified crossing position. As it can be seen, all pedestrians now use the installed crossings so that with no doubt this scenario is a better design solution for the analysed traffic situation.

4.2.4 Conclusions for the crossroads test case

By the example of a simple symmetric crossroad the influence of local quality assessment values on the routing choice was discussed theoretically and compared to model results. It was shown how the concept

of quality assessment values can be used to influence the routing decisions of the agents on a ”soft” basis by integrating the additional routing information dynamically into the decision process without modifying the basic behaviour rules.

Using two different quality assessment values for the horizontal and for the vertical street, the impact of the numerical value for $\Phi^{q,0}$ on the model results was shown. Admittedly, a simple and catchy example has been chosen here in order to present the general model mechanism. But the same principle can be used to analyse even more complex systems where the spatial relationship between the pedestrian walking routes and the environmental infrastructure is less obvious. A comparable example for such a study might be the analysis of the pedestrian behaviour at Trafalgar Square and the suggestion of re-design possibilities as done by Hillier et al. (1998) using their *Space Syntax* approach (Hillier et al., 1993).

5 Final conclusions

In this paper, the theory and application of the Multi-Agent model *PedWalk* for the simulation of pedestrian traffic in complex urban microscale environments has been presented. The basic behaviour rules driving the microscopic pedestrian traffic dynamics have been identified and been transformed into suitable numerical algorithms. Using the concept of assessment values and the Virtual Distance Metric, the outcomes of the different behaviour rules have been transformed into a numerical range between -1 (maximum negative assessment) and +1 (maximum positive assessment). The main advantage of this approach is that the *PedWalk* model remains open to add further assessment values e.g. obtained by assessing the environmental quality into the decision process without modifying the model logic.

As far as the selection of the crisp numerical values of these assessment parameters is concerned, it could be argued that their selection is relatively arbitrary and subjective. This is correct on the one hand, but, on the other hand, that does not mean that the operations, the whole simulation model or the results produced are arbitrarily – they are not, as long as the application of the numerical rules is consistent and standard mathematical functions are used. It has to be admitted that this point of view might appear strange at the first view, especially to scientists used to work with ”exact” physical models, but, as noted before, the main objective of the assessment values is to transform quality statements into a numerical scale so that they can be processed through numerical methods.

Using the demonstration cases of a simple street canyon and a symmetric street intersection, the performance of the model and the impact of different model parameters on the results have been shown.

The ability of the model to include additional quality information into the routing decision have been demonstrated in the last case study. In this example, the quality assessment values were assumed to be constant and explicitly known. In more complex model applications, these values might as well be calculated from a set of external parameters taking also into account the actual state of the individual agent.

Obviously, a simulation model for pedestrian traffic can only capture very basic features of the complex mechanisms that produce the patterns in human behaviour we observe day by day. Many other aspects play a role when trying to compare the behaviour predicted by a relatively simple model with the situation from the next street corner. This is true for all kind of models, but especially for those models where single human behaviour is in the focus of the calculations.

When reading the text, applying the model and analysing the results, it must be kept in mind that this is a tool designed to gather different assumptions and rules about pedestrian movement and integrate them in a consistent way using mathematics – not more, not less. It does not aim to reproduce every single situation found in urban pedestrian traffic, but it should be a good tool to analyse the complex spatial and temporal interactions between the virtual pedestrians and the model environment and to test the impact of changes in the environment on the pedestrian traffic flows.

References

Al Gahdi, S. and Mahmassani, H. (1991). Simulation of crowd behaviour and movemant: Fundamental relations and application. *Transp. Res. Board*, 1320:260–268.

Batty, M. (2003). CASA Paper 61: Agent-based pedestrian modelling. Technical report, Centre for advanced spatial analysis, University College London, London.

Batty, M., Jiang, B., and Thurstain-Goodwin, M. (1998). CASA Paper 4: Local movement: Agent based models of pedestrian flow. Technical report, Centre for advanced spatial analysis, University College London, London.

Bellman, R. (1958). On a routing problem. *Quaterly of Applied Mathematics*, 16:87–90.

Blue, V. and Adler, J. (1998). Emergent fundamental pedestrian flows from cellular automata microsimulation. *Transp. Res. Rec.*, 1644:29–36.

Blue, V. J. and Adler, J. L. (2001). Using cellular automata microsimulation to model pedestrian walkways. *Transp. Res.*, 35b:293–31.

Brilon, W., Großmann, M., and Blanke, H. (1993). *Verfahren für die Berechnung der Leistungsfähigkeit und Qualität des Verkehrsablaufes auf Straßen*. Bundesministerium f. Verkehr, Abt. Straßenbau, Bonn, Bad Godesberg.

Brustedde, C., Kirchner, A., Klauck, K., Schadschneider, A., and Zittartz, J. (2001). Cellular Automaton Approach to Pedestrian Dynamics – Applications. In *Pedestrian and Evacuation Dynamics*. Springer.

Coleman, J. S. (1964). *Introduction to Mathematical Sociology*. The Free Press of Glencoe, New York.

Corbusier, L. (1943). *Le charte d'Athènes*. Paris.

Dijkstra, E. W. (1959). A note on two problems in connexion with graphs. *Numerische Mathematik*, 1:269–271.

Dörner, D. (1993). Wissen, Emotionen und Handlungsregulation oder die Vernunft der Gefühle. *Zeitschrift für Psychologie*, 2:167–202.

Fruin, J. J. (1971a). Designing for pedestrians: A level-of-service concept. In *Highway Resreach Record No. 355: Pedestrians*, pages 1–15. Highway Research Board, Washington, D.C.

Fruin, J. J. (1971b). *Pedestrian Planning and Design*. Metropolitan Association of Urban Designers and Environmental Planers, New York.

Gipps, G. P. and Marksjö, B. (1985). A micro-simulation model for pedestrian flows. *Mathematics and Computers in Simulation*, 27:95–105.

Greenshields, B. D. (1934). A study of highway capacity. *Highway Res. Board*, 14:448–477.

GSS (1997). *London Travel Report 2003*. Transport for London, The mayor of London, London.

Hanking, D. D. and Wright, R. A. (1958). Passenger flows in subways. *Operational Research Quaterly*, 9.

Helbing, D. (1997). *Verkehrsdynamik. Neue physikalische Modellierungskonzepte*. Springer, Berlin, Heidelberg.

Helbing, D. (2001). Die wundervolle Welt aktiver Vierteilchensysteme. *Physikalische Blätter*, 1:27–33.

Helbing, D. and Molnár, P. (1995). Social force model for pedestrian dynamics. *Physical Review*, E51:4282.

Henderson, L. F. (1971). The statistics in crowd fluids. *Nature*, 229:381–383.

Henderson, L. F. (1974). On the fluid mechanics of human crowd motion. *Transportation Research*, 8:509–515.

Higgins, D. (2002). Generic A* Pathfinding. In Rabin, S., editor, *AI Game programming wisdome*, pages 114–121, Hingham, Massachusetts. Charles River Media.

Hillier, B., Hanson, J., Grajewski, T., and Xu, J. (1993). Natural movement: Configuration and attraction in urban pedestrian movement. *Environment and Planing B*, 20:29–66.

Hillier, B., Stonor, T., D., M., Major, and Spende, N. (1998). From research to design: Re-engineering

the space of trafalgar. *Urban Design Quarterly*, 68.

Jennings, N. R., Sycara, K., and Wooldridge, M. (1998). A roadmap of agent research and development. *Autonomous Agents and Multi-Agent Systems*, 1:7–38.

Jiang, B. (1999). SimPed:Simulating Pedestrian Flows in a Virtual Urban Environment. *Journal of Geographic Information and Decisionanalysis*, 3(1):21–30.

Kulka, R., Willis, A., Hine, J., and Kerridge, J. (2002). PEDFLOW: Development of an autonomous agent model of pedestrian flow. In *Transportation Research Record 1774*, pages 11–17, Washington, D.C. TRB,National Research Council, Transportation Research Board.

Kulka, R., Willis, A., and Kerridge, J. (2003). Application of context-mediated behavior to a multi-agent flow model (pedflow), revised version. In *Transportation Research Board 82nd annual meeting*, Washington, D.C. TRB, National Research Council, Transportation Research Board.

Lewin, K. (1951). *Field theory in Social Science*. Harper and Brothers, New York.

Lovas, G. G. (1994). Modelling and simulation of pedestrian traffic flow. *Transp. Res.*, 28b:429–443.

Matthews, J. (2002). Basic A* Pathfinding made simple. In Rabin, S., editor, *AI Game programming wisdome*, pages 105–113, Hingham, Massachusetts. Charles River Media.

Molnár, P. (1996). Microsimulation of pedestrian dynamics. In Doran, J., Gilbert, N., Müller, U., and Troitzsch, K., editors, *Social Science Microsimulation*. Springer, Berlin.

Muramatsu, M. and Nagatani, T. (2000a). Jamming transition in two-dimensional pedestrian traffic. *Physica*, 275:281–291.

Muramatsu, M. and Nagatani, T. (2000b). Jamming transition of pedestrian traffic at a crossing with open boundaries. *Physica*, 286:377–390.

Nagel, K. (1996). Particle hopping models and traffic flow theory. *Physical Review*, E53:4655–4661.

Nagel, K. and Rasmussen, S. (1994). Traffic at the edge of chaos. In *Artificial Life IV: Proceedings of the 4th international workshop on the synthesis and simulation of living systems*, pages 222–225. MIT Press, Cambridge, Massachusetts.

Nagel, K. and Schreckenberg, M. (1992). A cellular automaton model for freeway traffic. *Journal Physique I France*, 2:2221–2228.

Nash, J. (1950). The bargaining problem. *Econometrica*, 18:155–162.

Navin, F. P. D. and Wheeler, R. J. (1969). Pedestrian flow characteristics. *Traffic Engineering*, pages 30–36.

Oeding, D. (1963). Verkehrsbelastung und Dimensionierung von Gehwegen und anderen Anlagen des Fußgängerverkehrs. *Straßenbau und Straßenverkehrstechnik*, 22.

Older, S. J. (1968). Movement of pedestrians on footways in shopping streets. *Traffic Engineering and Control*, 10:160–163.

ONS (2001). National travel survey: Technical report 2000. Technical report, Office for National Statistics, London.

Prigogine, I. and Herman, R. (1971). *Kinetic theory of vehicular traffic*. American Elsevier, New York.

Pushkarev, B. and Zupan, J. (1975). *Urban Space for pedestrians*. The MIT Press, Cambridge, Massachusetts.

Reynolds, C. W. (1987). Flocks, Herds, and Schools: A distributed behavioral model. In *Computer Graphics 21(4): SIGGRAPH 87 Conference Proceedings*, pages 25–34, Anaheim, California. http://www.red.com/cwr/boids.html.

Reynolds, C. W. (1999). Steering behaviors for autonomous characters. In *Conference Proceedings of the 1999 Game Developers Conference*, pages 763–782, San Jose, California, http://www.red.com/cwr/steer/. Miller Freeman Game Group.

Sandahl, J. and Percivall, M. (1972). A pedestrian traffic model for town centers. *Traffic Quarterly*, 26:359–372.

Scheflen, A. E. and Ashcroft, N. (1976). *Human Theories: How We Behave in Space Time*. Prentice-Hall, Englewood Cliffs.

Schelhorn, T., O'Sullivan, D., Haklay, M., and Thurstain-Goodwin, M. (1999). STREETS: An agent-based pedestrian model. In *Computers in Urban Planing and Urban Management*, Venice, 8-10 September.

Schweitzer, F., Lao, K., and Family, F. (1997). Active random walkers simulate trunk trail formation by ants. *Biosystems*, 41:153–166.

Stilitz, I. B. (1969). The role of static pedestrian crowds in crowded spaces. *Ergonomics*, 12:821–839.

TRB (2000). *Highway Capacity Manual*. Transportation Research Board, Washington D.C., 4th edition.

Treiber, M., Hennecke, A., and Helbing, D. (2000). Conguested traffic states in empirical observations and microscopic simulations. *Phys. Rev.*, E62:1805–1824.

UK Department of Environment (DoE) (1996). *Planing Policy Guidance: Town Centers and Retail Developments*. Office of the Deputy Prime Minister, Department of Environment (DoE), London.

Weidmann, U. (1993). Transporttechnik für Fußgänger. In *Schriftenreihe des Instituts für Verkehrsplanung, Transporttechnik, Straßen- und Eisenbahnbau*. ETH Zürich.

Weiss, G., editor (2000). *Multi Agent Systems*, Cambridge, London. The MIT Press.

Wolff, M. (1973). Notes on the behaviour of pedestrians. In *People in places: The sociology of the familiar*. Praeger.

Zadeh, L. A. (1978). Fuzzy sets as a basis for a theory of possibility. *Fuzzy Sets and Systems*, 1:3–28.

Part III
Appendix

A Generating the virtual distance map Ξ^v

Although it is mathematically easy to calculate the virtual distance $\Xi^{\mathrm{v}}(i,j)$ of a point i,j once the quality assessment values are known, the task of creating the virtual distance map is far from being trivial, as there is normally more than just one possible combination of navigation nodes to get from $\Pi_{\mathrm{i,j}}$ to Π^*. In order to reproduce a logical behaviour of the agent, the virtual distance values of the nodes must always be based on the shortest (=best, as we use Δ^{v} instead of the real distance) possible route towards the destination node.

If the quality assessment of one or more nodes in the network change, the virtual distance value of all nodes connected to those nodes will change, too. As a consequence, routes that have been selected as the optimal paths towards the destination node may no longer be the best choice and it has to be checked, if alternative node combinations exists that might offer a more attractive connection to the destination node. If obstacles (non-passable nodes) exist in the map, these alternative paths might be totally different to the initial one.

The problem hidden behind this task is known as the *Shortest–Path–Problem* and is one of the classical mathematical problems which can be found in many different spatial or logical questions from finding the way out of a maze over graph theory up to Internet data package routing.

The main issue of path finding problems is not the complexity of the mathematical problem itself, but the huge number of different alternative solutions that have to be considered and compared with each other. A variety of different solution approaches exists to solve this problem numerically, which can be divided roughly into three types of algorithms:

1. Flooding algorithms
2. Heuristic algorithms (A*–Algorithm)
3. Improved single-source algorithms (Dijkstra's Algorithm)

Flooding algorithms like the *Bellman algorithm* (Bellman, 1958) are the most simple way to calculate the best path between two nodes and from the numerical performance point of view very close the worst-case scenario in which all possible connections need

to be checked before being sure that the shortest path has been found. As the name suggests, the main concept of the algorithm is to recursively ”flood” the network of nodes with distance values like flooding an uneven terrain with water: Nodes with a short connection to the source (=destination node) are flooded first, whereas nodes further away stay ”dry” for a longer time. Each time a new node is flooded, the distance value used is increased by a certain value as given by a cost function (compare eq. 2.3). Nodes which already hold a distance value that is lower than the value intended to be assigned remain unchanged because they are obviously already connected over a shorter path with the source of flooding.

The best route from any node inside the system to the destination node can then be found by simply connecting to the neighbouring node offering the best (=lowest) distance value and proceed until the destination node is reached. Flooding algorithms belong to the group of single-source approaches, which means they calculate the distance between the destination node and all other nodes in the system in one run. As each grid cell in the *PedWalk* model must be accompanied by a navigation node, the amount of nodes needed is very large. As speed and memory performance are crucial factors for the selection of the path finding algorithm and simple flooding algorithms fail to provided both of it, they are not a practical approach for this model.

Heuristic algorithms normally show a much better performance than flooding approaches because some prior estimate (”*heuristic*”) about the best path is used to optimise the search process. The so-called *A* (”A–Star”) algorithm* is probably the most prominent heuristic algorithm today and is implemented in a wide range of applications from computer games to car navigation systems (Higgins, 2002; Matthews, 2002). A* is an extremely fast algorithm and optimisations exist for almost all kind of problems. As a consequence of the heuristic approach A* estimates only the distance values of nodes belonging to the anticipated optimal path towards the destination node (”point-to-point algorithm”), the $\Xi^{\vee}$ values of nodes not belonging to this route remain unknown. Depending on the application, this might be sufficient, but in the context of the *PedWalk* model it imposes difficulties into the model that overrule the speed advantages of the algorithm. As shown in Figure 7 on page 13, normally more than one path of equal or almost equal quality exists from the starting node (green) to the destination node (red). A* would only return one path of them, for example the route highlighted in Figure 7. If one of the navigation nodes of this route becomes temporarily unavailable, for example because another agent is standing on this node, a complete new run of A* is necessary because no virtual distance information of the neighbouring alternative nodes have been calculated.

This brings finally the **Dijkstra’s algorithm** (Dijkstra, 1959) into play which is the algorithm selected for the *PedWalk* model. This algorithm is also based on the concept of flooding the node network, but uses two lists to optimize the flooding process. The Dijkstra algorithm is not as highly optimised as A* (A* builds up on the Dijkstra approach) but is still remarkably fast. As it is based on the flooding concept, it belongs to the group of single-source algorithms and returns the complete $\Xi^{\vee}$ matrix as shown in Figure 6 on page 13 in one run. If a node along the route becomes unavailable, the agent simply needs to check for the second best available navigation node to move to and finds the route to the destination node without re-running the algorithm.

B Agent object structure

This section lists the main properties and the interfaces of the methods of the *PedWalk* agent (BOT) implementation in the BOTworld system.

B.1 Properties

```
// ID that is unique to this BOT
myID:                 Integer;
// Color for graphical display
mycolor:              Integer;
// The given name of the BOT (taken from boysnames.txt and girlsnames.txt)
BOTName:              string;
// BOT sends output to a Stringlist via
hasconversion:        Boolean;
// active (True) or to-be-removed (False)
alive:                Boolean;
// Recent grid point position
Position:             TGridPos;
// fine x/y- position in meter assigned grid point
// (negative before passing the center)
deltax_m:             Single;
deltay_m:             Single;
// optimum position to recent target so far (reflective assessment)
MybestR:     Single;
// Co-ordinates of next grid point to move to
NextPosition:         Tgridpos;
// Pointer to exit point in global Routingpointlist
ExitPointIndex:     Integer;
// Pointer to my start point in global Routingpointlist
StartPointIndex:    Integer;
// Nr of targets in MyRoutingpointlist to be visited
NrTargets:            Integer;
// coords of the next target to move to
NextTargetCoords:     Tgridpos;
// explicit name of next target (string)
NextTargetName:       string;
// pointer to next target in the global (!!)  list RoutingPointList
NextTargetIndex:      Integer;
// pointer to next target in agents personal MyRoutingpointlist
NextMyTargetIndex:  Integer;
// true if next target is the final target before end
NextTarget_Exit:      Boolean;
// List of targets the BOT is going to visit...
//   .Targetindex  Pointer to this target in gobal list
//   .ActDistance  actual distance this target
//   .Visited      flag target visted?
MyRoutingpointlist:array[1..maxBOTTargets] of Record
                      Targetindex:Integer;
                      ActDistance:Single;
                      Visited:Boolean;
                      end;

// Variables for operating BOT inside of building
isInBuilding:        Boolean;
TimeInBuilding:      Single;

// Properties handling group interactions
// is BOT part of a multi-BOT group?
```

```
groupmember:          Boolean;
// ID of assigned group (=generation time in seconds)
groupID:              Integer;
// Flag for recent group dynamic mode
groupMode:            Integer;
// actual level to define successor-predecessor links
grouplevel:           Integer;
// index of the BOT that is the predecessor (0 if none)
predecessor,
// index of predecessing BOT (0 if none)
successor:Integer;

// Movement management
// Direction of actual move (ID see code)
MoveDir:              Integer;
// the last valid move dir (direction that wasn't standing)
lastValidDir:         Integer;
// True if last move had different direction than before
MoveChangedDir:       Boolean;
// counter in sec how long BOT stands still
// (will be decreased gradually as moving again)
StandingTime:         Single;
// True if the last move was the optimal choice
LastMove_BestMove:    Boolean;
// Random value between -0.5 (nearly never overtake)
// and +0.5 (nearly always overtake)
conflictPersonality: Single;
// Result of last overtaking decision
// 1: taken, -1: disclaimed
overtakingdecision:Integer;

// counter for standing-and-do-nothing
// if not zero, BOT stand still and decreases counter
timeout:              Single;
// Index of other BOT this BOT has talked to last time
lastTalkedTo:        Integer;
Talking:             Boolean;
nrknownBOTs:         Integer; // nr of BOTs in list of known BOTs

// List containing indices of known BOTs in the model
// used to decide if to talk to a BOT or not
ListKnownBOTs: array[1..MaxNrKnownBOTS] of Integer;

// Total life time of BOT since creation ( insec)
totaltime:            Single;

// General movement
// True if the next target grid is already entered
// (more than 50% of the distance is made)
nextgridentered:      Boolean;
// Distance moved since leaving the last grid
TotalDistanceMoved:   Single;
// distance to next target grid point in m
distanceToNextPoint:  Single;
// prefered walking speed if not disturbed
v_pref:               double;
// actual speed
v_act:                double;
// actual change of velocity (+:accelerate, -:decelerate)
dvdt:                 double;
```

```
// flag for "impatient" mode
impatient:            Boolean;
// time lost due to slower than desired velocity
losttime:             double;

// 2D fields that belong to the agent
// Actual virtual distance
VirtualDistance:   Array[1..Max_X,1..Max_Y] of Single;

// Time series logs
// nr of samples stored in MYdata
nrdatasamples:         Integer;
// second of modeltime, when the last sample was taken
// (used as countdown to determinate the next storage process)
lastsample:            Single;

// Main data structure in which the BOTs data will be saved during
// life cycle
// and written to Masterfile after reaching the final target
MyData: array[1..MaxSamples] of TclimBOTDatalog;
// History of Targets visted by BOT
NrTargetHistory: Integer;
TargetHistory: Array [1..MaxBOTTargets] of record
                       TargetPosition:TGridPos;
                       TargetName:String[20];
                       end;
```

B.2 Methods

```
// Routing and basics
// [BOT_basics] Creates BOTobject, inits all values except myID
Procedure SetInitialData;
// [BOT_basics] Ends the BOT object and releases list place
procedure QuitBOT;
// [BOT_basics] adds dt seconds time to the BOT
// (BOT walks, selects new targets etc
procedure Addtime(dt:Single);
procedure FindNextWayPoint;
// [BOT_routingmanage] Looks for and selects a closer alternative
// target from the actual one
Procedure ClearReservedGrids;
// [BOT_routingmanage] Clears all BOTposition except grid with BOT
function LookForAlternativeTargets:Integer;
// [BOT_RRoutines] copy pre-calculated R-fields into the BOTs memory
Procedure CopyWay(TargetIndex:Integer);
// [BOT_basics] Moves BOT to _pos. If _pos is not valid,
// BOT will be put to the closest possible location
Procedure SetPos(_pos:Tgridpos);
// [BOT_routingmanage] select next target out of list of targets
procedure SelectNextTarget;
// [BOT_routingmanage] resturns true if BOT has reached the assigned target
Function ReachedTarget:Boolean;
// [BOT_basics] Checks if position posi,posy is inside the model area
Function IsinArea(pos_i,pos_j:Integer):Boolean;
// [BOT_basics] Checks if the BOT is standing on grid _pos
Function IsOnGrid(_i,_j:Integer):Boolean;overload;
Function IsOnGrid(_pos:Tgridpos):Boolean;overload;
// [BOT_basics] Set the BOT to "talking"
procedure SetTalking(Talktime:Single;Talkpartner:Integer);
```

```
// [BOT_basics] End talk
procedure setFinishTalking;
// [BOT_basics] BOT enters building
procedure MoveIntoBuilding;
// [BOT_basics] BOT leaves building
procedure MoveoutofBuilding;
// [BOT_basics] Passes message s with priority level Messagelevel to out wnd
procedure Talk(s:string;Messagelevel:Integer);
// [BOT_basics] Sets a time out time for BOT, in which it does not move
procedure SetTimeout(_time:Single);
// [BOT_routingmanage] Removes BOT from _pos. Deletes conflict zone
procedure LeaveLocation(_pos:Tgridpos);
// [BOT_routingmanage] Enters BOT onto new location,
procedure EnterLocation(_pos:Tgridpos);
// [BOT_routingmanage] Plans route to the next target
procedure PlanRoute(_TargetIndex:Integer);
// [BOT_routingmanage] Generates the best way to the target
Procedure GenerateWay_Dijkstra(target:TGridPos;routeonly:Boolean);

// Display
// [BOT_graphics] Returns the property value according to _datatype
function GetDisplayedBOTProperty(_datatype:Integer):Single;
// [BOT_graphics] Draws the BOT to the screen
procedure DrawBOT;
// [BOT_graphics] Draw the BOT vector shape (used by @link(DrawBOT) method)
procedure DrawVectBOT(bodycolor,headcolor:Integer;
                      showMintrigger,showMaxtrigger:Boolean);
// [BOT_graphics] Removes BOT from screen
procedure DeleteBOT;

// Groups and other BOTs
// [BOT_managegroups] Removes BOT from a group
Procedure DelBOTfromGroup;
// [BOT_basics] Stores actual data (position, velocity) of BOT,
//             (Store_Biometdata)
procedure StoreData;
// [BOT_RRoutines] Generates new conflict zone. Called in (EnterLocation) event
procedure GenerateConflictzone;
// [BOT_RRoutines] Removes BOTs conflict zone. Called in (LeaveLocation) event
procedure RemoveConflictZone;
// [BOT_RRoutines] adjusts the conflict zone to new speed
// (checks is v_act has changed more than 0.2 m/s)
procedure UpdateConflictZone;
// [BOT_dynamics] Searches for another BOT in direction searchdir.
//  Returns distance and BOTindex if found or distance=-1 if no BOT found
Procedure GetDistanceToNextBOT(searchdir:Integer;
                               maxDistance:Single;
                               VAR distance:Single;
                               VAR BOTindex:Integer);
//  [BOT_basics]
//  Calculates simple euklidian distance from this BOT to BOT(_index)
//  distance is exact including fine dx,dy position
//  Returns -1 if BOT(_index) is not in list
//  Returns -2 if BOT(_index) is not alive }
function GetDistancetoIndexBOT(_index:Integer):Single;

// [BOT_basics]
//  Calculates the angel from BOT to BOT(_index)
//  0/360 is north
//  Returns -1 if BOT(_index) is not in list
```

```
//  Returns -2 if BOT(_index) is not alive }
function GetAngletoIndexBOT(_index:Integer):Single;

// Velocity
// [BOT_dynamics] Calculates change in speed due to other BOTs in the way
function GetDynamic_dvdt:Single;
// [BOT_dynamics] Calculates change in speed due to group coordinating
function GetgroupDynamic_dvdt:Single;
```


B

Module B

Simulating human thermal comfort in urban outdoor spaces using a simple dynamic model of the human thermoregulatory system linked to a Multi-Agent model system

Attractive public open spaces can serve as key design elements for enhancing life quality in urban areas and to diminish the negative effects of urbanisation. In order to fulfil this task and to serve as small oasis inside an artificial environment, open spaces must meet the expectation of potential users and offer the right mix of environmental, economic and social conditions. It is known that the microclimate conditions belong to the main factors driving the individual perception and assessment of an outdoor environment. The right mix of sun and shade or the shelter from wind – pleasant conditions will attract people who, in return, will make these areas more attractive for shops, restaurants or other facilities depending on pedestrian frequentation.

Traditionally, static indices like PMV are used to express the impact of local climate onto the thermal comfort of humans exposed to these conditions. These indices relate the average thermal comfort more or less directly to the local meteorological conditions assuming a balanced energy budget of the human body. However, under the complex and varying microclimate conditions found in urban areas, the response of the human thermoregulatory system is normally far from reaching equilibrium energy conditions, hence the assessment found by static indices often overrate the local conditions. Dynamic Multi-Node models of the human thermoregulatory system are a better approach to simulate the reaction of the human body on varying climate exposures. As these models are individual based, they are also able to simulate different human characters such as age, weight or climate adaptation which is not possible with community indices like PMV. In order to be practically applicable, Multi-Node models must be integrated into a computational framework which generates typical pedestrian movement patterns through the urban environment and provides the biometeorological models with the required microclimate data as input. One elegant way to construct such a system is to link the individual based thermal comfort model to a Multi-Agent Simulation system. In such a system, software agents take the role of the virtual humans moving through the model environment and different microclimate conditions while their thermal comfort is monitored constantly.

In part I of this paper, a simple dynamical Multi-Node model of the human thermoregulatory system (ITCM) is presented and it is shown, how this model can be linked with the Multi-Agent simulation system BOTworld. Example results are shown in part II and it will be discussed how and if these dynamical model helps to gain a better insight into the complex system of outdoor thermal comfort.

Keywords: Human thermal comfort, Multi-Node model, Human thermoregulatory system, Outdoor thermal comfort, Multi-Agent simulation, Microclimate, Individual based thermal comfort, PMV

Contents

List of Figures

List of Tables

Main Symbols (Alphabetical Index)

Main Symbols ITC Model		
Symbol	**Unit**	**Meaning**
A_{du}	m^2	Surface area of the body (*DuBois Area*)
A_{cl}	m^2	Surface area of the cloths
A_{sk}	m^2	Surface area of the unclothed body parts
ag	y	Age
BMI	-	Body Mass Index
C_{cl}	Wm^{-2}	Convection from the cloths
C_{sk}	Wm^{-2}	Convection of the skin
clo	clo	Static clothing insulation
c_p(Body)	$\text{Jkg}^{-1}\text{K}^{-1}$	Specific heat of human body
e_a, e^*	hPa	Vapour pressure of air and saturation vapour pressure
f_{cl}	-	Increase factor of surface area due to cloths
%fat	%	Percentage fat in body tissue
$G_{\text{sk-cl}}$	Wm^{-2}	Conduction between skin and cloths
h_c	$\text{Wm}^{-2}\text{K}^{-1}$	Convective heat transfer coefficient
h_e	$\text{Wm}^{-2}\text{hPa}^{-1}$	Convective vapour transfer coefficient
ht	m	Body height
$I_{\text{cl}}^{(s)}$	Km^2W^{-1}	(Static) intrinsic clothing insulation
$i_m^{(s)}$	-	(Static) vapour permability index of the cloths
LE	Wm^{-2}	Latent heat flux from skin
M	Wm^{-2}	Metabolism
m_d	$\text{kgm}-2\text{s}^{-1}$	Actual diffusive vapour flux
m_{pot}	$\text{kgm}^{-2}\text{s}^{-1}$	Potential transpiration vapour flux
m_{trans}	$\text{kgm}^{-2}\text{s}^{-1}$	Actual transpiration vapour flux
$Q_{\text{co-sk}}$	Wm^{-2}	Energy flux between core and skin
$Q_{\text{st,sk}}$	W	Energy stored in skin layer
$Q_{\text{st,core}}$	W	Energy stored in body core
R_{blood}	m^2KW^{-1}	Resistance of blood circulation to heat transfer
R_{tissue}	m^2KW^{-1}	Resistance of body tissue to heat transfer
R_{cl}	Wm^{-2}	Radiative budget of the cloths
R_{sk}	Wm^{-2}	Radiative budget of the skin
R_T	$\text{m}^2\text{hPaW}^{-1}$	vapour resistance of clothing
r_{cl2sk}	-	Ratio between clothed and unclothed surface area
SF	mm	Skinfold thickness
SW	kgm^{-2}	Amount of sweat on skin
sex	[male,female]	Gender
T_a	°C	Air temperature
T_{core}	°C	Core temperature of human body
T_{cl}	°C	Average clothing temperature
T_{mrt}	°C	Mean radiant temperature
T_{sk}	°C	Average skin temperature
W_{sk}	gh^{-1}	Amount of water lost through skin
W_{resp}	gh^{-1}	Amount of water lost through respiration
W_{ges}	gh^{-1}	Total water loss
$\dot{V}$	$\text{l min}^{-1}\text{m}^{-2}$	Ventilation rate
V_B	$\text{lm}^{-2}\text{h}^{-1}$	Blood volume transported into the peripheral tissue
v_{act}	ms^{-1}	Actual walking velocity
v_{wind}	ms^{-1}	Local wind speed
v_{wrel}	ms^{-1}	Local wind speed relative to moving agent
wg	kg	Weight
Γ	%	Fraction of wet skin
χ	μgm^{-3}	Local pollutant concentration
$\dot{\chi}_\Sigma$	μg	Inhaled pollutants

Part I
Model Theory

1 Introduction

Urban areas are the home for millions of people spending a substantial amount of their time between buildings, shopping malls and patches of green. Inside this artificial environment, public open spaces can act as vital and pulsating oases, attracting people for all kinds of business or leisure activities. Hence, these areas are an important contribution to improve urban life quality and can help to decrease the negative effects of urbanization.

Designing public spaces that are accepted and used by pedestrians is a challenging task for urban planers addressing a multitude of different architectural, technical and social aspects. One of the key factors determining whether an open space is succeeding or not is the environmental quality offered by the area. The mix of sun and shade, the presence of windy and calm areas, or, in short, the local microclimate is indisputably one of the main factors that drive the users perception of an outdoor space and influence their decision whether to stay or leave (compare Mark, 1987).

In urban areas, the average regional climate conditions are often replaced by heterogeneous and small scale local microclimate environments whose characteristics depend to a huge extend on the environmental design of the surrounding area. The magnitude of different materials used in the urban fabric and the arrangement of buildings, trees and other urban objects modify larger scale climate conditions and can produce typical microscale meteorological effects such as wind speed decrease, local jet effects, increased turbulence or increased thermal loads. Hence, environmental design can be used to shape the local microclimate towards agreeable conditions for the potential users of the open spaces. On the other hand, careless compilation of urban elements can easily create uncomfortable climate conditions and, in return, produce dissatisfied pedestrians or deserted urban areas.

In the context of urban microclimate, *thermal comfort* is the key indicator to describe the comfort of the users of open spaces as it summarizes the impact of sun, wind, air temperature and humidity on the thermal sensation. If the human body is not able to compensate hot or cold environmental conditions through thermoregulation, thermal discomfort arises

and the actual environment is assessed as too warm or too hot.

A sustainable design of urban open spaces is therefore a design, in which the expectations and wishes of the potential users meet with the functional requirements on the city structure. Hence, assessing the microclimate conditions of an urban open space means to find out,

- how the pedestrians feel under given climate conditions (in particular their thermal comfort, wind comfort etc)
- how those feelings will affect their behaviour within the urban structure (routing decision, seating locations,...)
- whether the urban design, the thermal preferences and the behaviour/demands of the citizens fit together or not.

There are a number of studies about the impact of different thermal environments on the human energy balance system (compare Matzarakis, 2001), but relatively few studies analyse the impact of the resulting thermal comfort on the behaviour of the exposed people. In 1971, Gehl (in Westerberg et al., 2003) has provided probably one of the earliest studies on the influence of microclimate on social life by counting people sitting on sunny and on shady benches. More recent studies in which the urban microclimate has been measured and the resulting behaviour of people has been monitored are described by Zacharias et al. (2001); Westerberg and Glaumann (1990); Nasar and Yurdakul (1990) or by Westerberg et al. (2003). The largest recent data pools containing measured microclimate conditions and associated people behaviour are probably the Australian data set collected by Richard de Dear (Potter and de Dear, 2000) and the database collected during the EU-funded RUROS project (Nikolopoulou et al., 2001). [1]

All these studies, as different as they might be in detail, have one idea in common concerning their approach: they focus on the comfort and the behaviour of the single individual to learn about the impact of local climate on the usage patterns of open spaces. This perspective differs to a huge extent from the assumptions made by more traditional assessment approaches such as the outdoor adopted PMV (VDI 3787, 1996) or OUT_SET* (Spagnolo and de Dear, 2003; Pickup and de Dear, 2000) indicators just to name two of them. These indicators, as practical as they might be, are not able to predict human thermal comfort at the scale of the single individual or to consider the time-space links that establish during the movement through the different microclimate conditions.

Recent studies (eg. Nikolopoulou et al., 2001; Potter and de Dear, 2000) have revealed a significant contradiction between the assessment of the local thermal conditions obtained from static assessment methods and those got by interviewing the actual users of open spaces. In fact, in nearly all of the cases, users found the local climate conditions much more comfortable than the assessment by PMV or OUT_SET* would suggest. Understanding and solving this contradiction is a task which has to be approached from at least two sides: On one side, it has to be analysed, if the impact of the thermal environment on the thermoregulatory system and human comfort is correctly represented by the assumptions used in the static indices. On the other side, the question arises, how this thermal comfort influences the assessment and the behaviour of the users of urban open space on the level of the single individual.

This paper focuses on the first of the two points: the calculation of the response of the human body on varying microscale conditions and its impact on the resulting thermal comfort. First, it will be analysed which are the drawbacks of the static thermal comfort indicators and how these problems can be solved using more advanced models such as Multi-Node models of the human thermoregulatory system. The question will be raised, how such individual based models can be applied practically to analyse the thermal comfort of an open space and the application of so-called *Multi-Agent simulation systems* will be suggested as a suitable approach to this problem. The first part of the paper describes the theory of a simple dynamic **I**ndividual based **T**hermal **C**omfort **M**odel (ITCM) and its embedding into the Multi-Agent system BOTworld. In the second part, selected model simulations are presented and the outcomes will be discussed.

1. see website `http://alpha.cres.gr/ruros/`

2 Human thermal comfort: Recent research, problems and potential solutions

2.1 Problems with static thermal indices applied to outdoor conditions

Static thermal indices like PMV (Fanger, 1982) or SET* (Gonzales et al., 1974) are widely used to assess the complex relationship between local climate and the resulting thermal comfort of humans exposed to these conditions. Originally, these methods have been developed for the assessment of homogenous indoor climate conditions, but through the time, several changes and extensions have been introduced to make them also applicable for the heterogeneous and more complex outdoor climate conditions (for example PMV based on VDI 3787 (VDI 3787, 1996; Jendritzky et al., 1990) or OUT_SET* (Spagnolo and de Dear, 2003; Pickup and de Dear, 2000). In addition, a number of more sophisticated models such as the Apparent Temperature (AT) used in the United States and in Australia (Steadman, 1994) or PET (Höppe, 1999) from Germany, just to name two of them, are applied to assess the thermal comfort of outdoor spaces.

In the last years, there has been increased criticism concerning the validity and reliability of static thermal comfort indices in general and on PMV/PPD which is proposed as standard method by ISO 7730 in particular (Olesen and Parsons, 2002; Humphreys and Nicol, 2002). The major points of criticism concerned on one hand the assumption of a balanced energy budget of the human body and on the other hand the oversimplifications used in the method to model the thermoregulatory system. This methodological aspect may explain the observed differences between the calculated PMV values and empirically obtained indices such as the *Actual Mean Vote* (AMV) to some extent (Olesen and Parsons, 2002; Humphreys and Nicol, 2002).

But not only the PMV/PPD method itself (which might be improved somehow) is criticised, there are also doubts that sensible input parameters for the model are obtained in the correct way: Especially the methods proposed to obtain the metabolic as proposed by ISO 8996 (Havenith et al., 2002) and the ISO 9920 method for estimating the clothing insulation values are questioned. For the latter, Holmér et al. (1999) and Havenith et al. (2002, 1999) showed in the framework of the BIOMED-II project that the currently used methods for the estimation of clothing convective and evaporative heat exchange are not adequate for moving persons or if the person is exposed to wind.

Last not least, it has to be mentioned that PMV/PPD and related indices are community-based indicators. Their statements represent average responses of a collective of people. It is almost impossible to analyse the effect of changes in individual body parameters such as acclimatisation or personal preferences on thermal comfort (compare Havenith, 2001, and related).

The observed discrepancies between thermal comfort assessed by static methods (in which *method* refers to the core method as well as to the estimation of the required parameters) become significant whenever the thermal conditions become more complex and dynamic than those observed in air-conditioned buildings or other controlled climate environments. For example, yet the presence of a natural ventilation in a building was found to result in an overestimation of thermal discomfort when using the PMV method (Olesen and Parsons, 2002).

When applying these methods to outdoor conditions, these uncertainties become even bigger, as the violation of the limits of PMV and similar indices (stationary heat balance, no effects of wind and walking, ...) are more the rule rather than the exception. Several studies in urban outdoor spaces have shown, that the thermal comfort predicted by PMV and the actual thermal sensation (ASV) [2] of the users of public open spaces differ significantly from the predicted thermal comfort indices (compare Thorson et al., 2004; Nikolopoulou et al., 2001; Potter and de Dear, 2000; Höppe and Seidl, 1991). This is no surprise as the relative shortness of an average urban outdoor stay plus the exposure to varying microclimate conditions while walking through urban structures makes it unlikely that the human thermoregulatory system reaches steady state conditions at all locations. Figure 1 shows as an example the comparison of the ASV ratings obtained by different interviews over the year with the corresponding PMV values calcu-

2. based on the ASHRAE 7-point scale ranging from -3 (cold) to +3 (hot) (ASHRAE, 1992)

lated using the local meteorological conditions at the outdoor location where the interviews took place.

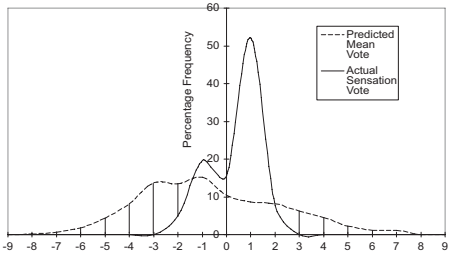

Figure 1: Example comparison between thermal assessment of outdoor locations based on interviews (Actual Sensation Vote ASV) and based on Predicted Mean Vote (PMV) values calculated for the location of the interviews (based on Nikolopoulou et al., 2001).

Höppe (2002) showed, using his model IMEM, that after entering a hot outdoor environment, steady state conditions for the skin temperature are reached after 28 min and for the core temperature after 56 min. This inertia of the human heat balance imposes a significant time-space component onto the thermal assessment process: The perception and assessment of the local climate conditions depends to a high degree on the thermal history (= the thermal conditions the subject was exposed to) of the assessing person. Consequently, the thermal sensation of a moving pedestrian at a location X can only be derived to a certain degree directly from the meteorological conditions at this very place.

Through their movement, pedestrians create linkages between different urban locations and microclimates. In order to asses the environmental quality of a certain location, we need to identify and understand those links. The classical example for such a non-local process is a sunny street segment, on one hand assessed by a person who walked through shade before and on the other hand by a person who has experienced hot conditions before.

When summarising the recent discussion on static thermal indices and the aspects mentioned in this paper so far, three main problems in the context of the assessment of urban outdoor climate can be emphasized:

- The usage of a stationary heat balance is inappropriate for the dynamic outdoor climate conditions in urban areas.
- Dynamic effects of walking and exposure to relative wind speed modify important components of the human energy balance (clothing properties, turbulent heat flux at the skin surface,...) which are not taken into account in stationary models.
- A personalisation of the models based on ISO 7730 to include the individual parameters such as acclimatisation or personal preferences is difficult or impossible.

These problems are known to the scientific community and have, for example lead to the proposal of a new version of ISO 7730 (Olesen and Parsons, 2002) or resulted in the establishment of a special commission of the International Society of Biometeorology targeting the development of a new Universal Thermal Climate Index UTCI (Höppe, 2002). One main step to overcome a number of the problems mentioned above is the application of so-called Multi-Node models which allow a more detailed and dynamic calculation of the human thermal regulatory system, plus, to some extent, a dynamic solution of the human energy balance. This aspect will be analysed in detail in the following section.

2.2 Application of Multi-Node models of the human heat balance

Multi-Node models of the human thermoregulatory system (for simplicity we will include two-node models in this group as they are based on the same principle) simulate the energy exchange processes inside the human body and between the human body and the environment based on the principals of thermodynamics applied to the different components of the thermoregulatory system.

In these models, each calculation node represents a certain component of the human body. Normally, one node is used to model the inner core of the body while the remaining (n-1) nodes are used to represent different skin surface areas of the human body such as hands, arms and legs. Additional nodes can be added to the numerical model to include helper variables such as the clothing temperature, which are required in the calculation process but do not belong

to the human thermoregulatory system, hence they are normally not counted in the node sum.

The first and the probably most well-known node model was introduced by Gagge et al. (1971). This model consists of two nodes, one representing the skin surface and the other node representing the body core. Gagge's initial model has been the fundament for numerous extensions and modifications. Lottens (1993) for example divided the skin surface area into an unclothed and a clothed fraction as well as in an radiated and non-radiated area, summing up to four skin nodes in total versus one node in the original model. Havenith (2001) extended the Gagge model furthermore by introducing additional parameters to consider individual properties such as body composition or acclimatization status.

Fiala et al. (2001, 1999) present another sophisticated model consisting of 21 nodes in the passive system describing the heat transfer through and at the different body components. This model is supposed to serve as the base for the previous mentioned Universal Thermal Climate Index. Finally, the model presented by Tanabe et al. (2002) should be mentioned as it is a fine example for the extensive use of skin nodes (65 in total).

2.2.1 Inherent problems using Multi-Node models

Multi-Node models are a promising approach to capture the dynamics of the human thermoregulatory system with greater accuracy. Those models can be applied even for complex constellations of body parameters or to simulate extreme climate conditions, given that the relevant physical and physiological processes can be formalised through equations. In addition, those models are able to simulate the dynamic character of the human thermoregulatory system, for example when the body is exposed to varying climate conditions and the heat balance does not reach steady-state conditions.

Unfortunately, there are drawbacks inherent to these types of models: Each simulation run of a Multi-Node model calculates the thermal response for the human body for one exactly defined constellation of human and meteorological parameters, or, in other words, the thermal comfort of *one* specific individual exposed to *one* specific climate environment or sequence of climate conditions. The question arises, how it can be possible to scale these calculations up to the community level and to consider inhomogeneous climate environments? Or, from the practitioners perspective, how can a model working on the scale of the individual be used to generate a representative spatial analysis of the thermal comfort conditions in a larger urban area?

One possible solution for the first part of the problem might be to perform a huge number of pre-calculations covering most possible combinations of human factors and meteorological conditions. In case of the Universal Thermal Climate Index, 6930 relevant combinations of meteorological and human parameters have been found (Jendritzky et al., 2002). Compared to the traditional indices such as PMV/PPD, this method would improve at least the general theory behind the methodology, but still a number of drawbacks remain. For example, once the pre-calculations have been finished and the results have been summarised, it is impossible to simulated the effects of a single parameter (e.g. acclimatization) without re-running the complete model set. Also, one of the main problems with static indices identified in Section 2.1, p. 4 remains: The inappropriate assumption of steady state thermal conditions. If a comfort index is based on pre-calculations with some Multi-Node model, it is impossible to include the effects of individual sequences of climate conditions while walking through the urban environment on the thermal sensation.

Even if we condemn the concept of pre-calculating a set of possible thermal comfort scenarios and keep the original Multi-Node model as the core method, there is still the problem to provide this model with the varying meteorological data that it requires as boundary conditions for the energy balance equations. Entering these data by hand might be possible for a few selected scenarios with pedestrians walking on pre-defined routes through the environment, but there is a certain limit on how many pedestrians and routes can be analysed that way.

Höppe (2002) for example used this approach to simulate the effects of entering a single sunny street segment. Also, the *dPET-Walkers* in former versions of the ENVI-met microclimate model (Bruse and Fleer, 1998) provided the option to analyse the impact of local climate on different body parameters for an

explicitly defined person walking on a pre-selected route through the environment. Figure 2 shows the results of such a dPET-Walker and the associated change of skin temperature taken from Bruse (2000).

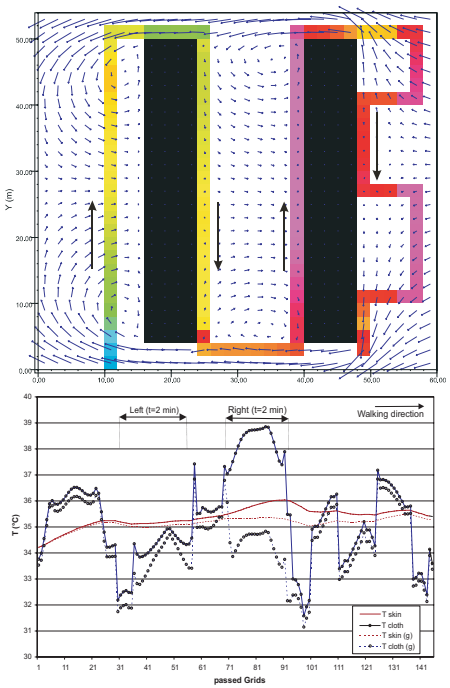

Figure 2: Example result from the so-called dPET-Walker implemented in the ENVI-met microclimate model. The upper panel shows the walker's route through and around a simple street canyon with colours indicating the skin temperature and arrows showing the wind field. The lower panel shows the associated evolution of skin and clothing temperature (T_{skin} and T_{cl}) for a street canyon without and with trees "(g)" (taken from Bruse, 2000).

In conclusion, the method of Multi-Node models of the human thermoregulatory system seems to be the best suitable method to simulate thermal comfort under complex conditions, but it needs to be integrated in a larger system to make it usable.

More precisely, this framework system should:

- automatically generate and run simulations representing different physiological and physical properties of the human body (age, clothing, walking speed) in agreement with the observed community properties,
- consider different pedestrian walking routes through the analysed urban area in order to simulate realistic sequences of exposure to varying microclimates,
- provide a certain level of internal intelligence to keep the model practically applicable. For example it should provide an autonomous routes generation based on some general information.
- be able to manage the required microclimate data and provide them to the Multi-Node model when required,

Fortunately, there is one relatively new approach in numerical simulation techniques that fulfils all these requirements: Multi-Agent systems.

2.3 Multi-Agent systems as simulation framework for individual based thermal comfort models

In Multi-Agent (MA) systems different natural entities such as humans or animals are represented through software "*agents*". These agents have a clearly defined spectrum of properties and methods to interact with the environment and with each other. Although their individual behaviour options are often quite limited, interesting and complex behaviour patterns and simulation results often establish through their iterative interaction and through self-organisation effects. One typical example is the simulation of an ant colony in which each single animal is represented through a software agent. Though each agent has a very limited set of behaviour options (find food, follow other ants, ...), very complex patterns can emerge if a few hundred of these simple ant-agents are released into the virtual software world.

There is an impressive amount of different theoretical approaches concerning the architecture and the classification of Multi-Agent models. In this paper, we will restrict ourselves to those aspects that are relevant in the context of using MA systems to simulate human thermal comfort. For further information, the books from Weiss (2000) and Jennings et al. (1998) are recommended starting points.

Multi-Agent systems offer a very suitable framework to analyse human thermal comfort based on the energy balance of a single individual. Each software agent inside the system represents an user of the urban open space with its own individual physiological and physical properties and equipped with an individualised model of the thermoregulatory system continuously simulating the thermal state of the agent. Based on a personal set of routing destinations, the agent moves autonomously through the model environment and is exposed to different microclimate conditions. The local meteorological conditions are stored as different data layers inside the MA system and provided as boundary conditions to the biometeorological model with respect to the actual position of the agent inside the model area. After simulating a sufficient number of virtual pedestrian routes through the virtual environment, the data generated by the thermal comfort model are gathered and aggregated with respect to the objective of the analysis. Typical aggregation methods are for example spatial aggregation, summarising the state of all agents visiting selected locations of the area, or individual aggregation which reports about the state of all agents at a given time.

Creating such a Multi-Agent model for the simulation of thermal comfort consists basically of two steps: First, the development (or selection) of the Multi-Agent simulation framework which takes care of the different administrative tasks involved in the simulation process and second, the design of the biometeorological model and its implementation into the MA environment.

In the next section, a brief overview over the Multi-Agent system BOTworld is given. BOTworld was developed to simulate the movement and the behaviour of pedestrians in complex microscale urban environments and it serves as the framework system for embedding the **I**ndividual-based **T**hermal **C**omfort **M**odel (ITCM) presented in this paper. Then, in Section 4, p. 10 ff, the design and numerical implementation of the ITCM model is presented.

3 The MA simulation system BOTworld

Hand in hand with the development of the biometeorological model ITCM, the simulation system BOTworld has been created as a framework system focusing on the simulation of pedestrian movement and behaviour in complex urban environments. BOTworld allows to control the movement and location of each single virtual pedestrian with respect to their individual routing plans and the interaction with other virtual pedestrians. Although the BOTworld system has been designed with the intention to provide a model framework for individual based thermal comfort models, it can also serve for other purposes, for example to evaluate microscale pedestrian traffic flows.[3]

Figure 3 shows a simplified scheme of the model system focusing on the **I**ndividual-based **T**hermal **C**omfort **M**odel (ITCM). The urban open space is digitally represented through a horizontal $I \times J$ array of rectangular grid cells, in which each cell i, j has the dimension of $\Delta xy \times \Delta xy$ m^2 summing up to a total model domain of $X \times Y = (I \cdot \Delta xy) \times (J \cdot \Delta xy)$ m^2. As the model focuses on microscale processes and on the individual agent, a fine model resolution is required with cell sizes typically in the range of Δxy= 0.5 to 2 m.

To represent the urban environment, different properties can be assigned to the single grid cells. Most important of these properties are the location of buildings and of non-walkable or less-walkable surfaces (water areas, roads) as these obstacles influence the route selection of the virtual pedestrians. In order to create movement through the environment, routing points representing typical sources and targets of pedestrian traffic are distributed over the model domain for example to simulate building entrances or places where the agents enter and leave the model area. With these data, an individual itinerary is created for each single agent when he is released into the virtual world.

When running the BOTworld simulation, the pedestrian movement model *PedWalk* takes care of a realistic behaviour of the virtual pedestrians: It calculates the optimal routes from routing target to routing target, navigates the agents through the model world with respect to their preferred walking velocity and manages possible conflict between agents competing for the same positions.

Table 2: Properties of the BOTworld environment and of the agent community concerning the implementation of the ITCM model. ([1]50-50 distribution, [2]Gaussian distribution).

Community Properties	
Gender distribution[1]	
Age distribution[2]	$\overline{ag}, \sigma(ag)$
	$ag \in [5, 80]$
Body target height distribution[2]	$\overline{ht^*}, \sigma(ht^*)$,
	$ht^* \in [1.60, 2.10]$
Body Mass Index distribution[2]	$\overline{BMI}, \sigma(BMI)$
	$BMI \in [17.0, 30.0]$
Static clothing insulation dist.[2]	$\overline{clo}, \sigma(clo)$
Preferred velocity distribution[2]	$\overline{v}_{\text{pref}}, \sigma(v_{\text{pref}})$
	$v_{\text{pref}} \in [0.5, 2.0]$
Environmental Properties	
Routing points with traffic data	
Non-passable grids	
Microclimate conditions in ca. 2 m:	
Wind speed and wind direction	$v_{\text{wind}}, \phi_{\text{wind}}$
Air temperature	T_a
Mean radiative temperature	T_{mrt}
Air humidity (Vapour pressure)	e_a
Pollutant concentration	χ

In order to simulate the thermal comfort of an agent at a given location inside the model area, the biometeorological relevant climate data are required for each grid cell i, j. These data are, as usual: Air temperature, wind speed and direction, mean radiant temperature and air humidity. If the exposure to air pollutants should be calculated, the local concentration values are needed additionally (compare Table 2). These microclimate data must be complete over the entire model domain and must fit with the physical and morphological properties of the environment. Hence, these data are normally taken from numerical simulations or from special measurements that are interpolated over the area. For the application of BOTworld it is not relevant how these data have been created. For this study, we use data from the microscale climate model ENVI-met (Bruse and Fleer, 1998) to feed the Multi-Agent system.

During the simulation, agents with different properties and different combination of routing targets are generated and released into the model environment.

3. compare Segment A *"PedWalk – A Multi-Agent model for the simulation of pedestrian traffic in complex urban microscale environments"* of this thesis

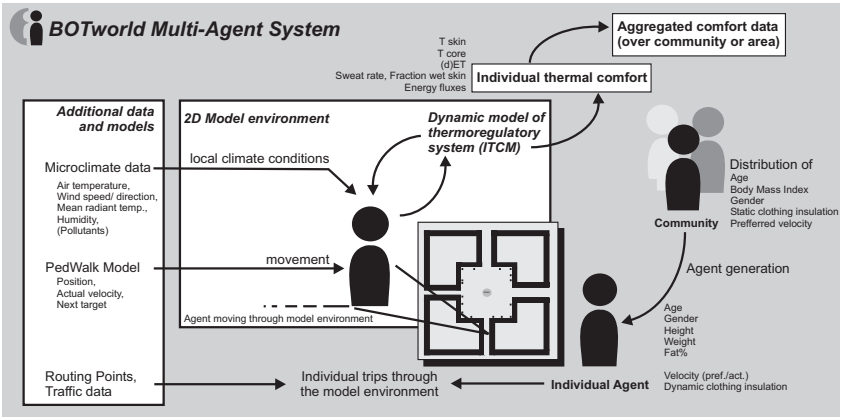

Figure 3: Schematic overview over the BOTworld system focussing on the embedded individual-based thermal comfort model ITCM.

Table 3: Main properties of the individual agent in the BOTworld system focussing on the ITCM model.

Basic Properties	
Gender (male, female)	*sex*
Age	*ag*
Height	*ht*
Weight (from BMI)	*wg*
Clothing Insulation	*clo*
Dynamical/ Routing Properties (from PedWalk)	
Preferred and actual velocity	v_{pref}, v_{act}
Relative wind speed	v_{wrel}
Actual position in model	i, j
Walking direction (angle)	ϕ
Main Physiological Properties	
Percentage fat (from BMI)	*%fat*
Mean skinfold thickness	*SF*
Body surface areas:	
DuBois area	A_{du}
Clothed surface area	A_{cl}
Skin surface area	A_{sk}
Main ITCM Biometeorological Variables	
Core temperature	T_{core}
Skin temperature	T_{sk}
Cloth temperature	T_{cl}
Metabolism	M
Energy flux core – skin	$Q_{\text{co-sk}}$
Conduction skin – cloths	$G_{\text{sk-cl}}$
Radiative budget skin	R_{sk}
Convection skin	C_{sk}
Radiative budget cloths	R_{cl}
Convection cloths	C_{cl}
Latent heat flux	*LE*
Sweat on skin	*SW*
Fraction wet skin	Γ

The amount of agents and the constellation of routing targets are based on traffic census data assigned to the routing points (number of pedestrians per minute, type of target). Depending on the size of the model area, 300 or more agents can be managed simultaneously.

In order to set up an individualised thermal comfort model considering the variance of human properties in real communities, detailed information about each single agent is required. This definition process works on two levels: On the community level as shown in Table 2, the general properties of the simulated virtual agent community are defined using classical statistical parameters such as mean values and standard deviations. From these general data, the exact parameters for the individual agent are created each time a new virtual pedestrian is generated and released into the model (see next section). Table 3 lists the most important properties and prognostic variables of the individual agent with respect to the thermal comfort model. Inside the BOTworld simulation system, a number of further properties are added for example to handle the movement behaviour of the agent.

4 The ITCM model: Theoretical background and model design

The primary design target for the model presented in this paper has been to produce an up-to-date but still simple and applicable model of the human thermoregulatory system. The model presented in this paper is a two-node model based on the approach from Gagge et al. (1971) updated with several extensions such as the suggestions from the BIOMED-II research project (Parsons et al., 1999; Havenith et al., 1999; Holmér et al., 1999) or the approaches for individualisation presented by Havenith (2001). Furthermore, some modifications are added to the basic model equations to take into account the different dynamic information resulting from the embedment into the Multi-Agent system.

4.1 Overview over the ITCM model

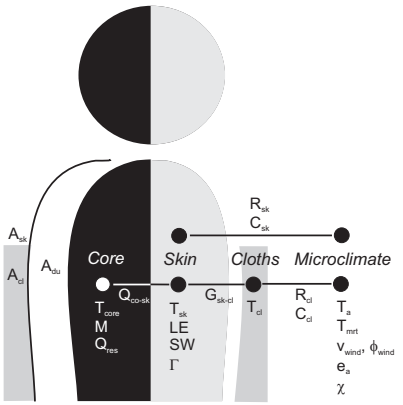

Figure 4: Overview over the main variables used in the ITCM model. For the explanation of the variables see also Table 3.

The Individual-based Thermal Comfort model is a dynamic two-node model in which the average core and skin temperature of the human body (T_{core} and T_{sk}) are the main prognostic variables. In addition, the average temperature of the clothing layer (T_{cl}) is calculated to estimate the energy fluxes at the clothed parts of the body surface. Figure 4 gives an overview of the model system including the most important model variables and the body surface areas (see also Table 3).

The following model description follows basically this scheme: First, the calculation of the basic body parameters is presented (Section 4.2, p. 10 ff). Then, the equations required for the estimation of the clothing temperature (Section 4.3, p. 13 ff) , the skin temperature (Section 4.4, p. 16 ff) and the core temperature (Section 4.5, p. 20 ff) are presented. Finally, some remarks on the model initialization (Section 4.8, p. 23) and on numerical aspects (Section 4.9, p. 25) are given.

4.2 Generation of individual agent parameters

4.2.1 Derivation of basic physiological properties

For each agent, the gender (*sex*), the age (*ag*), the body target height (*ht**) and Body Mass Index (*BMI*) are provided as initial properties by the BOTworld simulation framework. The gender of the agent is chosen randomly based on a 50-50 distribution, whereas age, target height and BMI of the individual agent are selected based on a Gaussian normal distribution with given mean value and standard deviation (see Table 2). Through the adjustment of the mean and standard deviation values, the user can force the model to generate agent communities with specific properties, for example only elderly people.

The body target height *ht** is understood as the height of a body in the state of adolescence (age=18), hence it needs to be corrected for virtual humans below this age. Based on the studies from Tuddenham and Snyder (1954), we assume that the body height increases linearly between 1.00 m at the age of 5 and the target height reached at the age of 18.

The height *ht(ag)* of an agent at the age of *ag* can then be calculated as

$$ht(ag) = \begin{cases} 1.00 + \frac{ht^* - 1.00}{15} \cdot (ag - 5) & ; ag < 18 \\ ht^* & ; ag \geq 18 \end{cases} \tag{4.1}$$

In order to relate the weight of a person to the height and the physiological shape of the body, the so-called *Body Mass Index* (*BMI*) was selected as reference

parameter (Keys et al., 1972). In general, the BMI value is defined as

$$\text{BMI} = \frac{\text{Weight}}{\text{Height}^2} \tag{4.2}$$

BMI values below 18.5 are indicators for underweight, 18.5 to 24.9 is considered as normal weight and a BMI above 25.0 indicates overweight, in which exceeding 29.9 is indicating obesity. Values outside the range of [17.0, 30.0] are not treated in the model as it can be assumed that for these conditions the human thermoregulatory systems behaves in a more specific way which is not covered by the standard model approaches used in this paper.

As the BOTworld system provides an individual BMI index for each agent, the related weight (*wg*) can easily be calculated from the body height (*ht*) and the BMI definition given in (4.2):

$$wg = BMI\sqrt{ht} \tag{4.3}$$

Although the BMI index provides a good representation of the state and shape of the human body, the level of detail used in this model requires a more sophisticated description. In detail, the amount of fat in the human body (*%fat*) and the so-called mean *Skinfold Thickness* (*SF*) are required by some of the calculation modules.

The derivation of both parameters from the BMI is not trivial and several approaches are available to relate them to the BMI, the age and gender of a person (compare Deurenberg et al., 1991; Gallagher et al., 1996; Jackson et al., 1980).

One specific problem arising from the BMI indicator applied to persons of different ages is the fact, that during the growth phase the BMI is not only a linear function of height and weight as assumed in (4.2) but also depends on the gender and the age of the person ("BMI-for-age", Pietrobelli et al., 1998).

Although Deurenberg et al. (1991) provides two separate equations for adults and non-adults, we have decided to use the approach from Jackson et al. (1980) in this model as the Deurenberg et al. (1991) equation makes unrealistic jumps when crossing the threshold value of 15 years.[4] Also, the Jackson approach gives realistic results when applied to the biometeorological reference person with 1.80 m, 75 kg and a BMI of 23.14. For this standard person, an amount of 15 % fat is assumed while the approach from Jackson after (4.4) gives the close result of 15,8 % fat.

After Jackson et al. (1980), the percentage of fat (*%fat*) in the human body can be calculated with

$$\%fat = 1.61 \cdot BMI + 0.13 \cdot ag - f_{\text{sex}} \cdot 12.1 - 13.9 \tag{4.4}$$

in which f_{sex} is a gender specific factor with 1 for male and 0 for female persons.

The *skinfold thickness* (*SF*) is the second parameter required by the model to estimate the composition and the physical properties of the peripheral body tissue.

Some additional steps have to be taken to calculate *SF* from the personal properties defined so far: In the first step, the body density (*BD*) has to be calculated from the amount of fat. Then, the skinfold thickness can be estimated from the body density.

Jackson and Pollock (1985) suggest the following relationship between the body density and the percentage of body fat:

$$\%fat = \left(\frac{4.95}{BD} - 4.5\right) \cdot 100$$

or, resolved for the body density,

$$BD = \frac{4.95}{0.01 \cdot \%fat + 4.5} \tag{4.5}$$

To estimate body density from the skinfold thickness, Jackson and Pollock (1985) propose for male persons the equation

$$BD = 1.112 - 10^{-6}(434.99 \cdot \Sigma SF + 0.55 \cdot \Sigma SF^2 - 288.26ag)$$

and for female persons:

$$BD = 1.097 - 10^{-6}(469.71 \cdot \Sigma SF + 0.56 \cdot \Sigma SF^2 - 188.28ag)$$

4. for example the results jump from 22.73 % fat at the age of 14 to 14.85 % at the age of 15 for a constant BMI of 23

in which ΣSF is the sum of the skin fold thickness taken at 7 points of the human body.

For the application in this model, the relationship must be reversed. If we drop the second order term which has only very little influence on the result, we get for the single skinfold thickness :

$$SF = \frac{1}{7} \cdot \frac{x_1 - BD - x_3 \cdot a}{x_2} \qquad (4.6)$$

with

$$x_1 = 1.112, x_2 = 434.99 \cdot 10^{-6}, x_3 = 288.26 \cdot 10^{-6}$$

for male and

$$x_1 = 1.097, x_2 = 469.71 \cdot 10^{-6}, x_3 = 188.28 \cdot 10^{-6}$$

for female persons.

4.2.2 Derivation of clothing properties

One of the main aspects influencing thermal comfort is the clothing that is actually worn. An inadequate selection of cloths can lead to almost any thermal sensation independent from the actual climate conditions, especially in the case of hot discomfort. Hence, a realistic and adequate selection of the clothing properties of the agent community is essential for a realistic simulation.

Table 4 lists a selection of different pieces of garments and the associated static clothing insulation *clo*. To obtain the overall insulation for a given clothing ensemble, the single insulation values are added according to the pieces of garment worn.

Like the other personal parameters, the individual *clo*-value of an agent is generated randomly based on a Gaussian standard distribution with the mean value $\overline{clo}$ and the standard deviation $\sigma(clo)$. Both values can be adjusted by the user in order to simulate different clothed communities.

4.2.3 Calculation of body surface areas

For the calculation of energy fluxes at the human body, the estimation of different body surface areas is required. The basic surface area of the human body without clothes A_{du}, the so-called *DuBois-Area*, can

Table 4: Selection of static insulation values for individual pieces of garments (taken from ISO 7933, 1989; ISO 7730, 1995).

Garment	*clo*
Underwear	
Panties	0.03
Underpants with long legs	0.10
Singlet	0.04
T-Shirt	0.09
Shirt with long sleeves	0.12
Shirts/ Blouses	
Short sleeves	0.15
Normal, long sleeves	0.20
Flannel shirt, long sleeves	0.30
Light blouse, long sleeves	0.15
Trousers	
Shorts	0.06
Light-weight	0.20
Normal	0.25
Flannel	0.28
Dresses/ Skirts	
Light skirt (summer)	0.15
Heavy skirt (winter)	0.25
Light dress, short sleeves	0.20
Winter dress, long sleeves	0.40
Sweaters	
Sleeveless vest	0.12
Thin sweater	0.20
Sweater	0.28
Thick sweater	0.35
Jackets	
Light summer jacket	0.25
Jacket	0.35
Outdoor clothing	
Coat	0.60
Down jacket	0.55
Sundries	
Socks	0.02
Thick ankle socks	0.05
Thick long socks	0.05
Nylon stockings	0.03
Shoes	0.03
Boots	0.10

be calculated after DuBois (1916) from the height *ht* and the weight *wg* of the virtual person:

$$A_{\mathrm{du}} = 0.203 \cdot wg^{0.425} ht^{0.725} \tag{4.7}$$

Due to the different layers of clothes, this surface area increases to a certain extent. As ISO 7730 (1995) suggests, this increase can be estimated using the isolation value of the clothes (*clo*) with

$$f_{\mathrm{cl}} = \begin{cases} 1.00 + 0.2clo & ; clo < 0.5 \\ 1.05 + 0.1clo & ; clo \geq 0.5 \end{cases} \tag{4.8}$$

Obviously, this increase concerns only those parts of the body which are actually covered by clothes. Hence, for a proper simulation of the energy exchanges, the overall surface area A_{du} must be divided into a clothed (A_{cl}) and a bare (A_{sk}) fraction:

$$A_{\mathrm{cl}} = A_{\mathrm{du}} \cdot (r_{\mathrm{cl2sk}} + f_{\mathrm{cl}} - 1) \tag{4.9a}$$

$$A_{\mathrm{sk}} = A_{\mathrm{du}} \, (1 - r_{\mathrm{cl2sk}}) \tag{4.9b}$$

Here, r_{cl2sk} is the ratio between the clothed and unclothed body surface which can be derived directly from the *clo* value (Morgan and Baskett, 1974):[5]

$$r_{\mathrm{cl2sk}} = 0.01 \cdot (-2.36 + 173.51 \cdot clo - 100.76 \cdot clo^2 + 19.28 \cdot clo^3) \tag{4.10}$$

4.3 Calculation of clothing temperature T_{cl}

Although the clothing temperature itself is not a biometeorological parameter, its value is required for the estimation of heat transfer between the clothed parts of the human body and the environment. In addition, due to its more rapid response on changes in the environmental conditions (compared to the skin temperature) the clothing temperature it is a good indicator for the impact of the local meteorological conditions and the energy balance.

For the calculation of the clothing temperature it is assumed, that the energy balance of the outer cloth surface is always in an equilibrium state. Hence, heat storage inside the clothing layer is neglected in the model and a homogeneous temperature distribution over the clothed body parts is assumed. These simplifications have only a small impact on the model results as long as the studies are restricted to cases where light to medium clothes are worn. Situations, in which thick clothes are used and severe cold stress conditions apply, go beyond the scope of this model and will not be treated.

Using these simplifications the energy balance equation of the outer clothing surface in steady-state conditions can be written as:

$$0 = R_{\mathrm{cl}} + C_{\mathrm{cl}} - G_{\mathrm{sk\text{-}cl}} \tag{4.11}$$

Here, the relevant energy fluxes are the net radiative flux at the clothing surface (R_{cl}), the heat convection from the cloth surface to the exterior air (C_{cl}) and the heat conduction between the outer cloth surface and the skin ($G_{\mathrm{sk\text{-}cl}}$).

4.3.1 Cloth net radiative flux R_{cl}

The net radiative flux between the clothes and the surrounding environment depends on the cloth temperature T_{cl} and the shortwave and longwave radiative fluxes from the environment, latter ones summarised in the mean radiative temperature T_{mrt}:

$$R_{\mathrm{cl}} = f_{\mathrm{eff}} \cdot \varepsilon_{\mathrm{cl}} \sigma_{\mathrm{B}} \left((T_{\mathrm{mrt}} + 273.15)^4 - (T_{\mathrm{cl}} + 273.15)^4 \right) \tag{4.12}$$

where $\varepsilon_{\mathrm{cl}}$ is the emissivity of the clothes and σ_{B} is the Stefan-Bolzman constant ($5.67 \cdot 10^{-8}$ $\mathrm{Wm^{-2}K^{-4}}$).

As not all parts of the human body are directly exposed to the environment (e.g. the inner sides of the legs or the arms are protected), the effective radiation area factor (f_{eff}) is used to calibrate the surface area which directly contributes radiation exchange. For a standing person, the values vary between 0.725 (Fanger, 1982) and 0.834 (Miyazaki et al., 1995). In this model we use the value of 0.74 proposed by Tanabe et al. (2000) as it is in between the other values and was derived using a sophisticated ray-casting simulation applied to a polygon model of the human

5. This approach is valid for *clo*-Values up to 2.4 clo.

body. If the simulated person is actually sitting instead of standing upright, the value of f_{eff} is set to 0.691 (compare Tanabe et al., 2000).

Some remarks on the usage of T_{mrt}

Care has to be taken when using mean radiant temperature data in the model. The T_{mrt} parameter is a complex parameter which is composed out of three different components: The longwave radiative fluxes from the environment, the diffuse shortwave fluxes (from the sky and reflected from the environment) and, most important if present, the direct solar radiation. For the correct application of T_{mrt} in human biometeorology the contribution of the different radiative fluxes have to be weighted depending on their direction of incidence so that the non-symmetric shape of the human body is taken into account (compare VDI 3787, 1996; Höppe, 1992). One of the most important components in this context is the body surface area directly exposed to the solar radiation which is a function of the solar elevation and the body position. If only the single T_{mrt} value is provided as input, it is impossible to introduce modification factors to include the effect of varying exposure angles. [6]

Hence, the equations used in the ITC model assume that the provided T_{mrt} data used as input are correctly composed to represent a typical average human exposure to the radiative fluxes. This is the case for example for T_{mrt} values provided by *ENVI-met* (Bruse and Fleer, 1998), *RayMan* (Matzarakis et al., 2000) or for values calculated using the methods proposed for OUT-SET* (Spagnolo and de Dear, 2003) or suggested in VDI 3787 (1996).

4.3.2 Cloth-air heat convection C_{cl}

The turbulent transfer of heat between the clothing surface and the surrounding air is given by the equation

$$C_{\text{cl}} = h_{\text{c}}\left(T_{\text{a}} - T_{\text{cl}}\right) \tag{4.13}$$

The convective heat transfer coefficient h_{c} [$\text{Wm}^{-2}\text{K}^{-1}$] is calculated after Kandjov (1999) with respect to the relative air velocity v_{wrel} at the clothing surface. In case of low wind speeds with free convection, the temperature difference $\Delta T = T_{\text{cl}} - T_{\text{a}}$ between the clothes and the air replaces the relative air velocity with

$$h_{\text{c}} = \begin{cases} 1.87\left(\Delta T\right)^{0.25} & ;v_{\text{wrel}} < 0.2 \\ 6.88\left(v_{\text{wrel}}\right)^{0.618} & ;0.2 \le v_{\text{wrel}} \le 2.0 \\ 6.08\left(v_{\text{wrel}}\right)^{0.805} & ;v_{\text{wrel}} > 2.0 \end{cases} \tag{4.14}$$

If ΔT is negative and the relative wind speed is below 0.2 ms^{-1}, convective heat transfer is assumed to be zero. The formulation above assumes standard air pressure p=p_0 conditions. For non-standard pressure, an additional correction term must be added (see Kandjov, 1999).

The relative wind speed v_{wrel} depends on the local wind speed v_{wind} and the actual walking velocity of the agent v_{act} on one hand and on the angle between wind direction ϕ_{wind} and walking direction ϕ of the agent on the other:

$$v_{\text{wrel}} = \sqrt{a^2 + b^2} \tag{4.15}$$

with

$$a = \left(\sin\phi_{\text{wind}} \cdot v_{\text{wind}} - \sin\phi \cdot v_{\text{act}}\right)^2$$
$$b = \left(\cos\phi_{\text{wind}} \cdot v_{\text{wind}} - \cos\phi \cdot v_{\text{act}}\right)^2$$

4.3.3 Cloth-skin heat conduction $G_{\text{sk-cl}}$

The heat conduction between the skin and the outer clothing surface represents the energetic exchange processes between the clothed skin surface and the outer surface of the clothing layer. There a several approaches how this multi-level exchange process can be parameterised and special attention has to be paid when using predefined clothing insulation values, to which of the different approaches they relate.

A frequently used definition relates the clothing insulation value I_{tot} to the overall heat transfer between the clothed skin and the surrounding air:

$$I_{\text{tot}} = \frac{T_{\text{sk}} - T_{\text{a}}}{DRY}$$

6. A coarse correction of T_{mrt} is possible to take into account the effect of varying clothing albedo. If the clothing albedo a_{cl} is different to the standard value of 0.7, a correction can be applied with

$$T_{\text{mrt}}^{'} = \left(1 - \left(a_{\text{cl}} - 0.7\right)\right) T_{\text{mrt}}$$

In this approach, the **dry heat transfer** coefficient (*DRY*) summarises different energy exchange processes such as convection, radiation or conduction occurring between the skin, the layer of cloths and the ambient air (Burton and Edholm, 1955).

With respect to the intention of the model developed here, this formulation is of limited use for two reasons: First, different types of energy exchange processes are combined into a single value. This makes it almost impossible to include dynamic effects such as wind effects or the influence of walking into the insulation value (see also Parsons et al., 1999; Holmér et al., 1999; Havenith et al., 1999). Second, the ITCM scheme provides the clothing surface temperature as an independent prognostic variable such as suggested in ISO 7730 (1995). Hence, the dry heat transfer coefficient is not usable here as it does not explicitly take into account the clothing temperature as an individual parameter.

To allow a more precise calculation, we use the **intrinsic clothing insulation**(I_{cl}) in the model. Using I_{cl}, the energy conductance between the skin and the clothing layer is treated independently from the exchange processes at the outer clothing surface. Hence, the conduction between the skin and the cloths can be written as:

$$G_{\text{sk-cl}} = \frac{1}{I_{\mathrm{cl}}} \left(T_{\mathrm{sk}} - T_{\mathrm{cl}}\right) \tag{4.16}$$

With this approach, the energy exchanges scheme between skin, cloths and outside is now composed as shown in Figure 5: The total insulation effect of the clothing layer (I_{tot}) is divided into the insulation effect of the clothing fabric including the internal air between the cloths and the skin (I_{cl}) and the air layer resistance between the outer clothing surface and the surrounding air (I_{a}). The first component I_{cl} is related to the conduction term $G_{\text{sk-cl}}$ in the ITC model whereas the I_{a} is represented by the convection component C_{cl} in the energy balance of the clothing layer.

4.3.4 Calculation of a dynamic I_{cl} value

The insulation values for different kinds of clothing found in literature always relate to a human body which is not in motion. If the analysed person begins to move, different effects begin to modify the insulation effect: On the one hand, the air layer resistance (I_{a}) at the outer surface of the clothing layer decreases. This effect is already included in the model through the convective heat transfer coefficient h_c (see eq. 4.14, p. 14). On the other hand, the intrinsic insulation of the cloths also reduces due to pumping effects that occur when the body begins to move. Through this effect the insulation effect of the air layer between the skin and the cloth layer is reduced.

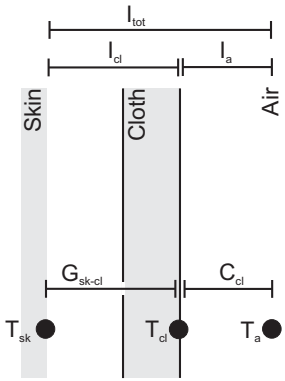

Figure 5: Schematic overview over the insulation values applying to a clothing layer.

In order to include the dynamic effects of wind speed and walking on the intrinsic clothing insulation, the correction procedure developed inside the framework of the BIOMED-II project (Parsons et al., 1999; Holmér et al., 1999; Havenith et al., 1999; Havenith, 1999) is included in the ITC model.

Following the scheme shown in Figure 5, the total insulation effect of the cloths can be written as

$$I^{\mathrm{s}}_{\mathrm{tot}} = I^{\mathrm{s}}_{\mathrm{cl}} + I^{\mathrm{s}}_{\mathrm{a}} / f_{\mathrm{cl}} \tag{4.17}$$

where the superscript "s" denotes that the insulation is referring to static conditions. The static intrinsic insulation of the clothing layer can be calculated directly from the given clo-value as

$$I^{\mathrm{s}}_{\mathrm{cl}} = 0.155 \cdot \mathrm{clo} \tag{4.18}$$

Here, $I^{\mathrm{s}}_{\mathrm{a}}$ is the air layer resistance under no-wind conditions which is assumed to be around 0.11. Finally f_{cl} is the correction factor given by (4.8) which

takes into account the effect of an increased clothing surface area on the total insulation.

To consider the dynamic effects of walking on the total insulation I_{tot}, Havenith et al. (2002) defines a correction factor $f_{\text{corr,tot}}$:

$$I_{\text{tot}} = I_{\text{tot}}^{\text{s}} \cdot f_{\text{corr,tot}} \tag{4.19}$$

Unfortunately, it is almost impossible to measure directly the effects of walking on the intrinsic clothing insulation. Therefore, the correction has to be made indirectly through the measurement of the total insulation under dressed and undressed conditions. From the datasets of clothed persons, the total dynamic insulation value I_{tot} can be derived and from the experimental data with unclothed persons, the changes in I_{a} can be extracted. Knowing both values, it can then be assumed that the difference between I_{tot} and I_{a} are due to changes in the intrinsic clothing insulation.

For the overall correction factor $f_{\text{corr,tot}}$, Havenith et al. (2002) and Holmér et al. (1999) propose the following relationship:

$$f_{\text{corr,tot}} = \left(\frac{0.6 - clo}{0.6}\right) f_{\text{corr,cl}} + \left(\frac{clo}{0.6}\right) f_{\text{corr,nude}} \tag{4.20}$$

in case of *clo* values lower or equal to 0.6. If the *clo* value is above 0.6, only the clothed correction factor is used:

$$f_{\text{corr,tot}} = f_{\text{corr,cl}} \tag{4.21}$$

The correction factors for the dressed ($f_{\text{corr,cl}}$) and the undressed ($f_{\text{corr,nude}}$) conditions are:

$$f_{\text{corr,cl}} = \exp\Big(0.043 - 0.398 v_{\text{rel}} + (0.066 v_{\text{rel}})^2 - 0.378 v_{\text{act}} + (0.094 v_{\text{act}})^2\Big)$$

and

$$f_{\text{corr,nude}} = \exp\Big(0.126 - 0.899 v_{\text{rel}} + (0.246 v_{\text{rel}})^2 - 0.313 v_{\text{act}} + (0.097 v_{\text{act}})^2\Big)$$

Here, v_{rel} is the relative wind speed calculated after (4.15), p. 14 and v_{act} is the actual walking velocity of the agent. Generally, due to their empirical background, the correction factors are only valid within the range of $v_{\texttt{rel}} \leq 3.5$ ms^{-1}and $v_{\text{act}} \leq 1.5$ ms^{-1}. If actual values exceed this range, the maximum allowed value will be used instead.

Once the correction factors are calculated, the dynamic total insulation and the dynamic air layer insulation can be calculated:

$$I_{\text{tot}} = I_{\text{tot}}^{\text{s}} \cdot f_{\text{tot}} \tag{4.22}$$

$$I_{\text{a}} = I_{\text{a}}^{\text{s}} \cdot f_{\text{c,nude}} \tag{4.23}$$

and the dynamic intrinsic insulation value can be extracted as the remaining difference:

$$I_{\text{cl}} = I_{\text{tot}} - \frac{I_{\text{a}}}{f_{\text{cl}}} \tag{4.24}$$

4.4 Calculation of skin temperature T_{sk}

Different to the clothing temperature which can be obtained directly using the stationary energy balance equation of the cloth surface, the calculation of the skin temperature is significantly more complex. On one side, the actual skin temperature T_{sk} is influenced by the meteorological conditions and on the other side by the thermoregulatory system of the human body. Through the effect of blood flow and due to heat storage and conduction capacity of the body tissue, the actual skin temperature cannot be estimated assuming steady-state conditions, but must be calculated as a prognostic variable.

The development of the skin temperature by time can be written as

$$\frac{\partial T_{\text{sk}}}{\partial t} = \frac{Q_{\text{st,sk}}}{\alpha \cdot c_{\text{p}}(\text{Body}) \cdot wg} \tag{4.25}$$

Here, $Q_{\text{st,sk}}$ represents the amount of energy gained or lost by the skin layer. The second important parameter is the effective specific heat $\alpha \cdot c_{\text{p}}(\text{Body})$ which equals the specific heat of the body tissue weighted with the coefficient α which takes into account the influence of the vasodilation status of the skin on the heat storage process.

The available energy at the skin surface can be written as

$$Q_{st,sk} = \underbrace{A_{sk} \cdot R_{sk}}_{\text{radiative e.-balance bare skin}} + \underbrace{A_{sk} \cdot C_{sk}}_{\text{convection bare skin}} - \underbrace{A_{cl} \cdot G_{sk\text{-}cl}}_{\text{conduction through cloths}} - \underbrace{A_{du} \cdot LE}_{\text{latent heat loss}} + \underbrace{Q_{co\text{-}sk}}_{\text{exchange with core}} \quad (4.26)$$

where R_{sk} and C_{sk} are the net radiative energy balance and the heat convection from the bare skin compartments, $G_{sk\text{-}cl}$ is the heat conduction from/to the clothing layer and *LE* is the energy loss through sweat transpiration and vapour diffusion. Finally, $Q_{co\text{-}sk}$ is the heat flow between the skin and the body core by blood circulation and through conduction.

The external energy fluxes are weighted with respect to the fraction of surface area they concern: R_{sk} and C_{sk} to the bare skin area (A_{sk}) and $G_{sk\text{-}cl}$ to the clothed surface area (A_{cl}). Exceptionally, *LE* is applied to the overall body area (A_{du}) as the influence of the clothing layer is handled implicitly when calculating *LE* (see Section 4.4.4, 18 ff). In the following sections, the estimation of the different components of the energy balance are presented in detail.

4.4.1 Calculation of specific heat of body tissue

In order to estimate how the storage of heat is distributed over the skin and the core body tissue, the *effective specific heat* is used in the prognostic equation for the skin and the core temperature. This artificial parameter depends on the specific heat of the body tissue $c_p(\text{Body})$ and on a weighting factor α describing the ratio of heat storage between skin and body core.

The average specific heat of the body $c_p(\text{Body})$ is composed out of two basic components: The body fat and other tissues like skin layer, skeleton or muscles. With respect to the relative amount of body fat (*%fat*) the specific heat of the body can be calculated as:

$$c_p(\text{Body}) = \frac{\%fat}{100} c_p(\text{Fat}) + \frac{100 - \%fat}{100} c_p(\text{Tissue}) \quad (4.27)$$

with $c_p(\text{Fat})$=2.51·10^3 Jkg^{-1}K^{-1} and $c_p(\text{Tissue})$=3.65·10^3 Jkg^{-1}K^{-1} (compare Havenith et al., 2002). [7]

The weighting coefficient α introduces the impact of the vasodilatation status of the skin on the heat distribution. Following Havenith (2001), α is derived from the body resistance to heat transfer $R_{co\text{-}sk}$ (see eq. 4.45, p. 20):

$$\alpha = 0.08 + 2R_{co\text{-}sk} \quad (4.28)$$

Values of α range between 0.1 (vasodilated skin under warm conditions) and 0.35 (vasoconstricted skin under cold conditions).

4.4.2 Skin net radiative flux R_{sk}

The equation for the skin net radiative flux equals more or less its counterpart for the clothing surface (4.12), except for the emissivity of the cloths that is replaced by the emissivity of the skin ε_{sk}:

$$R_{sk} = f_{eff} \cdot \varepsilon_{sk} \sigma_B \left((T_{mrt} + 273.15)^4 - (T_{sk} + 273.15)^4 \right) \quad (4.29)$$

4.4.3 Skin-air heat convection C_{sk}

Theoretically, the transfer of heat at the skin surface is composed out of a convective component and a conduction component if parts of the skin are in contact with other materials (chairs, surfaces,..). In this model, we will neglect the conductive part and will only treat the convective component, which should be accurate enough assuming a typical behaviour in outdoor spaces. Like for the radiative component, the equation for C_{sk} is equal to its counterpart for the clothing surface (eq. 4.13) except that T_{sk} is used instead of T_{cl}:

$$C_{sk} = h_c (T_a - T_{sk}) \quad (4.30)$$

with h_c calculated after (4.14) with $\Delta T = T_{sk} - T_a$.

7. For the standard person with an amount of 15% fat this expression gives the same value of $c_p(\text{Body}) = 3.5 \cdot 10^3$ Jkg^{-1}K^{-1} as used in the Gagge (1971) model

4.4.4 Sweat transpiration and vapour flux *LE*

The transpiration of sweat is one of the main mechanisms of the body to release surplus energy. In addition to the vaporisation of liquid sweat on the skin (m_{trans}) a constant diffusive flux of vapour through the skin (m_{d}) also contributes to the latent energy flux from the skin.

In total the latent energy flux is:

$$LE = L\,(m_{\text{trans}} + m_{\text{d}}) \tag{4.31}$$

Actual transpiration m_{trans}

The actual transpiration rate m_{trans} can be either limited through the amount of available sweat m_{avail} or through a restricted potential transpiration m_{pot} due to non-permeable clothing layers or high air humidity.

$$m_{\text{trans}} = \min(m_{\text{avail}}, m_{\text{pot}}) \tag{4.32}$$

Whereas the potential transpiration depends only on the actual meteorological and dynamical situation, the amount of available sweat might be higher than the actual produced sweat, as non-transpired sweat from preceding time steps can remain on the skin. To include this effect in the model, the amount of liquid sweat on the skin (*SW*) is introduced as a prognostic variable in the model.[8]

The amount of sweat *SW* available for transpiration at time t depends on the amount of sweat remaining from the last time step $SW(t-\Delta t)$ plus the additionally produced sweat during the actual time step:

$$SW(t) = SW(t-\Delta t) + m_{\text{prod}} \cdot \Delta t \tag{4.33}$$

from which the actually available sweat rate m_{avail} can be directly calculated with

$$m_{\text{avail}} = SW(t)/\Delta t$$

The amount of sweat produced m_{prod} is calculated after Höppe (1984) as

$$m_{\text{prod}} = f_{\text{sex}} \cdot 8.47 \cdot 10^{-5}\left(T_{\text{body}} - 36.6\right) \tag{4.34}$$

where f_{sex} is a gender specific factor taking into account the difference in sweat production of women and men with f_{sex}=1 for men and 0.7 for women.

T_{body} is an average body temperature calculated as

$$T_{\text{body}} = 0.1T_{\text{sk}} + 0.9T_{\text{core}}$$

If the body temperature is below the trigger of 36.6°C, no sweat is produced.

After the potential transpiration has been determined (see below), the actual transpiration during the time step Δt can be calculated from (4.32).

The amount of sweat remaining after this time step and serving as input to the next time step is then

$$SW(t+\Delta t) = SW(t) - m_{\text{trans}} \cdot \Delta t \tag{4.35}$$

Potential transpiration m_{pot}

The amount of potential transpiration depends mainly on the vapour pressure gradient between the skin surface and the ambient air plus, in case of the clothed skin fractions, on the vapour permeability of the clothing layer. To calculate the overall potential transpiration, the fluxes are distinguished into the vapour flux from the unclothed parts ($m_{\text{pot,sk}}$) and from the clothed parts ($m_{\text{pot,cl}}$) of the body, both weighted with the associated body surface area A_{sk} and A_{cl} respectively:

$$m_{\text{pot}} = \frac{A_{\text{cl}}}{A_{\text{cl}} + A_{\text{sk}}} m_{\text{pot,cl}} + \frac{A_{\text{sk}}}{A_{\text{cl}} + A_{\text{sk}}} m_{\text{pot,sk}} \tag{4.36}$$

The potential transpiration from the bare skin fraction $m_{\text{pot,sk}}$ is a function of the convective vapour transfer transfer h_{e} and of the saturation vapour pressure at skin temperature $e^*(T_{\text{sk}})$:

$$m_{\text{pot,skin}} = \frac{1}{L} h_{\text{e}}\,(e^*(T_{\text{sk}}) - e_{\text{a}}) \tag{4.37}$$

8. The approach used here is rather simple and does not take into account the absorption of sweat at the clothing layer and the consequences for the energy balance. A more sophisticated model including these effects can be found for example at Takada et al. (1999)

For the estimation of h_e the formulation proposed by Kandjov (1999) is used:

$$h_e = \begin{cases} 3.08\,(\Delta T)^{0.25} & ;v_{wrel} < 0.2 \\ 11.35\,(v_{wrel})^{0.618} & ;0.2 \le v_{wrel} \le 2.0 \\ 10.0\,(v_{wrel})^{0.805} & ;v_{wrel} > 2.0 \end{cases} \tag{4.38}$$

with $\Delta T = T_{sk} - T_a$, the relative wind speed v_{wrel} calculated after (4.15) and assuming standard air pressure p=p_0. No vapour transfer occurs if ΔT becomes negative and the wind speed is below 0.2 ms^{-1}. In addition, condensation is also neglected.

The potential transpiration through the clothing layer in can be written as:

$$m_{pot,cl} = \frac{1}{R_T \cdot L}\,(e^*(T_{sk}) - e_a) \tag{4.39}$$

in which R_T is the vapour resistance of the clothing. Following ISO 9920 (1993) R_T can be calculated based on the total thermal insolation I_{tot} of the clothing layer and the Woodcock vapour permeation index i_m :

$$R_T = 10\frac{I_{tot}}{i_m \cdot L_w} \tag{4.40}$$

using the Lewis relationship with L_w=16.7KkPa^{-1}.

Like the clothing heat resistance, the vapour resistance also depends not only on the clothing material but also on the relative wind speed and the walking velocity. To correct R_T, we use the same procedure as shown in Havenith et al. (1999), as this approach is well compatible to the method used for the thermal insulation of the clothing.

The static permeability index i_m^s is corrected into a dynamical permeability index i_m with:

$$i_m = i_m^s \cdot f_m \tag{4.41}$$

with the correction function

$$f_m = 1 + 1.3\,(1 - f_{corr,tot}) + 2.6\,(1 - f_{corr,tot})^2$$

The total clothing insulation I_{tot} and the correction factor $f_{corr,tot}$ are the same as used in the approach for the thermal component calculated after (4.19) – (4.21), p. 16.

Different input values for the static index i_m^s can be found in ISO 9920, but for normal permeable clothing, regardless of the number of layers, an average value of $i_m^s = 0.38$ is a good general approximation (Havenith et al., 2002, 1999).

Vapour diffusion through skin m_d

The direct and constant diffusion of vapour through the dry parts of the skin can be calculated as

$$m_d = (1 - \Gamma)\,\frac{1}{(R_{T,sk} + r_{cl2sk} \cdot R_T) \cdot L}\,(e^*(T_{sk}) - e_a) \tag{4.42}$$

where $R_{T,sk}$ is the vapour diffusion resistance of the skin layer (=3.215 m^{2}hPa W^{-1} after Höppe, 1984), R_T is the vapour resistance of the cloths calculated after (4.40) and r_{cl2sk} the ratio between clothed and unclothed body surface area after (4.10), p. 13. As only dry parts of the skin contribute to the vapour diffusion, the fraction of wet skin (Γ) needs to be taken into account in the equation.

Skin wetness indicator Γ and water loss M_{sk}

The estimation of the fraction of wet skin Γ is based on ISO 7730 (1995) which uses the amount of sweat produced compared to the potential sweat transpiration rate (m_{pot}), see eq. 4.36. However, instead of the sweat actually produced, the total available sweat m_{avail} which might contain sweat from previous time steps (compare eq. 4.33) is used in this model:

$$\Gamma = \frac{m_{avail}}{m_{pot}} + 0.06 \tag{4.43}$$

where Γ=0.06 is the minimal skin wetness due to vapour diffusion (Havenith et al., 2002).

The total amount of water lost by the body through the skin in one hour in grams per hour is then

$$W_{sk} = A_{du} \cdot \left(m_{prod} + m_d\right) \cdot 1000 \cdot 3600$$

4.4.5 Heat transfer between the skin and the body core $Q_{co\text{-}sk}$

The heat exchange between skin layer and body core is an important component of the human thermoregulatory system. It can be parameterised using $R_{co\text{-}sk}$ as the body's resistance to heat transfer:

$$Q_{co\text{-}sk} = A_{du} \cdot \frac{1}{R_{co\text{-}sk}}\,(T_{core} - T_{sk}) \tag{4.44}$$

Following Havenith (2001), the value of $R_{\text{co-sk}}$ includes the effects of advective heat transfer through the blood circulation (R_{blood}) plus the effect of heat conduction through the body tissue such as muscles, fat and skin (R_{tissue}):

$$R_{\text{co-sk}} = \left(\frac{1}{R_{\text{blood}}} + \frac{1}{R_{\text{tissue}}} \right)^{-1} \tag{4.45}$$

The resistance of the advective component R_{blood} is calculated as

$$R_{\text{blood}} = \frac{1}{\eta \cdot c_{\text{p}}(\text{Blood}) \rho(\text{Blood}) V_{\text{B,s}}}$$

where $V_{\text{B,s}}$ is the blood volume in [$\text{lm}^{-2}\text{s}^{-1}$ (=$V_{\text{B}}/3600$) and c_{p}(Blood),ρ(Blood) are the specific heat and density of blood (c_{p}(Blood) =$3.64 \cdot 10^3 \text{Jkg}^{-1}\text{K}^{-1}$, ρ(Blood)= 1.06 kgl^{-1}) after J. R. Geigy AG (1981).

The countercurrent heat exchange reduces the effective heat transport through the blood by the factor η. In this model, η is set to 1 which equals the formulation used in the original Gagge model.

The amount of blood that is transported in peripheral tissue (V_{B} in [$\text{l h}^{-1}\text{m}^{-2}$]) can be related to the skin and core temperature after Gagge et al. (1986, 1971) with

$$V_{\text{B}} = \frac{6.3 + 75.0\,(T_{\text{core}} - 36.6)}{1 + 0.5\,(34.0 - T_{\text{sk}})} \tag{4.46}$$

If terms in brackets become negative, they are set to zero. The threshold values for this equation are the physiological maximum blood volume with $V_{\text{B,max}} = 90 l\text{h}^{-1}\text{m}^{-2}$, and the required minimum volume with $V_{\text{B,min}} = 6.3 l\text{h}^{-1}\text{m}^{-2}$.

The second term of the body heat resistance, the resistance of the muscle, fat and skin layers is calculated as

$$R_{\text{tissue}} = 0.05 \cdot \left(1 + \frac{M - 65}{130} \right)^{-1} + (0.5SF - 2) \cdot 0.0048 + 0.0044 \tag{4.47}$$

using the metabolic rate M (see eq. 4.52) and the mean skinfold thickness *SF* as indicators for the body composition and state (Havenith, 2001). The first term on the right hand side of (4.47) represents the heat transfer resistance of the muscle layer, the second term stands for the heat resistance of the fat and skin layers.

4.5 Calculation of core temperature T_{core}

The temperature of the body core is a parameter that reacts only slowly onto changes in the environmental conditions. Nevertheless it is an important control value of the body and violating the acceptable range of the body core temperature might cause severe health implications.

In the ITC model, the development of the actual core temperature with time is given through the prognostic equation:

$$\frac{\partial T_{\text{core}}}{\partial t} = \frac{Q_{\text{st,core}}}{(1 - \alpha) c_{\text{p}}(\text{Body}) \cdot wg} \tag{4.48}$$

Here, α is the weighting coefficient to model the heat storage distribution in the body as introduced in (4.28), p. 17.

The energy balance of the core $Q_{\text{st,core}}$ is composed out of three components:

$$Q_{\text{st,core}} = \underbrace{A_{\text{du}}\,(M - W)}_{\text{internal heat}} - \underbrace{Q_{\text{co-sk}}}_{\text{exchange with skin}} - \underbrace{A_{\text{du}} \cdot Q_{\text{res}}}_{\text{respiratory heat loss}} \tag{4.49}$$

from which $Q_{\text{co-sk}}$ establishes the link to the energy balance of the skin and is given by eq. 4.44). The other two components, the internal heat and the respiratory heat loss, are treated in the following two sections.

4.5.1 Internal heat and metabolic rate M

The internal heat is composed out of the metabolic rate M and the effective mechanical power W which can be neglected in most of the cases. In this model, the metabolic rate M contains the basal metabolic rate M_{bas} plus the additional metabolism due to work (motion) M_{mot}:

$$M = M_{\text{bas}} + M_{\text{mot}} \tag{4.50}$$

For the estimation of M_{bas}, the approach from Gagge et al. (1971) is used:

$$M_{\text{bas}} = x_1 \cdot wg^{0.75} \cdot [1.0 + 0.004\,(30 - ag) + x_2 \cdot (z - x_3)] \quad (4.51)$$

with x_1=3.45, x_2=0.010 and x_3=43.4 for male and x_1=3.19, x_2=0.018 and x_3=42.1 for female persons. The parameter z relates to the body height and weight with

$$z = (ht \cdot 100)/wg^{0.33}$$

for both genders.

The additional metabolism M_{mot} due to motion can be related directly to the actual walking velocity of the virtual human v_{act} which is provided during the simulation from the pedestrian movement model *PedWalk* . In lack of a better approach and in order to obtain a smooth transition of the metabolism under changing walking velocities, a regression was calculated over the original values metabolism data given in VDI 3787 (1996).

From the regression analysis, the following expression for calculating the work metabolism from the walking velocity has been obtained:

$$M_{\text{mot}} = 42.81 + 21.11 \cdot (v_{\text{act}})^3 \quad (4.52)$$

For values of v_{act} between 0.89 and 1.78 ms^{-1} the function gives a satisfying R^2 better than 0.99. For values outside this range, comparison data are missing.

To avoid unrealistic oscillations of M_{mot} due to short term changes in walking velocity (jams, stops,...), an artificial inertia is added to the calculation of the work metabolism:

$$M_{\text{mot}}\,(t + \Delta t) = (1 - \xi\Delta t)\,M_{\text{mot}}(t) + \xi\Delta t\left(42.81 + 21.11 \cdot (v_{\text{act}})^3\right) \quad (4.53)$$

with an relaxation factor ξ arbitrarily set to 0.05 which results in an relaxation time of approximately 1.5 min under average conditions until the new metabolism is reached.

Figure 6 illustrates this concept showing the evolution of the metabolic rate M of an agent walking with a preferred velocity v_{pref} of 1.57 ms^{-1} making two stops. During the walking period, the total metabolic rate is around 200 Wm^{-2} and drops down to 120 Wm^{-2} while the agent stands.

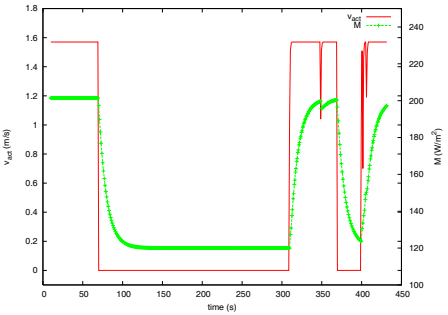

Figure 6: Example evolution of the metabolic rate M with the actual walking velocity v_{act} for an agent walking with a preferred velocity v_{pref} of 1.57 ms^{-1}.

4.5.2 Respiratory heat loss Q_{res}

The heat loss due to respiration can amount up to 15 to 25% of the body's total heat loss (Cain et al., 1990). This component summarises the convective heat needed to warm the breathed air up to 37°C (C_{res}) plus the energy required to saturate it with vapour (E_{res}):

$$Q_{\text{res}} = C_{\text{res}} + E_{\text{res}} \quad (4.54)$$

with

$$C_{\text{res}} = \rho\dot{V} \cdot c_{\text{p}} \cdot (T_{\text{ex}} - T_{\text{a}})$$
$$E_{\text{res}} = \rho\dot{V} \cdot 0.623\frac{L}{p}\,(e^*(T_{\text{ex}}) - e_{\text{a}})$$

Here, T_{ex} is the expiration temperature and $\rho\dot{V}$ is the ventilation rate in [kg s^{-1}m^{-2}]. The air pressure is assumed to be normal pressure p=p_0=1013 hPa in the model.

The expiration temperature depends on the exterior air temperature and on the air humidity. Varene (1986) proposes the relationship

$$T_{\text{ex}} = a + b \cdot T_{\text{a}}$$

where the choice of a and b depends on the relative humidity of the air (rH):

$$a = 24, b = 0.32 \quad ; rH < 35\%$$
$$a = 26, b = 0.25 \quad ; 35 \leq rH < 65\%$$
$$a = 27, b = 0.20 \quad ; 65 \leq rH < 100\%$$

For the ventilation rate $\dot{V}$ Livingstone et al. (1994) propose the following relationship with the metabolic rate M:

$$\dot{V} = 0.076 \cdot M \tag{4.55}$$

in which $\dot{V}$ is in [l min^{-1}m^{-2}] when M is in [Wm^{-2}]. For $\rho\dot{V}$ in [kgs^{-1}m^{-2}] the relation becomes

$$\rho\dot{V} = 1.6254 \cdot 10^{-6} M \tag{4.56}$$

Total water loss

Finally, the total respirative water loss in grams per hour can be calculated as

$$W_{\text{resp}} = \frac{E_{\text{res}}}{L} \cdot 3600 \cdot 1000$$

This loss adds to the loss of water through skin vapour diffusion and sweat evaporation, so that the overall water loss for the body writes

$$W_{\text{ges}} = M_{\text{sk}} + M_{\text{resp}}$$

4.6 Calculation of pollutant inhalation

Besides the thermal comfort, the local air quality is an important indicator for environmental quality. To evaluate the success of air improvement measures, it is useful to know the exposure of individuals to different pollutants. As the ITCM already provides the ventilation rate $\dot{V}$, it is easy to calculate the total amount of inhaled pollutants from the local concentration values.

The total amount of inhaled pollutants $\dot{\chi}_\Sigma$ is calculated as the product of local pollutant concentration χ and the ventilation rate $\dot{V}$ given by (4.55):

$$\dot{\chi}_\Sigma(t + \Delta t) = \chi_{\text{sum}}\,(t) + A_{\text{du}} \cdot \dot{V}/60 \cdot 0.001\chi \cdot \Delta t \tag{4.57}$$

with $\dot{\chi}_\Sigma$ in μg when χ is in μgm^{-3}.

$\dot{\chi}_\Sigma$ is summed up during the activity of the agent in the model and can afterwards be normalised with the trip duration of the agent to obtain a value comparable with other agents.

4.7 The Effective Temperature indicators (d)ET and (s)ET

Using skin and core temperature as thermal comfort indicators appear abstract and difficult to interpret to many people. One way to find a better interpretable representation of the thermal state of the body is to relate the actual skin and core temperature to the air temperature in a fictive room with no radiative input (T_{mrt}=T_{a}) and almost no air movement (v_{wind}=0.1 ms^{-1}) which would result in the same thermal conditions as the observed. For the indoor humidity, classically a constant value of e_{a}= 12 hPa is used which makes the humidity insensitive against the indoor air temperature.

This concept is used by many different thermal comfort indicators such as the *New Effective Temperature ET** (Gagge et al., 1986) including the outdoor extension *OUT_SET** (Pickup and de Dear, 2000), the *Physiological Equivalent Temperature PET* (Mayer and Höppe, 1987) or the *Perceived Temperature PT* (Jendritzky et al., 2002). However, the main difference between those methods is the approach that is used to calculate the corresponding skin and core temperature out of the given meteorological conditions, the remaining concept is the same.

Mayer and Höppe (1987) for example defined PET as follows

> "The Physiological Equivalent Temperature is defined as the air temperature at which in a typical indoor setting (without wind and solar radiation) the heat budget of the human body is balanced with the same core and skin"

The concepts of the other indices are more or less equal to this PET definition. Figure 7 (compiled after Höppe, 2002; Matzarakis and Mayer, 1997) shows a rough comparison of the thermal sensation expressed using the PMV scale and the corresponding PET values calculated for a metabolic rate of 80 Wm^{-2} and a *clo* value 0.8. However, this figure should be regarded only as a rough classification idea about the PMV and PET values and the associated thermal sensation as PMV values outside the interval -2 to +2 must be treated with caution due to the PMV model assumptions (Mayer, 2005, pers. comm.).

For further use in the ITCM model we will re-use the term "*Effective Temperature*", being aware that

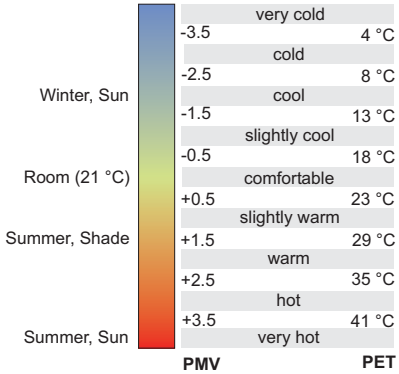

Figure 7: Thermal sensation scale and associated PMV and PET values (compiled after Höppe, 2002; Matzarakis and Mayer, 1997).

it is not totally conform with the standard calculation routine as proposed by Gagge et al. (1986). In the context of this dynamical model, two different types of Effective Temperature are distinguished: the *dynamic Effective Temperature (d)ET* which is based on the actual skin and core temperature of an individual agent at the time he passes a certain location (and where the heat budget is not necessarily balanced), and the *static Effective Temperature (s)ET*, which is a rough estimate of the Effective Temperature under a balanced energy budget assuming that no other parameter will change.

To obtain both (d)ET and (s)ET the following calculation steps are implemented into the model:

1. For each agent the actual skin and core temperature are taken as start values. Then, the following indoor conditions are assumed: T_{mrt}=T_{a}, v_{wind}=0.1 ms^{-1}, v_{act}=0.5 ms^{-1} (=light activity). The indoor humidity is set to a value of 50% relative humidity related to the indoor air temperature. For the clothing insulation and the vapour permeability index, the static values $I_{\mathrm{cl}}^{\mathrm{s}}$ and $i_{\mathrm{m}}^{\mathrm{s}}$ are taken.

   These values are inserted in the concerning equations of the ITC model.

2. The energy balance equation (4.58), p. 24 is solved for Q_{EB}=0, keeping T_{sk} and T_{core} constant but iterating over T_{a} and related T_{mrt} and e_{a} to find the equilibrium state.

3. The final air temperature T_{a} with which Q_{EB}=0 equals the dynamic Effective Temperature (d)ET.

4. To predict the static Effective Temperature (s)ET under a balanced heat budget, the energy balance equation is solved Q_{EB}=EB. Doing this, the resulting T_{a} is adjusted to compensate the actually missing ($EB < 0$, body cooling down) or surplus ($EB > 0$, body heating up) energy.

Normally, the Effective Temperature is related to static conditions, hence the static skin and core temperatures are estimated first before the equivalent air temperature is calculated. The last step for obtaining (s)ET is similar to this approach, but skips the calculation of the static skin and core temperatures. Instead, the energy balance equation is modified to compensate the non-balanced energy budget. This method normally returns values very close or equal to the Effective Temperature obtained through the standard procedure. Only in the case of important physiological changes between the actual and the static thermal state like changes in sweating the real static Effective Temperature will be over- or underpredicted (compare Section 5.3.2, p. 37 ff). For the practical implementation in the BOTworld system, the quick s(ET) estimate is more practical than two additional iterations for each agent at each position.

Although, from the theoretical point of view, (d)ET and (s)ET are not equal to the values obtained using the ET*, PET or other methods, their meaning is the same, hence their values can be directly compared to other indicators based on the same concept.

4.8 Model initialisation

The initial conditions of the biometeorological model represent the meteorological situation the virtual pedestrians have been exposed to before they enter the test area. Hence, these settings are of great importance for the resulting thermal comfort situation as they determine the initial thermal load of the agents.

In general, three different situations are possible: i) the climate conditions in the nearby areas are comparable to the average conditions in the analysed area,

ii) the nearby areas are characterised by patches of sun and shade, or iii) the surroundings are dominated by shady conditions or the majority of people are entering the area from indoors.

For each given situation one of these constellations makes more sense than the other and should be selected as the initialisation method for the model simulation.

The ITCM implemented into the BOTworld system offers four different ways to initialise the model, which can be selected by the user with respect to the best fit to the analysed situation:

1. Start with given skin and core temperature
2. Initialization from average climate data
3. Initialization from user defined climate data
4. Initialization with a "*Synthetic Environment*"

Predefining the initial skin and the core temperature is the most simple way of starting the ITCM model that leaves the responsibility of selecting appropriate values completely to the user.

The other three initialization procedures require the definition of the meteorological boundary conditions for the air temperature (T_a), mean radiative temperature T_{mrt}, vapour pressure e and wind speed v_{wind} as input. In case of the initialisation option (2), these climate data are extracted as averages of the actual climate data loaded for the simulation area whereas for option (3) the required data must be given by the user. Method (2) represents the case in which the climate conditions of the surrounding are comparable to the conditions inside the model area, whereas option (3) can be used to simulate any starting condition, including entering the model domain from indoors, air-conditioned car or similar environments.

Finally, method (4), the "*Synthetic Environment*" (*synthetic* as it does not exist in the model area), is the most complex, but also the most realistic method for most applications. In this procedure, the agent is exposed to 12 varying climate environments for a total initialisation period of 60 minutes. To construct these environments, the minimum, the maximum and the average value for each of the climate variables T_a, T_{mrt}, e and v_{wind} are extracted out of the climate data actually loaded in the model and assigned to one of the four condition indexes. In case of the radiative temperature, this assignment reads:

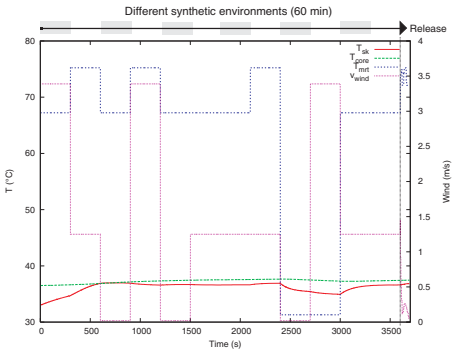

Figure 8: Variation of mean radiant temperature and wind speed during the "Synthetic Environment" initialisation and the calculated corresponding skin and core temperatures.

$$T_{mrt}[1] = \min(T_{mrt})$$
$$T_{mrt}[2 \text{ and } 3] = \overline{T}_{mrt}$$
$$T_{mrt}[4] = \max(T_{mrt})$$

For the other variables, the assignment is accordingly. To simulate a walk through the synthetic environment, individual random numbers between 1 and 4 are created for each climate parameter and the assigned minimum, average or maximum value is used to compose the climate condition the agent is exposed to over the period of 60/12= 5 minutes. Figure 8 shows an example of such an initialisation procedure by plotting the radiative and wind conditions during the initialisation phase versus the calculated skin and core temperature (the agent properties correspond to the agent "Marvin" introduced in Section 5.3, p. 30 ff)

After the boundary meteorological variables are known and the remaining parameters required in the ITC model are calculated, the prognostic equations for T_{sk} and T_{core} plus the associated fluxes are solved.

In case of the initialisation methods (2) and (3) the energy balance of the human body

$$Q_{EB} = A_{du} \cdot (M - W) - A_{du} \cdot Q_{res} - A_{du} \cdot LE_{sk} + A_{sk} \cdot C_{sk} + A_{sk} \cdot R_{sk} - A_{cl} \cdot G_{cl} \quad (4.58)$$

is then iterated until an equilibrium state is reached (Q_{EB}=0) or a maximum initialisation time was reached (default 60 min). [9] If the "*Synthetic Environment*" method is used, the initialisation routine equals the normal prognostic calculation loop.

After the biometeorological data have been initialised, the agent is released into the model environment and begins to visit the list of routing points.

4.9 Numerical aspects

The prognostic equations for the skin temperature (4.25), the core temperature (4.48) and the sweat balance (4.33) are solved forward in time with an explicit numerical scheme. As all of the thermal components included in this system react quite slowly, the choice of the required time step is more limited through the changes of the meteorological boundary conditions rather than by stability concerns. Hence, a fixed time step of 1 sec is considered small enough for all relevant processes. In case of the sweat balance *SW* equation (4.33), it is accurate enough to reset the solution to zero in case of negative values of *SW*.

The numerical solution of the ITCM model is embedded into the MA-system BOTworld which takes care of the movement of the agent through the virtual environment. From here (especially from the *PedWalk* model) an additional stability condition applies to all submodules of the BOTworld system, including the ITCM:

$$\Delta t_{\max} = 0.5 \frac{\Delta xy}{\max v_{\mathrm{act}}(1..n)}$$

where Δxy is the horizontal resolution of the grid mesh and $\max v_{\mathrm{act}}$ is the maximum actual velocity over all active n agents in the model system. This condition ensures, that no grid positions are overlooked in the case of fast running agents.

9. The prognostic equation for sweat accumulation is not used in the initialisation phase using the steady-state conditions

Part II
Model Results

5 Case studies with the ITCM: Thermal comfort conditions of a simple urban open space

The method of Multi-agent simulations offer a multitude of different view angles onto the simulation:

- Individual focussed analysis
- Spatial aggregation
- Community aggregation ("*Virtual interviews*")

The most detailed insight into the dynamics of the thermoregulatory system can be obtained by focussing on the state of a single agent walking through the model world. In this analysis, the temporal development of all physiological parameters with time can be studied exactly, but only few information can be obtained about the spatial distribution of the thermal comfort conditions inside the model area. Contrary, the method of spatial aggregation collects the data from the individual agents walking through the model. With this method, map-like two dimensional graphics can be generated which allow to assess the thermal conditions in the model area, but the information about the state of the individual agent is lost through averaging. Hence, this method is not well suited to understand the processes that lead to the observed values in the perspective of the single agent.

The third method, called "*Virtual Interview*" combines aspects of both other procedures. Like in a real world street interview, different areas of interest can be selected inside the BOTworld model environment. Each agent entering these survey areas will be electronically "questioned" about his actual state. These data will then be compiled and frequency distributions can be generated for all model parameters. The advantage of this method is that the it has a larger spatial relevance compared to the agent focussed analysis, but at the same time, the agent's individual data are preserved to a larger extent compared to one averaged value per grid point.

In this second part of the paper, the application of the ITC model embedded into the Multi-Agent simulation system BOTworld will be presented. Using the three analysis method mentioned above, typical situations will be presented and discussed using the example of a simple square urban open space.

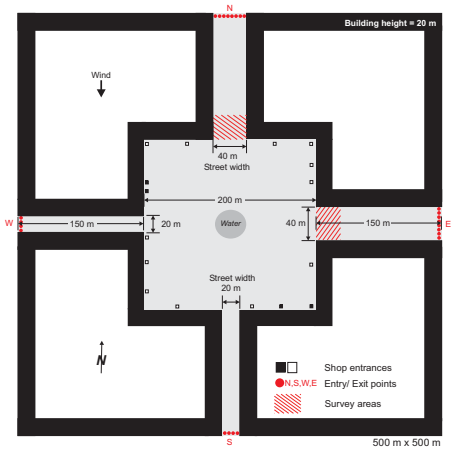

Figure 9: Model domain for the "Urban open space" test case. Red circles indicate routing points where agents enter and leave the model area, squares indicate internal targets visited by the agents (filled squares belong to the same location as for example different entrances to the same building).

In the following sections, some comparisons will be made between thermal comfort calculated with the BOTworld model and, on the other hand, calculated using the PMV method. Although PMV is not the most up-to-date static index as for example PET (Höppe, 1999) or OUT_SET* (Spagnolo and de Dear, 2003; Pickup and de Dear, 2000) are newer, we will use it as a counterpart example as it is still widely applied today.

5.1 The study domain and simulation settings

In order to present a typical application of the ITCM/BOTworld system and to analyse the simulation results, a simple test case of a symmetric bare urban open space have been chosen as shown in Figure 9.

Spatial model layout

The central place is a 200 m $\times$ 200 m large open space which can be accessed through four street canyons, each 150 m long. Two of these streets are 20 m wide (west and south street) and two are 40 m wide (north and east street). The morphology of the streets and of the central place is formed by closed building fronts with an uniform height of 20 m each. The total size of the study is 500 m $\times$ 500 m and is analysed in the BOTworld system with a spatial resolution of Δxy=2 m. In the center of the open place, a decorative water pond is placed which cannot be crossed by pedestrians. This element was introduced to prevent too straight lines of movement. It has almost no impact on the microclimate conditions.

The pedestrian traffic inside the model domain is created through routing points as indicated in Figure 9 ("*Shop entrances*" and "*Entry/ Exit points*"). In BOTworld, two different kinds of routing points can be distinguished: Routing points that serve as entry and/or exit points from/to the model domain and routing points that serve as internal targets.

Entry/ Exit points are the interface to the outside model world where the agents enter and leave the model area (e.g bus stops, parking lots or, as in this case, the lateral model boundaries). In the test domain, this type of points is used at the end of the four streets and is labelled with "N", "S", "W" and "E". For those points, a uniform agent flux rate of 10 agents per minute for the narrow streets ("W" and "S") and 20 agents per minute for the wide street ("N" and "E") is used.

Contrary, *internal targets* are routing points inside the model domain which are visited by pedestrians but cannot serve as entry or exit points (e.g. shops). These internal targets are used to create a list of intermediate targets for each agent, which will be visited before the agent steers towards his assigned exit point and leaves the model. For the following simulation a maximum of 3 internal targets have been assigned to each agent. In order to simulate differences in the popularity of the internal targets, each target has its own visitor frequentation rate. Target points with a higher frequentation rate will appear more frequent on the agent itineraries compared to those with a lower frequentation. However, for the simulation of human thermal comfort, the partition of pedestrian flows between the different routing points is of interest rather than the absolute traffic volumes. Therefore some arbitrary agent flux rates between 0.1 and 1.0 agents per minute have been assigned to the internal targets, where those buildings with two entrances

Table 5: Settings for the BOTworld agent community and for the microclimate simulation with ENVI-met.

Settings BOTworld Community	
Age distribution	$\overline{ag}$=40 y, $\sigma(ag)$=15 y
Body Mass Index distribution	$\overline{BMI}$=22, $\sigma(BMI)$=2
Static clothing insulation dist.	$\overline{clo}$=0.5 clo, $\sigma(clo)$=0.1 clo
Preferred velocity distribution	$\overline{v}_{\text{pref}}$=1.34 ms^{-1}, $\sigma(v_{\text{pref}})$=0.26 ms^{-1}
Settings Microclimate Simulation	
Simulated day	23th June
Simulated position	Bochum, Germany 7.5° e.Long., 53.0° n.Lat
Above-roof wind (10 m)	2.0 ms^{-1} from N
Reference temperature atmosphere	22.0°C
Initial relative humidity	50%
Dimension model area	500 m × 500 m
Resolution model area	
ENVI-met	Δxy=4 m
BOTworld	Δxy=2 m

(filled squares in Figure 9) get the maximum rate of 1 agent per minute.

Each simulation runs over a user-defined time period. In order to obtain statistically representative data, a simulation time of 30 to 60 min is a good choice for this test case. During this time, approximately 1500 agents with individual routes and properties are generated and analysed by the BOTworld system. It has to be noted that in the recent program version, the climate conditions do not progress during the simulation time, the 14:00 CET situation stays constant even after 60 min of simulation time.

Agent community settings

In contrast to traditional comfort indices based on average values for the analysed community in terms of age, walking speed, clothing etc., BOTworld generates an individual set of properties for each single agent based on the user-defined mean and standard deviation parameters (see *Settings BOTworld Community* in Table 5). For this simulation, average conditions have been used in terms of age and Body Mass Index. Also, the proposed mean value and standard deviation for the preferred walking velocity is typical for a standard urban traffic situation (Weidmann, 1993). For the clothing insulation values, it was assumed that the agent community wears light summer clothes with an average static insulation value of 0.5 clo.

To get an impression, what these settings actually

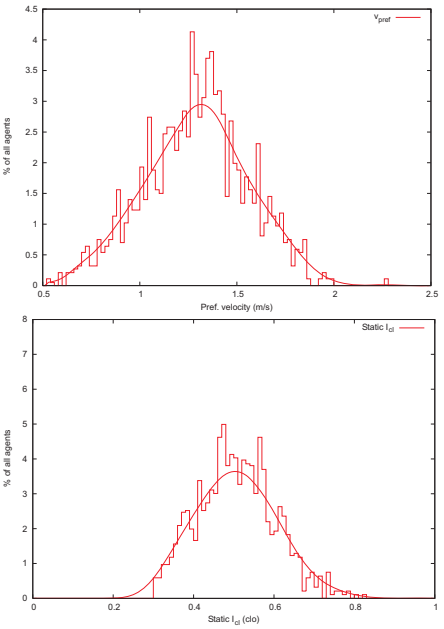

Figure 10: Example distribution of the agent properties "preferred velocity" (v_{pref}, top) and "static clothing insulation" (clo, bottom).

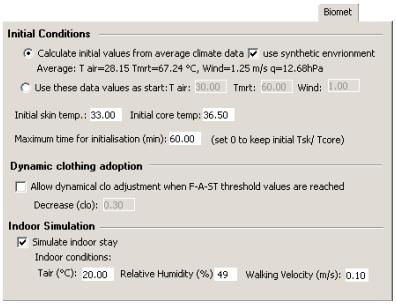

Figure 11: Interface for the biometeorological model offered by the BOTworld simulation system with example settings.

mean in the simulation, two example distributions for the agent properties "preferred velocity" (v_{pref}) and "static clothing insulation" (I_{cl}) are shown in Figure 10. It has to be noted that the generation of the individual agent properties are based on random functions, so each simulation run generates a unique distribution of properties slightly different to the ones generated before. The distribution shown in Figure 10 is just one example picked out of the multitude of different simulation runs performed.

Settings for the biometeorological model system

The implementation of the ITCM inside the BOTworld environment offers a large number of simulation settings that affect the results of the simulation. Some of these settings, for example the selection of the initialisation method, origin from the biometeorological model itself and have been discussed before. Other settings, like the simulation of indoor stays, are possibilities that arise from the combination of the ITCM with the Multi-Agent system and will be discussed later. Figure 11 shows the interface of the BOTworld system for the biometeorological model.

The options shown under "*Initial conditions*" refer to the different initialisation methods of the ITCM model as presented in Section 4.8, p. 23 f. For the simulations presented in the following sections, different settings have been used here that will be discussed in the related text sections.

The "*Dynamic clothing adaptation*" is a special feature for the behaviour-controlled simulation of thermal comfort that is not treated in this paper.

Finally, the "*Indoor Simulation*" is a feature of the BOTworld system that allows to simulate the effects of temporary indoor stays of the agents while they travel through the model area. The usage and the effects of this option will be discussed in Section 5.6, p. 45 ff.

5.2 Simulated microclimate conditions

Before the thermal comfort conditions of the model area can be assessed, the driving meteorological parameters are required for each grid cell. These data are, as already mentioned in Section 3, p. 8: Air temperature (T_{a}), wind speed and direction (v_{wind} and ϕ_{wind}), mean radiant temperature (T_{mrt} and air humidity as vapour pressure (e_{a}).

In general, it is irrelevant from which source these data come as long as they are complete over the entire model area and fit with the structure of the urban morphology. In this study, the microclimate model ENVI-met (Bruse and Fleer, 1998) is used to generate the required input data for the BOTworld system. For the microclimate simulations, the spatial resolution of the model area was reduced to Δxy=4 m and the results were then linearly interpolated to the Δxy=2 m resolution used for the Multi-Agent simulation.

The geographic position of the test area as well as the basic input data for the microclimate simulations are summarised in Table 5. The reference air temperature in 2500 m height was set to 22°C which results in ground level air temperatures between 28 and 29°C at 14:00 CET. The settings for the solar radiation input correspond to a clean atmosphere with no clouds giving a maximum global radiation of 1000 $\text{Wm}^{-}2$ at noon. Hence, these settings correspond to a hot, sunny summer day with moderate winds coming from north. This situation may be considered relatively untypical for a German summer as it usually happens only on a few days, if at all. However, the point in this choice of meteorological situation is to demonstrate the general behaviour of the ITC model which works best when all the influencing parameters are well developed. So, for more average conditions, the general statements of this analysis remain

the same but might be less elaborated. Alternatively, the test area can be considered to be somewhere in South Europe or somewhere else where this meteorological situation is more frequent.

Figure 12 shows the basic meteorological situation at 14:00 Central European Time (CET) close to the biometeorological relevant reverence level at 1.60 m above ground. [10] This time of day serves as the main analysis situation in the following sections because it normally offers the most severe conditions with respect to hot thermal discomfort.

The wind flow pattern (Fig. 12 a) shows a typical distinction between the N–S orientated street canyons with a street-parallel flow and the W–E canyons, which are perpendicular to the main wind direction. Consequently, the N–S canyons are dominated with high wind speeds whereas the wind in the W–E streets is calm. On the central place, the wind speed varies between a maximum of 1.75 ms^{-1} at the entrance to the northern street segment and a minimum of below 0.5 ms^{-1} in the corners of the place while most of the place show average wind speeds 1.25 ms^{-1}.

As far as the air temperature distribution (Fig. 12 b) is concerned, there are only small spatial variations with temperatures ranging between 28 and 29°C observable which is typical for a well-mixed urban boundary layer and does not require further analysis.

The spatial distribution of sun and shade and the resulting distribution of surface temperatures are well represented through the mean radiant temperature as shown in Figure 12 (c): Most of the area is in full sun, resulting in T_{mrt} values around 70°C and more due to the high solar input. The small patch of lower radiant temperature in the middle of the place is due to the reduction in ground surface temperature where the small water pond is situated.

Finally, Figure 12 (d) gives an impression over the resulting thermal comfort as predicted by the BOTworld system using the standard PMV method after VDI 3787 (1996). To calculate the PMV values, average data for the static clothing insulation (0.5 clo) and for the internal heat production (165 Wm^{-2}) have been used.

In conclusion, the average climate conditions found in the four street segments can be characterised as follows:

Table 6: Selected agents from the model simulation including their main physiological parameters and movement pattern.

Agent	Gender [m/f]	Age [y]	Height [m]	Weight [kg]	Route
”Marvin”	m	48	1.82	75	W→E, in shade
”Claire”	f	17	1.60	56	W←E in sun
”Antonio”	m	66	1.69	70	N↓S in shade
”Melissa”	f	49	1.86	76	S↑N in shade

- N: sunny and windy
- E: sunny and calm
- S: mix of sun and shade, windy
- W: mix of sun and shade, calm

5.3 Individual thermal comfort: Agent-focussed ITCM analysis

To start the analysis of the ITCM/BOTworld system, we will focus on the thermal comfort of selected agents moving through the environment. Four exemplary agents, ”Marvin”, ”Claire”, ”Antonio” and ”Melissa”, have been picked more or less randomly from the pool of simulated agents.[11] The only selection criteria has been, that each of these agents use a simple and direct walking route through the model area. In order to keep this initial analysis simple, no internal target points are used in this simulation.

Table 6 lists the selected agents, their basic properties and the walking routes they have chosen through the model domain. For each symmetry axis, one pair of agents has been chosen, ”Marvin” and ”Claire” for the W–E axis and ”Antonio” and ”Melissa” for the N–S axis. From each pair, one agents walks on the sunny side of the street canyon whereas the other one uses the shaded side and walks in the opposite direction.

10. Actually these values correspond to the 2.0 m level due to restrictions in the vertical model resolution

11. The names of the agents are picked randomly out of a gender specific names database to allow a better identification compared to numeric IDs

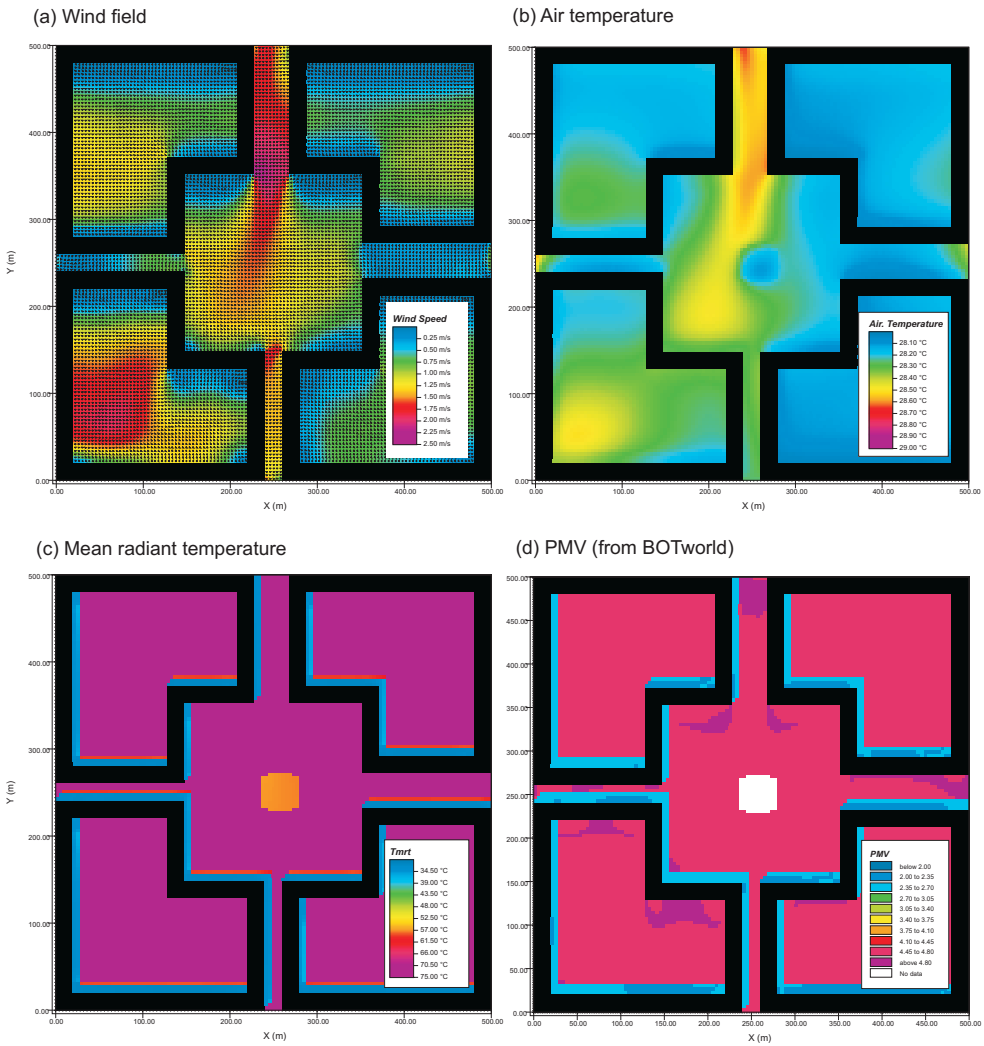

Figure 12: Biometeorological relevant microclimate conditions in 2 m height above ground at 14:00 CET simulated with ENVI-met: (a) wind flow pattern and wind speed, (b) air temperature, (c) mean radiant temperature and (d) corresponding PMV values calculated in BOTworld.

Table 7: Initial values of skin and core temperature for the four selected agents compared to the two-node models IMEM and ASHRAE.

Agent	v_{pref} [ms^{-1}]	clo [clo]	T_{sk} (ITCM) [°C]	T_{sk} (IMEM) [°C]	T_{sk} (ASHRAE) [°C]	T_{core} (ITCM) [°C]	T_{core} (IMEM) [°C]	T_{core} (ASHRAE) [°C]
"Marvin"	0.98	0.43	36.61	36.3	36.54	37.72	37.8	37.71
"Claire"	1.51	0.35	37.01	36.4	36.54	38.41	37.9	37.99
"Antonio"	1.19	0.41	36.60	36.3	36.53	37.75	37.8	37.73
"Melissa"	1.23	0.38	36.99	36.4	36.48	38.24	37.9	37.78

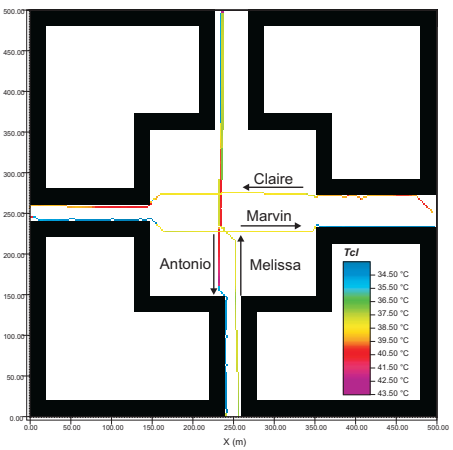

Figure 13: Routes of the four selected agents through the model environment. Trajectories are coloured with the actual clothing temperature T_{cl} at the respective positions.

5.3.1 Case A: Individual thermal comfort in case of entering the model area from similar climate conditions

For the first numerical test, we assume that the surrounding areas offer the same climate conditions as those found inside the model area. According to the different initialisation procedures mentioned in Section 4.8, p. 23 f, this corresponds to the procedure in which each new agent is exposed to constant climate conditions until a balanced energy budget is reached. In case of the 14:00 CET situation, these static conditions equal the average climate conditions extracted from the ENVI-met simulation data which are: T_{a}=28.15°C, T_{mrt} = 67.24°C, v_{wind}=1.25 ms^{-1} and e_{a}= 12.68 hPa. Hence, we assume a continuation of the sunny and warm conditions outside the observed model area. For the initial human parameters, a skin temperature of 33°C and core temperature of 36.5°C have been assumed.

Table 7 shows the initial T_{sk} and T_{core} values calculated by the ITCM model compared to the results obtained by the two-node models IMEM from Peter Höppe and a two-node model based on the equations from ASHRAE (1992) provided on the internet site from Richard de Dear, Macquarie University, Sydney (ASHRAE model hereafter). [12] As far as possible, all controllable parameter such as metabolic rate or wind velocity in both models have been adjusted to meet the properties of the four analysed agents. However, the models still differ significantly from the ITCM with respect to the personalisation of the agents and other non-adjustable parameters. Hence, this comparison should only serve as a very basic test

12. IMEM version from 1.5.1996 obtained as a part of VDI 3787 (1996) and ASHRAE accessed on the 4.6.2005 from `http://atmos.es.mq.edu.au/~rdedear/pmv/`

to check whether the values predicted by the ITCM are in the range of data calculated by other models or not.

Comparing ITCM to IMEM and ASHRAE, we find the maximum differences for the skin and core temperature for the agent "Claire". This is not surprising as this agent differs most in terms of gender, age, height and weight from the average conditions assumed by IMEM and ASHRAE (standard male person with age 35 y, height 1.75 m and weight 75 kg) from which ASHRAE at least allows to adjust the DuBois Area parameter. The same applies to a lower degree to the other female agent "Melissa". For the male agents, the simulated skin and core temperatures from ITCM fit well with the ASHRAE model (differences below 0.1 K) and, with slightly larger differences up to 0.3 K, with IMEM as well.

Starting the analysis of dynamic model behaviour, Figures 14 and 15 show the development of selected parameters of the thermoregulatory system while the four agents move through the model environment. On the abscissas, the life time of the agent relative to the time of release into the model area (but excluding the initialisation phase) is plotted. The grey bars in the diagrams indicate the period while the agents cross the open space. As the agents move with different walking velocities, the time required to cross the model area is of course different.

The diagrams labeled "(a)" show the radiative microclimate conditions in terms of T_{mrt} plus the resulting skin, core and clothing temperature (T_{sk}, T_{core} and T_{cl}). The "(b)" diagrams allow a closer look at the actual energy state of the agents. Here, the absolute energy gain or loss of the body (Q_{EB} according to eq. 4.58, p. 24) and the energy fluxes at the bare skin (R_{sk}, C_{sk} and LE_{sk} per skin area unit) are shown. Finally, the plots indicated with "(c)" take a look at the actual fraction of wet skin (Γ as described through eq. 4.43, p. 19) in relation to the local absolute and relative wind speed (v_{wind} and v_{wrel} respectively).

Starting the analysis with agent "Marvin" moving West to East in the shade, the effect of the local microclimate on the skin temperature can be well observed (Fig. 14 a): When entering the shady street section, the skin temperature drops from the initial 36.61°C down to 35.54°C. After 200 seconds total time, the end of the street is reached and the agent enters the open space where he is exposed to a high mean radiant temperature of around 72°C. Immediately, the skin temperature rises again until the agent reaches the shady street canyon on the opposite side of the place. The core temperature shows only little reaction on the exposure to different microclimates. Here, a general drop from the initial 37.72°C down to 37.54°C at the end of the complete walk can be observed. This small decrease is only slowed down while the agent walks through the sunny open space.

The energy balance of the body and the energy fluxes plotted in Figure 14 (b) allow a detailed analysis of the thermal processes taking place at the different locations of the model area. In principle, a positive energy balance Q_{EB} indicates that the body is heating up and has not reached a stable thermal state (yet). The more positive the actual energy balance is, the more intensive is the perception of heating up when entering a different tempered environment. In case of a negative energy balance, the same principle applies accordingly. Inside the shady street canyons a negative energy balance of around -250 W can be observed, hence this location will give the impression of a cool environment (compared to the initially assumed average climate conditions). While "Marvin" crosses the open space, the energy balance changes to positive values and the body heats up.

For "Claire" the situation is different: As this agent walks constantly through the sun, there is only a small variation in skin temperature and almost no change in the core temperature all through the simulated walk. As the initially assumed sunny and warm conditions endure during the walk through the model area with only small variations due to changing wind conditions, no significant change in the thermal state can be expected. While walking through the street canyons, the energy balance shows a small positive value around 50 W due to the reduced wind speed. Hence, this passage will give the impression of being slightly warmer compared to the initial conditions. Contrary, the open space is appearing a bit cooler due to the higher wind speed which becomes especially effective immediately after entering the open space with a relative high amount of sweat on the skin.

This aspect leads to the last two diagrams (c) of Figure 14 presenting the aspect of skin wetness while walking through the model environment. As explained in Section 4.4.4, p. 18 ff, the fraction of wet skin depends on the amount of sweat produced on

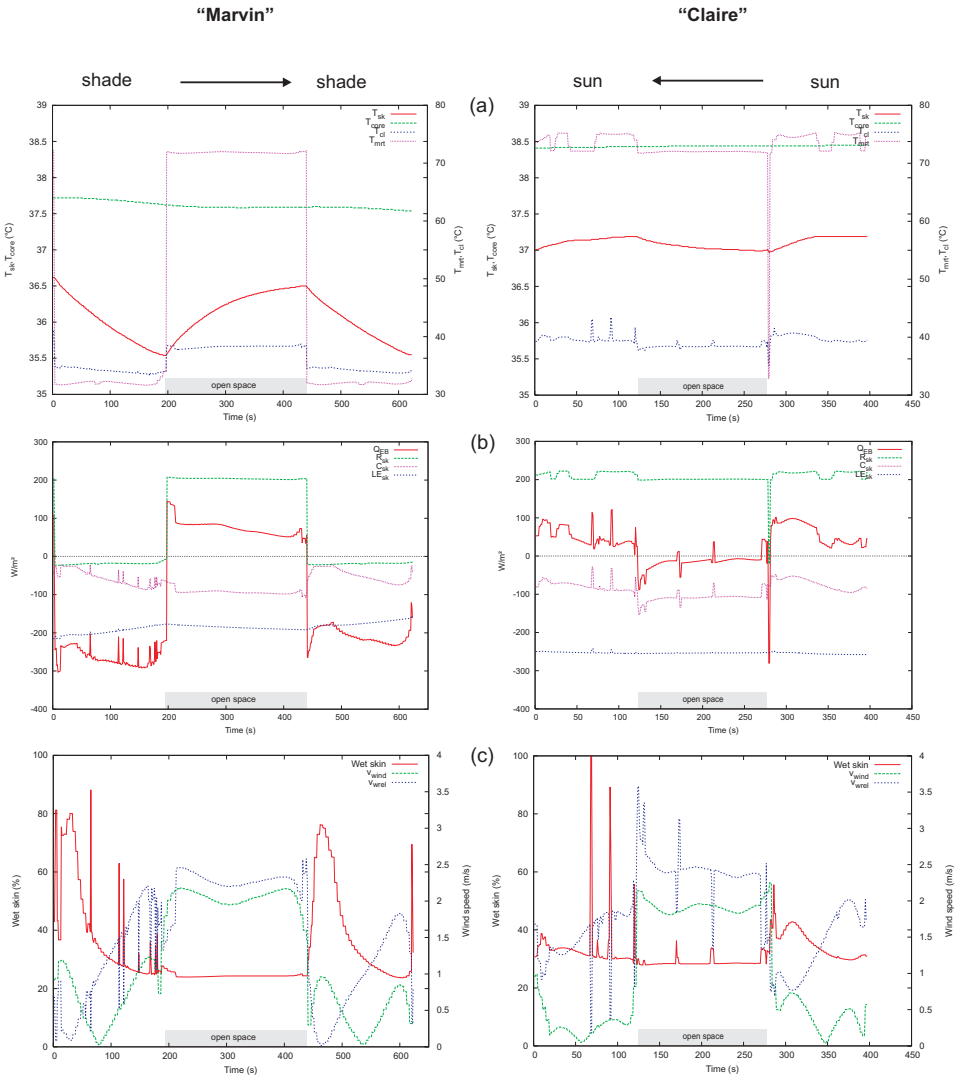

Figure 14: Evolution of selected parameters of the ITC model for the agents "Marvin" and "Claire" walking on the W–E axis of the study domain: Temperature of skin, core and clothing and the local mean radiant temperature (a), total energy balance and radiative, convective and latent energy fluxes per skin surface area (b) and fraction of wet skin and local absolute and relative wind speed (c).

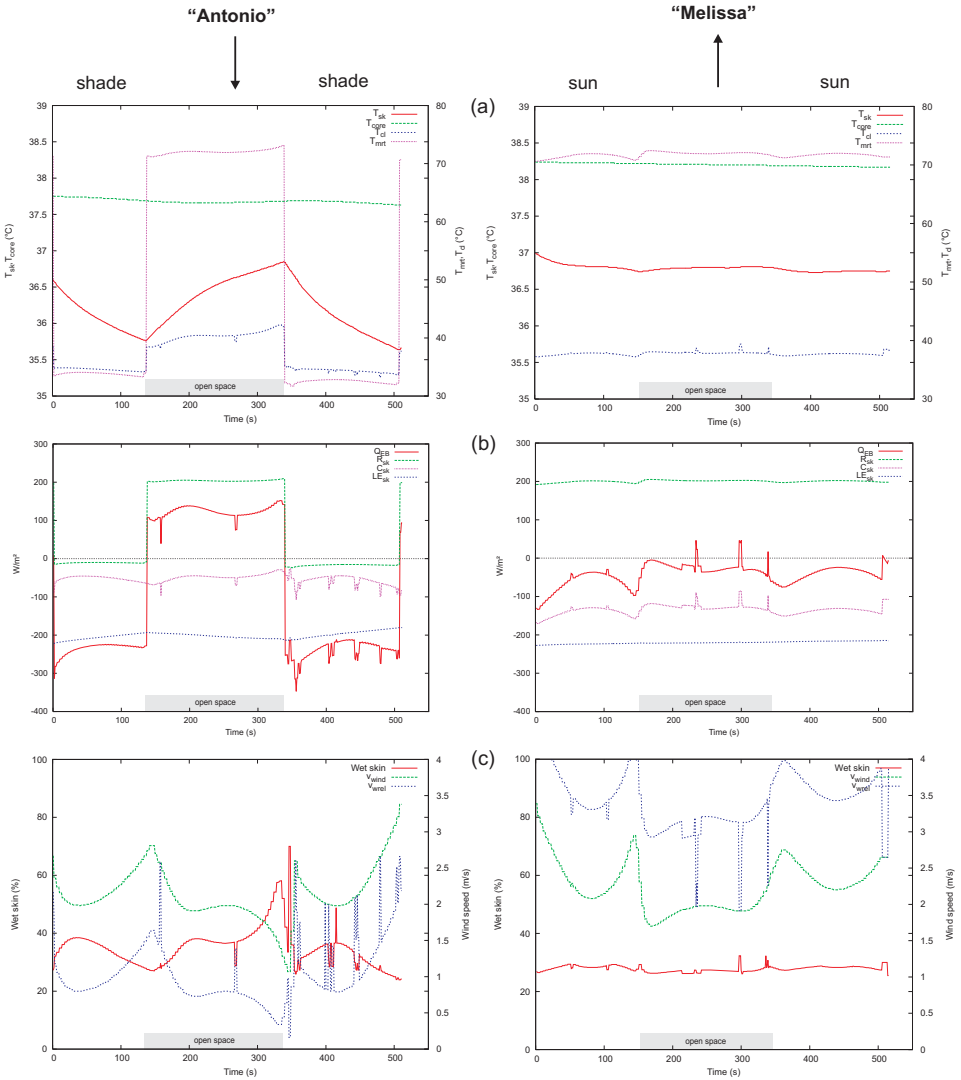

Figure 15: Evolution of selected parameters of the ITC model for the agents "Antonio" and "Melissa" walking on the N–S axis of the study domain: Temperature of skin, core and clothing and the local mean radiant temperature (a), total energy balance and radiative, convective and latent energy fluxes per skin surface area (b) and fraction of wet skin and local absolute and relative wind speed (c).

one hand and on the possibility to perspire it on the other. As it can be seen from Figure 14 (b), the transpiration of sweat contributes to a significant amount to the energy balance of the agents. For "Claire" who walks always in the sun, this contribution is at maximum with about -250 Wm^{-2}, but even for "Marvin" who walks mostly in the shade it stays around -200 Wm^{-2} during the walk. As the amount of produced sweat depends to 90% on the core temperature of the body (compare eq. 4.34, p. 18) which is relatively constant for all agents, the wet skin fraction shows its main variation in relation to the different relative wind speeds (v_{wrel}).

In the case of "Marvin", relative high percentages of wet skin can be observed inside the street canyons which can be explained mainly through the low relative wind speed as a consequence of the local wind speed and the walking velocity and direction. With amounts up to 80% wet skin, the street canyons will not appear comfortable to this agent, even if he walks in the shade (high strain according to VDI 3787, 1996). When crossing the open space, the fraction of wet skin stabilises around 24% for "Marvin" and around 30% for "Claire" due to high local wind speeds. This value indicates only light discomfort due to sweating (threshold value equals 25% according to VDI 3787, 1996).

Figure 15 shows the equivalent diagrams for the agents "Antonio" and "Melissa" walking on the N–S axis of the model area. In general, the same observations made for the previous figures also apply to these two agents. As both of them are exposed to relatively high wind speeds all the time, the curves of skin temperature and of the associated energy fluxes appear smoother and the peaks in the wet skin fraction are less developed here. Especially in the case of "Melissa" who experiences high relative wind speed all the time as she walks into the opposite direction of the wind flow (adding vector components), the fraction of wet skin stabilizes around 25% without exceeding 30% at any time.

As the general dynamics of the agent's thermal system is the same for both the W–E and the N–S axis, we will restrict the further analysis now on the agents walking on the W–E axis, and here especially on the walking route that leads through mixed climate environments of sun and shade used by "Marvin".

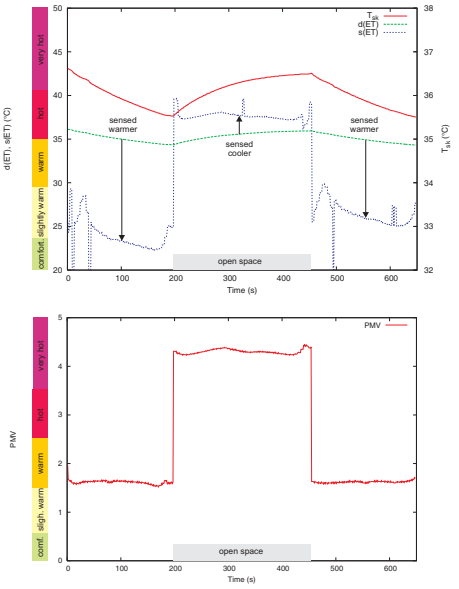

Figure 16: Thermal sensation of agent "Marvin" while walking through the model environment. Top: Evolution of skin temperature T_{sk} and dynamic and static Effective Temperature (d(ET) and s(ET)). Bottom: PMV values calculated using standard routines for the corresponding locations.

Effective Temperature and PMV

Figure 16 (top) shows the development of the dynamic and static Effective Temperature (d)ET and (s)ET for agent "Marvin". As the (d)ET value is linked to the skin and core temperature, it behaves similar: When the agent enters the first shady street section, he enters a thermal environment that is cooler than the assumed initial conditions, hence the dynamic Effective Temperature, which reflects the agent's *actual* thermal state begins slowly to decrease. After entering the sunny open space, it slowly rises again until the opposite shaded street segment is reached.

From Figure 14 (b) it is known, that at no time during the virtual trip through the model the energy budget of the agent reaches a balanced state. Hence, the predicted static Effective Temperature value differers significantly from the dynamic one: Inside the shady

street canyons, the actual thermal sensation is ”hot” with d(ET) values around 36°C while the s(ET) indicator shows values between 23 to 25°C indicating only ”slightly warm” conditions as they are typical for a shaded street on a sunny summer day (Höppe, 2002). When the agent enters the open space, the situation inverts: Here, the static Effective Temperature values increase up to 39°C while d(ET) indicates a cooler sensation with values between 34.5°C when entering the open space and 36°C before leaving it.

For comparison, the associated PMV values calculated for each agent position using the standard PMV method (VDI 3787, 1996) are shown on the lower panel of Figure 16. With values around 1.6 in the shady street segments and above 4 in the open space they correspond to the behaviour of s(ET) indicating moderate warm conditions in the streets and hot discomfort in the open space.

5.3.2 Case B: Individual thermal comfort in case of entering the model area from indoors

Entering an outdoor environment from indoors is the opposite situation compared to the case study presented before. Even if the indoor location is not air-conditioned, the thermal load of a person coming out of a building is normally quite low compared to someone exposed to outdoor conditions for some time. The same applies to people entering the area by car or using other climate-controlled means of transport.

To initialise the model with indoor conditions, the agents have been exposed to $T_a = T_{mrt}$=20.0°C and a wind speed of v_{wind}=0.1 ms^{-1} until a balanced energy budget was reached. For the agent ”Marvin” (the other parameters as listed in Tab. 6, p. 30 remain unchanged), this results in a start skin temperature of 32.12°C and a start core temperature of 36.64°C.

Figure 17 shows the evolution of the main parameters of the ITC model analogously to the study presented in the preceding section. After entering the outdoor environment, the body constantly shows a positive energy balance with about 150 Wm^{-2} in the shady street which reaches the impressive amount of around 450 Wm^{-2} in the open space. Consequently, the skin temperature rises constantly up to a value of T_{sk}= 35.10°C before entering the opposite shaded

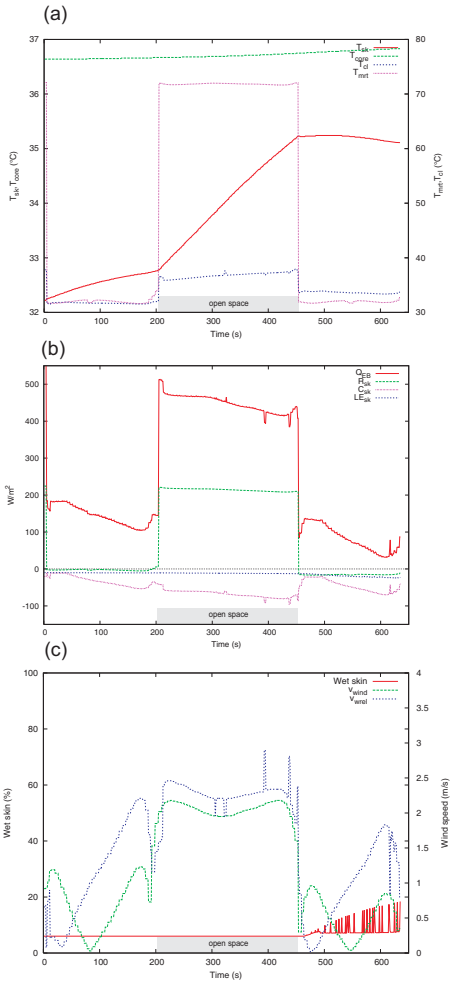

Figure 17: Evolution of selected parameters of the ITC model for the agent ”Marvin” entering the model from indoors and walking in the shade on the W–E axis: Temperatures of skin, core and clothing and the local mean radiant temperature (a), total energy balance and radiative, convective and latent energy fluxes per skin surface area (b) and fraction of wet skin and associated absolute and relative wind speed (c).

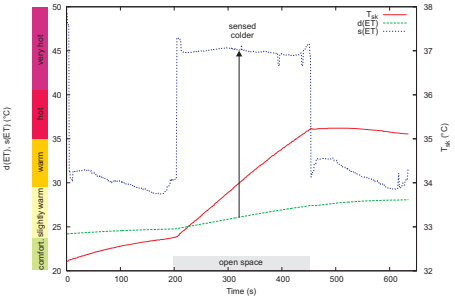

Figure 18: Thermal sensation of agent "Marvin" coming from indoors and walking through the model environment. Evolution of skin temperature T_{sk} and dynamic and static Effective Temperature d(ET) and s(ET).

street segment. While the skin temperature begins to decrease gradually here, a small but constant increase in core temperature can be observed here due to the still positive energy budget of the body.

Only very few latent energy is lost through transpiration and even when entering the wind shielded street sections, the fraction of wet skin does not exceed 20% all through the simulation.

Like in the previous case, Figure 18 shows the thermal sensation of the agent in terms of dynamic and static Effective Temperature.

Due to the significant lower thermal load, the local thermal sensation of the agent coming from indoors is much cooler compared to the static Effective Temperature and to the thermal sensation of agents exposed to outdoor conditions before (values around 27°C versus 36°C on the open space, see Fig. 16 top). During the complete walk, the d(ET) values indicate only "comfortable" to "slightly warm" conditions compared to the "hot" to "very hot" assessment in case A.

The predicted s(ET) values are approximately 5°C higher compared to those calculated by the agent exposed initially to outdoor conditions. Normally, one expects that for the same location and the same agent parameters, the same static Effective Temperature should result. This difference is an effect of the calculation method that was already mentioned in Section 4.7, p. 22: Due to the very low skin temperatures the cooling effect of sweating is not taken into account when predicting the steady state conditions through an extrapolation of the actual energy balance. Hence, the static temperature corresponds to an Effective Temperature if the agent would not sweat.

5.3.3 Conclusions

In this section, a detailed analysis of the energy exchange processes and the resulting thermal sensation of individual agents has been given. To study these aspects, two different initialisation procedures have been used. In case A, a continuation of the meteorological situation inside the model domain has been assumed whereas for case B the thermal sensation of an agent entering the outdoor environment from indoors has been analysed.

As the study area is dominated by sunny areas, the assumption of average initial conditions (case A) leads to relative high thermal loads of the virtual pedestrians when they first appear in the model area. Consequently, agents continuing to walk through the sun ("Claire" and "Melissa") experience only minor modifications of their thermal state compared to the initial conditions whereas agents walking in the shade ("Marvin" and "Antonio") cool down significantly. The relative wind speed was found to be the most influencing parameter when assessing the fraction-of-wet-skin indicator. As the relative wind speed depends both on the local wind velocity and the actual walking direction of the agent, this parameter shows a high temporal and spatial variability which becomes better interpretable when the model results are spatially averaged over the agent community.

In case B, the initially assumed indoor conditions result in much lower start skin and core temperatures. As the thermal load of the agent is much lower and the duration of the indoor stay is relatively short, these start conditions shift the thermal sensation significantly towards a cooler sensation of the environment. During the complete walk, this effect continues which underlines the impact of the thermal history when analyzing local thermal comfort conditions.

5.4 Outdoor thermal comfort: Spatial aggregation

The agent-focussed analysis in the previous section helped to show and analyse the detailed dynamics of the ITC model under various climate conditions. However, as stated in the introduction, in order to make the model practically applicable and to analyze the thermal comfort conditions of an outdoor space, the individual-based data need to be spatially aggregated. This section focuses on the spatial distribution of the main ITCM and thermal comfort parameters. To initialise the simulations, the "*Synthetic Environment*" method was used (compare Section 4.8, p. 23 f) in all cases. The remaining simulation parameters are the same as in the previous simulations.

Spatial data generation

In order to obtain a two-dimensional map of selected agent parameters, the state of all agents entering a grid cell are collected and averaged over the simulation cycle. Due to the random component of the Multi-Agent simulation it can happen that single grid cells are not visited by agents or by only very few agents. As a result, white spaces appear or the resulting averaged values differ from the values on the neighbour grids. In consequence, the generated map looks very noisy and is hard to interpret (compare Fig. 19 top). To improve the result, two post-processing steps are applied to the data: First, missing data are filled if valid data are found within a range of 5 m using a linear inverse distance weighted interpolation (Fig. 19 middle, the interpolation range limit can be modified by the user). Then, a smoothing filter using a 3×3 kernel mask is applied to each grid cell i, j containing valid data:

$$\Phi^*_{\mathrm{i,j}} = \sum_{\mathrm{n}=-1}^{+1} \sum_{\mathrm{m}=-1}^{+1} \frac{1}{x} \Phi_{\mathrm{i+n,j+m}}$$

where x is the number of valid data inside the 3×3 kernel and Φ is the original and Φ^* is the new smoothed value. Figure 19 (bottom) shows the result after this smoothing step. This two–step method was applied to all figures in this section,

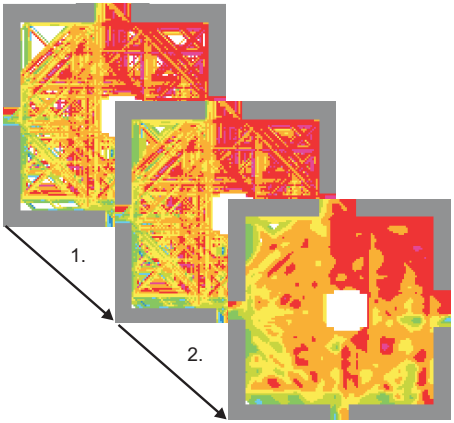

Figure 19: Post-Processing steps of the spatial model data. In step 1 missing values are filled, in step 2 the data are spatially smoothed.

5.4.1 Distribution of skin temperature and energy balance

Figure 20 shows the spatial and frequency distribution of the average skin temperature (a), the average energy balance (b) and of the average change of skin temperature per time (c, only spatial distribution) in the model area for the 14:00 CET situation.

The range of observable skin temperatures is sharply limited to the range between 36 and 37°C with the majority of values in the warmer half of the interval (see Fig. 20 a). Peak values of T_{sk} can be found along the sunlit side of the eastern street segment and in the north-east quarter of the open space while the minimum skin temperatures are located on the shady street sides with very few differences between the different street segments. It is interesting to see that the north-east quarter of the open space shows considerable higher skin temperatures compared to the other quarters although the meteorological conditions at those spots are very similar. To explain this phenomenon, the effect of the agent's movement patterns must be taken into account: The northern and eastern street segments are the two street canyons with the highest pedestrian traffic in the model area (20 agents per minute at their end routing points). Inside these street canyons, sunny conditions dominate and either the absolute wind speed is low (E

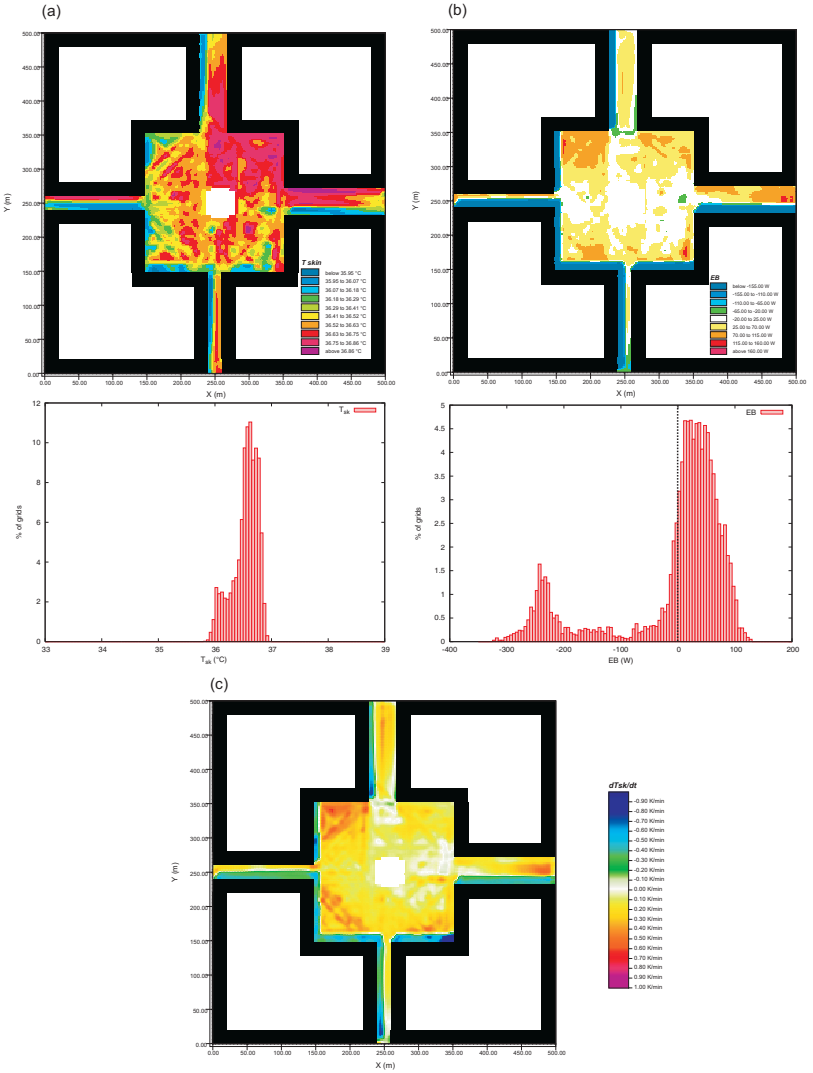

Figure 20: Spatial distribution and frequency distribution of average skin temperature T_{sk} (a), average energy balance EB (b) and average change of skin temperature by time dT_{sk}/dt (c, only spatial distribution) in the model area for the 14:00 CET situation.

segment) or the pedestrians going towards the open space walk with the wind (N segment) which results in low relative wind speeds. As a consequence, the majority of agents entering the open space from the E and N street segment have relative high skin temperatures. A considerable amount of these agents will walk on the N–E route and use the shortest connection by crossing the north-east quarter of the open space. Hence, higher average skin temperatures can be observed in this section compared to other spots where the thermal loads of the bypassing agents is more diverse.

In order to understand and assess the thermal conditions, it is important to know which thermal processes dominate the thermoregulatory system at the different locations: Heating up, cooling down or stationary conditions. Figure 20 (b) shows the distribution of the average energy balance inside the model area.

The core areas of the open space show an average energy balance close to zero which indicates relative stable thermal conditions. For these areas, static thermal indices will be sufficient accurate (compare also Section 5.4.3). However, in the corners of the open space and inside the street canyon the energy balance is far from being balanced. Especially in the shaded areas, cooling down is still in progress with values down to -300 W as the associated histogram shows. At these locations, the assumption of a stationary heat balance will overrate the effect of shade on thermal comfort by far. The same applies in principle for the positive average energy balance indicated in the corners of the open space, but here the thermal imbalance is much lower with values not exceeding +100 W.

One of the immediate effects of an unbalanced energy budget is a change in skin temperature as shown in Figure 20 (c). In general, this figure shows the same spatial distribution as discussed before for the energy balance with a maximum increase in skin temperature in the north-western quarter of the place and minimum values in the shaded zones. However, the link between energy balance and skin temperature is not linear as the absolute level of skin temperature and the impact of other physiological parameters must also be taken into account.

5.4.2 Distribution of skin wetness

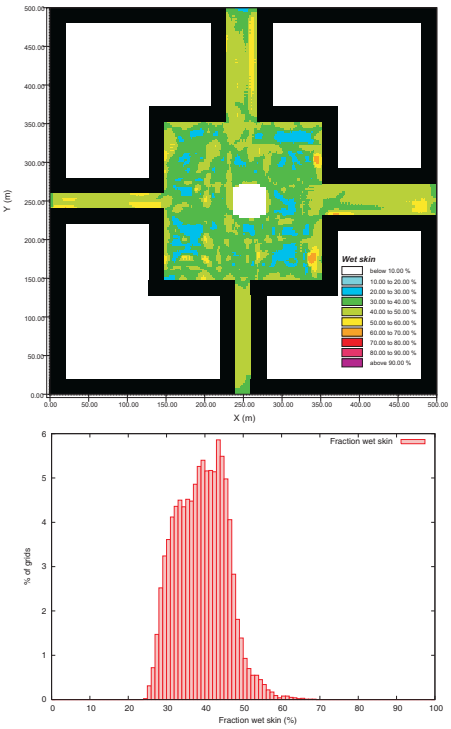

Figure 21: Spatial distribution and frequency distribution of average skin wetness (fraction of wet skin) in the model area for the 14:00 CET situation.

Contrary to the energy balance, the distribution of the fraction of wet skin as plotted in Figure 21 shows only little spatial variation and the differences between sun and shade can hardly be traced. The skin wetness values are basically within the range of 25 to 60% with only three small spots with slightly higher values. These local maxima can be explained by agents coming from the sunny eastern street segment and heading for the shop entrances on the shade-free side of the open space.

Comparing the situation with the threshold values for skin wetness given by VDI 3787 (1996), the average simulation values are all below the 75% threshold value for ”high strain” conditions. In the open space, the average values are close to the comfort thresh-

old of 25% whereas in all street canyons regardless to the local climate conditions, the skin wetness approaches 50%.

5.4.3 Effective Temperature and PMV

Figure 22 (a) shows the spatial distribution of the dynamic Effective Temperature at 14:00 CET. In the associated histogram, the frequency distribution of d(ET) is supplemented by the corresponding static (s)ET values for each location.

The simulated dynamical Effective Temperature values are within the range of 35.5 to 38°C thus indicating "hot", but not "very hot" conditions. The distribution of sun and shade in the area can be traced well in the (d)ET values with a difference of around 1 K between the sunny and the shady street sides. This differences can develop as the main walking direction of the agents is parallel to the sun–shade border and only very few agents switch between the sunny and the shady side while walking through the street canyon.

Similar to the distribution of the skin temperature shown in Figure 20 (a), the north-east corner of the open space holds the highest (d)ET values in the model area.

For a comparison between the dynamical thermal comfort index (d)ET and the results obtained from static indices, the frequency distribution of the static Effective Temperature (s)ET is shown as additional curve in histogram (a) and the spatial difference between both values is plotted in Figure 22 (c). From the frequency distribution is can be seen, that thermal comfort described by the dynamic indicator shows a significant different behaviour as the static index: While the high (s)ET values are well distributed between 36 and 43°C with a mean around 38.5°C, the (d)ET values appear, as mentioned above, quite concentrated between 35.5 and 38°C.

Inside the shaded areas the (s)ET values range around 25°C, indicating slightly warm conditions. This results in a secondary peak in the frequency distribution of (s)ET that cannot be observed in the distribution of the (d)ET values. As the virtual pedestrians are only exposed to the cooler conditions inside the shaded areas for a limited time and the sunny and hot conditions overweight in the area, the cooling effect of the shaded section leads to a small bias of the (d)ET peak towards the cooler conditions, but does not result in a single secondary peak.

Figure 22 (b) allows a comparison with the thermal comfort distribution using the PMV method. To obtain the distribution, the individual PMV values have first been calculated for each location and each agent according to VDI 3787 (1996) using the actual metabolic rate M, the relative wind speed and the static *clo*-value of the individual agent. Then, all single values have been averaged for each location. [13]

Like (s)ET, PMV shows a basically two-peaked data distribution with the major peak representing the sunny areas and the smaller peak with values from the shaded areas. The data from the sunny areas show PMV values between 3 and 4.5 with a clear emphasis of the values in the "very hot" range around 4. Hence, the PMV values for the sunny locations indicate slightly hotter conditions than the (s)ET counterpart.

When analysing the spatial distribution of the dynamic Effective Temperature (d)ET and its differences to the static index s(ET), the remarks made in relation with the distribution of skin temperature and the impact of non-balanced energy budgets can be repeated: At locations where the energy budget is almost balanced, the differences between (d)ET and (s)ET vanish and the static index gives an appropriate representation of the thermal conditions even under dynamic conditions. Contrary, locations with non-balanced energy budgets, here especially in the cooler areas, show large differences up to 10 K between the dynamic and static version of ET. Here, the static index overrates the impact of the local meteorological conditions on the individual thermal comfort.

5.4.4 Thermal comfort through the day

Finally, Plate 1 shows the development of the spatial distribution of the average (d)ET, PMV and energy balance (EB) during the day for the 08:00, 11:00, 18:00 and the 22:00 CET situation.

The general observations made for the 14:00 CET situation are basically also true for the other hours of

13. For the distribution shown in Figure 12 d, p. 31 only one PMV calculation for each location using community-averaged input values has been executed. Hence, the two figures differ.

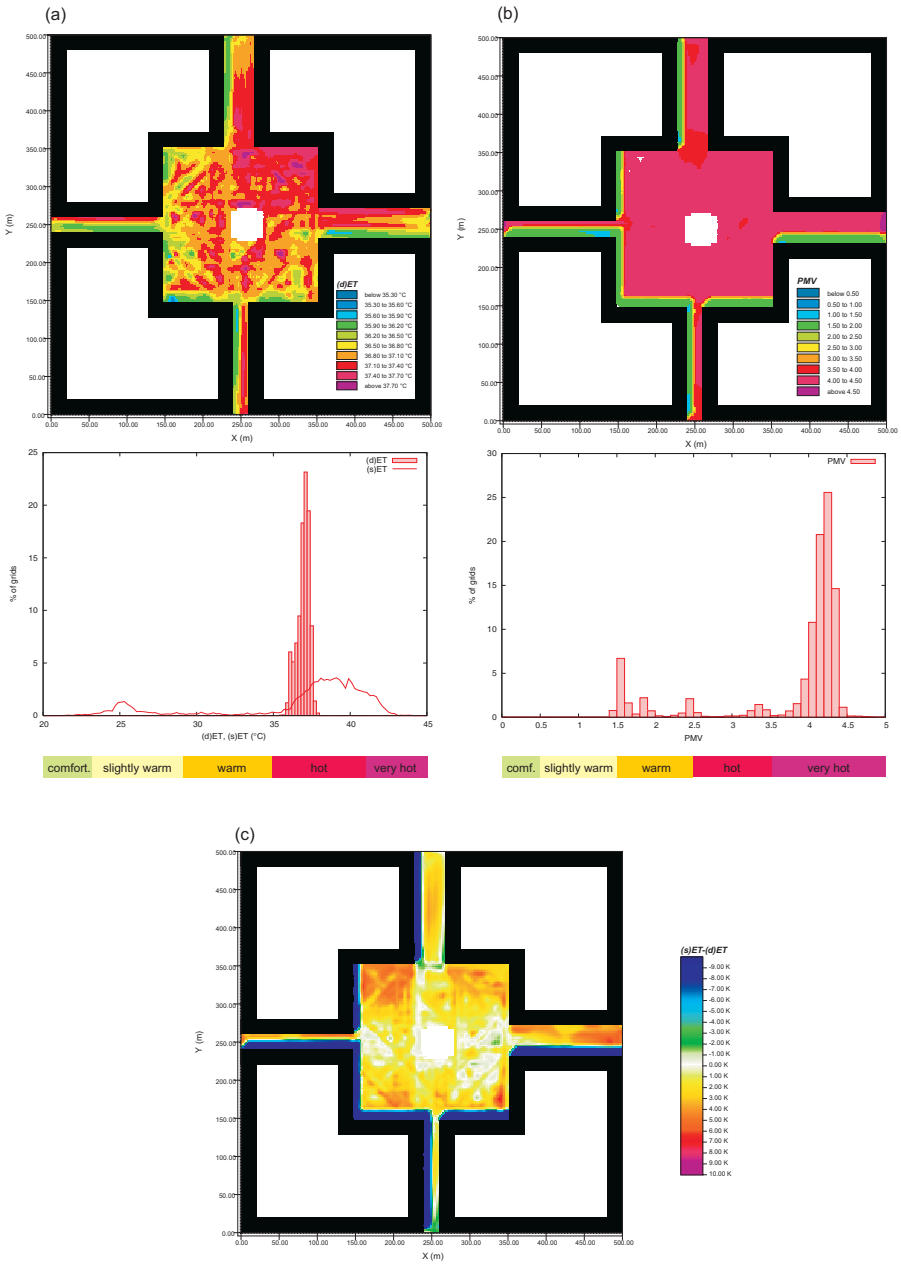

Figure 22: Spatial distribution and frequency distribution of the average dynamic Effective Temperature (a), PMV (b) and difference between static and dynamic effective temperature (c, only spatial distribution) in the model area for the 14:00 CET situation. The histogram for (d)ET also shows the (s)ET frequency distribution.

the day: On the central parts of the open space, the energy budget is almost balanced, hence the assessment through static indices such as PMV indicate the same thermal conditions like the dynamic Effective Temperature. Only in the case of the 22:00 CET situation when no direct solar input is available, the energy balances hold slightly negative values and static indices would indicate little cooler conditions than the dynamic indices for all outdoor locations.

The overestimation of the cooling effect of shaded areas can be observed all through the day and becomes particularly evident in the 18:00 CET situation: At that time of day, the northern and the southern street are in total shade but the (d)ET values still indicate "warm" to "hot" thermal conditions with only little spatial differences in these areas. In contrast, using PMV as an indicator, the same areas would be assessed as being only "slightly warm" conditions there.

5.4.5 Conclusions

The spatial aggregation method provides the possibility to analyse the results of the individual based thermal comfort simulation in their spatial context. The distribution of the average energy balance and the comparison between the dynamic Effective Temperature (d)ET and its static counterpart (s)ET showed prominently that the application of static thermal indices is problematic as soon as the thermal environment becomes more complex. In the center areas of the open space, the average energy budget approaches a balanced state, hence the application of static indices is reliable. As soon as the microclimate conditions deviate from the average conditions, static indices overrate their effect on thermal comfort. In the test case presented here the model domain is dominated by sunny conditions, therefore the impact of the relatively small patches of shade is overestimated. Conversely, if shady conditions would outweigh, the impact of sunny patches would be overrated.

5.5 Virtual Interviews: Community aggregation

In the last sections two different perspectives for analysing the thermal comfort conditions have been presented: The individual based approach which allows a detailed view on the dynamics of the thermoregulatory system of a single agent and the spatial aggregation, which transferred this individual thermal comfort into the spatial context. However, both methods have their drawbacks: The individual based approach does only show the thermal conditions of *one* single person moving on *one* specific route through the model environment. Contrary, the spatial aggregation provides information for the complete area, but looses the detailed information about the state of the individual agents due to data averaging.

In this section, a third possible analysis method provided by the BOTworld system, the "*Virtual Interview*" method is presented, which combines the advantages of both approaches.

The Virtual Interview method

The basic concept of the Virtual Interview method is similar to the way interviews are carried out in the real word: Inside the model area, one or more areas are selected as "survey areas". Each agent entering a survey area for the first time will virtually be "questioned", or, in other words, the actual state of the agent will be stored in a data pool. The data inside this pool have a spatial context as they are representative for the area where the survey took place but they also resolve the state of each single agent at the time he has entered the survey area.

Results from survey areas N and E

To demonstrate the results of the Virtual Interview method, two survey areas, one at the end of the northern and the other at the end of the eastern street segment close to the open space have been defined in the model area (compare Figure 9, p. 27). Both areas are 10 m long and cover the whole cross section of the street segments (40 m). In case of this 60 min simulation, a total of 760 agents have been "questioned" in the northern survey area and 779 agents have been analysed in the eastern area.

Figure 23 shows the frequency distribution of skin temperature (top) and of the (d)ET value (bottom) for the north (a) and west (b) survey area. While the averaged skin temperature values shown in Figure 20 (a) are all between 36 and 37°C (see marks in Fig. 23 top), the frequency distributions clearly indicate a

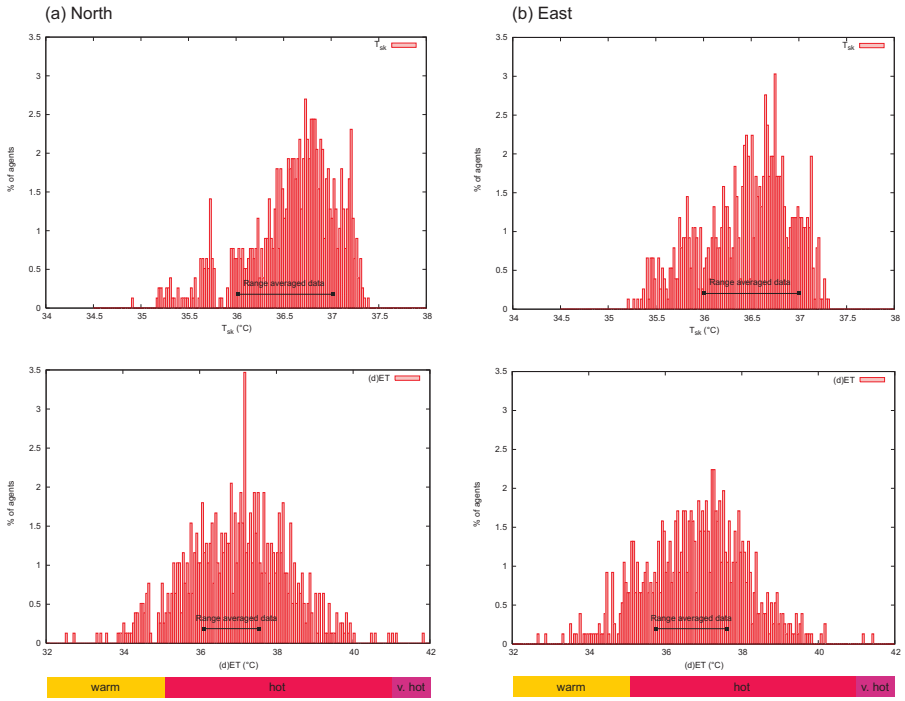

Figure 23: Frequency distribution of skin temperature (top) and (d)ET value (bottom) for the northern (a) and eastern (b) survey area. Black markers indicate the data range given by the spatially averaged values.

wider range of simulated skin temperatures. For example in the case of the northern survey area, the contribution of agents walking mainly in the shade can clearly be traced in the frequency distribution through a small secondary data accumulation around the 35.5°C value. The same observations apply even more drastic to the dynamic Effective Temperature values (Fig. 23 bottom). For the agents coming out of the shade, the thermal sensation stays ”warm” whereas the majority of agents feel ”hot” and a few reach the ”very hot” state. The information about the ”very hot” and ”warm” sensations would be lost through the averaging process.

When comparing real world interviews with simulated thermal comfort data, this mean variance of the data can be an important aspect when explaining the observed opinions. Especially if the urban situation is more complex and the meteorological conditions are more heterogenous, the usage of averaged data might not be sufficient to represent the actual human thermal comfort.

5.6 Impact of indoor stays on thermal comfort

In the different simulations analysed so far, the virtual pedestrians walked to their specified internal target points and, once reached the point, continued their trip immediately to the next target point. This differs to some extent with the real world, where people are normally occupied with location-specific activities once they reached their target. In the case of shops or other buildings, these activities normally include entering of an indoor environment and the exposure to the associated indoor climate conditions for some time.

As the indoor climate conditions normally differ significantly from the outdoor conditions, it can be anticipated that these interruptions of the outdoor stay will have a certain impact of the subsequent outdoor thermal comfort. Especially in the case of active air-conditioning we can expect a visible bias of the thermal comfort conditions towards the cooler sensation. In addition, tracing the thermal comfort of people entering buildings not only interesting for planning the outdoor environment, but also for those people responsible for defining the indoor climate conditions, e.g. through installing and operating the air conditioning system.

In order to simulate the impact of indoor stays, BOTworld distinguishes between indoor and outdoor targets. When an agent reaches an indoor target (and the simulation of indoor stays is enabled), the agent is exposed to an explicitly defined indoor climate environment for a random time period between 1 and 10 minutes. The indoor climate conditions are defined in terms of air temperature, relative humidity and the agent's walking velocity defining the relative indoor wind speed (compare example settings shown in Figure 11, p. 29). As usual for indoor conditions, the mean radiant temperature is set equal to the air temperature.

In this example, the impact of air-conditioned shops on the outdoor thermal sensation is analysed by setting the climate conditions of the internal targets to an air temperature of 18.0°C and a relative humidity of 50%. For the indoor walking velocity, a value of 0.5 ms^{-1} have been assumed as an average during the shopping process. Like in the previous studies, the model simulation has been run over 60 min model time resulting in a total of 1183 virtual pedestrians that have been analysed.

5.6.1 Impact of indoor stays on individual thermal comfort

To demonstrate the effects of air-conditioning on the outdoor thermal sensation, we start by looking at the thermal processes from the perspective of a single agent. The chosen agent "Sonja" is 24 years old, weighs 70 kg and has a static clothing insulation of 0.4 clo. Figure 24 shows the agent's route through the model environment using the skin temperature at the respective location to colour the route trajectory.

Figure 24: Route of agent "Sonja" visiting two shops in the model area. Route trajectory is coloured with the skin temperature at the respective positions.

The agent enters the model area through the southern street segment by walking on the shaded side. Then, two shops are visited (Shop 1: 5 min, Shop 2: 6 min stay) before "Sonja" returns and leaves the model area while walking on the sunny side of the southern street segment.

Figure 25 (a) shows the actual mean radiant temperature the agent is exposed to and the reactions of the cloth, skin and core temperature. In (b) the associated energy fluxes (b) during the simulated walk are plotted. The impact of the two indoor stays can well be observed in the change of the skin temperature: Before entering the first shop, the skin temperature behaves comparable to the dynamics observed for agent "Antonio" in Figure 15 (a) on page 35. Inside the first shop, the skin temperature drops by 1.5 K from 36.80°C to 35.30°C. After leaving the shop, the agent is exposed to direct solar radiation again and the skin temperature rises quickly and reaches the same value as before entering the shop. In the second shop, the same behaviour can be observed with a slightly larger decrease of 1.7 K down to 35.10°C due to the slightly longer indoor stay.

The energy exchange processes shown in Figure 25 (b) indicate that the indoor stay practically has the same effect like walking through a shaded environment. This might be a bit surprising as the indoor

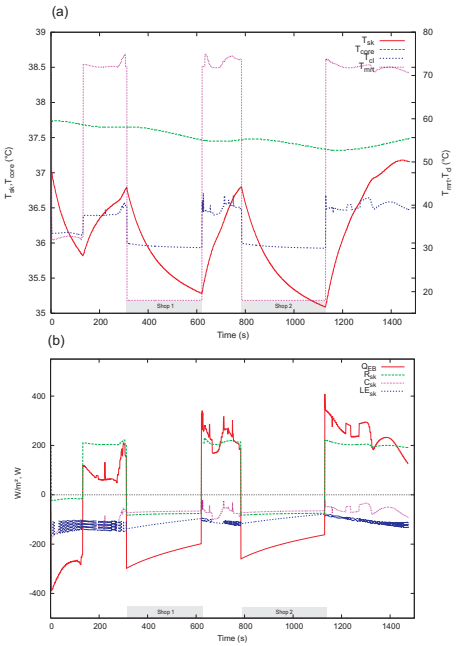

Figure 25: Evolution of selected parameters of the ITC model for the agent "Sonja" during the passage through the model and while entering two air-conditioned indoor environments: (a) temperatures of skin, core and clothing and the local mean radiant temperature, (b) total energy balance and radiative, convective and latent energy fluxes per skin surface area.

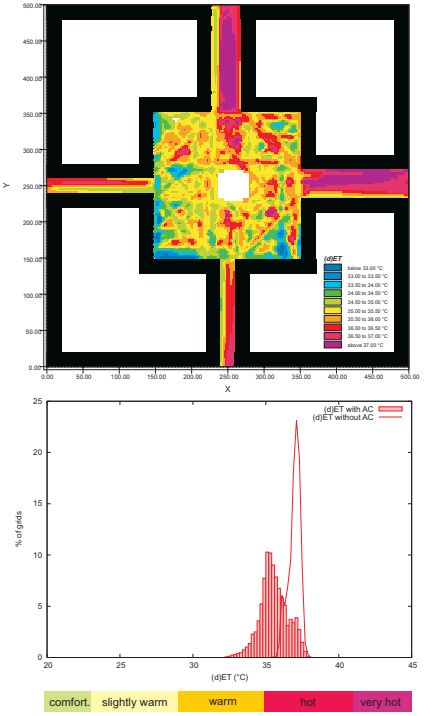

Figure 26: Spatial distribution and frequency distribution of the average dynamic Effective Temperature in the model area for the 14:00 CET simulation taking into account indoor stays in an air-conditioned environment. The frequency distribution includes the (d)ET distribution for the simulation without indoor stays.

air temperature is much lower compared to a shaded outdoor location, but due to the low relative wind speed in the indoor environment the convective heat transfer and the vapour transpiration are low. As it can be seen especially during the stay in shop 2, the convective heat loss C_{sk}, the radiative heat loss R_{sk} and the latent heat loss LE_{sk} contribute approximately with the same amount to the cooling process whereas in a typical shaded outdoor environment (e.g. in the first 100 sec in the walk of "Antonio", see Fig. 15 b, p. 35) the distribution is about 5% : 20% : 75% for $R_{sk} : C_{sk} : LE_{sk}$

5.6.2 Impact of indoor stays on spatially aggregated thermal comfort

Moving from the perspective of individual thermal comfort to the impact of indoor stays on spatially aggregated level, Figure 26 shows the spatial distribution of the average dynamic Effective Temperature. Compared with Figure 22, p. 43, it is obvious that the simulation of indoor stays decreases the dynamic Effective Temperature, in particular close to the shop entrances, by 3 K and more. Especially in the north-eastern corner of the open space which was dominated by the highest (d)ET values before, the effect is impressive. Comparing the frequency distributions

(Fig. 26 bottom) with and without the simulation of air-conditioned indoor stays, a clear bias towards the ”warm” thermal conditions can be observed. Also, due to the variations in the amount and duration of indoor stays, the band width of (d)ET values becomes wider. The mean of the distribution is now between the ”warm” and ”hot” assessment whereas it was clearly in the ”hot” region before. Even in the street canyons, where no shop entrances have been located, the effect of indoor stays is still traceable with a reduction of the dynamic Effective Temperature around 1 K.

5.6.3 Conclusions

Entering indoor environments has a strong impact on the thermal sensation not only during the indoor stay itself, but due to the inertia of the energy exchange processes also during the following outdoor passages. Comparing the dynamic Effective Temperature with and without consideration of air-conditioned indoor stays, a decrease in (d)ET of 3 K and more close to the shop entrances can be observed. Even in the more distant locations of the area without shop entrances, a decrease of around 1 K still is traceable.

Though the simulation of indoor stays has a proven impact on the thermal sensation during and after visiting the indoor environment it is quite difficult to find the correct simulation parameters for the indoor sequences. There are too many unknown variables in terms of indoor climate conditions, number of visited shops and length of indoor stays to allow a representative simulation for each case. Hence, this option should only be used if reliable data about these parameters are available or if only general mechanisms should be analysed.

6 Final conclusions

In this paper, the design of the **I**ndividual based **T**hermal **C**omfort **M**odel (ITCM) and its operation inside the Multi-Agent system BOTworld has been presented. Different analytical perspectives have been taken to demonstrate the impact of varying microclimate conditions on human thermal comfort. Even for the relatively simple example of a square urban open space it became evident, that the thermoregulatory system is a complex construct which depends on many spatial and temporal factors.

One of the main motivations for the development of the ITC model have been the reported discrepancies between local static thermal comfort indices and empirically observed opinions about the thermal conditions. Hence, one of the main aspects of the model analyses has been to compare the assessment of thermal conditions based on steady indices with the outcomes from the dynamic ITC model. It was found that even for the simple case study scenario there are only few locations where the human energy budget is balanced and static indices could be applied. In the presented case, the dominance of sunny locations had a large impact on the thermal sensation of the shaded areas. Using static parameters, the cooling contribution of shaded areas was largely overestimated compared to the outcomes of the dynamic model.

In reality, the situation is of course much more complicated than in this case study which was selected to demonstrate the functionality of the ITC model. When the urban structure becomes more complex, a multitude of different microclimate environments can be found. Through the pedestrian movement, these environments interact with each other and the thermal conditions at one place will influence the thermal situation at another place. Without a computer-based simulation such as BOTworld, it would be impossible to predict those effects.

The human energy balance model as it is presented and used here should be regarded as a first approach, a proof of concept of the idea to link the Multi-Agent method with a model of the human thermoregulatory system. Its design is relatively simple and there are quite a few aspects not included yet. However, the need of a few hundred up to a few thousand of agents for a realistic simulation imposes some restriction on the complexity of the biometeorological model linked to each of these agents. The more sophisticated a model gets, the more input parameter and assumptions are required to operate this model. Even for a simple model like ITCM, there are quite a few uncertainties and screws in the model with a large impact on the simulation results. The impact of different initial conditions or the effect of indoor stays on thermal comfort are just two of them that became obvious when running the case study simulations.

Last not least it has to be mentioned that the physiological component is only one aspect that drives the perception of thermal comfort. Besides skin and core temperature it is the physiological attitude towards the specific location that influences the individual thermal comfort. The example simulations of indoor stays showed that the skin temperature decreases only slowly when entering an air conditioned environment, hence the dynamic Effective Temperature also decreases slowly. In these cases it is the change in the energy balance that triggers the cold receptors and makes the thermal environment appearing more pleasant as the actual body parameters would indicate. Under such conditions, thermal comfort is not a function of the actual thermal state of the body, regardless of the method how it was calculated, but of the expectations about the future development of the personal thermal comfort.

One aspect that was not analysed in this paper is the effect of behaviour adaptation by the pedestrians. If a pedestrian feels uncomfortable hot and the choice between walking on the sunny or on the shady side of the road exists, the shady side would probably be chosen. Climate-controlled behaviour can improve the overall assessment of an urban area significantly if the users of the open space have the possibility to select the local climate conditions that fit best to their actual state and preferences. With the ITC model in combination with the Multi-Agent system BOTworld it is even possible to simulate such behaviour feedbacks and their impact of the assessment of the urban microclimate. This aspect will be highlighted in detail in Module D of this thesis.

References

ASHRAE (1992). *Physiological Principles, Comfort and Health*, chapter 8. Fundamentals Handbook. American Society of Heating, Refrigerating and Air Conditioning Engineers (ASHRAE), Atlanta.

Bruse, M. (2000). Assessing thermal comfort in urban environments using an integrated dynamic microscale biometeorological model system. In *Proceedings of the Third Symposium on the Urban Environment*, Davis, CA. Americal Meteorological Society.

Bruse, M. and Fleer, H. (1998). Simulating surface-plant-air interactions inside urban environments with a three dimensional numerical model. *Environmental Modelling and Software*, 13:373–384.

Burton, A. C. and Edholm, O. G. (1955). *Man in Cold Environment*. Edward Arnold, New York.

Cain, J. B., Livingstone, S. D., Nolan, R., and Keefe, A. A. (1990). Respiratory heat loss during work at various ambient temperatures. *Respir. Physiol.*, 79:145–150.

Deurenberg, P., Weststrate, J., and Seidell, J. (1991). Body Mass Index as a measure of body fatness: Age- and sex-specific prediction formulas. *Br. J. Nutr.*, 65(2):105–114.

DuBois, D. (1916). Clinical calorimetry: a formula to estimate the appropriate surface area if height and weight be known. *Arch. Int. Med.*, 17:863–871.

Fanger, P. O. (1982). *Thermal Comfort. Analysis and Application in Environment Engineering*. McGraw Hill Book Company, New York.

Fiala, D., Lomas, K., and Stohrer, M. (2001). Computer prediction of human thermoregulatory and temperature responses to a wide range of envrionmental conditions. *Int. J. Biomet.*, 45:143–159.

Fiala, D., Lomas, K. J., and Stohrer, M. (1999). A computer model of human thermoregulation for a wide range of environmental conditions: The passive system. *J. Appl. Physiol.*, 87:1957–1972.

Gagge, A., Fobelets, A., and Berglund, L. (1986). A standard predictive index of human response to the thermal environment. *ASHRAE Trans.*, 92(2):709–731.

Gagge, A., Stolwijk, J., and Nishi, Y. (1971). An effective temperature scale based on a simple model of human physiological regulatory response. *ASHRAE Trans.*, 77(1):247–262.

Gallagher, D., Visser, M., Sepulveda, D., Pierson, R., Harris, T., and Heymsfield, S. (1996). How useful is body mass index for comparison of body fatness across age, sex and ethnic groups. *Am. J. Epidemiol.*, 143:228–239.

Gonzales, R., Y., N., and Gagge, A. P. (1974). Experimental evaluation of standard effective temperature - A new biometeorological index of man's thermal discomfort. *Int. J. Biomet.*, 18(1):1–15.

Havenith, G. (1999). Heat balance when wearing protective clothing. *Ann. Occ. Hyg.*, 43(5):289–296.

Havenith, G. (2001). Individualized model of human thermoregulation for the simulation of heat stress response. *J. Appl. Physiol.*, 90:1943–1954.

Havenith, G., Holmér, I., den Hartog, E., and Parsons, K. (1999). Clothing evaporative heat resistance- proposal for improved representation in standards and models. *Ann. Occ. Hyg.*, 43(5):339–346.

Havenith, G., Holmér, I., and Parsons, K. (2002). Personal factors in thermal comfort assessment: clothing properties and metabolic heat production. *Energy and Buildings*, 34:581–591.

Holmér, I., Nilsson, G., Havenith, G., and Parsons, K. (1999). Clothing convective heat exchange-proposal for improved prediction in standards and models. *Ann. Occ. Hyg.*, 43(5):329–337.

Höppe, P. (1984). Die Energiebilanz des Menschen. In *Münchener Universitätsschriften- Fachbereich Physik, Wissenschaftliche Mitteilungen Nr. 49*. Meteorologisches Institut, Universität München, München.

Höppe, P. (1992). Ein neues Verfahren zur Bestimmung der mittleren Strahlungstemperatur im Freien. *Wetter und Leben*, 44:147–515.

Höppe, P. (1999). The physiological equivalent temperature PET- an universal index for the biometeorological assessment of the thermal environment. *Int. J. Biomet.*, 43(2):71–75.

Höppe, P. (2002). Different aspects of assessing indoor and outdoor thermal comfort. *Energy and Buildings*, 34:661–665.

Höppe, P. and Seidl, H. (1991). Problems in the assessment of the bioclimate for vacationists at the seaside. *Int. J. Biomet.*, 35:107–110.

Humphreys, M. and Nicol, J. (2002). The validity of ISO-PMV for predicting comfort votes in everyday thermal environments. *Energy and Buildings*, 34:667–684.

ISO 7730 (1995). Moderate Thermal Environments-Determination of the PMV and PPD indices and specification of the conditions for thermal comfort. Technical report, Int. Standards Org., Geneva.

ISO 7933 (1989). Hot environments - Analytical determination and interpretation of thermal stress using calculation of required sweat rate . Technical report, Int. Standards Org., Geneva.

ISO 8996 (1989). Ergonomics of thermal environments- Determination of metabolic heat production. Technical report, Int. Standards Org., Geneva.

ISO 9920 (1993). Ergonomics- Estimation of the thermal characteristics of a clothing ensemble. Technical report, Int. Standards Org., Geneva.

J. R. Geigy AG (1981). *Scientific Tables - Physical Chemistry; Composition of Blood; Hematology; Somatometric Data*, volume 3. J. R. Geigy AG, Basel, CH, 8th editon edition.

Jackson, A. and Pollock, M. (1985). Practical assessment of body composition. *Physician Sports Med.*, 13:76–90.

Jackson, A., Pollock, M., and Ward, A. (1980). Generalized equations for predicting body density of women. *Med. Sci. Sports Exercise*, 12:175–182.

Jendritzky, G., Maarouf, A., Fiala, D., and Staiger, H. (2002). An update on the developement of a universal thermal climate index - Progress report of the ISB Commission 6 on UTCI. In *Proceedings of the 15th Congress of Biometeorology*, Kansas City. Int. Soc. Biomet.

Jendritzky, G., Menz, G., Schirmer, H., and Schmidt-Kessen, W. (1990). Raumbezogene Bewertung der thermischen Komponente im Bioklima des Menschen (fortgeschriebenes Klima-Michel Modell). In *Beiträge der Akademie f. Raumordnung und Landesplanung 114*. Akademie f. Raumordnung und Landesplanung, Hannover.

Jennings, N. R., Sycara, K., and Wooldridge, M. (1998). A roadmap of agent research and development. *Autonomous Agents and Multi-Agent Systems*, 1:7–38.

Kandjov, I. (1999). Heat and mass exchange processes between the surface of the human body and ambient air at various altitudes. *Int. J. Biomet.*, 43:38–44.

Keys, A., Fidanza, F., Karvonen, M., Kimura, N., and Taylor, H. (1972). Indices of relative weight and obesity. *Journal of Chronic Disease*, 25:329–343.

Livingstone, S., Nolan, R., Cain, J. B., and Keefe, A. (1994). Effect of working in hot environments on respiratory air temperatures. *Eur. J. Appl. Physiology*, 69:98–101.

Lottens, W. (1993). *Heat transfer from humans wearing clothing*. PhD thesis, Delft Univ. of Technology, Delft, The Netherlands.

Mark, F. (1987). Control as a dimension of public space quality. In Altman, I. and Zube, E., editors, *Public Places and spaces*. Plenum Press, N.Y.

Matzarakis, A. (2001). *Die thermische Komponente des Stadtklimas*. Berichte des Meteorologischen Instituts der Universität Freiburg, Volume 6. Univ. Freiburg, Freiburg i. Br., D.

Matzarakis, A. and Mayer, H. (1997). Heat Stress in Greece. *Int. J. Biomet.*, 41:34–39.

Matzarakis, A., Rutz, F., and Mayer, H. (2000). Estimation and calculation of the mean radient temperature within urban structures. In de Dear, R., Kalma, J., Oke, T. R., and Aulicems, A., editors, *Biometeorology and urban climatology at the turn*

of the millenium. Selected papers from the Conference ICB-ICUC '99, pages 273–278. World Meteorological Organisation, World Climate Application and Service Program. (WCASP-50).

Mayer, H. and Höppe, P. (1987). Thermal comfort of man in different urban evironments. *Theor. Appl. Climat.*, 38:43–49.

Miyazaki, Y., Saito, M., and Seshimo, Y. (1995). A study of evaluation of non-uniform environments by human body model. *Journal of human and living environment*, 2(1):92–100.

Morgan, D. and Baskett, R. (1974). Comfort of man in the city- An energy balance model of man. *Int. J. Biomet.*, 18(3):184–198.

Nasar, L. J. and Yurdakul, A. R. (1990). Patterns of behavior in urban public spaces. *Architectural and Planning Res.*, 7(1):71–85.

Nikolopoulou, M., Baker, N., and Steemers, K. (2001). Thermal comfort in outdoor urban spaces: understanding the human parameter. *Solar Energy*, 70(3):227–235.

Olesen, B. and Parsons, K. (2002). Introduction to thermal comfort standards and to the proposed new version of EN ISO 7730. *Energy and Buildings*, 34:537–548.

Parsons, K. C., Havenith, G., Holmér, I., Nilsson, H., and Malchaire, J. (1999). The effects of wind and human movement on the heat and vapour transfer properties of clothing. *Ann. Occ. Hyg.*, 43:347–352.

Pickup, J. and de Dear, R. (2000). An outdoor thermal comfort index (OUT-SET*). Part I- The model and its assumptions. In de Dear, R., Kalma, J., Oke, T. R., and Aulicems, A., editors, *Biometeorology and urban climatology at the turn of the millenium. Selected papers from the Conference ICB-ICUC '99*, pages 279–283. World Meteorological Organisation, World Climate Application and Service Program. (WCASP-50).

Pietrobelli, A., Faith, M., Allison, D., Gallagher, D., Chiumello, G., and Heymsfield, S. (1998). Body Mass Index as a measure of adiposity among children and adolescents: A validation study. *Journal of Pediatrics*, 132:204–210.

Potter, J. and de Dear, R. (2000). Field study to calibrate an outdoor thermal comfort index. In de Dear, R., Kalma, J., Oke, T. R., and Aulicems, A., editors, *Biometeorology and urban climatology at the turn of the millenium. Selected papers from the Conference ICB-ICUC '99*, pages 315–320. World Meteorological Organisation, World Climate Application and Service Program. (WCASP-50).

Spagnolo, J. and de Dear, R. (2003). A field study of thermal comfort in outdoor and semi-outdoor environments in subtropical Sydney, Australia. *Building and environment*, 38:721–738.

Steadman, R. (1994). Norms of apparent temperature in Australia. *Aust. Met. Mag.*, 43:1–16.

Takada, S., Hokoi, S., Kawakami, N., and Kudo, M. (1999). Effect of sweat accumulation in clothing on transient thermophysiological response of human body to the environment. In *Proceedings of building simulation '99, Vol. 1*, pages 385–392. International Building Performance Society.

Tanabe, S., Kobayashi, K., Nakando, J., Ozeki, Y., and Konishi, M. (2002). Evaluation of thermal comfort using combined multi-node thermoregulation (65mn) and radiation models and computational fluid dynamics (cfd). *Energy and Buildings*, 34:637–646.

Tanabe, S., Narita, C., Ozeki, Y., and Konishi, M. (2000). Effective radiation area of human body calculated by a numerical simulation. *Energy and Buildings*, 32:205–215.

Thorson, S., Lindqvist, M., and Lindqvist, S. (2004). Thermal bioclimatic conditions and patterns of behaviour in an urban park in Göteborg, Sweden. *Int. J. Biomet.*, 48:149–156.

Tuddenham, R. and Snyder, M. M. (1954). Physical growth of california boys and girls from birth to eighteen years. Technical report, University of California, Berkley and Los Angeles.

Varene, P. (1986). Computation of respiratory heat exchanges. *J. Appl. Physiol.*, 61(4):1586–1589.

VDI 3787 (1996). Richtlinie VDI 3787: Methoden zur human-biometeorologischen Bewertung von

Klima und Lufthygiene für die Stadt- und Regionalplanung Teil 1: Klima. Technical report, Verein deutscher Ingenieure.

Weidmann, U. (1993). Transporttechnik für Fußgänger. In *Schriftenreihe des Instituts für Verkehrsplanung, Transporttechnik, Straßen- und Eisenbahnbau*. ETH Zürich.

Weiss, G., editor (2000). *Multi Agent Systems*, Cambridge, London. The MIT Press.

Westerberg, U. and Glaumann, M. (1990). Design criteria for solar access and wind shelter in the outdoor environment. *Energy and Buildings*, 15–16:425–431.

Westerberg, U., Knez, I., and Eliasson, I. (2003). Urban Climate Spaces: A Multidisciplinary Research Projct. In Klysik, K., Oke, T., Fortuniak, K., B., G. C. S., and Wibig, J., editors, *Proceedings of the Fith International Conference on Urban Climate, Vol. 2*, pages 107–110, Lodz, Poland. University of Lodz.

Zacharias, J., Stathopoulos, T., and Wu, H. (2001). Microclimate and downtown open space activity. *Environment and Behavior*, 33(2).

Module C

The F-A-ST approach: A Fuzzy Logic based assessment model for the use in Multi-Agent model environments

Numerical simulation systems have established as powerful tools for analysing the behaviour of complex dynamic systems under controlled conditions. In case the observed system becomes very complex in its logical, temporal or spatial dimension, individual-based simulation systems such as Multi-Agent (MA) systems are well suited to break down the complexity of the complete system through focussing onto the behaviour of the individual agent. In this paper, a simple Fuzzy Logic based assessment model (F-A-ST model) for the use in Multi-Agent simulation systems is presented. The F-A-ST model provides a simple but still very flexible mechanism to assess a given environmental situation in dependency to the individual state of the assessing agent. Using an example from human biometeorology it is shown, how the F-A-ST model can be applied to assess the thermal conditions of an urban open space on a hot summer day.

Keywords: Fuzzy Logic, Multi-Agent simulation, assessment model, F-A-ST model, Biometeorology, Thermal comfort analysis

Contents

List of Figures

List of Tables

1 Introduction

Numerical simulation systems have established as powerful tools for analysing the behaviour of complex dynamic systems under controlled conditions. In traditional model approaches, the behaviour of the regarded system and the interactions between its components interactions are implemented using a priori formulated analytical rules and decision trees describing the system dynamics from an outside observer's perspective. However, if the observed system becomes too complex in its logical, temporal or spatial dimension, it often turns out to be impossible to formulate such general analytical rules considering all aspects of the observed system satisfactory and fit for all possible situations. In these cases, a change of the perspective away from the observer watching the system from the outside towards the view of an internal actor assessing the system from inside can help to reduce complexity and to resolve potential contradictions emerging in analytical approaches.

Multi-Agent (MA) simulation systems are a prominent and up-to-date method for an individual based analysis of complex and non-linear systems. In Multi-Agent systems, different natural entities such as humans or animals are represented through software "*agents*". These agents have a clearly defined spectrum of properties and methods allowing them to interact with the environment and amongst each other based on the information gathered and the individual goals followed. Even though the agents' individual behaviour options are often quite limited, interesting and complex behaviour patterns and simulation results can establish through iterative interaction between the virtual actors and the emerging self-organisation effects. In MA systems there are no central functions controlling the behaviour of the individual agents or of the complete system. The dynamics of the complete system results only from the activities of the single agents trying to fulfil a given task using the best available strategy.

In order to act as an autonomous object, each agent needs a certain level of intelligence providing him with the ability to assess the actual situation, based on the outcomes of this assessment, to select the optimal behaviour strategy. Hence, the correct assessment is the crucial part in any software system requiring autonomous decisions.

The individual assessment of a given situation depends not only on the objective conditions found, but also to a huge extent on the subjective impressions, the personal expectations and associated emotions of the individual assessing the situation. These personal preferences can not only bias the assessment into the positive or negative direction, but can also be the all-decisive information to choose between alternating options. Especially the impact of emotions on a decision process is a point that confuses many people as the classical dichotomy between "rational decisions" (logical and predictable) and "emotional behaviour" (subjective and unpredictable) seems to contradict the consideration of emotional components in computer-based decision making. The idea that a computer might be able to reproduce an emotional process or even to generate some kind of autonomous feelings is something that tends to cause a certain degree of discomfort and sounds a bit like "Star Wars".

Computer simulation of emotions?

The question if and how it might be possible to simulate emotion-influence decision processes using numerical models occupies scientists from different disciplines with different motivations. People with a scientific background in psychology are mainly interested to use numerical models to test complex theories using a computer framework. They explore the role of emotions as a positive component in human cogitation and intelligence (Izard, 1977; Ekman, 1992) or analyse the impact of emotions on memory, thinking and judgement (Bower and Cohen, 1982; Forgas, 1995) using numerical models.

On the other side, the simulation of emotions is used more practically motivated in order to improve the behaviour and level of realism of computer-based interaction systems (compare Dautenhahn, 1998). In the context of Multi-Agent systems, the FLAME model presented by El-Nasr et al. (2000) is a recent approach to model individual-based behaviour feedback shown by the example of an artificial pet.

At this point it should be clearly stated that the objective of such an "emotional modeling" is NOT to produce a system that becomes to life somehow. The intention of these models is to provide additional rules that modulate other processes such as assessment or cognition. Dörner and Hille (1995) summarise "To have an emotion means that the processes of be-

haviour regulation are brought into a certain form according to the conditions of a situation".

Bartl and Hille (2001) name four main reasons, why computer (models) can and should be used to simulate psychological processes:

- even complex theories remain controllable
- temporal developments can the traced
- computer simulations force a formalisation of theory and concepts, contradictions are exposed
- the dynamics of the theory can be tested under different external and internal conditions (scenarios)

These four points are exactly in line with the aims of Multi-Agent simulations in general and the purpose of the F-A-ST concept presented in this paper in particular: Depending on a given internal state which stands for the agent's actual needs and desires, the F-A-ST method evaluates environmental conditions whether they support the agent's needs and associated goals or contradict them. Hence, the F-A-ST model is both a method to formalise different assumptions how the recent state of the agent influences the perception and assessment of the environment and to express this assessment as a numerical value obtained using comprehensible mathematical operations.

The F-A-ST concept

The F-A-ST model presented in this paper provides a simple but still very flexible mechanism to assess a given environmental situation in dependency to the actual state of the agent. It basically consists out of three components:

Environmental parameter F (Input) The environmental conditions which should be assessed

Internal state ST The internal state of the agent which has an impact on the assessment of F

Assessment value A^* (Output) The output of the assessment process as a numerical value

Seen from the perspective of the F-A-ST model, the assessment process can be understood as a projection of the environmental parameter F onto the assessment value A^* biased by the internal state ST:

$$F \xrightarrow{ST} A^*$$

Each combination of external parameter, internal state and resulting assessment value is called a "*F-A-ST set*". In order to assess different parameters of the environment or different impacts on one assessment process, several F-A-ST sets can be defined and evaluated parallel to each other.

As most assessment processes are based on soft, qualitative evaluations rather than on crisp numerical threshold values, the method of *Fuzzy Logic* is used as the core method to operate the F-A-ST model. Different to the classical binary logic, Fuzzy Logic is able to deal with imprecise, uncertain or ambiguous data and rules and is therefore well suited to simulate a human-like decision process.

In the following sections, the theory and design of the "*Fuzzy-Assessment-by-State (F-A-ST)*" model is presented. Using an example from human biometeorology it will then be shown how the F-A-ST model can be applied to assess the thermal conditions of an urban open space on a hot summer day.

2 Theory of fuzzy logic

2.1 The basic concept

The basic concept of Fuzzy Logic was introduced in 1965 by Lofti Zadeh as a new approach to handle uncertain and "fuzzy" data using standard mathematical methods (Zadeh, 1984, 1965). The main components of a fuzzy system are the so-called "*fuzzy sets*" that group data into sets with similar qualitative properties, e.g. low temperatures, average temperatures and high temperatures. The main difference to conventional Aristotelian logic is constituting in the fact that some value X can belong partly to one fuzzy set and partly to another. Contrary, in conventional logic, X can only be a 100% member of one set of data or be no member of it. Figure 1 illustrates this circumstance using classification "low", "average" and "high" once seen from conventional logic (top) and seen from the Fuzzy Logic approach (bottom).

In conventional logic, the usage of sharp threshold values to group data values imposes a strong pressure on the correct estimation of the threshold values (compare x_l and x_h shown in Fig. 1): Once a value X has been classified to one of the data sets, the information whether this value is close to the upper or to the lower boundary is lost. A typical example for the problematic application of this sharp classification can be found in the definition of environmental threshold values, for example for air quality. Once the critical boundary values are fixed, every situation below the threshold is considered as tolerable, regardless how close or far it is to the actual limits. Contrary, the concept of Fuzzy logic allows a smooth transition between the different fuzzy sets as shown in Figure 1 (bottom). As a value X approaches the limit x_l, it begins to loose its "membership" in the set of "low" data and increases its "membership" in the set of "average" values. At the point where $X = x_l$ it belongs to the "low" and "average" fuzzy set to the same degree. In Fuzzy logic, this degree is called the "*membership grade* (μ)" and ranges between 0 (no membership) to 1 (complete membership).

Although Fuzzy logic demands the definition of some transition values such as x_l or x_h as well, the impact of these values on the decision logic is much lower compared to the concept of crisp threshold values used in conventional sets. Hence, the impact of possible errors is much lower and it is possible to "guess" values to some extent.

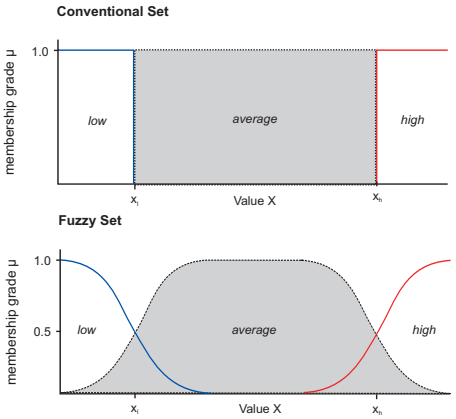

Figure 1: Definition of data sets using conventional logic (top) and Fuzzy Logic (bottom).

In order to process logical decisions, Fuzzy Logic allows arithmetic operations with and between different fuzzy sets. These operations are defined in terms of decision rules (IF *condition* THEN *conclusion*) similar to Boolean logic. The result of such an IF...THEN rule is again a fuzzy value indicating to which degree the conclusion applies for the given variables. Finally, after applying the designed set of decision rules, the fuzzy results are re-transformed into crisp numerical values usable outside the fuzzy system.

In overview the sequence of fuzzy logic processing can be divided into three steps (compare Fig. 2):

1. Fuzzification
2. Fuzzy-Interference
3. De-Fuzzification

In the following paragraphs, the basic characteristics of these three steps are described with an emphasis on their role in the F-A-ST model. The exact mathematical implementation of the F-A-ST will then be shown in Section 3 p. 6 ff.

It has to be noted, that fuzzy logic is an extremely complex topic so that in this paper we will only concentrate on those aspects of fuzzy logic that are relevant for the F-A-ST model.

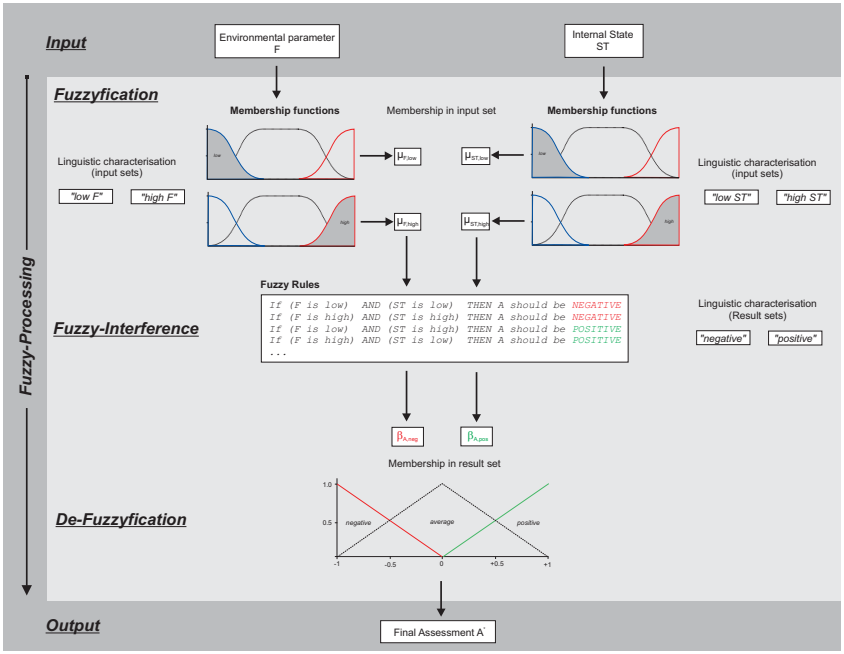

Figure 2: Schematic overview of the different steps of data processing in the F-A-ST model: Fuzzyfication (top) calculates the membership degree of the input values in the defined input sets, Fuzzy-Interference (middle) applies the given logic rules to the membership grades and the De-Fuzzyfication (bottom) re-transforms the final result into a crisp numerical output value.

2.2 Fuzzification

The objective of the Fuzzyfication step is to transform the crisp numerical input values (F and ST respectively) into membership values μ indicating to which degree the input values belong to the respective fuzzy sets. The main problem to be solved in this step is to classify the spectrum of possible input values into useful fuzzy sets and to define the definition boundaries of these sets. There are two basic approaches to solve this problem: The first approach, called *Similarity Relation Model* (Robinson, 1988) is based on a statistical analysis of data sets similar to a statistical factor analysis. By processing a reasonable amount of data, the computer can automatically identify the amount of required fuzzy sets, generate the shape of the membership function (e.g. bell-shaped like in Fig. 2 top or triangular, linear, trapezoidal, ...) and select the boundary values. Typical applications for this approach range from self-learning systems for remote sensing image classification for climate classification (McBratney and Moore, 1985) over salinity mapping (Metternicht, 1998) to temperature control systems (Lin, 2004). Using the Similarity Relation Model, the quality of the fuzzification process and of the complete following data processing depends largely on the choice of the training data and of the statistical methods used to classify the data.

The second approach, known as *Semantic Import Model*, relies on human expert knowledge when formulating the membership functions. Here, the fuzzification process begins with the linguistic formulation of the required fuzzy sets and then the required boundary parameters are defined. Typical applications can be found in noise annoyance mod-

elling (Botteldooren et al., 2003), the simulation of soil erosion (Metternicht and Gonzales, 2005) or in the development of filters for air quality monitoring (Kürbis, 2002). In this approach, the quality of the membership functions depends totally on the expert's knowledge and the ability to express this knowledge in terms of mathematical functions.

For the F-A-ST model, the second approach was used to define the fuzzy sets for the input parameters F and ST. For the input sets, the data are only distinguished into "low" and "high" values. A third fuzzy set of "average" values results implicitly as the complement of the "low" and "high" sets. The outcomes of the fuzzification process are membership values μ $[0...1]$ for each of the defined fuzzy set. In case of the F-A-ST model, we obtain $\mu_{\text{F,low}}$ and $\mu_{\text{F,high}}$ for the membership of F in the "low" and "high" fuzzy set and the membership values $\mu_{\text{ST,low}}$ and $\mu_{\text{ST,high}}$ for ST accordingly. This set of membership functions serves then as input for the next step of the fuzzy process, the Fuzzy-Interference.

2.3 Fuzzy-Interference

Fuzzy-Interference can be seen as core of the fuzzy data processing as it incorporates the knowledge about the logical relations between the fuzzy sets into the process. The Fuzzy-Interference step is based on a set of rules ("*Implications*") parameterised through "IF...THEN" conditions expressing the conditions one or many fuzzy sets have to fulfill to make a certain conclusion (result) become true (see Fig. 2 middle). Different to boolean logic, in which each "IF" condition (=factum) can only result in a "TRUE" or "FALSE" evaluation, Fuzzy-Interference can work with conditions that are between "TRUE" and "FALSE". Hence, if the condition is only partly true, the assigned conclusion ("THEN..." part) will only be fulfilled partly, or, in other words, the conclusion is only true with a given certainty. Consequently, the result of a Fuzzy-Interference rule is not a crisp numerical value but again a membership value indicating to which extend the result belongs to one of the predefined fuzzy result sets (see next section).

In the case of the F-A-ST model, the design of the Fuzzy-Interference is relatively simple as the different fuzzy input sets are only checked against one single result, the assessment value A^*. The outcomes of this step of the Fuzzy process are presented in terms of two membership values $\beta_{\text{A,neg}}$ and $\beta_{\text{A,pos}}$ expressing the membership of the result in the set of "negative" assessment values and in the set of "positive" assessment values (the set of "average" values is again the complement of the two other sets). In order to obtain a clear numerical value of A^* in the expected range between -1 and +1, these membership values must be de-fuzzyficated in the next and final step.

2.4 De-Fuzzyfication

After the successful application of the Fuzzy-Interference step, the outcomes of the rule system exists as membership values for the different result sets. In order to be applicable outside the fuzzy process, these membership values must be compiled into concrete numerical values. This transformation is done in the final step of the fuzzy processing, the De-Fuzzification. In principle, this process is the inverse of the Fuzzyifcation step and like the Fuzzification step it demands the exact definition of the membership function in terms of shape (in case of the F-A-ST model triangular as shown in Fig. 2 bottom) and boundary transition values. Like for the definition of the fuzzy input sets, these result sets have to be defined a priori either automatically through statistical methods or manually through expert knowledge.

After the final step, the fuzzy processing is finished and a crisp numerical value A^* as the outcome of the input values F and ST logically evaluated through a set of rules has been generated.

3 F-A-ST model: Mathematical implementation

In the following sections, the mathematical implementation of the fuzzy logic process into the F-A-ST model is presented. The structure of this description follows the general outline of the fuzzy logic process as presented in the previous section.

First, some general mathematical aspects of the fuzzy logic process are defined in Section 3.1. Then, the three steps of the fuzzy processing are explained in detail: Fuzzyfication (Section 3.2, p. 6), Fuzzy-Interference (Section 3.3, p. 9) and De-Fuzzyfication (Section 3.4, 10). Finally, some remarks on the usage of several F-A-ST sets (Section 3.5, p. 3.5) and on possible linguistic interpretations of the fuzzy results are made (Section 3.6, p. 3.6).

3.1 Numerical Definition Space

The purpose of the F-A-ST model is to provide a general mechanism to assess an external environmental parameter F with respect to the recent internal state ST of an agent. The result of the F-A-ST model is the assessment value A^* representing the actual evaluation of the external condition F.

In order to simplify the numerical implementation of the F-A-ST rules, the two input variables F and ST are first normalised to F^* and ST^*, or, in fuzzy terms, mapped from the original metric onto the universe U. In this model, the interval $[-1, +1]$ was chosen as universe U, in which -1 equals the lowest and +1 the highest possible fuzzy input value of F and ST.

To map F onto U, a simple linear function is used with

$$F \longrightarrow F^* :$$
$$F^* = \begin{cases} -1 & ; F \leq F_{\min} \\ -1 + 2\frac{F - F_{\min}}{F_{\max} - F_{\min}} & ; F_{\min} < F < F_{\max} \\ +1 & ; F \geq F_{\max} \end{cases} \tag{3.1}$$

with $F^* \in U \rightarrow [-1, +1]$. $F_{\min}$ and $F_{\max}$ are the boundary values between which the membership grade of the environmental factor F to the "low" or "high" fuzzy set will be calculated. Input values of F exceeding this range are cropped to the minimum or maximum value.

Analogously, the transformation of ST to ST^* can be written as

$$ST \longrightarrow ST^* : ST^* =$$
$$\begin{cases} -1 & ; ST \leq ST_{\min} \\ -1 + 2\frac{ST - ST_{\min}}{ST_{\max} - ST_{\min}} & ; ST_{\min} < ST < ST_{\max} \\ +1 & ; ST \geq ST_{\max} \end{cases} \tag{3.2}$$

with $ST^* \in U \rightarrow [-1, +1]$ and $ST_{\min}$ and $ST_{\max}$ as the boundary values for the expected range of input values for the internal state ST.

The advantage of this normalisation procedure is that the fuzzy process can easily be adopted for different input parameters by simply adjusting the threshold values while the rest of fuzzy rules can remain unaltered.

Finally, the expected range of the result variable A^* needs to be defined. To be coherent with the definition of the input variables, we define

$$A^* \in [-1, +1]$$

where -1 denotes the worst possible negative assessment and +1 is the best possible positive assessment of F. Values of A^* approaching 0 indicate a neutral assessment.

Each F-A-ST set defines only *one* combination of a selected F-ST relation. If the impact of several internal states ST on the same F parameter should be considered, additional F-A-ST sets must be defined and monitored parallel to each other (compare Section 3.5, p. 11). The same applies if different environmental aspects need to be assessed at the same time.

3.2 Step 1: Fuzzification

3.2.1 Definition of fuzzy input sets

The first step in fuzzy processing involves the definition of the required fuzzy sets to classify the input

variables F^* and ST^* as described in Section 2.2, p. 4.

For the input variables F^* and ST^* we define two Fuzzy sets for each variable: one set containing "low" values and the other containing "high" values. The complete formal definition of the fuzzy set *F,low* describing the membership $\mu_{F,low}$ of the variable F^* in the group of low values can be written as:

$$F,low := \{(F^*, \mu_{\text{F,low}}(F^*)) \mid F^* \in U; \mu_{\text{F,low}} \in M \longrightarrow [0,1]\}$$

in which M is the definition space $[0,1]$ of the membership function $\mu_{\text{F,low}}$ which will be defined in detail in the following section.

Analogously, the remaining fuzzy set *F,high* for high F^* values is defined as

$$F,high := \left(F^*, \mu_{\text{F,high}}(F^*)\right)$$

with $\mu_{\text{F,high}} \in M$ as assigned membership function.

For the normalised internal state ST^*, the same principle applies resulting in two fuzzy sets *ST,low* and *ST,high* with

$$ST,low := (ST^*, \mu_{\text{ST,low}}(ST^*))$$
$$ST,high := \left(ST^*, \mu_{\text{ST,high}}(ST^*)\right)$$

For both variables F and ST, a third fuzzy set for average values can be defined implicitly using the complement (inverse "¬") of the junction of the high and the low Fuzzy sets of the related variable:

$$F,average := \neg(F,low \cup F,high)$$
$$ST,neutral := \neg(ST,low \cup ST,high)$$

3.2.2 Definition of membership function

In order to estimate the exact membership value $\mu(x)$ of a variable x in a fuzzy set, the geometric shape and the boundary transition values for the membership function needs to be defined.

Theoretically, each valid mathematical function can be used to describe the membership function in Fuzzy logic. Hence, there is an almost infinite repertoire of membership functions that is used over the scientific community (for an in-depth discussion on that topic compare Mitaim and Kosko, 2001). However, most of more complex functions are only relevant when the fuzzy sets are generated automatically by computer algorithms using the Similarity Relation Model (compare Section 2.2, p. 4). If the sets are generated manually as in this case, the shape of the membership functions is normally limited to bell-shaped, triangular, trapezoidal or linear functions.

Figure 3: Membership functions for the fuzzy input sets "low", "average" and "high" for F^* and ST^*. x_1, x_2 and x_m are the main form parameters for the functions (shown only for the "low" set here).

From these classical options, we have chosen the *bell-shaped S-curve* to formalise the membership functions of F^* and ST^* in the fuzzy input sets. In contrast to the linear membership functions such as the triangle or trapezoid forms, the S-curve form represents well the first slowly but then increasingly distinct association of the input variables with the terms "low" and "high". However, it has to be noted that the selection of the shape of the membership curve is more intuitive rather than being based on hard mathematical theory supporting this decision (compare also Mitaim and Kosko, 2001).

Figure 3 shows the distribution of the "low" and "high" fuzzy input sets and the complement "average" set for both F^* and ST^*. In general, the exact shape and position of the bell-shaped curve is described using the three form parameters x_1, x_2 and x_m. For a better differentiation between the fuzzy sets, we will use $x_{1,l}$, $x_{m,l}$ and $x_{2,l}$ for the "low" and $x_{1,h}$, $x_{m,h}$ and $x_{2,h}$ as form parameters for the "high" fuzzy sets in the following text.

In the case of the "low" sets $x_{1,l}$ is located at the point where μ=1, $x_{2,l}$ is located at μ=0 and $x_{m,l}$ at μ=0.5. For the curve of the "high" sets the same principle

applies, except that the position of the respective values x_1 and x_2 are swapped.

The exact formulation of the membership function for the "low" fuzzy input set for a variable x can be written as:

$$\mu_{\text{x,low}}(x) = \begin{cases} 1 & ;x \leq x_{1,\text{l}} \\ 1 - 2\left(\frac{x - x_{2,\text{l}}}{x_{2,\text{l}} - x_{1,\text{l}}}\right)^2 & ; x_{1,\text{l}} < x < x_{\text{m,l}} \\ 2\left(\frac{x - x_{2,\text{l}}}{x_{2,\text{l}} - x_{1,\text{l}}}\right)^2 & ; x_{\text{m,l}} \leq x < x_{2,\text{l}} \\ 0 & ; x \geq x_{2,\text{l}} \end{cases}$$

and for the "high" fuzzy input set:

$$\mu_{\text{x,high}}(x) = \begin{cases} 0 & ; x \leq x_{1,\text{h}} \\ 2\left(\frac{x - x_{1,\text{h}}}{x_{2,\text{h}} - x_{1,\text{h}}}\right)^2 & ; x_{1,\text{h}} < x < x_{\text{m,h}} \\ 1 - 2\left(\frac{x - x_{2,\text{h}}}{x_{2,\text{h}} - x_{1,\text{h}}}\right)^2 & ; x_{\text{m,h}} \leq x < x_{2,\text{h}} \\ 1 & ; x \geq x_{2,\text{h}} \end{cases}$$

As only symmetric curves are used in the F-A-ST model, we can simplify $x_{\text{m,l}} = 0.5(x_{1,\text{l}} + x_{2,\text{l}})$ and for $x_{\text{m,h}}$ accordingly.

The membership value to the "average" fuzzy input set can be calculated as the complement of the junction of $\mu_{x,low}$ and $\mu_x, high$ once these values are known:

$$\begin{aligned} \mu_{\text{x,average}}(x) &= \neg\left(\mu_{\text{x,low}}(x) \cup \mu_{\text{x,high}}(x)\right) \\ &= 1 - \max\left(\mu_{\text{x,low}}(x), \mu_{\text{x,high}}(x)\right) \end{aligned}$$

Here, the "max" operator is used according to standard fuzzy rules to construct the complement of two fuzzy membership values.

3.2.3 Individualisation of fuzzy sets

In the model as it was presented so far, the assignment of the external parameter ST to the fuzzy input set depends only on the active range of ST given through $ST_{\min}$ and $ST_{\max}$ (see eq. 3.2) and on the form parameters $x_1(ST^*)$ and $x_2(ST^*)$ defining the start and the end value of the fuzzy input set. For practical reasons, these setting should be fixed in the model settings for the different F-A-ST combinations. However, in reality people do not react all in the same way on changes in their internal state. Some are more tolerant to high or low ST values, others are more sensible. To include this effect into the assessment process of the individual agent, an offset parameter x' is added to the definition of the ST^* membership functions. Using x', the form parameter $x_{2,\text{l}}(ST^*)$ for the *ST,low* input set is modified with

$$x_{2,\text{l}}(ST^*) = x^0_{2,\text{l}}(ST^*) + x'$$

For the *ST,high* set, the parameter $x_{1,\text{h}}(ST^*)$ is modified accordingly with

$$x_{1,\text{h}}(ST^*) = x^0_{1,\text{h}}(ST^*) - x'$$

where $x^0_{1,\text{h}}(ST^*)$ and $x^0_{2,\text{l}}(ST^*)$ are the original form parameters for the $\mu(ST^*)$ membership functions that apply to all agents.

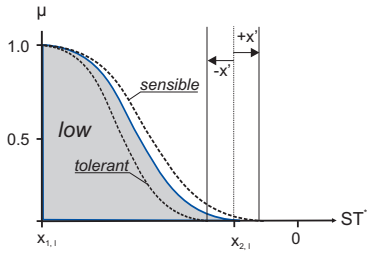

Figure 4: Individualisation of fuzzy sets by adding an offset x' to the form parameters. Figure shows the *ST,low* fuzzy set in which the grey area indicates the definition range of the "low" membership function without an individual offset applied.

Figure 4 shows the application of the x' offset by the example of the *ST,low* fuzzy set: For positive values of x', the upper boundary of the *ST,low* set shifts to the right. As an effect, small ST values will be classified earlier as "low" ST values. This condition can be associated with a *sensible* person who considers the actual state ST as "low" more quickly compared to a *normal* person with no x' offset applied. Analogously, the *ST,high* fuzzy set is also extended by the same offset, hence the same principle applies for high ST values.

Contrary, a negative offset x' decreases the definition range of both the *ST,low* and the *ST,high* fuzzy

set. As a consequence, a wider range of ST values will be considered as "average" (nor "low" neither "high"). This case would correspond to a more *tolerant* person (compare Fig. 4).

3.3 Step 2: Fuzzy-Interference

In the Fuzzy-Interference step, the connections between the input parameters F and ST and the resulting assessment A^* are established through a set of logic rules. Like for the design of the fuzzy sets in the previous step, the formulation of these rules are based on expert knowledge about how the assessment of the environmental parameter F is influenced by the internal state ST.

3.3.1 Linguistic formulation of fuzzy rules

As stated in the introduction, the concept of the F-A-ST model is rather simple compared to other models such as FLAME (El-Nasr et al., 2000). In our model, each environmental parameter is assessed independently from the other and each assessment depends on only one internal state variable at a time. Each given combination of an environmental parameter F, an associated internal state ST and the final assessment is called a "F-A-ST set".

For each F-A-ST set, a number of fuzzy rules need to be defined in order to transform the input data into an assessment value. These rules are rather simple and there are only two different cases that need to be distinguished.

The first one, called "*normal*" relationship is characterised by the following set of four rules:

(A1) `IF (`ST` is low) AND (`F` is low) THEN `A^*` should be NEGATIVE`

(A2) `IF (`ST` is high) AND (`F` is high) THEN `A^*` should be NEGATIVE`

(A3) `IF (`ST` is low) AND (`F` is high) THEN `A^*` should be POSITIVE`

(A4) `IF (`ST` is high) AND (`F` is low) THEN `A^*` should be POSITIVE`

In this set of rules, it is assumed that there is an inverse relationship between the magnitude of the external factor F and the internal state ST. If, for example, the internal state ST is high, an external factor F which is low will be assessed positive. This kind of relationship is typically used when a positive correlation between ST and F exists, in other words exposure to high F conditions will result in an increase of ST and hence a high ST state will result in an avoidance of further high F conditions.

The second set, called "*inverse*" relationship, handles the opponent case:

(B1) `IF (`ST` is high) AND (`F` is low) THEN `A^*` should be NEGATIVE`

(B2) `IF (`ST` is low) AND (`F` is high) THEN `A^*` should be NEGATIVE`

(B3) `IF (`ST` is high) AND (`F` is high) THEN `A^*` should be POSITIVE`

(B4) `IF (`ST` is low) AND (`F` is low) THEN `A^*` should be POSITIVE`

This relationship is typical for a negative correlation between F and ST in which high F values lead to a decrease in ST.

Different to boolean logic, the outcomes of the fuzzy rules are not exact numerical values, but again membership degrees to fuzzy sets, in this case to the fuzzy result sets. For the F-A-ST model, two fuzzy result sets have been defined: *A,negative* for negative assessment values with the membership grade $\beta_{\text{A,neg}}$ and *A,positive* with $\beta_{\text{A,pos}}$ for positive assessment values. Like for the input data sets, a third set of "neutral" assessment values results implicitly as the complement of the two other sets.

At this stage it is sufficient to define the fuzzy result sets only through linguistic description. The exact definition of the membership functions for the result sets will be required only in the last step of the Fuzzy processing, the De-Fuzzyfication.

3.3.2 Numerical implementation of fuzzy rules

This sub-step of the Fuzzy-Interference process deals with the translation of the linguistic rules presented in the previous section into standard numerical equations. Although the fuzzy system itself works with unsharpened data in this step, the rules must be defined using precise mathematical formulation in order to be applicable in a computer program.

The translation of the linguistic rules into mathematical equations can be distinguished into two parts:

First, the "IF x is y THEN" cases of the individual fuzzy rules must be transformed. Second, the results of the single rules defined in the fuzzy system must be compiled into one single result.

There are several different ways how the operators "*OR*" and "*AND*" in the fuzzy IF-conditions can be transferred into classical algebra. Originally, Zadeh (1965) proposed the usage of the **min**-operator to apply the fuzzy "*OR*" ($\vee$) between two variables the the application of the **max**-operator to calculate the fuzzy "*AND*" ($\wedge$).

Using this approach, rule A1 could be written as:

$$\beta_{\text{A,neg}} = \mu_{\text{ST,low}} \wedge \mu_{\text{F,low}} = \min\left(\mu_{\text{ST,low}}, \mu_{\text{F,low}}\right)$$

One problem with the min/max approach is that only the membership grade of *one* input parameter is taken into account in the final result. Hence, a non-continuous behaviour of the result function can be observed at switch points (compare Kürbis, 2002, p. 95 f). To overcome these problems, the set of possible fuzzy operators have been extended by several authors (see e.g. Börcsök, 2000; Zimmermann, 2001).

In this model, we will apply the "*Prod*" method which uses the algebraic product to represent the fuzzy "AND" operator. This method provides a finer resolution of the output value as it takes into account the state of *both* input variables, which seems more reasonable for this application. So, the rules (A1) to A4 can be written as:

(A1) $\beta^{\text{A1}}_{\text{A,neg}}(ST^*, F^*) = \mu_{\text{ST,low}}(ST^*) \cdot \mu_{\text{F,low}}(F^*)$

(A2) $\beta^{\text{A2}}_{\text{A,neg}}(ST^*, F^*) = \mu_{\text{ST,high}}(ST^*) \cdot \mu_{\text{F,high}}(F^*)$

(A3) $\beta^{\text{A3}}_{\text{A,pos}}(ST^*, F^*) = \mu_{\text{ST,low}}(ST^*) \cdot \mu_{\text{F,high}}(F^*)$

(A4) $\beta^{\text{A4}}_{\text{A,pos}}(ST^*, F^*) = \mu_{\text{ST,high}}(ST^*) \cdot \mu_{\text{F,low}}(F^*)$

And for the inverse rule set:

(B1) $\beta^{\text{B1}}_{\text{A,neg}}(ST^*, F^*) = \mu_{\text{ST,high}}(ST^*) \cdot \mu_{\text{F,low}}(F^*)$

(B2) $\beta^{\text{B2}}_{\text{A,neg}}(ST^*, F^*) = \mu_{\text{ST,low}}(ST^*) \cdot \mu_{\text{F,high}}(F^*)$

(B3) $\beta^{\text{B3}}_{\text{A,pos}}(ST^*, F^*) = \mu_{\text{ST,high}}(ST^*) \cdot \mu_{\text{F,high}}(F^*)$

(B4) $\beta^{\text{B4}}_{\text{A,pos}}(ST^*, F^*) = \mu_{\text{ST,low}}(ST^*) \cdot \mu_{\text{F,low}}(F^*)$

3.3.3 Fuzzy composition

In the last sub-step of the Fuzzy-Interference, the so-called *Fuzzy Composition*, the outcomes of the different rules which have been treated independently from each other so far, need to be summarised into a single value. This is realised through linking the different membership grades in the fuzzy result sets β through then fuzzy "OR" ($\vee$) represented through by the **max**-operator. This method of using the algebraic products in the evaluation of the single rules and then the max-operator in the final result compilation is a popular approach in Fuzzy logic also known as the "**Prod-Max**" method.

For the case of a "normal" F–ST relation ship (see above), the Fuzzy composition writes:

$$\begin{aligned}
\beta_{\text{A,neg}}(ST^*, F^*) &= \beta^{\text{A1}}_{A,neg} \vee \beta^{\text{A2}}_{\text{A,neg}} \\
&= \max\left(\beta^{\text{A1}}_{A,neg}, \beta^{\text{A2}}_{\text{A,neg}}\right) \\
\beta_{\text{A,pos}}(ST^*, F^*) &= \beta^{\text{A3}}_{A,pos} \vee \beta^{\text{A4}}_{\text{A,pos}} \\
&= \max\left(\beta^{\text{A3}}_{A,pos}, \beta^{\text{A4}}_{\text{A,pos}}\right)
\end{aligned}$$

If the F-A-ST relationship is of the "inverse" type, the steps above are written analogously using rules B1-4.

It has to be noted that in the F-A-ST model as it is designed here, the "low" and the "high" Fuzzy sets do not overlap. Hence, only one of the rules can apply (or, in fuzzy terms, "fire") at a time, so the membership value of this rule could be taken immediately as the final result of the rule system. However, to allow a more general application of the model and cover the case of overlapping fuzzy sets, the complete evaluation procedure was implemented into the model.

3.4 Step 3: De-Fuzzyfication

The objective of the final step of the fuzzy logic process is to transform the fuzzy output of the fuzzy interference step into crisp numeric value(s) that can be used outside the Fuzzy logic system. As the name suggests, it is the inverse method to the Fuzzyfication described in Step 1.

The two fuzzy result sets *A,negative* and *A,positive* have only been defined linguistically so far. In order to transfer the results of the fuzzy rules given in terms

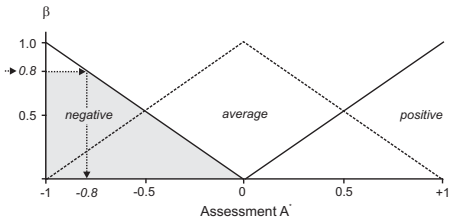

Figure 5: Membership functions for the fuzzy result sets "negative", "positive" and the complement set "average". As an example, the De-Fuzzyfication of $\beta_{\text{A,neg}}$=0.8 is indicated.

of membership grades $\beta_{\text{A,pos}}$ and $\beta_{\text{A,pos}}$ into a crisp assessment value A^* ranging from -1 to +1, the shape of the result fuzzy sets needs to be defined precisely as it has been done for the fuzzy input sets.

Based on the initial definition of A^* (see Section 3.1, p. 6), the formal definition of the fuzzy result sets is quite easy: Negative assessments are defined as A^* values between -1 and 0 whereas positive assessments are in the range between +1 and 0.

Hence, the result fuzzy sets can be defined as:

$$A_{\text{pos}} := \left\{ \left(A^*, \beta_{\text{A,pos}}\right) \mid A^* \in [+1, 0]\,; \beta_{\text{A,pos}} \in M \right\}$$

and

$$A_{\text{neg}} := \left\{ \left(A^*, \beta_{\text{A,neg}}\right) \mid A^* \in [-1, 0]\,; \beta_{\text{A,neg}} \in M \right\}$$

The third fuzzy result set containing the average assessment values is again the complement of the two other sets.

Whereas for the fuzzy input sets a bell-shaped membership function was chosen, a linear transition of A^* over the definition range seems more appropriate for the fuzzy result sets. To model this linear transition, the simple triangle form as shown in Figure 5 has been selected for the two result sets.

In a complex fuzzy system with several fuzzy result sets, the De-Fuzzyfication process can be the most complicated step of the whole fuzzy processing, which, for example, can require a geometric mapping of all fuzzy result membership grades onto a single axis to obtain the final result as a numerical value ("Center-of-Gravity"-Method). However, for the F-A-ST model this step is much more simple as only two fuzzy result sets exist. Due to this simple structure, the final assessment value $A^* \in [-1, +1]$ can be calculated directly from the weighted average of the membership functions $\beta_{\text{A,neg}}$ and $\beta_{\text{A,neg}}$ and the associated maximum values -1 and +1: [1]

$$A^* = \frac{\beta_{\text{A,neg}} \cdot (-1) + \beta_{\text{A,pos}} \cdot (+1)}{\beta_{\text{A,neg}} + \beta_{\text{A,pos}}}$$

Figure 5 shows as an example the De-Fuzzyfication for a membership grade $\beta_{\text{A,neg}}$=0.8 leading to the assessment A^*=-0.8.

3.5 Interactions between different F-A-ST sets

Up to this point, only the outcomes of one F-A-ST set have been considered in the assessment value. As the model allows different F-A-ST sets to be active and analysed at the same time, it has to be defined how they are linked with each other and how the results are evaluated.

There are basically two possible approaches to solve this problem: The first way could be to summarize the suggestions of the different F-A-ST sets on the level of the single membership values β in the fuzzy result sets and then construct one final A^* value out of them.

The second option is to calculate an individual A^* value for each F-A-ST set and then summarize these values into a common A^*. In fact, there is no big difference between both methods as they both include an aggregation of the individual suggestions. In this model we use the second method and first calculate the single A^* values for each active F-A-ST set and then summarize them into one final value:

$$A^* = \min\left\{A^*(\text{Set } 1), A^*(\text{Set } 2), \ldots, A^*(\text{Set}n)\right\}$$

1. In the model as it is now, only either $\beta_{\text{A,neg}}$ or $\beta_{\text{A,neg}}$ can hold values different to zero. Hence, the De-Fuzzyfication could be even more simple but would restrict the application to non-overlapping fuzzy input sets

Using the **min**-operator, the F-A-ST set with the highest negative impact "wins" and defines the final assessment value. Like in the case of the fuzzy logic operators, it can be annotated that the assessment values of all other F-A-ST sets will be lost when the max-operator is used. However, if the F-A-ST sets define very different aspects of the assessment process it is of limited use anyway to combine them in one single value. In those cases, the results of the single F-A-ST sets should be analysed and interpreted independently from each other in different simulation runs.

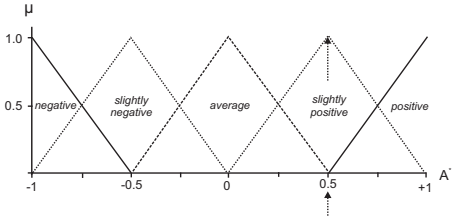

Figure 6: Membership functions for the Re-Fuzzyfication of the assessment value into finer linguistic groups. As an example, the Re-Fuzzyfication of A^*=0.5 is indicated.

3.6 Linguistic Interpretation of assessment results

Besides calculating a crisp numerical value as outcome of the fuzzy assessment process it is also possible to use the basic idea of fuzzy logic to provide a linguistic interpretation of the results.

Through the membership degree β in the fuzzy result sets it can be directly derived, to what degree a statement about the assessment value is true. If, for example, the outcomes of the fuzzy process show a membership degree of $\beta_{\text{A,pos}}$= 0.7 in the fuzzy set of positive assessment values, then the statement "*The assessment is positive*" is 70% true (and 30% false).

In addition to these basic statements, fuzzy logic allows to model more detailed information similar to the usage of adjectives and adverbs in a natural language through the application of so-called "*hedges*". Using hedges, the statement "A^* is positive" can be refined into "A^* is *very* positive" by adjusting the membership degree $\beta_{\text{A,pos}}$:

$$\beta_{\text{A, very pos}} = \left(\beta_{\text{A,pos}}\right)^2$$

Other typical hedges are "*more or less* X" (typically defined through $\beta_{\text{A,more/less X}} = \sqrt{\beta_{\text{A,X}}}$) or "*somewhat*", "*rather*" or "*sort of*".

A second option to transform the results of the fuzzy process into linguistic terms is a Re-Fuzzyfication of the result into linguistic groups. Whereas it was easier for the formulation of the fuzzy rules to deal with as few result sets as possible, it might be of advantage to have a finer interpretation of the final result afterwards. For example a value A^* of +0.5 indicates that the assessment is 50% "positive" and 50% "average". No one would speak like this in real live, rather the situation would be described as "*slightly* positive". To model the meaning of "slightly", it is possible to use the fuzzy hedges as described below, or to re-fuzzy the result. The advantage of the latter is that the formal definition of these linguistic fuzzy sets can be chosen freely. Figure 6 shows as an example the Re-Fuzzification of the $A*$ value into five linguistic fuzzy sets.

Combining the assessment value with the information about the quality of the environmental parameter F, the result can be further refined into "negative due to high F value", "negative due to low F value" and the other combinations accordingly.

4 Assessing thermal conditions: An example from human biometeorology

In the previous sections, the theoretical concept and the numerical implementation of the F-A-ST model have been presented. In order to make the application of the F-A-ST model as a component of a Multi-Agent simulation system more transparent, a relative simple example from human biometeorology related to the thermal conditions in urban areas is presented in the following section.

4.1 Thermal comfort: Theoretical background

Controlling and keeping the body temperature inside a quite limited range is one of the basic tasks the human body is continuously occupied with. Though the thermal conditions in daily life normally do not reach values that can lead to dangerous conditions for the body's health, it is quite frequent that we feel uncomfortable with the actual conditions. If our immediate environment appears too warm or too cold, the body begins to counteract by trying to compensate the energy surplus or deficit. However, this mechanism of thermoregulation can only adjust the thermal state of the body within a certain range. If the actual thermal conditions are outside this range, thermal discomfort arises.

While it is possible to control the climate conditions of indoor locations in a way that thermal comfort is achieved for most of the users, this is not practicable for outdoor locations. As soon as we enter the outdoor environment, the human body is exposed to a variety of energy inputs and losses due to wind, air temperature and solar radiation. Through the selection of adequate clothing it is possible to react on cold conditions over a wide range of temperatures, but there is no protection against heat stress. Hence, hot discomfort is the most frequent problem when dealing with human thermal comfort in outdoor locations. Especially in urban areas the local design with artificial surface materials and often very few green spaces can result in unpleasant hot local climate conditions. These conditions can have a significant impact on the popularity and usage of open spaces and streets and thus imply economic consequences for shops, restaurants or other facilities depending on pedestrian frequentation.

There are a lot of different approaches for the estimation of human comfort based on the climate conditions humans are exposed to. ISO 7730 (1995) for example defines the well known "*Predicted Mean Vote*" (PMV) index which predicts thermal comfort based on the air temperature, wind flow, humidity and, for outdoor locations, solar radiation of the respective location. In this example we will approach the problem from the perspective of the individual user of an urban outdoor location. Using the Multi-Agent simulation system BOTworld including the dynamical model of the human thermoregulatory system (ITCM), we will assess the thermal comfort conditions in a simple open space depending on both the actual thermal state of the individual agent and of the local climate conditions. It will be demonstrated, how the F-A-ST model can be used as an universal method to link these two parameters in order to get a situation-specific assessment of the (thermal) environmental conditions.

The following sections will focus only on the F-A-ST model as a method to combine internal and external parameters into one assessment value. The way, how these input data are generated and how they can be interpreted will be addressed only very briefly here. Details on this aspect can be found in Module B of this thesis.

4.2 The BOTworld Multi-Agent system

In this example, the Multi-Agent system BOTworld is used to apply the F-A-ST model to assess human thermal comfort in urban areas. BOTworld is a microscale Multi-Agent system that allows simulating pedestrian traffic in urban areas based on the simulation of the individual behaviour. Figure 7 gives a schematic overview over the system focussing on the F-A-ST model as an integrated component of the system used to assess local climate conditions.

In BOTworld, each virtual pedestrian is represented through a software agent who navigates autonomously through the model environment. Based on different routing points distributed over the 2D model environment, individual trip itineraries are created for each agent. To create realistic movement

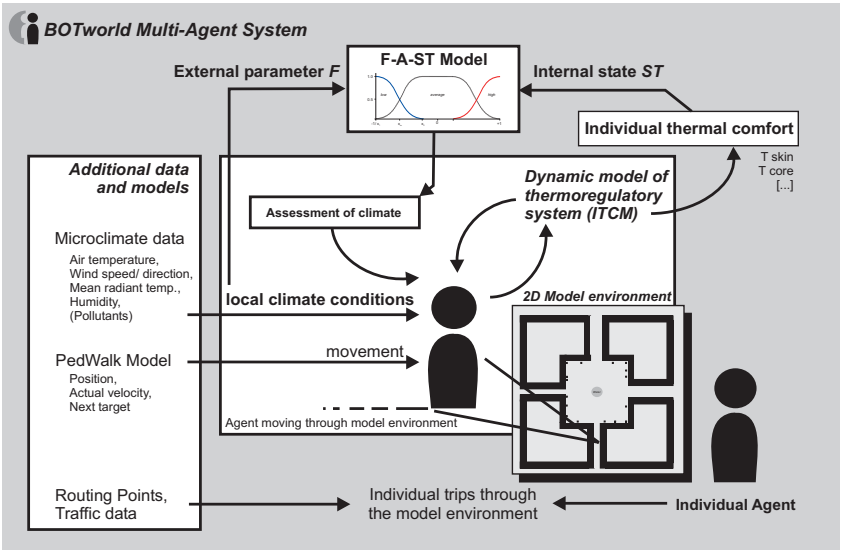

Figure 7: Schematic overview of the different components and the architecture of the BOTworld system focussing on the F-A-ST assessment model.

patterns, the *PedWalk* model component of BOTworld (compare Module A of this thesis) takes care of the agents' route choice, position control and conflict behaviour when meeting other agents inside the virtual model world.

In order to simulate thermal comfort of the virtual pedestrians, the BOTworld system needs detailed information about the microclimate conditions inside the selected urban environment. The main data required are: Air temperature, wind speed and direction, air humidity and, the "mean radiant temperature". The latter is a synthetic temperature that is defined as the uniform temperature of an imaginary black enclosure which would result in the same radiative energy balance as the actual enclosure (compare ISO 7730, 1995).

For an outdoor location, the mean radiant temperature (T_{mrt}) is the main indicator for the solar radiative input. In the shade, T_{mrt} is close to the air temperature values whereas in the sun it can easily reach values of 70°C and more. We will use this parameter later on to characterise the environmental conditions in terms of thermal conditions.

While moving through the model environment, the agents are exposed to different microclimatic conditions influencing the energy budget of their body. In order to analyse the reaction of the human thermoregulatory system onto these conditions, the Individual Thermal Comfort Model (ITCM) continuously monitors the thermal state of each agent with respect to his individual body properties and location in the model area. The ITCM is a complex biometeorological model (compare module B of this thesis) that provides detailed information about the actual thermal state of the individual agent. From the different parameters provided, we will use the *average skin temperature* T_{sk} in this paper as indicator for the actual internal thermal state of the agent when assessing the local climate conditions.

4.3 The test scenario: Spatial layout and microclimate conditions

To demonstrate the functionality of the F-A-ST model, the scenario of a simple square urban open space has been chosen as a demonstration case. The model domain as shown in Figure 8 consists of a 200

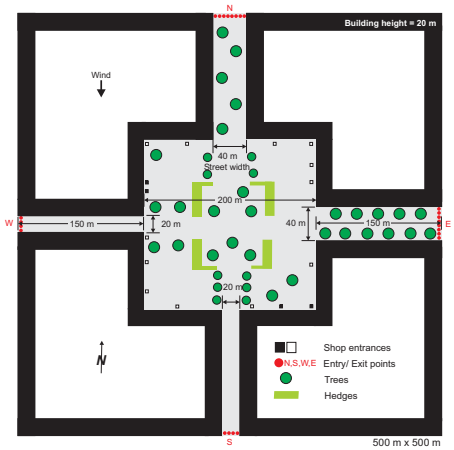

Figure 8: Model domain for the F-A-ST model test study. The entry/ exit points as well as the shop entrances are used to generate pedestrian traffic inside the model environment.

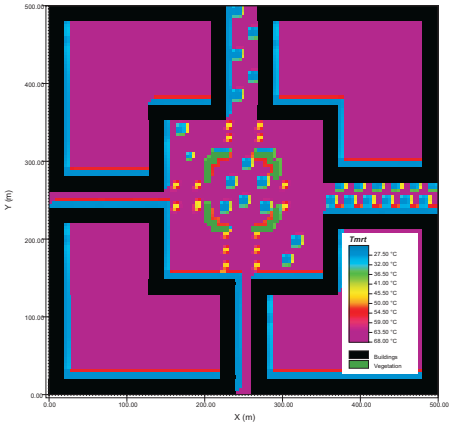

Figure 9: Distribution of mean radiant temperature in 1.60 m above ground for a hot summer day in Central Europe at 14:00 CET.

m × 200 m large central place which can be accessed through four lateral street canyons, each 150 m long. On the open place, several trees are located that provide local shade and wind shelter. Routing points at the end of the streets serve as interfaces to the world outside the model domain where agents can enter and leave the model area. Inside the model domain, the virtual pedestrians are randomly attracted by different shop entrances distributed over the buildings on the open place (little squares in Fig. 8).

In order to obtain information about the microclimate conditions of the urban space, the microclimate model ENVI-met (Bruse and Fleer, 1998) has been used to generate the required input data for the BOTworld system. Table 1 lists the most important initial and boundary conditions for the microclimate simulation. For this case study, a cloudless summer day in Central Europe with moderate northern winds (2 ms^{-1} have been chosen. From the different climate data provided by ENVI-met, Figure 9 shows as an example the distribution of the mean radiant temperature in 1.60 m above ground at 14:00 CET. At that time of day, the local air temperature in the model area has warmed up from the initially assumed 22°C to values around 26°C with a difference less than 2 K between the coldest and the hottest spot. It has to be noted, that the microclimate simulations with ENVI-met have been made using a coarser spatial resolution of Δxy=4 m while the Multi-Agent system BOTworld used a finer resolution of Δxy=2 m. The climate data have been linearly interpolated to the finer model resolution.

Table 1: Settings for the ENVI-met microclimate simulation.

Simulated day	23th June
Simulated position	Bochum, Germany
	7.5° e.Long.
	53.0° n.Lat
Above-roof wind (10 m)	2.0 ms^{-1} from N
Reference temperature atmosphere	22.0°C
Initial relative humidity	50%
Dimension model area	500 m × 500 m
Resolution model area	
ENVI-met	Δxy=4 m
BOTworld	Δxy=2 m

Figure 9 shows well the distribution of sun and shade in the model area: In the unshaded areas, the mean radiant temperature reaches values up to 70°C due to the high solar input. Contrary, in the shade of the buildings and of the larger trees, T_{mrt} drops down to 26°C which equals more or less the local air temperatures. Hence, the mean radiant temperature is a

well suited indicator to describe the thermal conditions inside the model area.

4.4 Defining the T_{mrt}–T_{sk} F-A-ST set

In this example, the F-A-ST model is run with only one active F-A-ST set. The first and basic step in the definition of a F-A-ST set is the choice of the environmental parameter F to be assessed and the selection of the associated internal state ST that has an impact on the assessment of F.

As noted before, the mean radiant temperature (T_{mrt} represents a good indicator to describe the solar input at a given location. Using the T_{mrt} value, the local microclimate conditions can easily be distinguished into "*sunny*" and "*shady*" conditions. Hence, the mean radiant temperature is used as the external parameter F in this F-A-ST set.

The question, whether a person prefers a sunny or a shady location is highly influenced by the actual thermal state of the person: If someone already feels hot, shade is preferred, if someone feels cold, sunny conditions will be given preference. From the different parameters that are supplied by the human thermal comfort model ITCM we have chosen the *average skin temperature* (T_{sk}) as ST parameter to represent the actual thermal state of the agent.

Following the description in Section 3.2.1 p. 6, we define the boundary values for the fuzzy range of external parameter F as:

$$\begin{aligned} F_{min} = 25°C \quad &\rightarrow T_{mrt} \text{ indicates } \textit{"shady"} \\ \updownarrow & \\ F_{max} = 65°C \quad &\rightarrow T_{mrt} \text{ indicates } \textit{"sunny"} \end{aligned}$$

where "shady" and "sunny" equal the linguistic descriptions of the respective end of the fuzzy range. The closer a value of T_{mrt} approaches these boundaries, the more clearly it will be assigned to the *F,low* or *F,high* fuzzy input set.

Analogously, the boundaries for mapping the skin temperature ST onto ST^* are defined as:

$$\begin{aligned} ST_{min} = 34°C \quad &\rightarrow T_{sk} \text{ indicates } \textit{"cold"} \\ \updownarrow & \\ ST_{max} = 38°C \quad &\rightarrow T_{sk} \text{ indicates } \textit{"hot"} \end{aligned}$$

with "cold" and "hot" describing the thermal state of the agent parameterised through the skin temperature.

Obviously, the T_{mrt}–T_{sk} F-A-ST set is of the relationship type that is called "normal" in Section 3.3.1: If the skin temperature is high (hot state), high mean radiant temperature values (sunny conditions) will be assessed negative and the other way round.

For the mathematical definition of the fuzzy input sets, the form parameters of the membership function need to be defined. For both sets, the default settings provided by the BOTworld system have been used:

$$\begin{aligned} x_{1,l} = -1.0, \quad x_{2,l} = -0.25 \\ x_{1,h} = +0.25, \quad x_{2,h} = +1.0 \end{aligned}$$

and for the individualisation of the fuzzy sets the following offset values have been used:

$$\begin{aligned} x' = +0.10 \text{ (sensible agents)} \\ x' = -0.10 \text{ (tolerant agents)} \end{aligned}$$

Figure 10 shows the BOTworld software interface for the definition of F-A-ST sets showing the previously defined set. The diagram in the interface shows the membership functions of the fuzzy sets [*F,low*], [*F,high*] and the resulting complement set [*F,average*] plotted for a "normal" agent (x'=0).

To get an impression over the behaviour of the T_{mrt}–T_{sk} F-A-ST set, Figure 11 shows the resulting assessment values plotted over the F^* and ST^* definition space. Surface areas plotted above the 0.00 level indicate parameter combinations that will be assessed positive whereas areas below zero indicate a negative assessment. The flat regions are those conditions that are assessed neutral by the F-A-ST model.

4.5 Simulation results

4.5.1 Individual assessment

The first example of selected F-A-ST simulation results focuses on the assessment process seen from the perspective of a single agent. The following scenario has been constructed to show how the assessment of the local situation is influenced by the actual thermal state of the agent: An agent named "Jacob" leaves an

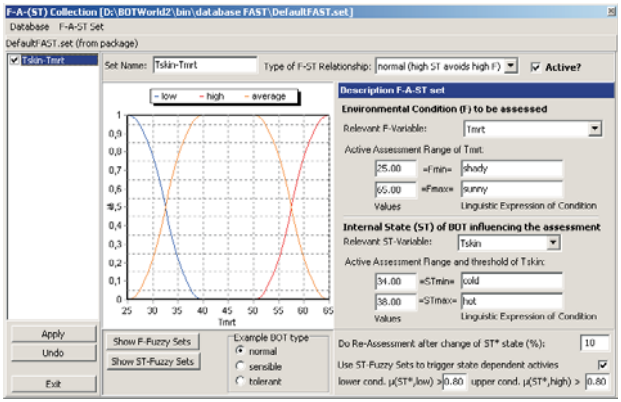

Figure 10: GUI of the BOTworld system for the definition of F-A-ST sets showing the T_{mrt}–T_{sk} F-A-ST set. Example plot illustrates the membership functions of the F-fuzzy sets.

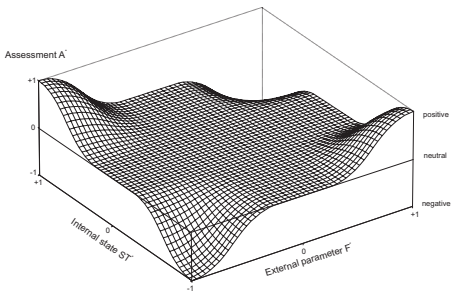

Figure 11: Assessment values A^* resulting from the T_{mrt}–T_{sk} F-A-ST set over the definition range of the normalised parameters F^* and ST^*.

indoor environment with an assumed air temperature of 20°C and enters the model area from the western street segment. While walking on the sunny side of the street, he meets somebody and stops his walk for a long conversation. During that time, he is exposed to a mean radiant temperature of about 67°C.

Figure 12 (a) shows the evolution of the skin temperature during this scenario as it is provided by the individual thermal comfort model: When "Jacob" enters the outdoor environment, his initial skin temperature is about 34.5°C. According to the settings of the ST fuzzy input sets in Section 4.4, this internal state is classified with a certainty of 81% as "cold" ($\mu_{\mathrm{ST,low}}$=0.81) and with a certainty of 65% as "*very* cold" using the fuzzy hedge "very" with $\mu_{\mathrm{ST,very\ low}}=(\mu_{\mathrm{ST,low}})^2$=0.65 (compare Fig. 14 a).

While the agent stands in the sun, he begins to heat up and the skin temperature increases up to 37.8°C after approximately 20 min. This state approaches the end of the fuzzy definition range of ST with a membership grade of 0.97 in the "hot" and 0.95 in the "very hot" fuzzy set (compare Fig. 14 b).

The BOTworld system also allows using the F-A-ST model to influence the agents' behaviour. For example, an upper and a lower threshold value of ST^* can be defined to trigger situation specific activities. In this example, the termination of the conversation would be a realistic response to such a high discom-

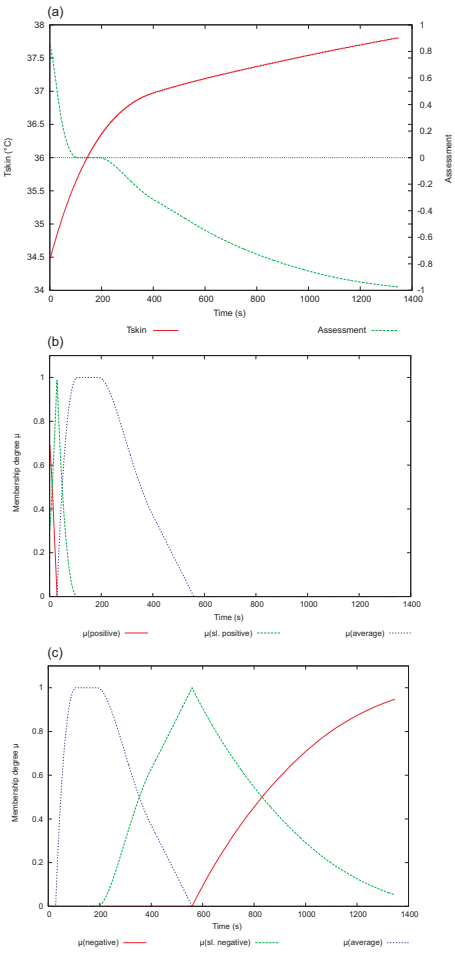

Figure 12: Evolution of the skin temperature and associated change in the local assessment during the simulated conversation scenario: Skin temperature versus actual assessment of position (a) and membership functions for A^* in the linguistic result sets ”positive”, ”slightly positive”, ”average”, ”slightly negative” and ”negative” (b,c).

fort.

Obviously, the observed change in the internal state must have an impact on the assessment of the local situation the agent is exposed to. At the beginning of the conversation, the ”cold” internal state results in a positive assessment of the ”hot” local microclimate conditions with A^*=+0.81 (compare Figs. 12 a and 14 a) the agent is standing in. As the skin temperature increases, the assessment changes: When approaching a value of T_{sk}=36°, the assessment enters the neutral range until a skin temperature of 36.5° is reached and A^* turns into the negative range of assessment values almost reaching the maximum negative assessment of -1 at the end of the virtual conversation (see Fig. 14 a).

Figures 12 (b) and (c) show the membership degrees of the respective assessment values based on the Re-Fuzzyfication into the five linguistic terms ”positive”, ”slightly positive”, ”average”, ”slightly negative” and ”negative” as suggested in Section 3.6 and Figure 6 p. 12. Especially in the case of negative assessment values, the distribution into three assessment sub-ranges provide a more detailed information about the actual situation compared to the analysis of the single A^* curve only.

The internal assessment map

The actual internal state does not only influence the assessment of the actual position of the agent, but also has an impact on the agent’s view on the complete model environment. In a Multi-Agent system that considers feedbacks between the environmental assessment and the resulting behaviour of the agents, this internal assessment map is the main information base for the agents’ decision processes.

In Figure 13, the individual assessment map of agent ”Jacob” at the beginning of the conversation while his internal state is still ”cold” can be seen as an example. Areas with an assessment value larger than 0 (shades of green) are assessed positive and regarded as pleasant and desirable locations by the agent. Contrary, location with negative assessment values (shades of red) are locations, where the agent expects to maintain or even increase his actual ”cold” discomfort state. In this example, the spatial distribution of positive and negative assessment values correspond with the distribution of sun and shade: Areas in the shade of buildings and larger trees are as-

Figure 14: BOTworld interface for online monitoring of the F-A-ST model: Assessment process at the beginning of the simulation (cold state,a) and situation at the end of the simulated conversation (hot state,b).

sessed negative while the sunlit parts get positive assessment values. The semi-shade of the smaller trees is assessed as neutral conditions neither improving nor worsen the actual thermal state.

At the end of the virtual conversation, when the agent has reached the ”hot” internal state in the meantime, the distribution of assessment values is inverse: Now the sunlit areas have become unattractive while the shaded regions are assessed positive (not shown as figure here).

Online monitoring of the F-A-ST process

In order to monitor and understand the dynamics of the F-A-ST assessment process, the BOTworld system allows the online monitoring of the different F-A-ST sets defined in the model. Figure 14 (a) shows the state of the assessment process at the beginning of the example simulation (cool skin temperature of the agent ”Jacob”) while Figure 14 (b) shows the situation after 20 min when the agent's internal state has shifted to ”hot” conditions. The respective fuzzy classification of the internal state ST/ST^* is indicated with a green and a red dot in the figure, the other variables shown follow the definitions used in this paper.

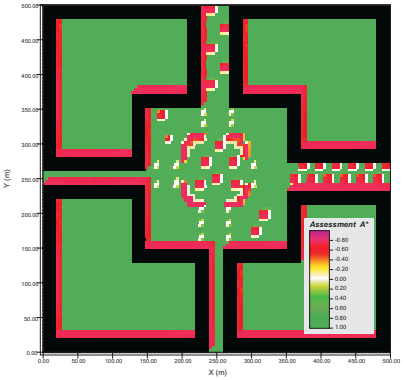

Figure 13: Spatial distribution of the local assessment value A^* seen from agent "Jacob" at the beginning of the simulation ("cold" internal state).

4.5.2 Spatially aggregated assessment

The agent-focussed model analysis presented in the previous section allowed a detailed insight into the dynamics of the F-A-ST system, but does not provide enough information to assess the complete model area. To obtain spatial representative data, a large amount of agents with different properties and routes through the model environment is required. The local assessment values can then be extracted by averaging the individual assessments of agents as they pass by.

To generate a map of local assessment values, a simulation over a period of 30 min model time has been executed in BOTworld. During this time, approximately 1700 agents have populated the virtual urban open space and contributed to the maps shown in Figure 15. [2]

Figure 15 (a) shows the averaged local internal state ST^* over the model area. The maximum values can be found in the north-eastern corner of the open space with ST^* values going up to +0.50. In this corner, no trees or buildings shade the area and due to the wind sheltering effect of the building corner, the skin temperatures can reach their local maxima here. A second peak can be observed on the sunny side of the western street segment. Due to the small width of the street and its perpendicular orientation to the wind direction, the local wind speed is also low here, causing comparably high skin temperatures. Con-

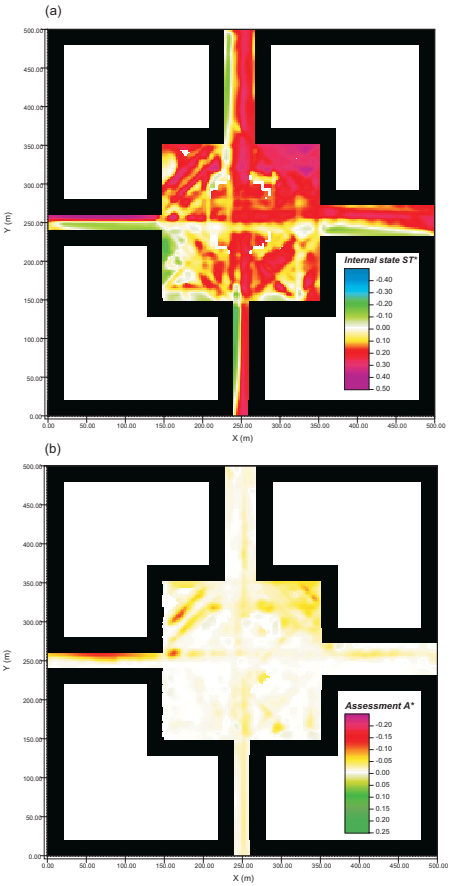

Figure 15: Spatial aggregated results from the F-A-ST model: Internal state ST^* (a) and resulting assessment value A^* (b).

trary, the lowest values ST^* can be found on the shaded sides of the streets and in the south-western corner of the place. Here, the internal state values go hardly lower than -0.25 which is just the beginning of the range covered by the *ST,low* fuzzy input set (selected threshold value $x_{2,l}$=-0.25). Hence, those lo-

2. In Figures 15 and 16, missing data from grid points without any agent visits have been linearly interpolated using an inverse distance weight method and the resulting data have then been spatially smoothed to filter unrepresentative excess values.

cations will not give a cool or even cold impression using the actual F-A-ST parameters.

While the previously discussed map of the internal state reflects the actual state of the agents when entering a certain location, the map of the average assessment values as shown in Figure 15 (b) now combines this information with the local microclimate conditions. The simulated thermal state of agents in this case study only reaches moderate hot conditions with ST^* values not exceeding 0.50, hence the resulting assessment values are also close to a neutral assessment at most locations. The "worst" conditions with values of around A^*= -0.15 can be found on the sunny side of the western street canyon and on some spots on the open space.

Concluding the results of the F-A-ST model, the thermal comfort situation of the case study shows in average a certain tendency towards the warm conditions, but, except maybe of the western street, does not show areas where hot internal states and hot microclimate environments meet in an unacceptable combination. However, it must be kept in mind, that the threshold values of the input fuzzy sets are selected more or less arbitrarily based on personal impressions rather than on hard empirical facts. With the transparent concept of the F-A-ST model it is always possible to refine the model settings and adjust them to empirical data e.g. from questionnaires if such information is available.

Impact of street trees on the assessment

To answer the question, to which extent the comparable high amount of trees in the case study scenario contributes to the thermal situation, a second simulation has been carried out in which all the vegetation has been removed and a small water pond in the middle of the place has been installed (compare to the simulations in Module B of this thesis). The remaining parameters of the simulation have not been changed.

In Figure 16 the spatial distribution of the average assessment values for the treeless scenario is shown. Two changes are obvious when comparing the results of the two scenarios: First, the overall level of the assessment values has shifted slightly towards more negative values in the treeless case and second, the removal of the trees in the eastern street changed the assessment of this street from the more or less neutral range towards a new local maximum in negative evaluation with A^* values around -0.20. In the northern street segment the change is less drastic but still traceable.

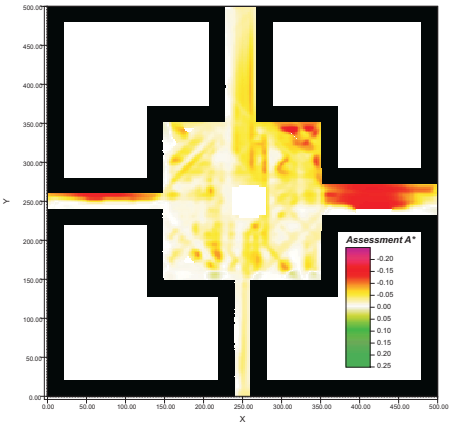

Figure 16: Spatial aggregated assessment of the open space without trees.

As the thermal state of the agents react with a certain inertia on the actual microclimate conditions, the removal of the trees has an impact even in those areas where no trees have been anyway. This can be well observed in the case of the north-eastern corner of the open space which is treeless in both scenarios. The assessment of this area is highly influenced by the thermal state of the agents entering the open space through the eastern street segment. Through the removal of the trees in this segment, the thermal load of agents using this passage is increased which also shifts the assessment of the following locations visited towards a warmer thermal impression.

4.6 Conclusions for the test scenario

To demonstrate the functionality of the F-A-ST model as a component of the Multi-Agent system BOTworld, the assessment of human thermal comfort when walking over a square urban open space has been chosen as case study. In order to operate the model, one F-A-ST set assessing the local thermal conditions (mean radiant temperature) in dependency to the internal thermal state of the agent (skin

temperature) has been constructed. By the example of an agent standing motionless in the sun and slowly heating up it was demonstrated, how the individual assessment of the actual position changes as the relevant internal state changes.

For obtaining spatial representative assessment data, model simulations have been executed over a 30 min time period with 1700 agents that used the virtual open space. By comparing the assessment results for the open space with trees to a situation where all trees have been removed it was shown, that local changes effect the thermal comfort assessment of the complete area, not only of those locations where the change took place.

As stated previously, the selection of the boundary values for the fuzzification of the external parameter F and the internal parameter ST have been chosen relative arbitrarily based on guesses which temperatures are assessed as hot and which are considered as cold. To calibrate the model to a specific situation and a given community of users, the different threshold values of the fuzzy input sets can easily be adjusted to the observations.

5 Final conclusions

In this paper the "*Fuzzy-Assessment-by-state (F-A-ST)*" model has been presented. The F-A-ST model is a simple general purpose approach to assess a given external parameter F in dependency to an internal state ST that influences the assessment process. The main area of application for this model are software systems in which decision processes are modified by the actual state of the decision making unit, most prominently Multi-Agent systems in which each single agents needs an autonomous assessment and decision system.

With a relatively simple example from human biometeorology it was shown how the the F-A-ST model can be used to assess the local microclimate conditions with respect to the internal thermal state of the agents. Like in a real world decision process, the F-A-ST approach considers both local (microclimate) and non-local (thermal state of the moving agent) aspects in the assessment process. Hence, if the model is properly defined in terms of relevant F–ST combinations and the associated boundary values for the fuzzy sets are correctly adjusted, this model should be able to produce more realistic results than indicators that are only based on either local or non-local parameters.

Of course it must be clearly admitted, that even if based on observations, the definition of the boundary values and other relevant parameters are, at least partly, subjective. However, as marked in the introduction, the aim of such a model is not to reproduce the exact perception of a single individual at a certain time at a certain location, but to formalise theories, how different variables interact with each other and trigger the assessment of an external situation. So, even if the exact values are uncertain, the operations how they are linked and transformed are consistent. Hence, the model can be used to test complex theories by using standard mathematical functions which force the user to formulate his or her assumptions in a concrete and systematic way instead of assessing the available data with some rule-of-thumb.

References

Bartl, C. and Hille, K. (2001). Computermodellierung psychischer Prozesse – Eine ”künstliche Seele”. Technical report, Universität Bamberg, obtainable from `www.unibamberg.de/ppp/insttheopsy/psiliteratur.html`.

Börcsök, J. (2000). *Fuzzy control*. Verlag Technik, Berlin.

Botteldooren, D., Verkeyn, A., and Lercher, P. (2003). Noise annoyance modelling using fuzzy rule based systems. *Journal of the Acoustic Society of America*, 114(3):1487–1498.

Bower, G. H. and Cohen, P. R. (1982). Emotional influences in memory and thinking: Data and Theory. In Clark, M. and Fiske, S., editors, *Affect and Cognition*, pages 291–331. Lawrence Erlbaum Assoc. Pub., London.

Bruse, M. and Fleer, H. (1998). Simulating surface-plant-air interactions inside urban environments with a three dimensional numerical model. *Environmental Modelling and Software*, 13:373–384.

Dautenhahn, K. (1998). The art of designing socially intelligent agents: science, fiction and the human in the loop. *Applied Artificial Intelligence J.*, 12(7–8):573–619.

Dörner, D. and Hille, K. (1995). Artificial souls: Motivated emotional robots. In *Proceedings of the International Conference on Systems, Man and Cybernetics*, pages 3828–3832, obtainable from `www.uni-bamberg.de/~ba2dp1/psi.htm`.

Ekman, P. (1992). An argument for basic emotions. In *Cognition and Emotion*, pages 169–200. Lawrence Erlbaum Assoc. Pub., London.

El-Nasr, M. S., Yen, J., and Ioerger, R. (2000). FLAME- Fuzzy logic adaptive model of emotions. *Autonomous Agents and Multi-Agent system*, 3:219–257.

Forgas, J. P. (1995). Mood and judgement: The affect infusion model (AIM). *Psychological Bulletin*, 117:39–66.

ISO 7730 (1995). Moderate Thermal Environments-Determination of the PMV and PPD indices and specification of the conditions for thermal comfort. Technical report, Int. Standards Org., Geneva.

Izard, C. E. (1977). *Human emotions*. Plenum Press, New York.

Kürbis, I. (2002). *Fuzzy-Logic Filter für das Global Atmosphere Watch Program*. PhD thesis, Ruhr-University Bochum, Bochum, Germany.

Lin, C.-J. (2004). A AI-based neural fuzzy system for temperature control. *Fuzzy sets and systems*, 143:311–333.

McBratney, A. and Moore, A. (1985). Application of fuzzy sets to climate classifications. *Agricultural and Forest meteorology*, 35:165–185.

Metternicht, G. (1998). Fuzzy classification of JERS-1 SAR data: an evaluation of its performance for soil salinity mapping. *Ecological modelling*, 111:61–74.

Metternicht, G. and Gonzales, S. (2005). FUERO: foundations of a fuzzy exploratory model for soil erosion hazard prediction. *Environmental Modelling and Software*, 20:715–728.

Mitaim, S. and Kosko, B. (2001). The shape of fuzzy sets in adaptive function approximation. *IEEE Transactions on fuzzy systems*, 9(4):637–656.

Robinson, V. (1988). Some implications of fuzzy set theory applied to geographic databases. *Computer Environment and Urban Systems*, 12:89–97.

Zadeh, L. (1965). Fuzzy sets. *Information control*, 8:338–353.

Zadeh, L. (1984). Making computers think like people. *IEEE Spectrum*, 8:26–32.

Zimmermann, H. J. (2001). *Fuzzy set theory and its applications*. Kluwer Academic Publishers, Boston, Dordrecht, London.


D

Module D

Simulating human thermal comfort in urban open spaces using the Multi-Agent simulation system BOTworld

In this module, the complete Multi-Agent system BOTworld is applied to analyse human thermal comfort in urban open spaces. Using the example of two simple symmetric urban street canyons, different morphological and microclimatic conditions and the resulting thermal comfort conditions are analysed in detail. It will be shown, how the dynamic simulation of the human thermoregulatory system provided by the ITC model can be linked to the F-A-ST assessment model and which impact the consideration of thermal state dependent routing behaviour has on the model results. To compare thermal comfort assessment based on the static PMV index with results obtained using the BOTworld system, a case study of planting additional trees in the street canyon is presented. From the results of the case study it becomes obvious, that if non-local effects created through pedestrian movement are considered in the analysis, even local changes of the microclimatic conditions can have a significant impact on the overall human thermal comfort.

Keywords: Thermal comfort, Multi-Agent simulation, BOTworld, PMV, Urban microclimate

Contents

List of Figures

List of Tables

1 Introduction

In the previous segments, the basic components of the BOTworld Multi-Agent system have been presented bit by bit. In Module A, the pedestrian movement model *PedWalk* for the simulation of pedestrian movement in complex urban environments has been presented. This was followed by the description of the individual-based biometeorological model ITCM allowing to simulate the reaction of the human thermoregulatory system on variable microclimate conditions. Through linking both *PedWalk* and ITCM, the thermal comfort of individual agents moving through urban open spaces have been analysed and the differences to the results obtained from local static indices have been discussed in Module B. Finally, the Fuzzy Logic based assessment model F-A-ST has been presented in Module C. Using the F-A-ST approach, local environmental conditions can be assessed with respect to the actual individual state of the assessing agent.

Now, the missing and final step in the design of the BOTworld system consists of linking the assessment model back to the *PedWalk* model in order to simulate the impact of the environmental assessment on pedestrian behaviour. Following the BOTworld schemes presented in the Segments B and C, Figure 1 shows the outline of the complete BOTworld system including the feedback loop between the F-A-ST assessment model and the *PedWalk* model.

In the BOTworld system presented so far, the results of the assessment model have only been collected and analysed afterwards, but did not have an impact on the routing behaviour of the agents. Compared to the real world this approach can produce potentially unrealistic behaviour as the agents always cling to their initial shortest-way routing plan regardless of their personal internal (thermal) state. In reality, pedestrians try to adopt their routing with respect to their personal comport situation: If a persons feels uncomfortable hot and the choice between a sunlit and a shaded street exists, the shaded side would be preferred if the resulting route is equal long or the increase in distance lies within a tolerable range. Hence, the information about the quality offered by the different possible routes through the model environment must also be taken into account when calculating the optimal path to a given destination.

Figure 2 offers a different view onto the BOTworld system by focussing on the decision flow as seen from the perspective of the individual agent: Based on the location of routing points and the general morphology of the analysed area (especially the location of non-walkable and less favourable areas) an initial shortest-path routing to the target is calculated.

Depending on the F-A-ST assessment sets actually used in the model simulation, different aspects of pedestrian comfort are then evaluated for the actual position of the agent: From the *PedWalk* model, information about the dynamical comfort is provided. This aspect covers basically all parameters associated with comfortable navigation through the model area such as walking with the preferred velocity or avoidance of waiting times. As a second comfort aspect, the thermal comfort conditions inside the model area are analysed with respect to the actual internal state of the agent. It is possible to extend the BOTworld system by further modules, this list can be extended by other comfort aspects such as air quality or exposure to noise, if the required input data are supplied and the associated F-A-ST sets are constructed.

Based on the outcomes of the comfort assessment, the environmental situation on possible routes towards the actual target is analysed in the next step. Summing up all available information, the optimal next navigation node towards the agent's target can be identified and the agent moves, if possible, towards this node.

In this paper, the application of the complete BOTworld system is presented by a simple example analysing the thermal comfort conditions in two street canyons. It will be shown, how the feedback loop between the agents' thermal state and their routing behaviour influences the thermal comfort assessment of the area and how the impact of additional trees can be analysed using the BOTworld system.

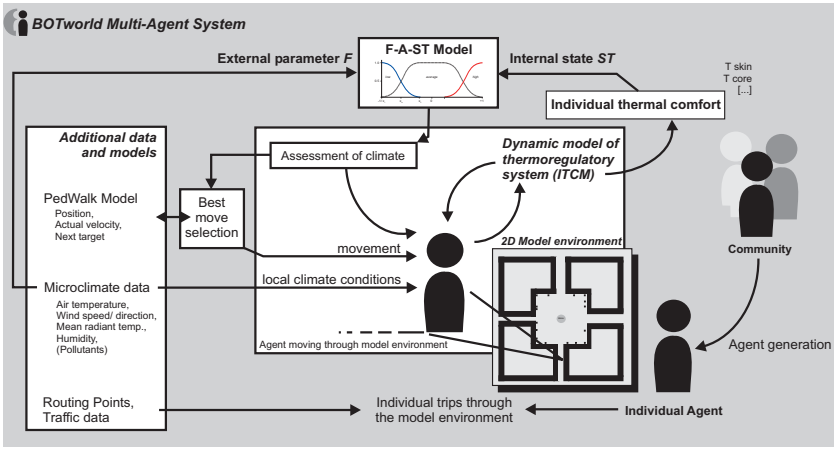

Figure 1: Schematic overview over the complete BOTworld system including the feedback loop between the F-A-ST assessment model and the *PedWalk* pedestrian movement model.

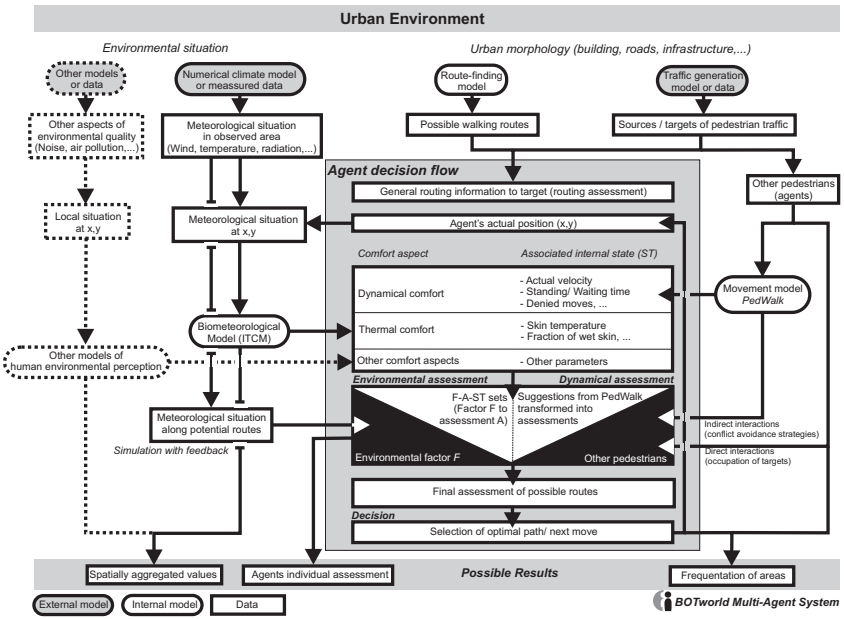

Figure 2: Decision flow in the BOTworld system with behaviour feedback as seen from the perspective of the individual agent. Dotted lines indicate possible extensions of the BOTworld system to assess other environmental aspects than thermal conditions.

2 Integrating state-dependent behaviour control into the BOTworld system

In order to consider the individual assessment of the local environmental conditions in the final routing decision of the agents, the path-finding algorithm of the *PedWalk* must be supplied with the quality information generated by the F-A-ST model.

The concept of local *Quality Assessment Values* introduced in the *PedWalk* model (compare Segment A of this thesis), offers a simple mechanism to incorporate such external quality information into the agents' routing decisions. By definition, a quality assessment value Φ^q is defined within the range of [+1,-1] where +1 denotes the maximum positive assessment and -1 represents the minimum negative assessment. It is no incident that the outcomes of the F-A-ST model, the assessment value A^*, follow the same concept and hence can be directly linked with the *PedWalk* model.

To integrate the results of the F-A-ST model into the *PedWalk* model, the local assessment values are added as global quality assessment values into the *PedWalk* system:

$$\Phi^{q,0}(\text{F-A-ST}) = \omega_q(\text{F-A-ST}) \cdot A^*(\text{F-A-ST})$$

Here, ω_q(F-A-ST) is the individual impact factor expressing the level of importance the environmental assessment should have on the routing decision ranging from 0 (no impact) to 1 (maximum impact). A^*(F-A-ST) is the assessment value as it is provided by the F-A-ST model.

This local quality assessment adds to the other assessment values that are used inside the *PedWalk* model. Hence, the impact of environmental assessment on the final routing decision depends on the respective constellation of all relevant assessment values for the agent's actual situation and their selected impact factors (see Figure 3).

As pointed out in Segment A, the local assessment values are used to transform the real distance Δ between two navigation nodes into a virtual distance Δ^v with

$$\Delta^v = \Delta\,(1 - \Phi)$$

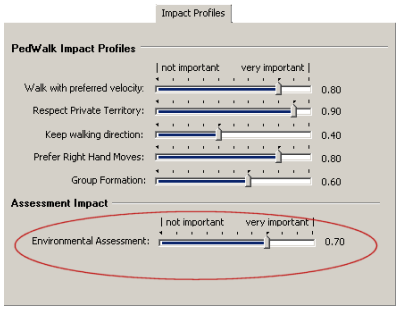

Figure 3: GUI for adjusting the different impact factors ω_x in the BOTworld system. The marked setting ω_q(F-A-ST)=0.7 for the impact of the environmental assessment on the routing decision is used for the simulations in this paper.

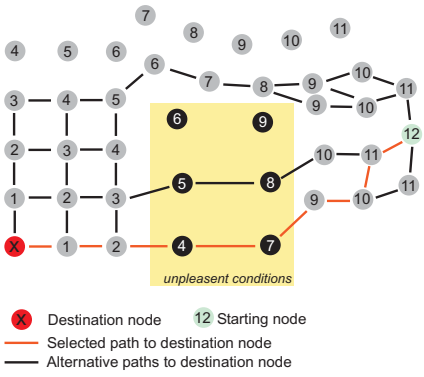

Figure 4: Example layout of the navigation network with an area of unpleasant conditions evaluated with $\Phi^{q,0}$(F-A-ST)=-1 The diagonal connections between the nodes are not shown or taken into account in this schematic figure.

where positive assessment values result in a virtual distance shorter than the real distance while negative assessment values produce a larger virtual distance. Using this definition, the worst assessment of $\Phi^{q,0}$(F-A-ST)=-1 for ω_q(F-A-ST)=1 and A^*=-1 will double the distance between two nodes. Figure 4 illustrates the virtual distance concept for a simple network of navigation nodes (real distance Δ=1) including an area with unpleasant environmental conditions that have been assessed with -1.

With this constellation of parameters, the local environmental conditions will be considered in the routing decision up to an increase in path length of 100% compared to the shortest possible route.

Of course, the numerical fixation of the impact of environmental conditions on the route choice is relatively arbitrary. There is lack of appropriate empirical studies confirming or rejecting the assumptions used in the model. Hence, we have chosen a value of ω_q(F-A-ST)=0.7 that seems realistic from our personal experience and gives satisfying results in the model simulations. In most of the cases, the exact value of the impact factors had only little influence on the model results as long as the values did not approach zero (compare studies in Segment A). However, if future studies will reveal that different values should be used, it is easy to modify the settings.

3 Simulation case study with the complete BOTworld system

3.1 The test scenario: Spatial layout and microclimate conditions

Like in the previous modules, a relatively simple urban situation will be used to test the behaviour of the BOTworld system and the impact of different model settings on the simulation results. The test area selected for this paper consists for two North-South orientated street canons (vertical streets hereafter), each 100 m long and 20 m wide as shown in Figure 5. The surrounding buildings have an uniform height of 20 m, which results in width–to–height ratio of 1. In addition, three small West-East orientated street sections (horizontal street hereafter) are used to complement the model domain.

At the ends of the horizontal streets, the entry and exit points of the model area are situated. Here, the virtual pedestrian can leave and enter the model. For all entry/ exit points a uniform pedestrian flux rate of 5 agents per minute has been assumed. In order to generate individual walking routes for each agent, several shop entrances are defined as internal target points on both sides of the vertical streets (small squares in Fig. 5). An uniform distribution of 0.1 shop visitors per minute has been applied to these internal targets, so that the route compositions are not biased by a different shop popularity. The maximum of internal targets has been set to three targets per agent.

In the default configuration, no vegetation is placed in the model area as shown in Figure 5 left ("bare" case). The "green" case shown on the right side of Figure 5 will be analysed in detail later in Section 3.4.3, p. 15f.

The microclimate data inside the model domain have been simulated using the microclimate model ENVI-met (Bruse and Fleer, 1998). The basic input parameters for the ENVI-met simulations are summarised in Table 1 (top). The spatial resolution for both the ENVI-met and the BOTworld simulation has been Δxy= 2 m. In order to simulate a summer day with relatively fresh air temperatures in the morning and hot conditions at noon, two reference temperature values have been used in ENVI-met: At 07:00 CET, a large scale background air temperature of 16°C has

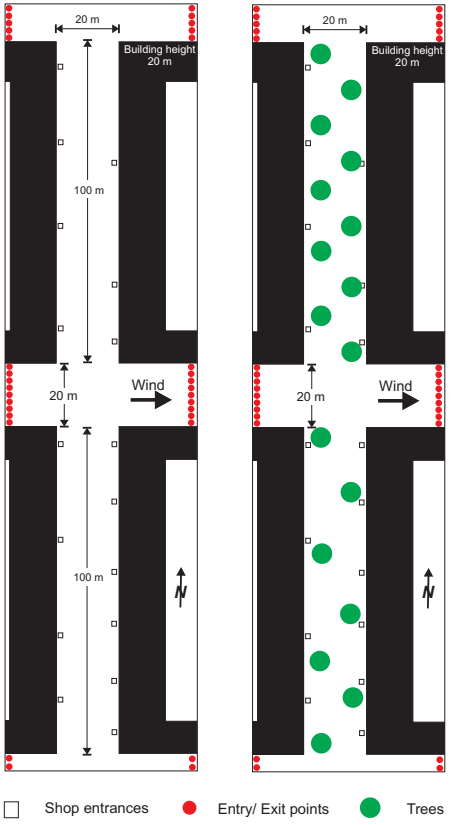

Figure 5: Layouts for the test scenario model domain for the simulations using the complete BOTworld system. The left figure shows the default situation with no trees ("bare" case), the right figure shows the "green" test case.

Table 1: Settings for the ENVI-met microclimate simulation and for the BOTworld agent community.

Settings Microclimate Simulation	
Simulated day	23th June
Simulated position	Bochum, Germany
	7.5° e.Long.
	53.0° n.Lat
Above-roof wind (10 m)	2.0 ms^{-1} from W
Reference temperature atmosphere	
07:00 CET	16°C
14:00 CET	24°C
Initial relative humidity	50%
Dimension model area	60 m × 240 m
Resolution model area	Δxy=2 m
Settings BOTworld Community	
Age distribution	$\overline{ag}$=40 y, $\sigma(ag)$=15 y
Body Mass Index distribution	$\overline{BMI}$=22, $\sigma(BMI)$=2
Static clothing insulation dist.	$\overline{clo}$=0.5 clo, $\sigma(clo)$=0.1 clo
Preferred velocity distribution	$\overline{v}_{\text{pref}}$=1.34 ms^{-1}, $\sigma(v_{\text{pref}})$=0.26 ms^{-1}
Impact factor environm. assessment	ω_q(F-A-ST)=0.7

been fixed which then linearly increased to 24°C at 14:00 CET.

In this section, two hours of the day will be analysed in detail: the 10:00 CET situation and, like in the previous papers, the 14:00 CET conditions. Figure 6 shows the ENVI-met simulation results for the "bare" model configuration at the respective times in terms of wind speed (a), air temperature (b1 and b2) and mean radiant temperature (c1 and c2). In case of the wind speed, the meteorological situation does not change significantly between 10:00 and 14:00 CET.

3.2 BOTworld community settings

The basic settings for the generation of BOTworld agents are summarized in Table 1 (bottom). For both the 10:00 and the 14:00 CET simulation, the same conditions, especially in terms of clothing insulation have been used. For the individualisation of agents, all three available agent types "normal", "sensible" and "tolerant" as defined in the F-A-ST model (see Module C of this thesis) are used in the model. The impact of the environmental assessment has been set to ω_q(F-A-ST)=0.7, which equals a moderate high importance of the environmental quality assessment on the agents' moving decisions.

The remaining community parameters represent average conditions which correspond to the settings used in the preceding simulations in Modules B and C.

3.3 Definition of the F-A-ST set

For the assessment of the thermal comfort conditions, one F-A-ST set has been defined in this study. As external factor F, the mean radiant temperature T_{mrt} has been chosen like in the examples before. To normalise F to F^*, the following boundary values and their respective linguistic expressions have been used:

$$\begin{aligned} F_{\text{min}} = 25°\text{C} \quad &\rightarrow T_{\text{mrt}} \text{ indicates } \textit{"shady"} \\ \updownarrow & \\ F_{\text{max}} = 65°\text{C} \quad &\rightarrow T_{\text{mrt}} \text{ indicates } \textit{"sunny"} \end{aligned}$$

For the associated internal state ST, the dynamic Effective Temperature (d)ET has been selected as indicator. Here, the selected range is:

$$\begin{aligned} ST_{\text{min}} = 18°\text{C} \quad &\rightarrow \text{(d)ET indicates } \textit{"cold"} \\ \updownarrow & \\ ST_{\text{max}} = 40°\text{C} \quad &\rightarrow \text{(d)ET indicates } \textit{"hot"} \end{aligned}$$

with the terms "*cold*" and "*hot*" describing the thermal state of the agent at the selected minimum (ST=18°C, ST^*=-1), and maximum (ST=40°C, ST^*=+1) threshold values of (d)ET.

Figure 7 shows the definition of the T_{mrt}-(d)ET set using the BOTworld software interface. The example chart in the GUI represents the distribution of the ST fuzzy input sets by plotting the internal state variable (d)ET versus the membership value μ in the "low", "high" and "average" fuzzy input set.

3.4 Model results

3.4.1 Individual-based assessment of the environment

To start the presentation of model results, we will focus on the assessment of the thermal conditions from the perspective of a single agent visiting the virtual

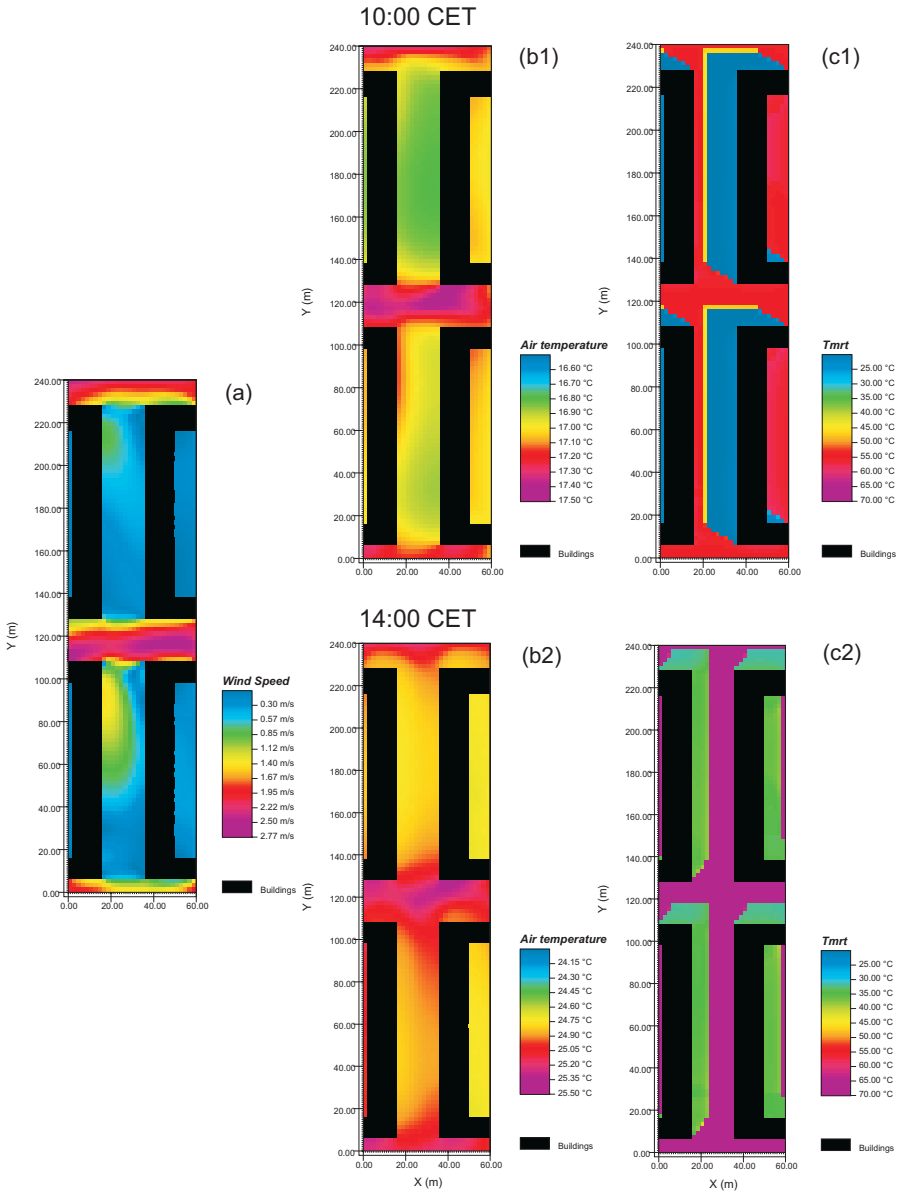

Figure 6: Biometeorological relevant microclimate conditions in 2 m height above ground at 10:00 CET (top) and 14:00 CET (bottom) simulated with ENVI-met for the "bare" configuration: Wind speed (a), air temperature (b1,b2) and mean radiant temperature (c1,c2).

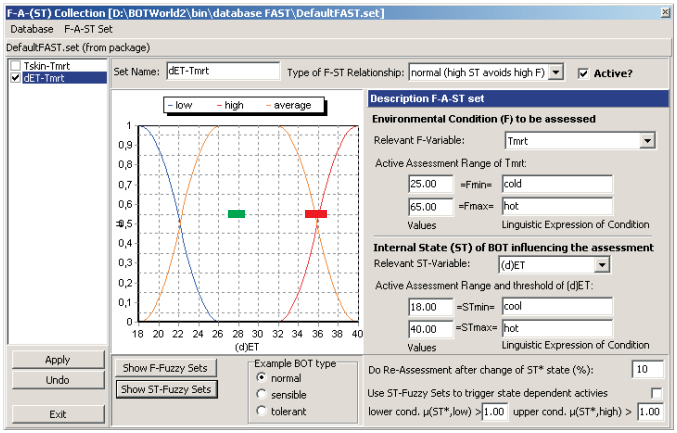

Figure 7: Definition of the T_{mrt}–(d)ET F-A-ST set in the BOTworld software. The bars inside the example plots indicate the typical range of observed (d)ET values for the 10:00 (green bar) and the 14:00 CET (red bar) situation.

street canyons at 14:00 CET. The agent in focus is called ”Daniela”, female, 53 years old and 1.90 m tall with a weight of 82 kg. Figure 8 shows the actual routing situation of ”Daniela” as a snapshot of a single moment during the model simulation. At this very moment, ”Danielas” actual dynamic Effective Temperature is 36.73°C which equals a normalised internal state ST^* of 0.70. Hence, the actual thermal sensation of the agent can be classified as a warm discomfort condition.

In Figure 8 (a) the location of ”Danielas” next target and the resulting real distance (Δ) to each point of the model domain is shown. In the given model geometry, the shortest path towards the target is only restricted by the surrounding buildings, hence the real distance is distributed almost radial around the target point.

In sub-figure (b) the spatial distribution of the quality assessment value $\Phi^{q,0}$ based on the actual thermal state of ”Daniela” is shown. $\Phi^{q,0}$ corresponds to the local assessment value A^* calculated by the F-A-ST model weighted with the impact factor ω_q(F-A-ST)=0.7 (see Section 2, p. 3 ff). As the actual thermal state of the agent is inside the warm to hot range, the shaded areas in the model are assessed positive (shades of green) while the unshaded sections with high mean radiant temperatures values get negative assessment values (shades of red).

Finally, Figure 8 (c) presents the Virtual Distance map showing the virtual distance Δ^v towards the next target taking into account both real spatial distance and the quality assessment values. For a better comparison between real and virtual distance, subfigure (d) shows the difference between Δ^v from (c) and Δ from (a). It has to be noted that in the presented simulation, only negative assessment values have been used to calculate the increase in virtual distance while the positive assessment values have been neglected. Considering also positive assessment values in the virtual distance calculation holds the danger of generating secondary local distance minima which would overwrite the routing information to the target and the agent would be lost (see also the annotations in Module A of this thesis). However, as the decisions of the agent are based on relative comparisons between the available options, considering only the negative assessment information is sufficient for this case study. For the simulation of less purposeful pedestrians such as tourists, the consideration of positive assessment values can be turned on in the BOTworld system.

Comparing real and virtual distance, the impact of the negative assessed sunny sections of the streets (eastern half of the street canyons, compare red areas in Fig. 8 b) can clearly be traced in a change of distance. Using the sunny sections of the north-

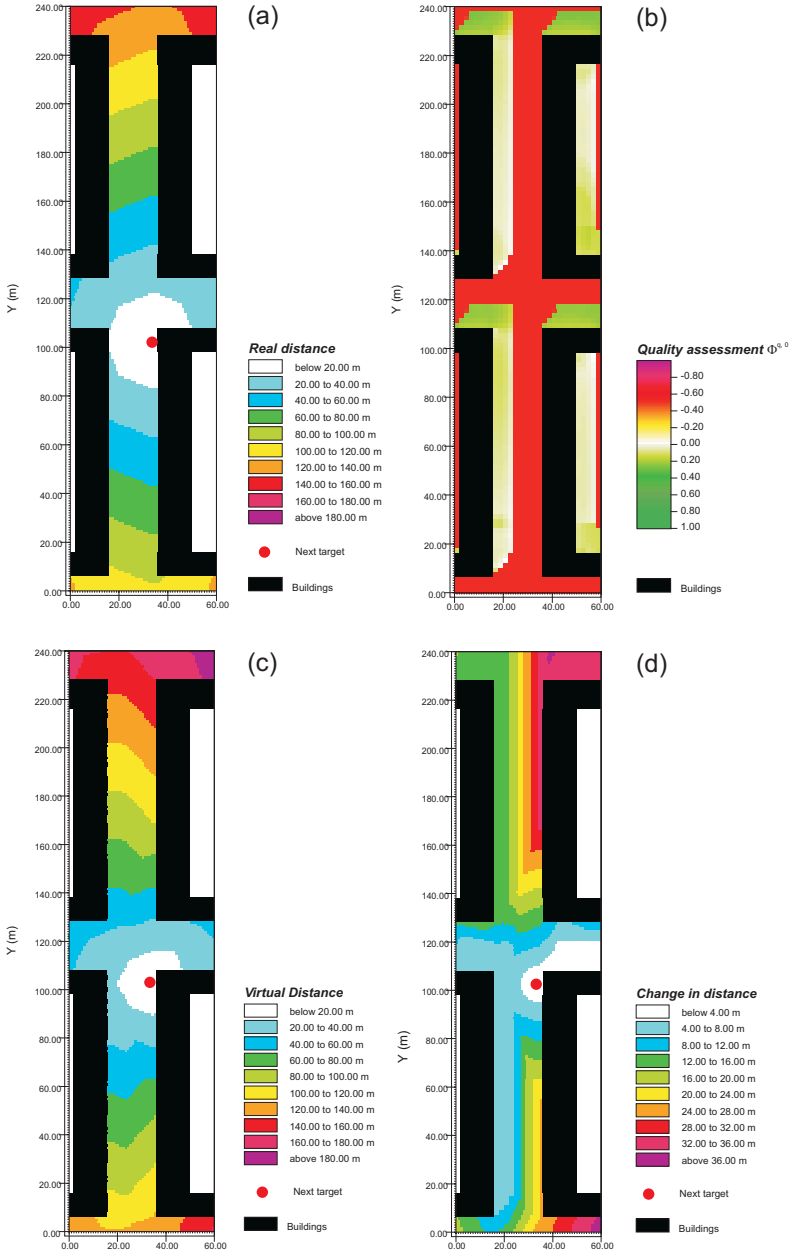

Figure 8: Spatial distribution of the main parameters for the routing decision of agent "Daniela" at 14:00 CET while the agent is in a warm to hot thermal state: Real distance Δ to the next routing target (red dot, a), actual weighted quality assessment $\Phi^{q,0}$ (b), resulting virtual distance Δ^v (c) and difference between virtual and real distance (d).

ern vertical street canyon to reach the target would result in an increase of virtual distance up to 36 m. Contrary, walking on the shady side would only lead to an increase up to 16 m. This remaining increase in virtual distance is caused by the unavoidable passage through sunlit areas to reach the target on the other side of the street.

Conclusions

Using the F-A-ST model, the local microclimate conditions can be assessed in dependency to an associated internal state of the respective agent. Once these assessment values are known, it is possible to replace the real distance towards the agent's actual target with a virtual distance which takes into account the microclimate conditions of the route. As the agent uses the virtual distance to choose between different possible routes through the model environment, this mechanism allows to simulate the feedback of thermal comfort assessment on the routing decision. In the following section it will now be shown, how this behaviour feedback influences the model results when running the BOTworld model with a few hundred virtual pedestrians.

3.4.2 Spatially aggregated assessment of the environment

In order to obtain information about the spatial distribution of the environmental assessment and to learn about the impact thermal comfort has on the movement patterns in the model area, complete BOTworld simulations have been carried out over a period of 60 min model time each. During this time, approximately 1900 agents entered the model area, visited virtual shops and left the domain afterwards. [1]

In this section we will analyse four different simulations: Two simulation runs have been executed analysing the 10:00 CET situation and two runs have been carried out using the 14:00 CET meteorological conditions (compare Fig. 6). From each simulation pair, one simulation has been run without a feedback loop between the thermal comfort and the moving decision of the agents while the other considered the local quality assessment in the routing decision.

The 10:00 situation

Figure 9 shows selected results from the 10:00 CET simulation without (top) and with (bottom) behaviour feedback: (a1) and (a2) display the dynamic Effective Temperature (d)ET averaged over all agents visiting the respective grid cells. The associated assessment values A^* are then shown in (b1) and (b2) and the number of agents entering a grid point is shown in (c1) and (c2). [2]

In the case of the simulations without feedback, the distribution of (d)ET allows a coarse division of the street canyons into a warmer (values around 28.5°C) and a cooler (values around 27°C side) side. According to the definition scale of the Effective Temperature (compare Module B and the scales in Fig. 10), this can be interpreted as "*slightly warm*" conditions in both cases.

Comparing the (d)ET values with the boundary values used in the T_{mrt}–(d)ET F-A-ST set, it is obvious that the observed (d)ET values are all within the "average" fuzzy input set (compare green bar in Figure 7, p. 8). Hence, no thermal discomfort is evident in this situation and the resulting local assessment values are close to neutral (A^*=0) all over the model area (Fig. 9 b1).

From Figure 9 (c1) an almost homogenous distribution of pedestrian traffic between both sides of the street canyon can be seen. As the agents always follow *exactly* the optimal route towards the next target point the traffic is very concentrated on the grid cells close to the building facades. In future versions of the model, a certain random component should be introduced here to distribute the traffic more over the available place.

Comparing the distribution of the dynamic Effective Temperature from the simulation with behaviour feedback (Fig. 9 a2) with the results from the non-feedback simulation, the two patches of lower (d)ET values in the northern street canyon are the only remarkable difference. The reason why these two spots develop is not really obvious. As only very few

1. In the example simulations, the impact of the indoor stay on thermal comfort has not been considered.

2. In this section we are not focussing on the impact of the local assessment on the routing decision process in detail. For that reason we have used the absolute assessment value A^* in the following figures rather than the impact weighted values $\Phi^{q,0}$ shown before.

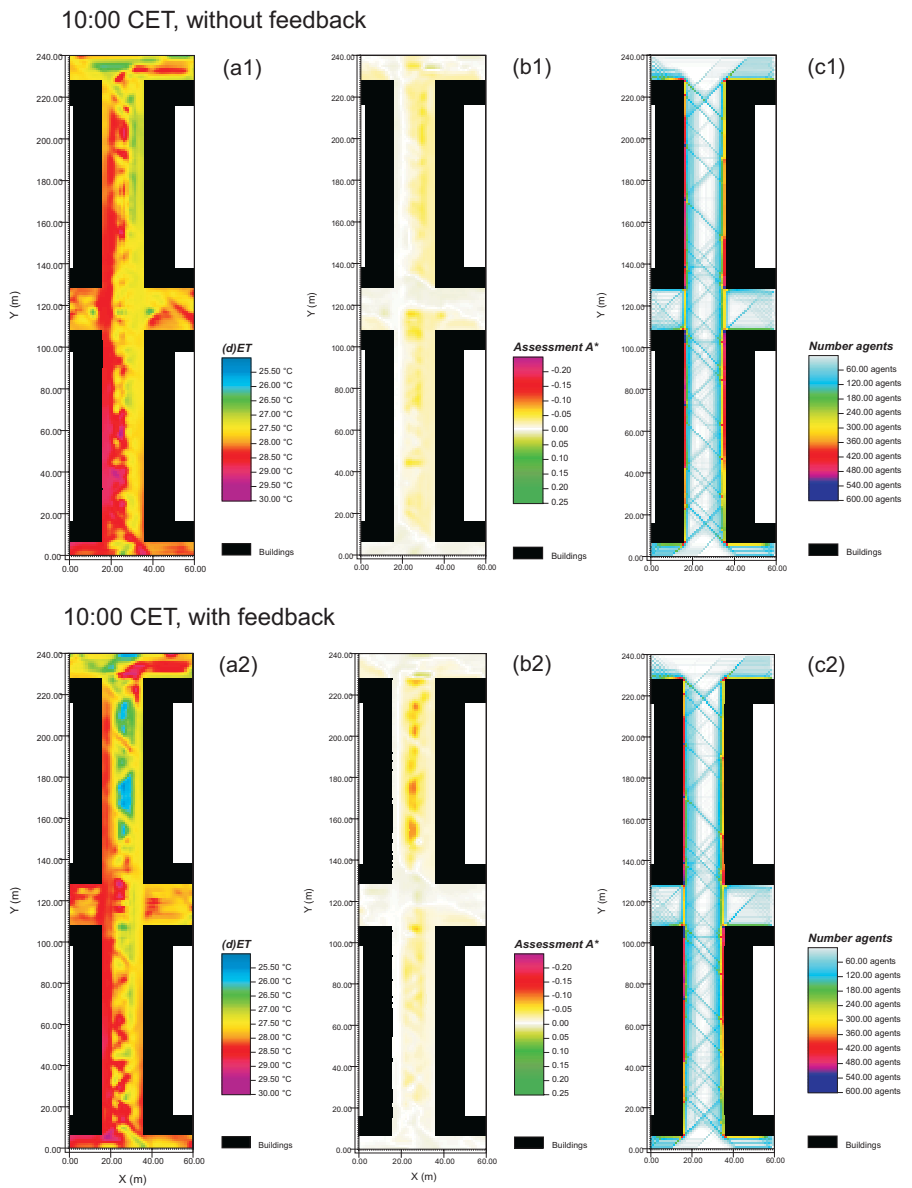

Figure 9: Spatially averaged distribution of selected simulation results for the 10:00 CET simulation for the "bare" scenario: Dynamical Effective Temperature (d)ET (a1,a2), local assessment values A^* (b1,b2) and number of agents entering the respective grid cell (c1,c2).

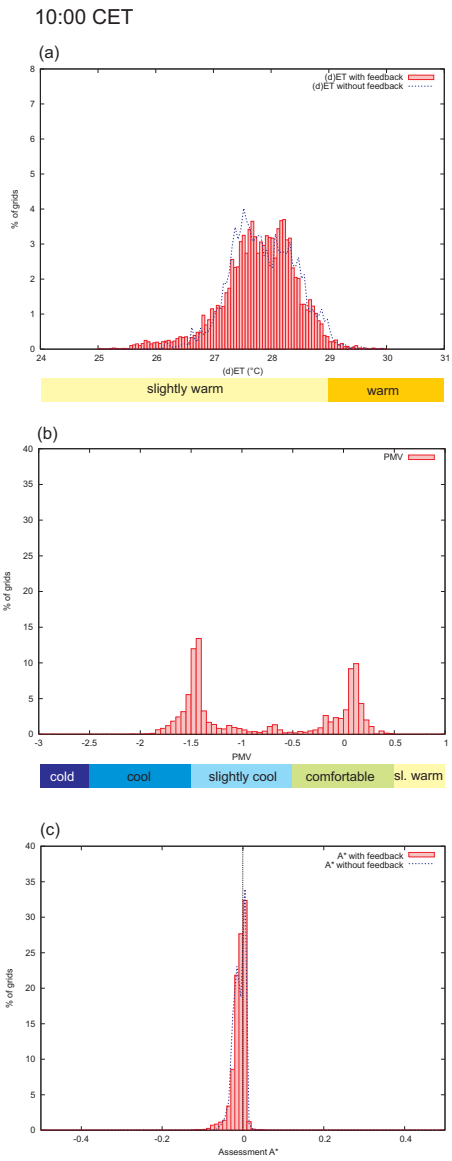

Figure 10: Frequency distribution of dynamic Effective Temperature (d)ET (a), predicted mean vote PMV (b) and local assessment value A^* (c) for the 10:00 CET situation. The results from the simulation without feedback are shown as dotted lines in (a) and (c).

agents (less than 60 agents, see Fig. 9 c2) pass over these two areas, the averaged values are quite sensitive to small changes in movement patterns. As the assessment values are still very close to the neutral conditions all over the area, this effect is close to numerical noise and should not be over-interpreted.

Figure 10 offers a different view onto the simulation results for the 10:00 CET situation: Sub-Figure (a) shows the frequency distribution of the averaged dynamic Effective Temperature over the model domain for the simulation with (bars) and without (dotted line) behaviour feedback. The subdivision into thermal sensations ("*cold*" to "*very hot*") used in this an the following figures follow the scheme from Höppe (2002) and Matzarakis and Mayer (1997) that has already been discussed in Modul B of this thesis.

In order to compare the results obtained from the dynamic ITC model with data generated by a classical static model, the frequency distribution of the associated *Predicted Mean Vote* (PMV) values is shown in Figure 10 (b).

As the PMV method is a static index assuming a balanced energy budget of the human body, the differentiation into sunlit and shaded sections inside the model is clearly reflected in the frequency distribution of the PMV values. The shaded areas are assessed as being "*cool*" to "*slightly cool*" locations which seems reasonable if one assumes that a person pauses in the shade until a stationary energy balance is reached. In the BOTworld model, the agents are only exposed to these conditions for a limited time and hence the cool conditions cannot be traced in the (d)ET distribution. On the other hand, the sunny locations are assessed as "*comfortable*" by the PMV model. According to Höppe (2002) "*comfortable*" conditions can be expected when the Effective Temperature is in the range between 18 and 23°C. Here, the BOTworld model indicates again slightly warmer conditions (values around 28.5°C). [3]

However, the assessment values for both the simulation with and without feedback indicate neutral conditions for all areas of the model with a very small tendency towards the cooler conditions but far away from any discomfort conditions.

3. In his paper, Höppe (2002) relates to the index PET, but as mentioned in Module B, we assume that despite of the different models used to calculate PET and (d)ET, the meaning of the values can be compared.

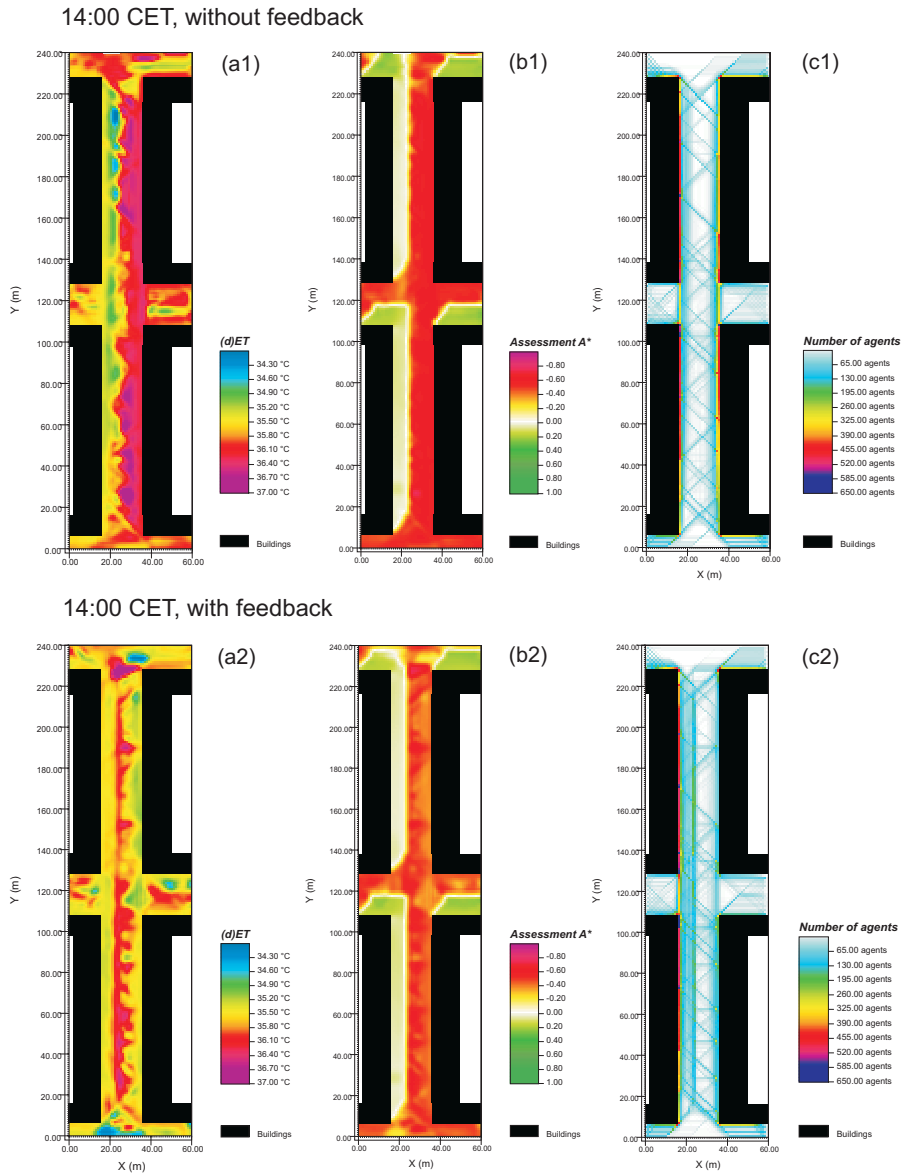

Figure 11: Spatially averaged distribution of selected simulation results for the 14:00 CET simulation for the "bare" scenario: Dynamical Effective Temperature (d)ET (a1,a2), local assessment values A^* (b1,b2) and number of agents entering the respective grid cell (c1,c2).

The 14:00 situation

Analogously to the 10:00 CET situation analysed before, Figure 11 shows the BOTworld model results for the situation at 14:00 CET from which we will start by looking at the results from the simulation without feedback (a1–c1).

Due to the generally higher air temperature and the increased radiative input at that time of day, the thermal comfort has shifted clearly towards the warm and hot conditions. The dynamic Effective Temperature (Fig. 11 a1) now shows values up to 37°C for the sunny street sides which can be classified as "*hot*" conditions. Contrary, on the shady side of the street the (d)ET values remain around 35°C which is the border between the "*warm*" and "*hot*" classification. Interpreting these values with respect to the definition of the T_{mrt}-(d)ET F-A-ST set, a clear tendency towards the "hot" internal state can be observed all over the model domain (compare red bar in Fig. 7, p. 8). As the internal state of the agents is now in a non-neutral condition, a clear pattern of positively and negatively assessed areas can be observed (Fig. 11 b1): The shaded areas are assessed positive as they promise to reduce the thermal load whereas the sunlit parts of the model domain show negative assessment values.

The agent frequentation pattern shown in Figure 11 (c1) is comparable to the 10:00 situation analysed before, which seems logical as no interactions between the thermal state and the routing behaviour are defined in the simulations without feedback.

Looking at the simulations with behaviour feedback (a2–c2), the situation is remarkably different. Now, the sunlit side of the street canyons are much less frequented compared to the 10:00 situation or to the simulation without feedback: The frequentation drops from approximately 350 agents down to less than 100 agents in the northern street and down to values of around 130 agents in the southern street. Accordingly, the frequentation of the shaded street sides increases as the agents try to walk in the shade whenever it is possible. This behaviour adoption has an obvious effect on the distribution of (d)ET values as shown in Figure 11 (a2). The dynamic Effective Temperature values both on the shaded and the sunny side now show values around 35.5°C, only in the middle of the street patches of higher values can be observed. As the agents return into the shade whenever their individual routing allows, the absolute level of their thermal load is much lower compared to the simulation where no impact on the routing choices has been simulated.

Figure 12 shows the associated frequency distribution of (d)ET (a), PMV (b) and the local assessment A^* (c) for the 14:00 CET situation. Like in Figure 10, the distributions for the simulation without feedback are shown as dotted lines while the solid bars show the simulation results with behaviour feedback.

The frequency distribution of the (d)ET values (Fig. 12 a) now shows a mono-peaked distribution in which the frequency of (d)ET values above 36°C is clearly reduced while the amount of values between 35.5 and 36°C has increased. While the PMV values shown in Figure 12 (b) still have the typical bimodal distribution with one peak for the shaded (values around 1) and the other peak for the sunlit zones (values around 3), this difference is no longer traceable in the dynamic Effective Temperature.

The behaviour feedback also has an impact on the agents' assessment on the area. Due to the reduced thermal stress level, the assessment of the unpleasant areas has improved slightly while it stayed the same for the positive evaluated areas (Fig. 12c). In both simulations, the meteorological conditions were the same, hence this change in assessment is related to the improvement of the thermal state of the agents due to the choice of alternative routes through the model area.

Conclusions

The example simulations presented in this section focussed on the effects of thermal state dependent routing behaviour on the spatial distribution of thermal comfort and the associated assessment parameters. In case of the near-neutral thermal conditions at 10:00 CET, the differences between the simulations with and without behaviour feedback was found to be minimal. When no thermal stress is present, the local microclimate conditions have no traceable effect on the routing behaviour of the agents. Contrary, for the 14:00 CET situation in which almost all agents suffer from warm to hot conditions, it could be shown that the consideration of a thermal state dependent routing choice has a clear impact on the thermal assessment of the area. Whenever possible, the agents try to avoid the sunny section. Therefore

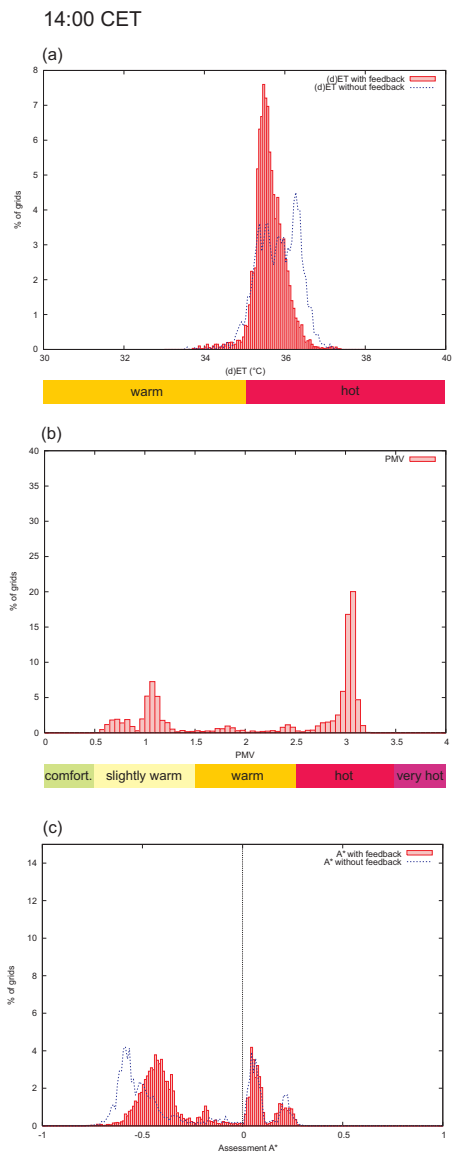

Figure 12: Frequency distribution of dynamic Effective Temperature (d)ET (a), predicted mean vote PMV (b) and local assessment value A^* (c) for the 14:00 CET situation.

the shady street sides are more frequently used and due to the temporary escapes into the shade, the general level of thermal discomfort has decreased compared to the simulation without feedback. A comparison of both simulations with the static PMV index showed that the bimodal PMV distribution which results from the independent assessment of the sunny and shady locations does not occur when using a non-local dynamical biometeorological model.

3.4.3 Effects of additional trees on thermal comfort

Looking at the simulated thermal comfort conditions, the question arises, how the actual situation could be improved through planning measures. One of the most obvious changes to improve thermal comfort is the plantation of trees along the street. However, trees are expensive in purchase and maintenance and therefore the obtainable improvements in microclimatic conditions should be analysed carefully. To test the effect of trees on thermal comfort, the configuration of the street canyon used so far has been modified with two rows of additional 20 m high trees in each street canyon (”green” test case, see Fig. 5, p. 5 right). In the northern street, the trees have been planted a bit denser than in the southern street canyon. The other simulation parameters remained the same as in the simulations before. For the simulation of the ”green” case study, only simulations with behaviour feedback have been executed.

Figure 13 shows the effect of the new trees on the meteorological parameters air temperature (a) and mean radiant temperature (b) for the 14:00 CET situation.

The shading and the transpiration of the trees lead to a decrease in air temperature within a 0.3 K limit. It can be anticipated, that this small change will not have a traceable impact on the biometeorological conditions of the model area. The larger effect of the trees can be found in the distribution of the mean radiant temperature. Here, local reductions around 30 K can be observed on the sunlit side of the street (Fig. 13 b).

Like in the previous examples, Figure 14 shows the results of the BOTworld simulation over a virtual time of 30 min in terms of average dynamic Effective

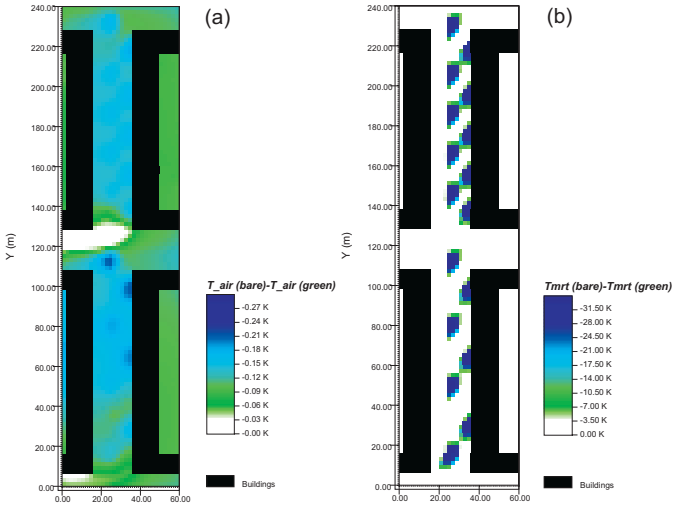

Figure 13: Differences between air temperature (a) and mean radiant temperature (b) simulated for the ”bare” and for the ”green” test case at 14:00 CET.

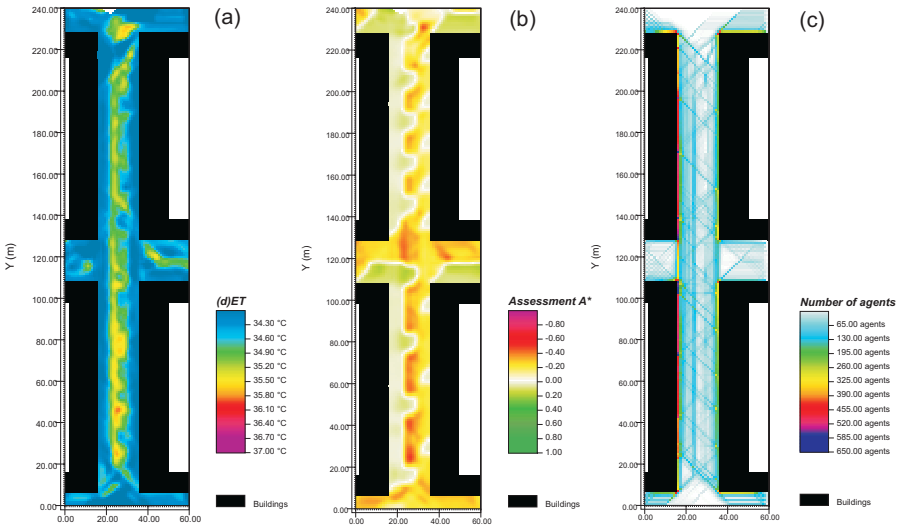

Figure 14: Spatially averaged distribution of selected simulation results for the 14:00 CET simulation for the ”green” scenario: Dynamical Effective Temperature (d)ET (a), local assessment value A^* (b) and number of agents entering the respective grid cell (c).

Temperature (a), local assessment (b) and number of by passing agents (c).

Comparing these figures with the results for the ”bare” simulation with feedback (Fig. 11 a2–c2), a significant improvement of the thermal conditions can be noticed: The (d)ET temperature now shows values with a mean around 34°C and a few warmer spots in the middle of the street canyons. This is an improvement of around 2 K compared to the situation without trees. This change is also reflected in the spatial distribution of the assessment values as shown in Figure 14 (b): The majority of the area is now assessed with A^* values better than -0.2 compared to the ”bare” case with a significant peak around the -0.5 level (see also Fig. 15 c). Also, the distribution of visiting agents (Fig. 14 c) shows a pattern different to the previous results. Although the left street side is still more frequently used, the pedestrians now distribute more equal over the available space.

Figure 15 shows the effect of the additional trees as frequency distributions allowing a direct comparison between the ”bare” and the ”green” scenario. The results form the ”bare” simulation with feedback is plotted as dotted lines while the ”green” simulation values are drawn as solid bars.

Seen from the perspective of the PMV distribution (Fig. 15 b), the additional trees have only a limited effect as they reduce the frequency peak of high PMV values (around PMV 3) only by approximately 5%. Contrary, the distribution of (d)ET values in Figure 15 (a) shows a very clear effect of the trees by decreasing the mean (d)ET values around 2 K from 36°C down to 34°C. Here, the non-local effects of the trees become obvious: Due to the temporary exposure to shade while walking through the model environment, the thermal load of the pedestrians remains much lower than in the case without trees. This lower thermal stress still remains while the pedestrians pass through a sunlit section of the street canyons.

The frequency distribution of the assessment values (Fig. 15 c) underline the previous conclusions: Although only a limited fraction of the model area is directly influenced by the additional trees, the resulting general decrease in thermal stress improves the assessment of the overall area significantly. By just looking at the spatial distribution of T_{mrt} or PMV,

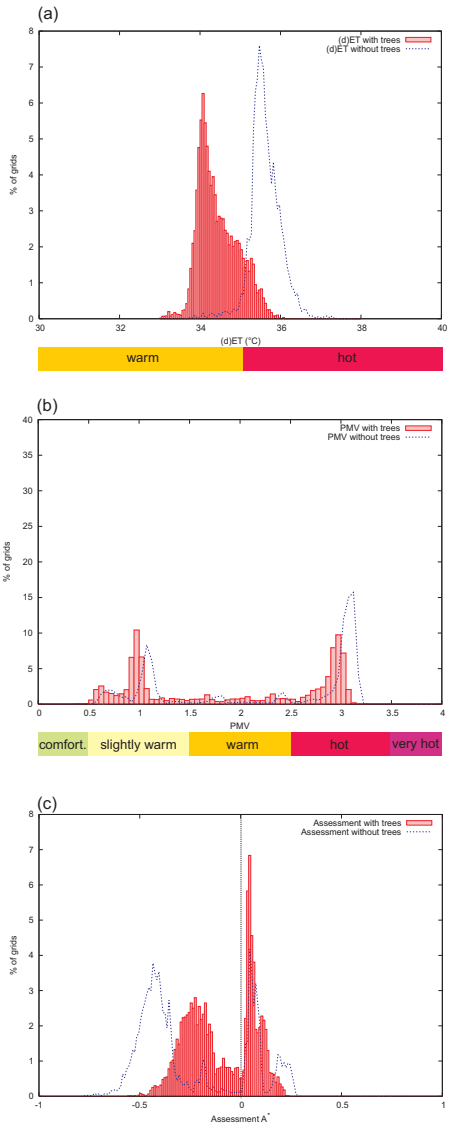

Figure 15: Frequency distribution of dynamic Effective Temperature (d)ET (a), predicted mean vote PMV (b) and local assessment value A^* (c) for the 14:00 CET situation with trees. The results from the ”bare” simulation are shown as dotted lines.

this effect would be largely underestimated.

Conclusions

In this section, the effect of two additional rows of trees on the thermal comfort conditions in the case study street canyons have been analysed. It was found, that even though the trees shade only a fraction of the model area, they have a large impact on the thermal comfort of the complete model domain. Contrary to the impression given by looking at the PMV value distribution, the trees significantly decrease the level of thermal stress inside the model area. The distribution of sunny and shady patches allow the virtual pedestrians to adopt their routing decisions to their actual thermal state without being forced to take too long deviations from the optimal shortest route.

4 Final conclusions

In this paper the application of the complete BOTworld model to the problem of assessing thermal comfort in a complex urban environment has been demonstrated. The different models presented in the previous modules of the thesis have been linked with each other and it was shown how the simulation of thermal state depended routing behaviour affects the simulation results.

Even when restricting to the simple case of a symmetric urban street canyon, it was obvious that both the application of the dynamic biometeorological model ITCM and the consideration of behaviour feedback had a major impact on the simulation results. Assessing the benefits of additional trees on thermal comfort using a classical steady-state comfort index such as PMV results in a much lower effect compared to the simulation results obtained with BOTworld. This difference enlarged with increasing thermal stress and growing complexity of the microclimate conditions (patches of sun and shade).

With the BOTworld model, several conclusions can be drawn from the simulation results obtained. Similar to the application of static indices such as PMV, BOTworld can produce two-dimensional maps showing the spatial distribution of the thermal conditions inside a given domain. Depending on the selected F-A-ST assessment sets, the impact of individual routing optimisation can be implicitly considered in these maps, which is not possible with simple local approaches.

As the BOTworld model also provides the number of by passing agents, the user is able to analyse how the urban structure and the resulting microclimate conditions influence the pedestrian movement patterns and how the thermal state of the visiting pedestrians will be. This information is of great importance if for example the optimal location of shops, restaurants or other facilities depending on a consumption-friendly attitude of the by-passers should be evaluated.

In conclusion, the BOTworld model provides a very sophisticated approach to simulate thermal comfort conditions in complex urban environments taking into account both non-local effects and the individual route optimisation. However, to get these results, the user has to process a number of additional steps (generation of traffic data, definition of F-A-ST sets,...) which introduce a certain amount of uncertainty into the model and might require an empirical calibration. But, in our point of view, this is still a major improvement and a step towards a realistic simulation of human thermal comfort compared to static indices which do not consider these effects at all.

The special strength of BOTworld lies in the simulation of complex and heterogeneous thermal environments. The more homogenous the environment is, the smaller is the difference between the assessment results obtained by static and local approaches and by dynamic non-local approaches like BOTworld.

References

Bruse, M. and Fleer, H. (1998). Simulating surface-plant-air interactions inside urban environments with a three dimensional numerical model. *Environmental Modelling and Software*, 13:373–384.

Höppe, P. (2002). Different aspects of assessing indoor and outdoor thermal comfort. *Energy and Buildings*, 34:661–665.

Matzarakis, A. and Mayer, H. (1997). Heat Stress in Greece. *Int. J. Biomet.*, 41:34–39.

VDI 3787 (1996). Richtlinie VDI 3787: Methoden zur human-biometeorologischen Bewertung von Klima und Lufthygiene für die Stadt- und Regionalplanung Teil 1: Klima. Technical report, Verein deutscher Ingenieure.


E

Module E

Simulating pedestrian exposure to traffic-induced air pollutants in urban areas using a Multi-Agent model system

In urban areas, the exposure of pedestrians to traffic induced air pollution is one of the most severe environmental risks. In order to fulfil legislative air quality criteria, a traffic redistribution between differen urban streets is often the most efficient way to decrease the air pollution at critical spots. However, a redistribution of the traffic leads to an increase of emissions at some other places and the question, whether the overall situation has improved through the measures or not, is not always easy to answer.

In this paper, a simple case study is presented to illustrate how the Multi-Agent system BOTworld can be used to simulate the exposure of pedestrians to PM10 (fine dust particles) pollutants. It will be shown, how traffic redirection measures change the spatial air pollutant distribution and how these effects can be assessed with respect to the exposure of pedestrians to PM10 using the Multi-Agent simulation approach.

Keywords: BOTworld, Multi-Agent system, Air pollution, Exposure to pollutants, PM10

1 Introduction

In urban areas, the exposure of pedestrians to air pollution caused by car traffic is one of the most severe environmental risks. According to the WHO, about 65.000 additional deaths can be related in Germany directly or indirectly to the exposure of traffic air pollutants (World Health Organisation, Regional Office Europe, 1999). Most recently, the new EU guideline 99/30/EG[1] defining the maximum acceptable concentration of fine dust particles with a diameter smaller or equal to 10 μm (PM10) has become relevant as one of the most stringent air quality guidelines for urban areas. In almost all of the bigger European cities, hot spots can be found that do not meet this quality criteria. Hence, urban managers and planners are forced to seek for effective measures to reduce the PM10 concentration at these spots.

Unfortunately, as long as there are no better technical solutions for diesel exhaust cleaning available, the only immediately effective measure to improve the local air quality is to reduce the traffic load at the concerned locations. However, urban car traffic consists to a huge part of local traffic which means that cars removed from one street will probably appear as additional traffic on a nearby road. As an effect, the lower pollutant concentrations obtained at one hot spots are often bought on the expense of other locations which suffer from higher air pollution afterwards. Therefore it is not easy to establish universal indicators for assessing the effects of a proposed measure on the overall air quality situation.

Looking at the problem of air pollution from an impact orientated point of view, it is not only important to know, *where* the air pollution increases or decreases, but also to take into account *how many* people are finally affected by the expected changes. The conclusions based on this perspective might differ from an assessment focussing on keeping the air quality limits.

In this paper, another application case for the Multi-Agent system BOTworld is presented: The pedestrian movement simulated by BOTworld will be used to assess the exposure of pedestrians to PM10 pollutants. We will analyse the effects of traffic redistribution on the spatial pollutant distribution and will compare the results with those obtained using an exposure orientated analysis.

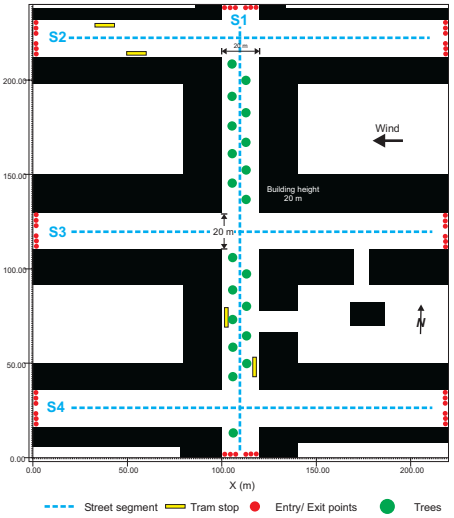

Figure 1: Layout of the 220 m×240 m model domain for the test scenario.

This paper is a proof-of-concept aiming to show that a Multi-Agent system like BOTworld can be applied to many different aspects of environmental analysis and assessment beyond the analysis of thermal comfort presented in the previous modules of this thesis.

2 Application of BOTworld to air quality assessment: The test case

To demonstrate the application of BOTworld to air quality assessment, the urban situation shown in Figure 1 has been constructed. The model area represents a section of a densely built-up urban area with a simple block structure.

The model domain is dominated by three 20 m wide West-East orientated street canyons (labeled ”S2”, ”S3” and ”S4” in Fig. 1, called ”horizontal streets” hereafter) and one 20 m wide North-South orientated canyon (”S1” in Fig. 1, ”vertical street” hereafter). The surrounding buildings have a uniform height of

1. excess of the daily average PM10 concentration above 50 μgm^{-3} only allowed at maximum 35 day per year

20 m, hence the width-to-height ratio of all canyons equals 1.

The total size of the test domain is 220 m×240 m and it was resolved into 110 × 120 grid cells with a spatial resolution of 2 m to simulate the pollutant dispersion using the microclimate model ENVI-met (Bruse and Fleer, 1998). For the Multi-Agent simulations in BOTworld, this resolution was refined to a 1 m grid (220 × 240 grid cells in total) with a linear interpolation of the calculated pollutant distribution.

For this case study, we have selected PM10 as an example air pollution component. As meteorological background scenario for the pollutant dispersion simulation, a day with light winds coming from the East with a velocity of 1.5 ms^{-1} above roof level have been assumed. As this papers deals only with very basic aspects of pollution modelling, the impact of thermal effects on the pollutant dispersion has not been taken into account. Further details on the traffic constellation and the resulting emission situation are summarized in the next section but one.

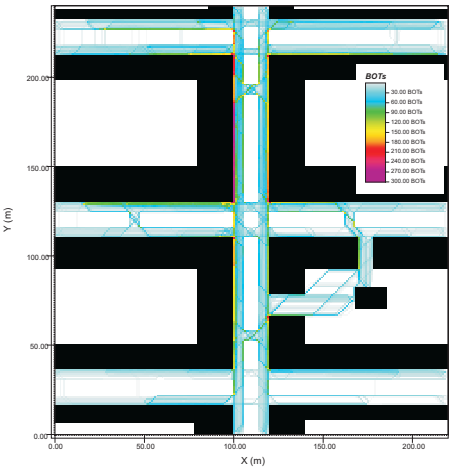

Figure 2: Agent frequentation pattern in the model domain after 30 min of simulation time in the BOTworld Multi-Agent system.

2.1 Pedestrian traffic situation

In order to generate pedestrian traffic inside the study area, entry and exit points have been placed at the end of each street canyon (red dots in Fig. 1). In addition, two tram stops have been located in the S1 and S2 street canyon. Here, like at the end points of the streets, the agents can enter and leave the model area. Furthermore, several shop entrances have been defined along all streets and in the backyard of the right block to serve as internal traffic targets for constructing the agents' personal itinerary (not shown in Fig. 1 for the sake of clarity).

The pedestrian traffic inside the model domain is supposed to be distributed non non-uniformly: The streets S1 and S3 are assumed to be the most attractive streets in the area with a pedestrian flux rate of 10 agents/ minute at each end of the street segment. With a pedestrian flux rate of 5 agents/minute street S2 is only as half as frequented as S1/S3 and street S4 finally is comparably deserted with only 1 agent/minute leaving or entering the model domain at the ends of this street. Accordingly to this distribution, the visitor frequencies of the shops located along the streets have been selected: For shops in the streets S1 and S3 a customer flux rate between 0.4 and 0.9 agents/minute have been used while in street S2 a maximum of 0.3 agents/minute and in street S4 of 0.1 agents/minute is defined. Figure 2 shows as an example the frequentation pattern in the model area after a simulation time of 30 min in the BOTworld Multi-Agent system.

To simulate the dynamics of pedestrian movement, a standard pedestrian community with a mean preferred velocity of $\overline{v}_{\text{pref}}$=1.34 ms^{-1} and a standard deviation of $\sigma(v_{\text{pref}})$=0.26 ms^{-1} according to Weidmann (1993) (compare Module A, Section 3.1 of this thesis) have been chosen. The other details of the BOTworld agent community are also set to the default values and need not be analysed in detail here. The different BOTworld simulations have been run over a model time of 30 min which resulted in approximately 1000 agents that have been analysed.

2.2 Car traffic and air quality situation

In this case study we will analyse the effects of a traffic rearrangement between the streets S4 and S2/S3 on the air quality situation. In the initial configuration ("old traffic"), the S4 horizontal street has a high traffic load with 30.000 cars per day and di-

Table 1: Car traffic volumes assigned to the four street segments in the test scenario and associated emission rates calculated for the 07:00 rush hour.

Street	old traffic [cars per day and direction]	new traffic [cars per day and direction]	change [cars per day and direction]	old PM10 emission 07:00 [μg s^{-1}]	new PM10 emission 07:00 [μg s^{-1}]
S1	16.000	16.000	0	13.28	13.28
S2	7.500	13.500	+6.000	6.26	10.41
S3	7.500	13.500	+6.000	6.26	10.41
S4	30.000	18.000	-12.000	22.64	15.36

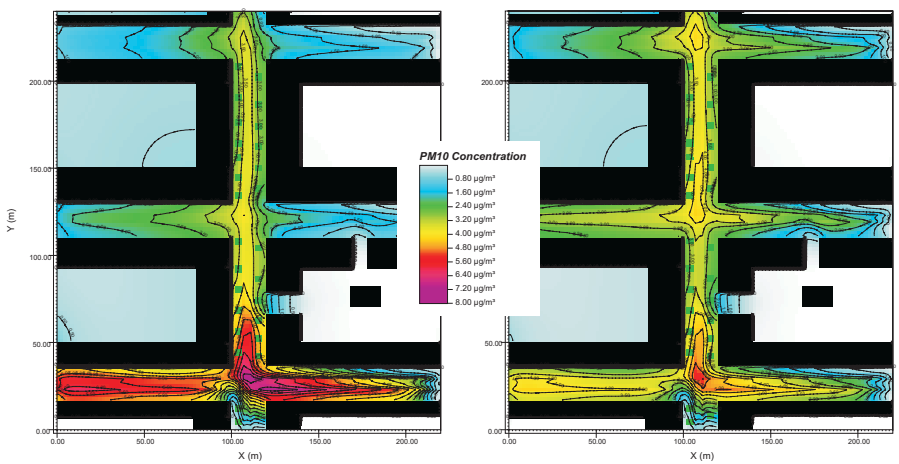

Figure 3: Local PM10 concentration in 1.8 m height simulated with ENVI-met for the old (left) and the new (right) traffic distribution. Isoline interval 0.5 μgm^{-3}.

rection while the remaining streets have significant lower loads with 16.000 cars per day and direction (S1) and 7.500 cars per day and direction (compare Table 1). According to their traffic volume, the emission of air pollutants differs significantly between the four street segments. Table 1 shows the emission rate of PM10 particles in the associated street segments for the morning rush hour peak at 07:00 calculated using the traffic emission model ISIS-Kfz (Beckröge and Bruse, 1999).

Due to the high emission rate, a local peak of PM10 concentrations can be anticipated in the S4 street canyon and at the intersection between S4 and S1. Figure 3 (left) shows the local PM10 concentrations in 1.8 m above ground level calculated with ENVI-met (Bruse and Fleer, 1998) for the 07:00 situation.

The maximum PM10 concentration can be found at the S4/S1 intersection with values between 7.5 and 8 μgm^{-3} while inside the S4 street canyon the concentrations are around 5 μgm^{-3}. These values alone do not reach the critical values of 50 μgm^{-3} according to EU guideline 99/30/EG, but as regional and local background concentration levels add to this local concentration, a strategy for a reduction of the local PM10 concentrations seem reasonable.

For this test scenario it was assumed that, as in most real cases, it is not possible to remove buildings to improve the local ventilation situation. Hence, the most efficient measure for reducing the local pollutants is to redirect the traffic from the critical street segment onto other streets.

A typical result of such a local traffic redirection is shown in Table 1 ("new traffic"): It was assumed that due to traffic re-routing, about 12.000 cars per day and direction could be removed from the critical S4 street. As these cars are assumed to be mainly local traffic, they must appear on other roads, in this case on the street segments S2 and S3 (+6.000 cars per direction each).

These changes in the traffic distribution cause an emission decrease in the S4 street from 22.64 μs^{-1} down to 15.36 μs^{-1} while the emissions in the streets S2 and S3 increased from 6.26 μs^{-1} up to 10.41 μs^{-1} (compare Tab. 1). As a consequence of the new emission situation, the local PM10 concentrations decrease down to values around 5.5 μm^{-3} at the S1/S4 intersection and down to values around 4 μm^{-3} in the S4 street canyon. Contrary, in the street canyons S2 and S3, the local PM10 values increase by approximately 1 μm^{-3} due to the higher traffic load (compare Fig. 3 right).

2.3 Analysing the effects of the measure

The first (and sometimes the only) step for assessing the effects of air quailing improvement measures is to compare the spatial distribution and the peak values of the pollutant concentration before and after the intended change. As already discussed above, the imposed changes in the traffic structure have led to a substantial decrease of the peak concentration values at the S1/S4 intersection while the values in the S2 and S3 canyons have increased slightly.

Figure 4 illustrates this situation by showing the frequency distribution of PM10 concentrations for the complete model area before (dotted line) and after (solid boxes) the traffic change analogous to the spatial distribution shown in Figure 3. The distribution chart confirms, that the amount of high concentration values (above 5 μm^{-3}) has decreased while in return the amount of PM10 concentrations between 2 and 4.5 μm^{-3} has increased. Assessing this change with respect to the relevant threshold values, it can be concluded that the situation has improved as it is now less likely that the local concentration exceed these thresholds. However, the increase of PM10 at other locations strikes the eye and should lead to a more sophisticated analysis of the results.

Using the BOTworld Multi-Agent system, the movement patterns of pedestrians and the resulting frequentation distribution can be calculated for the model area. If this information is merged with the spatial pollutant distribution, an exposure weighted pollution map can be generated. However, it is by far not obvious how this map should be generated numerically: Simply multiplying the local concentrations with the visitor frequency seems an obvious approach, but results in a map showing the distribution of a variable with a non-interpretable unit (concentration times visitors). Also, a linear operation between both variables would imply that reducing the local pollutant concentration by 50% has the same health effect than decreasing the amount of pedestrians by 50%, which is a doubtful theory.

Using the BOTworld system, a more realistic and

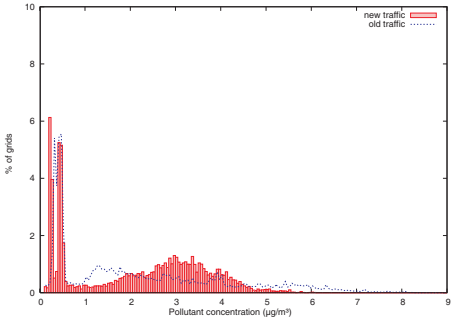

Figure 4: Frequency distribution of PM10 concentrations over the model area before (dotted line) and after (solid boxes) the traffic changes.

systematic analysis of the exposure to pollutants can be performed: From the biometeorological model ITCM, the ventilation rate is known for each agent at any time during the simulation. Linking this information with the local pollutant concentration, the amount of breathed pollutants can be calculated and summed up (compare Section 4.6 of Module B of this thesis).

To monitor the exposure of agents to PM10 pollutants, the so called ”Virtual Interview” method from BOTworld has been applied. In this method, selected areas of the model domain are marked as ”Survey Areas” in which the agents are virtually questioned as they pass by. In our study, we have defined survey areas at the end of each street and at the intersection of the streets S1 and S3 (”central survey area”).

Figure 5 shows the frequency distribution of the inhaled PM10 mass monitored during the simulation in the center survey area (top) and in all other survey areas (bottom). Obviously, an improvement of the air quality situation cannot be traced looking at the situation from this perspective: The reduced air pollution in street S4 and at the intersection of S1 and S4 has almost no impact on the exposure of pedestrians to PM10 particles. This is mainly due to two reasons: First, the locations where the local pollutant concentration decreased have only little pedestrian traffic while at the same time an increase of pollutants was found in the streets S2 and S3 with a much higher amount of bypassing pedestrians. Second, the main reduction of the PM10 concentration can be found

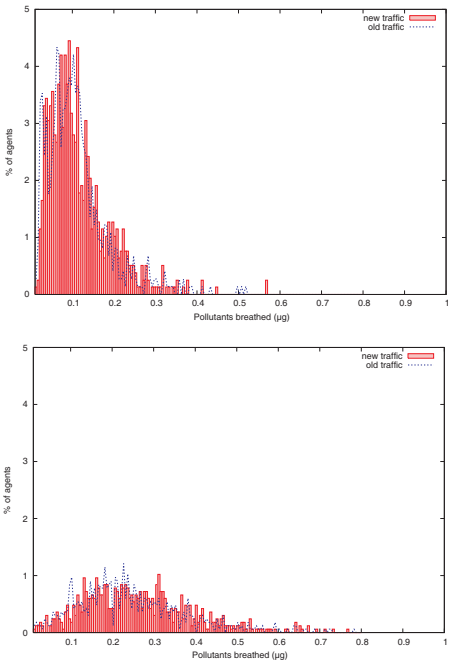

Figure 5: Frequency distribution of breathed PM10 mass monitored in the central survey area (top) and all other survey areas (bottom).

close to the emission source in the middle of the street. As the pedestrian traffic is restricted mostly to a 6 m broad pavement on both sides of the street, only very few pedestrians are directly affected by this improvement (compare Fig. 2). Closer to the building front, where the pavements are located, the changes in PM10 concentration are lower, hence the decrease of the amount of inhaled pollutants is lower compared to the maximum observable changes of PM10 concentrations.

In conclusion, the traffic redirection measures might help the local authorities to avoid exceeding the relevant threshold values for PM10, but it does not improve the general air quality situation if the exposure of pedestrians is taken into account.

3 Conclusions

In this paper, the application of the Multi-Agent system BOTworld for the analysis of pedestrian exposure to traffic induced pollutants has been presented. When assessing the impacts of purposed changes in the emission situation, it is often difficult to weigh up local improvements in air quality against opposing effects at other locations. If the situation is analysed only with regard to keeping the respective air quality threshold values, an analysis of the spatial pollutant distribution might be enough to assess the effects of a measures. However, looking at the situation from a more general perspective and with respect to pedestrian health, the overall exposure of pedestrians in the concerned area need be taken into account. Here, Multi-Agent systems simulating the individual pedestrian movement in urban areas can serve as powerful tools to analyse the air quality situation with respect to human exposure to pollutants.

Using the Multi-Agent system BOTworld, the effects of traffic redirection measures on the exposure of pedestrians to PM10 particles have been analysed in this paper. It was shown, that though the local peak PM10 concentrations have decreased, the pedestrian exposure to pollutants did not change significantly. Due to the movement of the pedestrians, the redistribution of pollutants from one place to another resulted in an equal rate of inhaled pollutants averaged over a virtual community of about 1000 agents.

The case study presented in this paper should serve as a proof-of-concept for the application of BOTworld to pollutant exposure simulation. With a more complex and larger street network, the advantages of using a Multi-Agent simulation would become even more clear.

References

Beckröge, W. and Bruse, M. (1999). ISIS-Traffic. A monitoring model for car induced air pollution in built-up areas. *Science of the total environment*, 235:371–374.

Bruse, M. and Fleer, H. (1998). Simulating surface-plant-air interactions inside urban environments with a three dimensional numerical model. *Environmental Modelling and Software*, 13:373–384.

Weidmann, U. (1993). Transporttechnik für Fuß gänger. In *Schriftenreihe des Instituts für Verkehrsplanung, Transporttechnik, Straß en- und Eisenbahnbau*. ETH Zürich.

World Health Organisation, Regional Office Europe (1999). Health Costs due to Road Traffic-related Air Pollution. An impact assessment project of Austria, France and Switzerland.

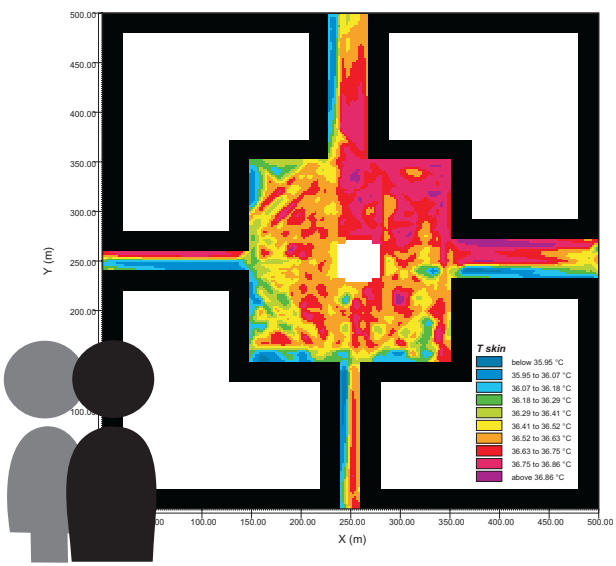
500.00
450.00
400.00
350.00
300.00
250.00
200.00
Y (m)
100.00
150.00
200.00
250.00
300.00
350.00
400.00
450.00
500.00
X (m)
T skin
below 35.95 °C
35.95 to 36.07 °C
36.07 to 36.18 °C
36.18 to 36.29 °C
36.29 to 36.41 °C
36.41 to 36.52 °C
36.52 to 36.63 °C
36.63 to 36.75 °C
36.75 to 36.86 °C
above 36.86 °C